EVALUATION OF A NANOPARTICLE DRUG DELIVERY VEHICLE IN MEDULLOBLASTOMA AND ORGANOTYPIC BRAIN CELL CULTURES

Weina Meng, BPharm

Thesis submitted to the University of Nottingham for the degree of Doctor of Philosophy

March 2006

CONTENTS

CHAPTER 6: EVALUATING UPTAKE OF RHODAMINE B ISOTHIOCYANATE LABELLED NANOPARTICLES IN THREE DIMENSIONAL CELL CULTURE

ABSTRACT

It has been widely reported that cell culture dimension and microenvironment influence cell proliferation, differentiation, and gene expression, which lead to different interactions between drug delivery systems and cells. The development in evaluation of drug delivery systems has reached the stage where investigations are now concentrating on intracellular uptake and subcellular localization of drug delivery systems. This thesis investigates the use of three-dimensional (3-D) tissue culture models to study how nanoparticles (NPs) may behave *in vivo*.

Poly (glycerol-adipate) (PGA) NPs can degrade into glycerol and adipate, which are not having toxic and any undesirable local or systemic effects in the host. Following on the initial physicochemical characterization of PGA NPs loaded with drug and fluorescent dyes, investigations moved on to the biological studies of NPs in various cell culture model, e.g. monolayer culture, 3-D culture models, and brain tumour invasion model.

Particle size, surface charge, and hydrophobicity are important features affecting the amount of particles taken up by cells and intracellular localisation of particles. Thus, the physicochemical properties of drug and fluorescent dye loaded PGA NPs were assessed by Photon Correlation Spectroscopy, Laser Doppler Anemometry, and drug/fluorescent dye loading studies. These studies indicated that physicochemical properties of drug, fluorescent dyes and PGA polymer could influence drug /fluorescent dye loading, which results in different particle size and surface charge of PGA NPs.

Quantitative and qualitative investigations into the influence of cell culture

dimension on uptake of NPs by cells, both by confocal fluorescence microscopy and flow cytometry, revealed that DAOY cells took up NPs more effectively when in 3-D spherical aggregate culture than in 2-D monolayer culture while uptake of NPs by normal brain cells was lower in 3-D cell culture than that seen in 2-D monolayer culture. This resulted in intracellular fluorescence intensity about 6 times higher in DAOY aggregates than normal brain cell aggregates while in monolayer culture mixed brain cells took up 2 times as many NP as the DAOY cells. The results from studies of NPs migrating through aggregates and tissue slices also indicated that penetration of NPs in 3-D culture models was affected by the structure of the interstitial compartment and composition of extracellular matrix.

Microscopic investigation of the histology of a co-culture invasion model of DAOY aggregates and a organotypic brain slice confirmed that DAOY cells massively invaded into cerebellum slices after a 4-day co-culture while the invasion of DAOY cells were limited within cerebral cortex slices even after a 6-day co-culture. Selective uptake of NPs by host cells and brain tumour cells were also assessed in this 3-D brain tumour invasion model. It showed that most NPs were taken up by DAOY cells instead of brain cells.

ACKNOWLEDGEMENTS

This work could not have been completed without the invaluable assistance by the following people, whom I would like to sincerely thank:

First of all my supervisors Dr. Martin C. Garnett and Dr. Terry L. Parker for their advice, ideas and support throughout my research.

Dr. Paraskevi Kallinteri (School of Pharmacy, Nottingham) for all her technical assistance and providing physicochemical data of PGA series polymers with C18 substitution. Dr. Lisa Storer (School of Biomedical Sciences, Nottingham) for teaching me the technique of tissue culture and technical assistance of tissue culture. Dr. Trevor Gray (Department of Histopathology, Queen's Medical Centre, Nottingham) for cutting thin sections of organotypic brain slice samples, and providing facilities and assistance for TEM studies. Ian Ward (school of Biomedical Sciences, Nottingham) for technical assistance for Confocal fluorescence microscopy and flow cytometry studies. The whole of the technical staff in the department especially Christine Grainger-Boultby, Colin Rowe and Barbara Stevenson and other postgraduate students in our group for their help.

Dr. G. A. Hutcheon and Dr. S. Higgins (Liverpool John Moores University, Liverpool) for the synthesis and supply of polymers for this research work, and BBSRC for funding the polymer synthesis.

The Graduate School at the University of Nottingham for providing partial funding for my trip to the 32nd Annual Meeting & Exposition of the controlled Release Society in Miami, Florida, in June 2005.

The Children's Brain Tumour Research Group (CBTR) for funding for consumables and instrumentation.

Finally, I must send a special thanks to my family for their love and support. Without their encouragement, I could not have finished my project and thesis.

ABBREVIATIONS

BBB	Blood Brain Barrier
BSA	Bovine Serum Albumin
CFPT	Critical Flocculation Point
CLSM	Confocal Laser Scanning Microscopy
DAPI	4', 6-diamidino-2-phenylindole, dilactate
DAMP	3-(2,4-dinitroanilino)-3'-amino-N-methyldipropylamine
DMEM	Dulbecco's Modified Eagle's Medium
DXM-FL	Dexamethasone Fluorescein
DXM-P	Dexamethasone Phosphate
ECM	Extracellular Matrix
ECS	Extracellular Space
FBS	Fetal Bovine Serum
FDA	Food and Drug Administration
GABA	γ-Amino Butyric Acid
GPC	Gel Permeation Chromatography
GFAP	Glial Fibrillary Acidic Protein
HBSS	Hank's Balanced Salt Solution
HEPES	N-(2-hydroxyethyl) piperazine-N'-(2-ethanesulphonic acid)
HPLC	High-performance Liquid Chromatography
LDA	Laser Doppler Anemometry
LDL	Low Density Lipoprotein
MFI	Mean Fluorescence Intensity
MPS	Mononuclear Phagocyte System
MEM	Minimum Essential Medium
NCS	Newborn Calf Serum heat inactivated
NEAA	Non-essential Amino Acid
NF	Neurofilament
NP	Nanoparticle
PACA	Poly (alkylcyanoacrylates)
PBS	Phosphate-Buffered Saline

PBCA	poly (butylcyanoacrylate)
PCL	poly- ε -carprolactone
PCPP	poly (carboxyphenoxypropane)
PCS	Photon Correlation Spectroscopy
PDL	Poly-D-Lysine
PFA	Paraformaldehyde
PGA	Poly (glycerol-adipate)
PLA	poly (lactic acid)
PLGA	poly (lactic acid-co-glycolic acid)
PVA	poly (vinyl alcohol)
RB	Rhodamine B
RBITC	Rhodamine B Isothiocyanate
SA	Sebacic Acid
SUPW	Super Ultra Pure Water
TEM	Transmission Electron Microscopy
Tg	glass transition temperature
Tri-HCl	2-Amino-2-(hydroxymethyl)-1,3-propanediol, hydrochloride
U-86983	2-(4-morpholinyl)-8-(3-pyridinylmethoxy)-4H-1-benzopyran -4-one
2-D	Two Dimension
3-D	Three Dimension

,

LIST OF FIGURES

LIST OF TABLES

CHAPTER 1

INTRODUCTION

1.1 BIODEGRADABLE POLYMER BASED NANOPARTICLES

1.1.1 The concept of nanoparticles (NPs)

In recent years, an extensive variety of drug carrier systems have been developed for the purpose of providing site specific or targeted drug delivery coupled with optimal drug release profiles. Among these carriers, biodegradable polymer NPs have been investigated as a promising drug delivery system. Biodegradable NPs, solid colloidal particles ranging in size from 10 to 1000 nm, are made from various macromolecular materials, which come from natural or synthetic sources. There are two types of systems with different inner structure, nanospheres and nanocapsules. Nanospheres are a matrix-type system composed of an entanglement of oligomer or polymer units, in which drug or other biological active molecules are encapsulated, chemically attached to the polymers, or adsorbed on the surface of the nanospheres (Fig. 1.1).

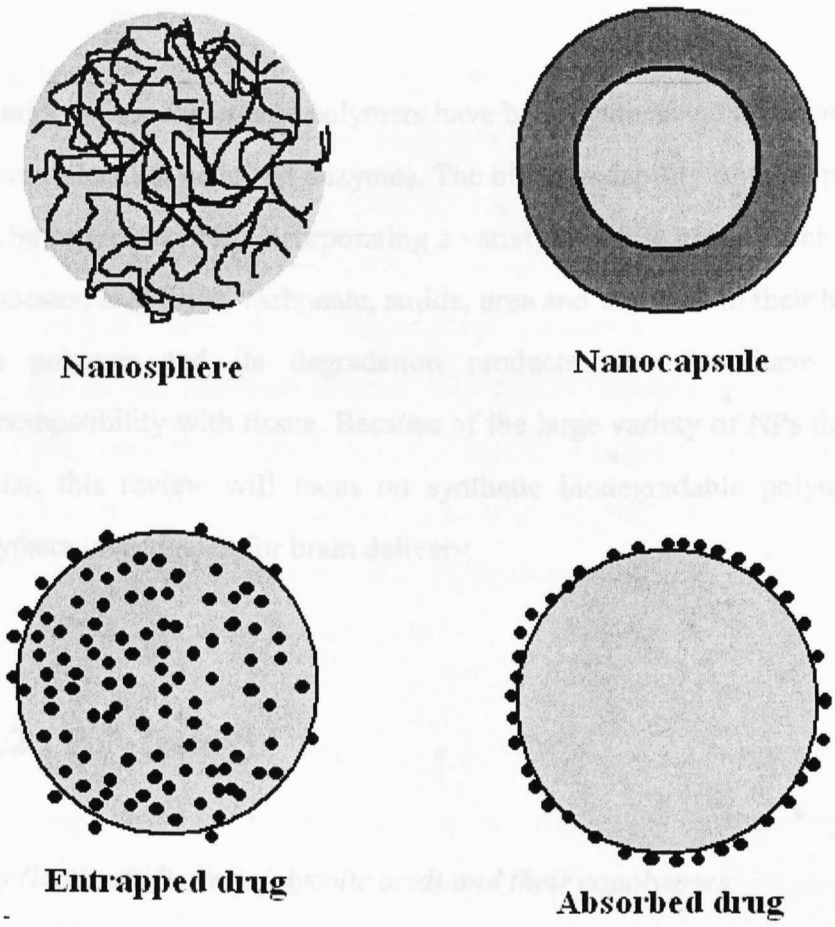

Fig. 1.1 Different types of polymeric NPs and drug loading

1.1.2 Biodegradable polymers for controlled release delivery systems

A variety of biodegradable polymers have been synthesized to deliver drugs, macromolecules, cells and enzymes. The biodegradability of these polymers can be manipulated by incorporating a variety of labile groups such as ester, orthoester, anhydride, carbonate, amide, urea and urethane in their backbone. The polymer and its degradation products can also have a good biocompatibility with tissue. Because of the large variety of NPs developed so far, this review will focus on synthetic biodegradable polymers and polymers investigated for brain delivery.

1.1.2.1 Poly (esters)

Poly (lactic acid), Poly (glycolic acid) and their copolymers

Poly (esters) (Fig. 1.2) based on poly (lactic acid) (PLA), poly (glycolic acid) and their copolymers, poly (lactic acid-co-glycolic acid) (PLGA) are the best characterized and have been widely studied. They have been used as biodegradable drug delivery systems or in the field of orthopaedics especially as fracture fixation devices, and to fabricate scaffolds on which cells can be cultured *in vitro* prior to implantation to regenerate tissue (Athanasiou *et al.*, 1996). PLA and PLGA have been used in the clinic since the 1960s, and so far PLGA has become the "gold standard" biodegradable polymer exemplified by more than 500 patents (Pillai *et al.*, 2001). The popularity of these polymers can be ascribed in part to their approval by Food and Drug Administration (FDA) for use in humans and their success as a biodegradable implant.

PLA, PLGA, or poly (glycolic acid) degrade through hydolysis of the backbone ester bonds into lactic acid and glycolic acid, which *in vivo* are then incorporated into the tricarboxylic acid cycle and excreted. In general, these polymers have shown satisfactory biocompatibility and absence of significant toxicity both in local tissues and systemically. *In vitro* cytotoxicity studies of PLA, PLGA, or poly (glycolic acid) demonstrated that they were well tolerated, increased cellular activity (Leenslag *et al.*, 1987), and resulted in no inflammatory or foreign body reaction (Schwope *et al.*, 1976, and Matsusue *et al.*, 1992). *In vivo* biocompatibility studies of these polymers from animal to human appear to support the view that these polymers and their degradation products seldom cause an abnormal response in local tissue and don't produce toxic effects either locally or systemically (Athanasiou *et al.*, 1996).

Degradation of PLA or PLGA occurs by auto catalytic cleavage of the ester bonds through spontaneous hydrolysis into oligomers and monomer of D, L-lactic acid or/and glycolic acid (Li *et al.*, 1996). The degradation rate depends on the hydrolysis rate constant (depending on the molecular weight, the lactic/glycolic ratio, and the morphology), amount of water absorbed, diffusion coefficient of the polymer fragments through the polymer matrix and the solubility of the degradation products in the surrounding aqueous medium (Shive and Anderson, 1997). Generally, burst release of drug from drug loaded PLGA/PLA NPs can be observed (Peracchia *et al.*, 1997, Cascone *et al.*, 2002, and Sant *et al.*, 2005). This might lead to insufficient concentration of drug being delivered to the target site and a high drug concentration near or above toxic levels to normal tissues (Shively *et al.*, 1995 and Jeong *et al.*, 2000).

Poly (esters):

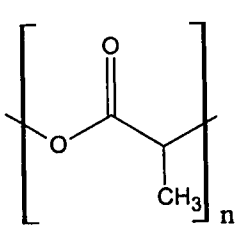

poly (lactic acid)

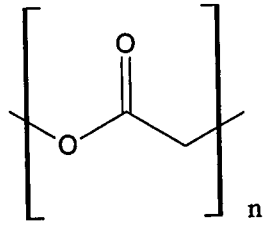

poly (glycolic acid)

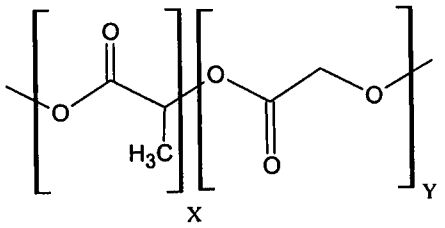

poly (lactic acid-co-glycolic acid)

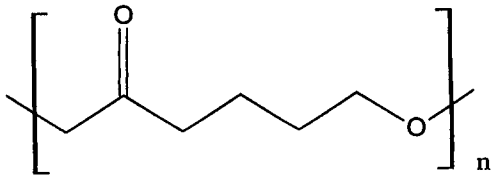

Poly-ϵ-caprolactone

Poly (alkylcyanoacrylates)

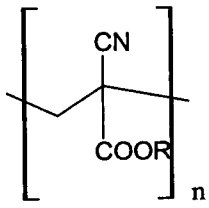

Polyanhydrides

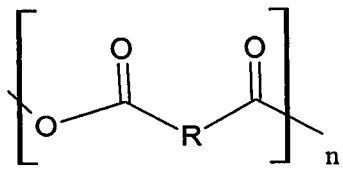

Fig. 1.2 Chemical structures of polymers cited in this chapter

Poly-ϵ-caprolactone

It was in the 1930s that the ring-opening polymerization of poly- ε -caprolactone (PCL) (Fig. 1.2) was first studied (Van Natta *et al.*, 1934). PCL is suitable for controlled drug delivery due to its high compatibility with many drugs (Sinha *et al.*, 2004) and non-toxicity (Murthy, 1997). Many drugs have been successfully incorporated into PCL microspheres and nanospheres, e.g. non-steroidal anti-inflammatory agent (Flurbiprofen) (Lacoulonche *et al.*, 1999), proteins (Jameela *et al.*, 1996), Steroids (Buntner *et al.*, 1996). Biocompatibility of PCL with tissue was studied in the brain of Wistar rats by Menei (Menei *et al.*, 1994). It was shown that no necrosis was observed, which accounts for biocompatibility of PCL microspheres with brain tissue. But a pronounced inflammatory reaction was observed and the author attributed it to a high concentration of PCL degradation products. Study of cytocompatibility in L929 mouse fibroblasts showed that neither cell cycle nor membrane integrity appeared affected by PCL films. These results underlined the good cytocompatibility of PCL films and fibroblast cells (Serrano *et al.*, 2005). The disadvantage of PCL polymer is that biodegradation of this polymer is very slow, extending over a period of more than one year in comparison to the shorter periods shown by other polymers such as PLA and PLGA (Sun *et al.*, 2006 and Sinha *et al.*, 2004). Although biodegradation of this polymer can be enhanced by copolymers like PLA and polyglycolic acid, it was reported that poly (lactide-co-caprolactone) can't be used for drugs with a narrow therapeutic window because particle shape and size was not precise (Fournier *et al.*, 2003)

1.1.2.2 Poly (alkylcyanoacrylates)

Poly (alkylcyanoacrylates) (PACA) NPs have attracted much attention for use in cancer thermotherapy and are already in clinical development for cancer drug delivery systems (Stella *et al.*, 2000 and Brigger *et al.*, 2001). PACA used as NPs was first reported by Couvreur and co-workers (Couvreur *et al.*, 1979a). A range of NPs with different properties could be produced by varying the size of the alkyl ester group (generally from methyl to octyl).

To design and evaluate the suitability of a polymer as drug carrier systems for humans, several aspects should be considered: a polymer has to be biocompatible, possibly biodegradable or at least should be able to be excreted by the kidneys or liver. The predominant degradation mechanism of PACA is mainly due to the hydrolysis of ester bonds of the alkyl side chain of polymer (Vansnick *et al.*, 1985 and Langer *et al.*, 1994). PACA was degraded into alkylalcohol and poly (cyanoacrylic acid), which can be eliminated *in vivo* via kidney filtration. This degradation has been shown to be catalyzed by esterases from serum, lysosomes and pancreatic juice (Mü ller *et al.*, 1990, and Scherer *et al.*, 1994). The cytotoxicity of PACA is related to the length of alkyl side chain. Studies examining cell morphology, cell viability and cell proliferation showed that polymers with short alkyl chains appeared more toxic than polymers with longer alkyl groups (Gipps *et al.*, 1987, Kubiak *et al.*, 1989, and Tseng *et al.*, 1990).

PACA has a wide range of applications, especially in cancer treatments and passage across the blood-brain barrier (BBB). Tight junction of brain microvessel endothelial cells that formed BBB is the major barrier to the passage of active molecules from the blood compartment to the brain. Thus

PACA used as a drug carrier for transport of therapeutic agents across BBB has been looked at in detail by many researchers. In studies by Kreuter and his co-workers, it was demonstrated that poly (butylcyanoacrylate) (PBCA) NPs represent the only NPs so far successfully used for the *in vivo* delivery of drugs to the brain (Kreuter *et al.*, 1997, and Kreuter, 2001). Drug loaded PBCA NPs coated with polysorbate-80 were taken up very rapidly by human and bovine primary brain capillary endothelial cells which leaded to about 10-20 fold higher amounts of polysorbated-80 coated PBCA NPs than uncoated PBCA NPs (Ramge *et al.*, 1999, Ramge *et al.*, 2000, and Gulyaev *et al.*, 1999). So far many research papers have shown that after incorporation into polysorbate-80 coated PBCA NPs, drugs including dalargin (Alyautdin *et al.*, 1995, and Kreuter *et al.*, 1995), loperamide (Alyautdin *et al.*, 1997), tubocurarine (Alyautdin *et al.*, 1998), the dipeptide kytorphin (Kreuter, 2001), the NMDA receptor antagonist MRZ 2/576 (Friese *et al.*, 2000) and doxorubicin (Gulyaev *et al.*, 1999), have been successfully transported into the brain. Enhancement of polysorbate 80-coated PBCA NPs across BBB was attributed to adsorption of apoliporotein E from blood plasma on the surface of NPs and thus may be mimicking low density lipoprotein, which has specific receptors at the surface of endothelial cells of the BBB. Apart from the mechanism described above, other processes such as tight junction modulation or P-glycoprotein inhibition may also occur (Kreuter, 2001).

1.1.2.3 Polyanhydrides

For degradable drug delivery systems in controlled release applications, it is expected that completion of polymer erosion coincides with the end of drug release and the drug is delivered by surface erosion of polymer matrix,

which leads to near zero-order release of the drug and enhances stability of the drug in the polymer (Uhrich *et al.*, 1999). This is hard to achieve with PLA and PLGA because PLA/PLGA NPs are degraded under bulk erosion and initial burst release can be observed in most drug loaded PLA/PLGA NPs in the first few hours. Therefore polyanhydrides were made with the intention that the polymer matrix could degrade with the longer time frame of their applications. The first application of polyanhydrides as a bioerodable matrix for controlled drug delivery was developed by Rosen in the early 1980s (Rosen *et al.*, 1983). Polyanhydrides are composed of diacid monomers, such as carboxyphenoxypropane (CCP) and sebacic acid (SA), connected to each other by anhydride bonds (Fig. 1.2).

The metabolic disposition and elimination process of poly (carboxyphenoxypropane) (PCCP)-SA at a ratio of 20:80 was studied *in vivo* by Domb and co-workers (Domb *et al.*, 1994). Domb demonstrated that PCCP degraded into its monomers CCP, whose main route of elimination is by macrophages and inflammatory cells after its disintegration into small fragments, and SA is eliminated as carbon dioxide due to its extensive metabolism in the body via the fatty acid degradation process. PCCP-SA polymer and its degradation products showed absence of acute cytotoxicity on cells as measured either by cell morphology or ability to proliferate (Leong *et al.*, 1986 and Attawia *et al.*, 1995).

Polyanhydrides constitute the only class of surface eroding polymers approved for clinical trial use by the FDA (Brem, *et al.*, 1991). In this phase I-II study, carmustine (BCNU) loaded polyanhydride polymer wafers were implanted intraoperatively in the resection cavity of 21 patients with recurrent malignant glioma. The polymer released BCNU for approximately 3 weeks and no adverse effect from the BCNU-polymer wafer was observed. Therefore, the therapy was well tolerated and safe. Consequently, extensive

research has been carried out focused on developing novel polyanhydride-based polymers. Other drugs of interest including anticancer drugs (cisplatin, fluorouracil, and methotrexate) (Shikani *et al.*, 2000), insulin (Carino *et al.*, 2000), and proteins (Tabata *et al.*, 1993) have been loaded into polyanhydride wafers, microspheres, and nanospheres. The polyanhydrides can be tailored to obtain the desired degradation profile via varying composition of polyanhydrides. Aliphatic polyanhydrides degrade in a few days combined with a near-constant rate without any large initial burst (Tabata *et al.*, 1993), while some aromatic polyanhydrides degrade over several years (Leong *et al.*, 1985).

1.1.3 General methods for the preparation of NPs

Several methods described in the literature have been developed for preparing NPs and the selection of the appropriate method for preparing drug loaded NPs depends on the physicochemical properties of polymer and drug. Generally, NPs can be prepared according to procedures of salting-out (Ibrahim *et al.*, 1992 and Galindo-Rodriguez *et al.*, 2004), emulsification-diffusion (Galindo-Rodriguez *et al.*, 2004), and nanoprecipitation (Fessi *et al.*, 1989).

1.1.3.1 Salting-out

The salting-out technique was first applied to the preparation of pseudolatex-loaded biodegradable NPs (Ibrahim *et al.*, 1992). In this method, a hydrophobic polymer is dissolved in an organic solvent, such as acetone, chloroform, tetrahydrofuran, and an emulsion is formed after

adding organic phase into a saturated electrolyte (magnesium chloride) containing colloid stabilizer, poly (vinyl alcohol) (PVA). Pure water is then added to the resulting emulsion in a sufficient amount for the organic solvent to diffuse into the aqueous phase, thus leading to formation of NPs. Solvent and salting-out agents are then eliminated by cross-flow filtration. This method can be used to encapsulate either hydrophilic drugs (Mani *et al.*, 2004) or hydrophobic drugs (Konan *et al.*, 2002) because polar (e.g., acetone) and non-polar (e.g. chloroform) solvents can be chosen for dissolving drugs. However, this technique is more suitable for loading lipophilic drugs because water-soluble drugs partition into the external water phase during emulsification. Varying PVA concentration, organic solvent, electrolyte, and percentage of polymer in organic phase can influence NP size and drug loading (Allémann *et al.*, 1993 and Konan *et al.*, 2002)

1.1.3.2 Solvent evaporation method

This is a well known technique (Bodmeier, 1986) that basically consists of the formation of a bi-phase, oil in water (o/w), or tri-phase (w/o/w) emulsion. In this technique, a hydrophobic polymer is dissolved in a non-polar solvent (e.g. chloroform, ethyl acetate or methylene chloride) and is emulsified in an aqueous phase containing a colloid stabilizer, such as PVA, polysorbate-80, or poloxamer-188. The resulting emulsion is then exposed to a high-energy mixer (e.g. ultrasonic device) to reduce the globule size. After the formation of a stable emulsion, the organic solvent is evaporated either by heat/vacuum or by continuous stirring. O/W emulsion is usually used for hydrophobic drug loaded NPs and w/o/w has been used to prepared hydrophilic drug loaded NPs (Zambaux *et al.*, 1998). This

method is widely used for preparation of microparticles, NPs, or micelles, which are made using various polymers, such as PLA, PLGA, and PACA. However, these procedures require the use of organic solvents, which are hazardous to the environment and physiological systems (Birnbaum *et al.*, 2000).

1.1.3.3 Interfacial deposition or nanoprecipitation

Nanoprecipitation, which has been developed by Fessi and co-workers (Fessi *et al.*, 1989), differs from salting-out and solvent evaporation methods in that no colloidal stabilizer needs to be used during NP preparation. Basically, this technique is based on interfacial turbulence or spontaneous agitation of the interface between the organic phase and the aqueous phase, involving flow, diffusion and surface processes. In the standard procedure, polymers are dissolved in a water-miscible solvent, such as acetone, ethanol, or methanol. This organic phase is then poured into the aqueous phase under slight magnetic stirring. The organic solvent diffuses instantaneously to the external aqueous phase followed by precipitation of polymer. Then as solvent diffuses further into the aqueous, the polymer chains aggregate resulting in NP formation. The original nanoprecipitation method is mostly suitable for hydrophobic drug, which is soluble in acetone or ethanol but displays very limited solubility in water. This results in reduction of drug leakage into aqueous phase. However, it was reported in the recent literature that lower encapsulation of hydrophilic drug also can be enhanced by changing the nature of the aqueous phase, such as pH, which can reduce drug ionization and lower its aqueous solubility (Govender *et al.*, 1999). The NP size and drug incorporation is also determined by the percentage of polymer in the organic phase, the

nature of the polymer, and the nature of the organic and aqueous solvents.

1.1.4 Drug loading

Drug loading is an important factor to evaluate in a successful NP system, because drug loading reflects the amount of drug entrapped into particles as a function of the total weight of polymer. Ideally when designing and evaluating a drug carrier, the drug should be well associated with the drug carrier with little drug in the unbound form. Therefore, a successful NP system is expected to have a high loading capacity, which leads to a decrease in the mass of the carrier required for administration. Drug encapsulated into NPs is achieved either by incorporation during NP formulation or by adsorbing the drug after formulation of NPs by incubating them in the drug solution (Couvreur *et al.*, 1979a, and Illum *et al.*, 1986b). Apart from the above two methods, drug-polymer conjugate has been reported for formulation of water-soluble drug loaded NPs (Yoo *et al.*, 1999). It is obvious evidence in the literature that a larger amount of drug can be loaded into NP by the incorporation method compared with the adsorption method when adsorption isotherms were considered (Illum *et al.*, 1986b, and Alonso *et al.*, 1991). NP formed by drug-polymer conjugates has a higher drug loading compared with non-conjugated drug. The drug loading in doxorubicin-PLGA conjugate and non conjugate was 3.5% and 0.3%, respectively.

The drug loading is highly dependent on factors such as the solubility of the drug, the nature of the organic solvent, the phase ratio of whole system, and the polymer composition. For drug adsorbed on the NP surface, the greatest drug adsorption can be achieved for hydrophobic unionized molecules.

Therefore, drug loading is quite sensitive to pH sorption medium (Couvreur *et al.*, 1979b, and Illum *et al.*, 1986b). Both Illum and Couvreur reported that the fluorescent dyes, fluorescein and rose bengal, are strongly adsorbed at low pH in their non-ionized form and rapidly desorbed as the pH increases. Apart from the properties of the drug, drug loading also can be enhanced by NPs composed of high ratio of hydrophobic moiety or by varying the colloid stabilizer, such as Dextran (Alonso *et al.*, 1991). In the case of drug incorporation, the rate of polymer precipitation at the droplet surface is of primary importance for the successful encapsulation of drug. The longer the time taken for precipitation to occur, the longer the time the drug has to diffuse into to the aqueous phase (Bodmeier *et al.*, 1988). Therefore, hydrophobic drugs are more readily incorporated than hydrophilic compounds not only because the hydrophobic drug has some solubility in the polymer matrix but also because its water-immiscible property delays hydrophobic drug diffusion into the aqueous phase prior to polymer precipitation (Bodmeier *et al.*, 1988 and Galindo-rodriguez *et al.*, 2004). Generally, up to 90% or even 100% of hydrophobic drug can be entrapped into NPs (Fessi *et al.*, 1989, Chacon *et al.*, 1996, and Barichello *et al.*, 1999) while drug loading of hydrophilic drug is about 10 time lower than that of water insoluble drug (Barichello *et al.*, 1999, and Govender *et al.*, 2000). Although water-soluble drugs have a relatively lower drug loading, recent research has provided encouraging results, which were reported in literature that hydrophilic drug, for example procaine hydrochloride, was more efficiently entrapped when the aqueous phase pH was set at a value that reduced drug ionization, hence hampering the amount of drug wastage by leakage (Govender *et al.*, 2000). In addition, drug loading also can be increased by an increase in the ratio of hydrophobic moieties and alkyl chain lengths of polymers. The higher the hydrophobic property the polymer has, the stronger the interaction that can occur between polymer and drug during NP formulation leading to higher drug

loading (Kim *et al.*, 1998, Fonseca *et al.*, 2002, and Zhang *et al.*, 2004).

1.1.5 Drug release

1.1.5.1 Mechanisms of drug release from NPs

Drug release from the NPs and subsequent polymer degradation and erosion are important for development of successful drug delivery devices. Drugs are often incorporated into both the hydrophilic and hydrophobic segment of NPs by chemical conjugation or by physical adsorption, so drug release may occur by (Kreuter, 1994):

(i) desorption of surface-bound drug;

(ii) diffusion through the NP matrix;

(iii) A combined erosion diffusion process;

(iv) In case of nanocapsules, diffusion through the polymer wall.

1.1.5.2 Methods for the determination of release

A number of methods have been applied for the determination of drug release from NPs and are discussed below (Washington, 1990).

(1) Membrane diffusion techniques: Dialysis bags/tubes and horizotal diffusion cells with artificial or biological membranes. Although membrane acts as an additional diffusion barrier leading to retardation of the drug release, membrane diffusion techniques, which are the most popular methods, avoid tedious and time-consuming separation.

(2) Ultracentrifugation, ultrafiltration and centrifugal ultrafiltration: These methods are unable to effectively and rapidly separate NPs from release medium, which leads to additional drug coming out from NPs during

the separation.

(3) *In situ* method: It avoids tedious separation and effectively reflects drug release from NPs *in vitro*. Researchers have to establish an effective assay method.

(4) Continuous flow methods: It also faces the problem of how to effectively separate sample and NPs.

In vitro drug release may have very little in common with delivery and release situation *in vivo*, but the release profiles describe the structure and behavior of NPs and drug-carrier interaction, and allow comparison between different formulations.

1.1.5.3 Release Kinetics

Diffusion dependant drug release from NPs

When NPs are stable and the rate of degradation is slow, the drug release from NPs is mainly controlled by diffusion. It has been reported that drug release from the NPs appeared to have two components with a rapid initial release at first sampling time followed by a gradually reduced release for a period of days (Song *et al.*, 1997, Cascone *et al.*, 2002, and Govender *et al.*, 1999). Drug release studies in U-86983 loaded PLGA NPs observed an immediate release of about 40% U-86983 release for the first day followed by a slower release for 18 days (Song *et al.*, 1997).

The rate of drug release is usually influenced by a number of factors: physical characteristics of drug; the physical state of NPs; the amount of drug loaded; the ratio of hydrophilic/hydrophobic segment of polymer; molecular volume of the drug, etc. In order to explain clearly, these factors will be discussed separately because most of them are interactive.

Drug hydrophilic/lipophilic characteristics and physical state of drug encapsulated in NP Hydrophobic NPs become increasingly hydrophilic when compounds such as water-soluble drugs are incorporated into the polymer matrix with consequent increase of the hydrolysis rate and drug diffusion (Vihola *et al.*, 1998). Thus, hydrophilic drugs are generally released more rapidly than hydrophobic drugs. Song reported that very poorly water soluble drugs did not display an initial burst release and the overall release rate was nearly constant (zero-order) (Song *et al.*, 1997). The physical state of the drug inside of NPs plays a key role in the drug diffusion from NPs. When drug is well dissolved or solubilized in the NPs, it may act as a plasticizer and lower the glass transition temperature (Tg) of NPs, which will accelerate the rate of drug release (Hombreiro-Pérez *et al.*, 2003).

Amount and molecular volume of drug It is reported that drug release rate increased with the amount of drug loaded (Jeong *et al.*, 2003, and Chorny *et al.*, 2002). When interaction between drug and NPs was studied, Song observed that drug release from PLGA NPs was accelerated as drug content increased (Song *et al.*, 1997). The size or molecular volume of drug will affect its rate of diffusion from NPs (Hintz *et al.*, 1989 and Jain *et al.*, 2000). Drug localized at the inner core of NPs with larger molecular volumes will have a smaller diffusion constant leading to a decreased release rate. However, release rate of drug localized at the surface of NPs is not dependent on the molecular volume (Teng *et al.*, 1998).

Physical state of NPs Under normal physiological conditions, whether NPs exist as an amorphous glassy state or liquid-like state will have a large influence on the rate of drug release from NPs. The thermal attributes of polymer, such as Tg, will prominently affect the physical state of NPs.

Below Tg, polymer is in a solid-like state, while above it the polymer is in a liquid-like state and free volume of polymer will increase, which permits greater local segmental chain mobility along the polymer backbone. Consequently, the diffusion of drug from glassy NPs will be slower than that from liquid-like NPs (Jeong *et al.*, 2003). However, if drug or other additives, such as surfactant, dissolve in NPs and solvent diffuses into NPs, they will act as plasticizers and be likely to lower the Tg (Jeong *et al.*, 2003). On the contrary, greater chain rigidity, bulky side groups and ring structures would tend to increase Tg (Markland *et al.*, 2000). Additionally, if NPs exist in crystal form, the rate of solvent movement in and solute or drug out of NPs will be lower in comparison with NPs formed from the more hydrophilic polymers, which contains appreciable amounts of water (Teng *et al.*, 1998).

The relative ratio of hydrophobic/hydrophilic segment In addition to the physical state of the NPs, polymer composition may be manipulated to change NP properties. Generally, the more the hydrophilic polymer segment, the faster drug comes out from the NPs. Cascone reported that the release rate of dexamethasone from PLGA 50/50 was higher than that from PLGA 75/25 NPs (Cascone *et al.*, 2002). It is known that glycolic units are more hydrophilic than lactic units and this increases the absorption rate of solvent and thus enhances solvent dissolvability to drug within PLGA matrix.

Presence of charged groups on structure of NPs The presence of charged groups on a polymer also can affect the rate of drug release from NPs. When there are ionized groups on the polymer, interaction between polymer and drug or polymer and polymer occurs. The extent of such interaction depends on the number and density of charged groups along the polymer backbone, on the side-chain groups, or at the terminal end-groups (La *et al.*, 1996 and Markland *et al.*, 2000).

Interaction strength between polymer and drug The stronger the interaction between the drug and NPs, the slower the diffusion of drug from NPs (La *et al.*, 1996, Puttipipatkhachorn *et al.*, 2001, and Chorny *et al.*, 2002). When the drug is chemically conjugated with PLGA NPs, the release takes place over 25 days, whereas, a rapid release in about 5 days occurred with those NPs containing unconjugated free drug (Yoo *et al.*, 1999).

Release from NPs depending on the rate of degradation and erosion

According to the literature, degradation of NPs is another important factor determining the profile of drug release from polymer matrix. Most biodegradable polymers have hydrolysable bonds in their backbone or on the side-chain group, ester, orthoester, anhydride, and so on. Their most important degradation mechanisms are chemical degradation via hydrolysis or enzyme-catalysed hydrolysis and physical processes, namely bioerosion.

Hydrolytic degradation The process of degradation describes the chain scission process during which polymer chains are cleaved to form oligomers and finally to form monomers (Gophferich, 1996). Basically, the hydrolytic degradation of aliphatic polyester consisting of polyester bonds proceeds according to the following reaction:

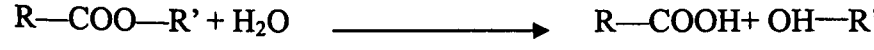

Hydrolytic degradation is a complex process, which involves water diffusion into NPs, ester bond cleavage, diffusion of soluble oligomers, and solubilization of fragments. Therefore these phenomena depend on the nature of the active compounds, i.e. drug properties, size of NPs and hydrophobic/hydrophilic segment within polymer, which have been discussed in the preceding paragraphs.

Acidic/basic properties of the incorporated drug The acidic/basic properties of incorporated drug may influence degradation rate of NPs because NPs have ester bonds and terminal carboxyl groups. An acidic drug can accelerate degradation rate and drug release from NPs because of faster hydrolysis of ester bonds. By contrast, basic drug has two different roles for controlling degradation of NPs: (1) basic drug acts as a basic catalyst catalyzing ester bond cleavage in polymer chains, which improve drug release from NPs (Li *et al.*, 1996); (2) Basic drug can slow down the rate of degradation and hence drug release from NPs can be suppressed (Govender *et al.*, 1999). Some authors have suggested that basic drug neutralises the carboxyl end groups of polymer chains, thereby decelerating the autocatalytic effect of the acidic chain ends on polymer degradation and water penetration into the matrix (Miyajima *et al.*, 1998). Li (Li *et al.*, 1996) explained why caffeine had two effects on polymer degradation. At an early stage, basic catalysis could occur because only a few carboxyl end groups were present and the molecular weight of the matrix was high. As degradation proceeded, some new carboxyl end groups were formed and caffeine could diffuse through the matrix. The caffeine was provided with more chances for interaction with carboxyl end groups. Thus in this stage the neutralization of newly formed carboxyl end groups became the main factor governing the degradation of matrix.

NP size Dunne investigated the influence of particle size on the degradation of PLGA (Dunne *et al.*, 2000). Three different size ranges, < 50, < 20 and $< 1\mu m$, were used to study PLGA degradation in Phosphate-Buffered Saline (PBS) buffer. It was found that rate of degradation in large particles is faster than in small particles. The author suggested that the influence of particle size can be attributed to more aqueous spaces or a larger radius of microparticles. In smaller particles products formed by degradation can easily diffuse to the surface of particles,

which would decrease the autocatalytic effect. In contrast, in the larger particles degradation products had a longer path to the surface of particles.

1.1.6 Colloidal stabilisation

Colloidal systems consist of a dispersed phase (or discontinuous phase) distributed uniformly in a finely divided state in a dispersion medium (or continuous phase). Colloidal particles in dispersion medium always show Brownian motion and thus particles may adhere to one another and form aggregates of successively increasing size. There are two basic interactions: one being Van der Waals attraction forces and another electrical double layer repulsive force. When attraction dominates, the particles will adhere with each other and finally form aggregates settling down under the influence of gravity. When repulsion dominates, the system will be stable and remain in a dispersed state (Napper, 1989).

1.1.6.1 Methods to stabilise colloids

To maintain the stability of the colloidal system, it is necessary to provide long range repulsive forces between the particles. This repulsion should be at least as strong as the attractive force and comparable to the range of the attractive interaction. Stability can be obtained by two fundamental methods (Napper, 1989):

(1) *Electrostatic or charge stabilisation*: This is the effect on particle interaction due to the distribution of charged species in the system. In liquid dispersion media, ionic groups can adsorb to the surface of a colloidal particle to form a charged layer. To maintain electroneutrality,

an equal number of counterions with opposite charge will surround the colloidal particles and give rise to overall charge-neutral double layers. Thus it is the mutual repulsion of these double layers surrounding particles that provides stability.

(2) *Steric stabilisation*: Steric stabilisation of colloidal particles is achieved by attaching (grafting or chemisorption of) macromolecules to the surfaces of the particles. If the thickness of the coating is sufficient to keep particles separated by steric repulsions between the macromolecule layers, the Van Der Waals forces are too weak to cause the particles to adhere. It has several distinct advantages over electrostatic stabilisation: relative insensitivity to the presence of electrolytes; equal efficacy in both aqueous and nonaqueous dispersion media; equal efficacy at both high and low solids content; reversibility of flocculation.

1.1.6.2 Steric stabilisation mechanism

When two particles with adsorbed polymer layers approach each other at a distance of less than twice the thickness of the adsorbed layer, interaction of the two layers takes place. The degree of stabilisation can be defined quantitatively in terms of the energy change occurring upon the interaction of the adsorbed layers. The Gibbs free energy change ΔG of the overlap interaction of the adsorbed layers is expressed as $\Delta G = \Delta H - T\Delta S$. If ΔG is negative upon the overlap of the adsorbed layers, flocculation or coagulation will result, and if ΔG is positive, stabilisation will result.

Many theories for explaining the steric stabilisation mechanism have been proposed and many theoretical equations for calculating the energy change with the overlap of the adsorption layer have been devised. Here the generally accepted entropic stabilisation theory is used. In this theory, it is

assumed that a second surface approaching the adsorbed layer is impenetrable. Thus, the adsorbed layer is compressed and the polymer segments present in the interaction region lose configurational entropy. That is, the polymer segments occupy fewer possible configurations in the compressed state than in the uncompressed state. This reduction in entropy increases ΔG, producing the net effect of repulsion between the particles and thus preventing the particles from flocculating. (Napper, 1989).

1.1.7 Uptake of particles by cells

1.1.7.1 Mechanism of Intracellular Uptake

To increase therapeutic effect and decrease both total dose and side effects associated with drug, it is not only important to deliver a drug into a specific tissue, but sometimes also to deliver it within a specific cellular compartment. Intracellular delivery of drug carriers has been paid some attention. It has long been clear that there are at least two mechanisms of uptake into the cells, generally classified as phagocytosis, receptor-mediated endocytosis and pinocytosis. Phagocytosis is usually defined as the internalization of large particles that must bind to specific plasma membrane receptors capable of triggering their own uptake. Phagocytosis is typically restricted to specialized mammalian cells, including macrophages, monocytes and neutrophils. Pinocytosis, which occurs in all cells, more commonly refers to the constitutive formation of smaller vesicles carrying extracellular fluid and macromolecules nonspecifically bound to the plasma membrane. Receptor-mediated endocytosis includes clathrin-mediated endocytosis and caveolin-mediated endocytosis (Conner and Schmid, 2003). After macromolecules, large complexes or whole cells are taken up by phagocytosis or receptor - mediated endocytosis into the cytoplasm, they are

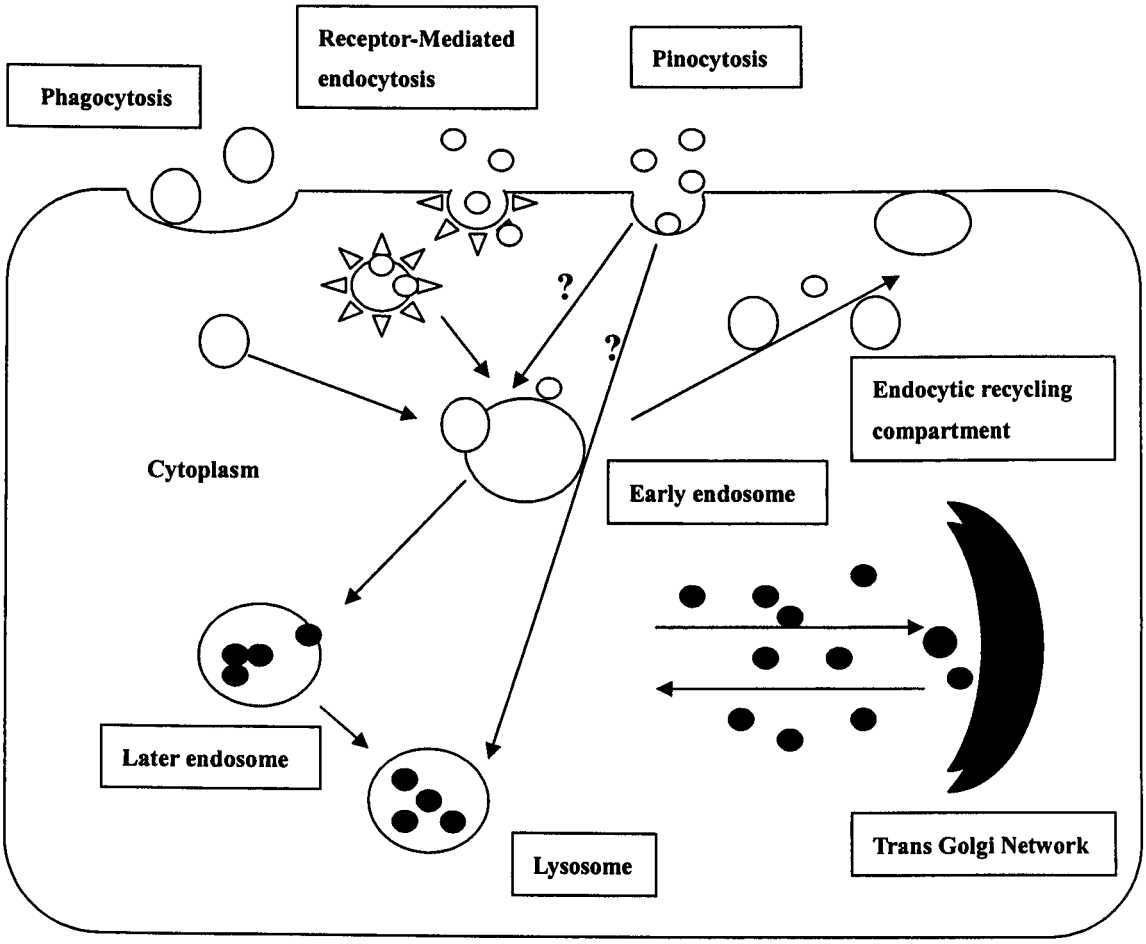

Fig. 1.3 Schematic depiction of particle uptake and sorting: particles with large size are taken up by phagocytosis. Particles with small size will be taken up by pinocytosis or receptor-mediated endocytosis. After entering vesicles at plasma membrane, particles taken up by phagocytosis or receptor-mediated endocytosis are transported to early endosomes. According to the properties of particles, some will enter into later endosome and lysosome, where they are degraded by lower pH and the high concentration of lysosomal enzymes and some, like most receptors, may be recycled to the plasma membrane. For pinoctyosis, it is not very clear that whether particle will be sorted into endosome or be directly sorted into lysosome so far.

transported to early endosomes and then sorted into different intracellular compartments (Fig. 1.3). The early endosomes, which have slightly acidic pH (pH≈6.0-6.8), are responsible for the dissociation and sorting of macromolecular-receptor complexes. The receptor may be recycled to the surface by vesicles that bud from the endosome and then target the plasma membrane; The remaining fraction is transported to later endosome and lysosomes, in which these fractions are degraded by lower pH (pH≈5) and the high concentration of lysosomal enzymes (Mellman, 1996, and Van Deurs, 1989). For pinocytosis, it is not very clear that whether particle will be sorted into endosome and then into lysosome or will be directly sorted into lysosome so far.

1.1.7.2 Properties affecting particles taken up by mononuclear phagocyte system (MPS)

The MPS is a collective name for a group of highly phagocytic mononuclear cells and consist of monocytes and macrophages. These cells are widely distributed and strategically placed throughout the body, either at fixed sites or free in the circulation, to recognize and clear altered and senescent cells, invading particles, and macromolecular ligands via a multitude of specialized plasma membrane receptors (Moghimi *et al.*, 2001). The rapid uptake of drug carrier systems by MPS especially macrophages *in vivo* was one of the major problems in applying colloid particles as drug carriers. It has been repeatedly emphasized that the physicochemical properties (e.g. particle size, surface properties) of an injected drug delivery system will affect its *in vivo* clearance behaviour and tissue distribution (Moghimi and Davis, 1994, and Douglas *et al.*, 1987)

Effect of particle size and shape Normally, following i.v. injection, large particles (> 200nm) are rapidly cleared by macrophages in liver and spleen, whereas small particles are cleared more slowly and show a greater tendency to accumulation in bone marrow. Frier showed that size of antimony sulfide colloids (200nm to 400nm) was rapidly cleared by liver macrophages and particles with sizes below 10nm were cleared more slowly and accumulated in bone marrow (Frier, 1981)

Effect of surface hydrophobicity/hydrophilicity Colloidal particles after i.v. administration generally adsorb various plasma proteins on the particle's surface. The adsorbed protein entities are able to interact with specific plasma membrane receptors on monocytes and various subsets of tissue macrophages, thus promoting particle recognition by these cells (opsonization process). Cells of the MPS possess membrane receptors for various subclasses of immunoglobulins and complement proteins, like C3 fragments (Moghimi *et al.*, 2001). In order to avoid the MPS uptake of colloidal particles, alteration of particle surface hydrophobicity/hydrophilicity was expected to bring about changes in MPS uptake. Gessner *et al.* found that decreasing surface hydrophobicity leads quantitatively to decreasing amounts of adsorbed proteins and to changes in the obtained protein adsorption patterns (Gessner *et al.*, 2000). This result was also supported by the observation in a new formulation for liposome (Ishida *et al.*, 2001) and ^{131}I-labelled polystyrene particles (Illum *et al.*, 1986a), which have been developed by coating with a hydrophilic polymer (e.g. poloxamer and poly (ethylene glycol)). As expected, these particles showed a significant reduction in particles uptake by the MPS cells, resulting in a reduction of the liver and spleen uptake of the polystyrene NPs from 90 to 46%. Additionally, surface coverage of hydrophilic polymer on the surface of colloidal particles also affects uptake of particles by the MPS. This was supported by the observation that attachment of polystyrene

microparticles to Kupffer cells *in vitro* was obviously decreased with increasing amounts of hydrophilic poly (ethylene oxide), which provides steric stabilisation to these micropheres (Harper *et al.*, 1995).

Effect of surface charge Surface charge also influence the phagocytosis of colloidal particles by the MPS (Douglas *et al.*, 1987). Roser *et al.* found a good correlation between phagocyotosis of albumin NPs and particle zeta potential. The lower the surface charge of particles, the lower the phagocytic activity of U-937, a macrophage cell line. An increase in phagocytic response was observed using particles with a high surface potential especially high positive net charges (Roser *et al.* 1998). It was also observed that cationic lipid loaded solid lipid microparticles were efficiently phagocytosed by phagocytic antigen-presenting cells (Erni *et al.*, 2002). Further studies revealed that cytotoxic effects of cationic solid lipid micropheres were more pronounced in the phagocytic cells. Erni *et al.* deduced that cytotoxic effects of cationic solid lipid resulted from the rapid uptake of these microspheres by phagocytic cells.

1.1.7.3 Physical properties affecting uptake of particles by target cells and intracellular targeting of particles

Nowadays, many authors study factors affecting the cellular uptake of NPs, intracellular trafficking and the sorting mechanism to further explore NPs as efficient delivery vehicles. It is found that particle size, surface charge, and hydrophobicity are important features affecting the amount of internalized particles and intracellular targeting. *In vitro* experiments using brain blood vessel endothelial cells were conducted to gain insight into the quantitation and possible mechanism of NP-mediated transport of drugs into the brain

(Borchard *et al.*, 1994). Borchard had observed the highest and fastest uptake (>300% compared to uncoated controls) after NPs were coated with polysorbate-80. In a further experiment, it was found that polysorbate-80 seemed to act as an anchor for apolipoprotein E, which was absorbed onto the NPs surface. Then particles seem to mimic low density lipoprotein (LDL) particles and could interact with the LDL receptor leading to their uptake by the endothelial cells (Ramge *et al.*, 2000).

Previous groups have shown that the surface charge of the drug carrier is critical for both increasing particle uptake and reaching intracellular targets. By altering the surface charge of particles with different groups, it has been reported that positively-charged particles were taken up by cells to a greater extent than uncharged particles and anionic particles appeared to be largely excluded by cells (Foster *et al.*, 2001). Labhasetwar also found greater uptake by modifying the surface of NPs with cationic agents such as didodecyldimethylammonium bromide (Labhasetwar *et al.*, 1998). These results might be due to a net negative charge on the cell membrane. In addition, by varying surface charge, part of NPs could be potentially directed either to lysosomes or to cytoplasm (Murphy *et al.*, 2000, and Wattiaux *et al.*, 2000). Panyam (Panyam *et al.*, 2002) observed that PLGA NPs can escape from lysosome compartments and could act as intracellular reservoirs for sustained release of the encapsulated drug. By further studies they deduced and confirmed that it is attributed to the pH sensitivity of PLGA, which shows a transition in surface charge from anionic in cytoplasm (pH 7.0) to positively-charged particles within endo-lysosomes (pH 5.0).

1.1.7.4 Visualisation of acidic organelles in intact cells by microscopy

Considerable evidence has accumulated over the past decade that endosome and lysosome compartments can maintain a pH lower than that of the surrounding cytoplasm (Anderson and Orci, 1988). The lysosome is a relatively spherical, single lipoprotein membrane-bound vesicle that contains glycosidases, acid phosphatases, elastase, cathepsins, carboxypeptidases and a variety of other proteases (Brown, 1974). A variety of techniques have been used to label and track lysosome compartments in intact cells. Anderson *et al.* visualised lysosome compartments under electron microscopy by using 3-(2,4-dinitroanilino) -3'-amino-N-methyldipropylamine (DAMP) (Anderson and Orci, 1988). DAMP is a basic congener of dinitrophenol that readily diffuses into intact cells. Its primary and tertiary amino groups allow it to be concentrated in acidic organelles, in which amino groups become protonated and positively charged at lower pH. The primary amino group also allows the DAMP molecule to become covalently linked to proteins which allows acidic compartments to be visualised in the electron microscope after fixation and reaction with appropriately tagged anti-dinitrophenol antibodies. Lysosome compartments also can be visualised under fluorescence microscopy by using LysoTracker probes. LysoTracker probes, which comprise a fluorophore linked to a weak base that is only partially protonated at neutral pH, are freely permeant to cell membranes and typically concentrated in spherical acidic organelles. Thus LysoTracker probes, which are colourless at physiological pH, show fluorescent colour at the acidic pH present in lysosome compartments (Panyam *et al.*, 2002, and manufacture's instruction, invitrogen, UK). Recent work has demonstrated that several LysoTracker probes have been widely used, such as LysoTracker Red, which had red

fluorescence at acidic compartment, LysoTracker Yellow, LysoTracker Green, and so on. LysoTracker probes have been used to study intracellular localisation of NPs. To confirm that PLGA NPs were sorted into lysosome compartments, human arterial smooth muscle cells were incubated with cell culture medium containing 6-coumarin loaded PLGA NPs, which has green fluorescence, and LysoTracker Red for 30 mins (Panyam *et al.*, 2002). Confocal fluorescence micrographs demonstrated that NPs were co-localized with LysoTracker in the lysosomal compartment, as evident from the appearance of red/green to yellow fluorescence.

1.2 THE ROLE OF CULTURE DIMENSION ON CELL BIOLOGY

1.2.1 Function of neurons and supporting cells

The nervous system, no matter how complicated in shape and structure, is made up of two types of cells: the neuronal cell with its processes and conducting axon and glial cells (Peters, 1976, and Pannese, 1994).

Neurons are the functional unit of the nervous system for transmitting signals through the body. They regulate the contraction of muscles and secretion of hormones. Neurons consist of the cell body (soma), dendrites, and axon. Dendrites are short extensions of the cell body. They receive impulses from another neuron or sensory receptors, and transmit it to the cell body. The axon, a thin tube that can be up to 3 feet long, takes impulses away from the cell body. In vertebrates most neurons are provided with several dendrites, but only one axon.

In the mammalian central nervous system glial cells are far more numerous

than the neurons. The glial cells can be divided into two major classes, the macroglia (astrocytes, oligodendrocytes and ependymal cells) and microglia, which act as phagocytes. Glial cells are generally small cells and do not participate in the active generation of signals (impulses), nor do they have a direct role to play in the information processing functions of the nervous system. Some, however, are influenced by neuronal activity and help regulate the ionic environment of the neurons and also remove some transmitters released by neurons. A number of functions for glia are known or suggested. These include: 1) Structural support for the neurons of the central nervous system, that is, to act in the same way as connective tissue in other parts of the body; 2) Phagocytosis of dead cells and debris after nervous system injury. Microglial cells, whose sites of origin are regarded as the pial adventitia of the large and medium-sized blood vessels, display moderate phagocytic activity, eliminating debris resulting from neuronal or glial degeneration; 3) Ionic regulation and neurotransmitter removal, for example, astrocytes; 4) A role in development for guiding growing neurons along appropriate paths; 5) The formation of an insulating cover, the myelin sheath, around certain axons in the central nervous system (e.g. oligodendrocytes).

1.2.2 Morphology of neurons and supporting cells

Neural Cells

Typically, neurons (Fig. 1.4) have a large, round nucleus located in the centre of the cell body. In small neurons the nucleus occupies most of the cell body with only a thin husk of cytoplasm surrounding it. In larger neurons it floats free in the cytoplasm, circumscribed by a thin nuclear membrane and often separated from the other organelles by a distinct clear

halo. The karyoplasm of neurons is distinguished by its lack of chromatin particles and its typically clear vesicular appearance. In large and medium-sized neurons, the chromatin is widely and homogeneously dispersed so that the nucleus appears as a pale vesicle under the light microscope even after staining with basic dyes. In the largest neurons, their nucleus can contain a few deeply stained, irregular bodies. In many small neurons (e.g. granule cells in the cerebellar cortex), the chromatin is instead condensed into clumps which stain deeply with basic dyes. It appears as speckled as that of any plasma cell or lymphocytes. In all types of neurons, except the smaller granule cells, the nucleus is marked by a conspicuous, large, spherical nucleolus. According to measurements by Marinesco (1909) in a variety of nerve cell types in several mammalian species, the diameter of nucleolus, 3 to 7 microns, can be one-third to one-fourth that of the nucleus. It is common to find clear round vacuoles or open spots in the otherwise dense and deeply stained nucleolus. Thus, in electron micrographs the nucleolus of a neuron appears as an extremely dense, large, roughly spherical mass clearly demarcated from the rest of the karyoplasm. Apart from prominent characteristics of the nucleus, Nissl bodies and neurofilaments are unique to neurons. Under the electron microscope, each Nissl body appears to consist of a number of cisternae whose membranes are studded with polysomes and free polysomes occurring in the cytoplasm. Neurofilaments appear to lie in the spaces between much more prominent and much more electron dense organelles (e.g. Nissl bodies, mitochondria, Golgi complexes), and occur individually scattered or loosely aggregated into small bundles (Peters, 1976, and Pannese, 1994).

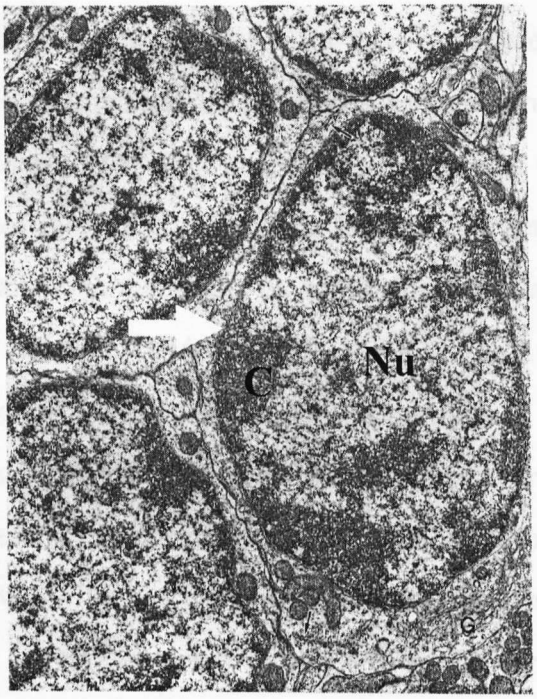

Fig. 1.4 Electron micrographs of neurons: The nucleus (Nu), which occupies most of the cell body, displays clumps of chromatin (C), some of which lie adjacent to the nuclear envelope (arrow). Rat cerebellar cortex, x2000 (Pannse, 1994)

Glial cells

Macroglial cells, like neurons, are of ectodermal origin, but they differ from neurons in having only one type of process. They don't form synapses, and they retain the ability to divide throughout life, particularly under the influence of damage to the nervous system. In contrast, microglia are of mesodermal origin and enter the brain either in the neonatal period or as reticuloendothelial cells via the blood crossing the capillary endothelium in the case of brain trauma injure.

Astrocytes

Astrocytes (Fig. 1.5I) can be of two types, fibrous astrocytes and

protoplasmic astrocytes, based on their morphology and location. Fibrous astrocytes lie in white matter. In electron micrographs, the nuclei of fibrous astrocytes are often bean-shaped or irregular and the nuclear envelope may be thrown into deep folds. The karyoplasm generally has a fairly even density, although there may be some clumping immediately adjacent to the nuclear envelope, and occasionally a nucleolus is present. The most prominent cytoplasmic component of the fibrous astrocyte is the numerous fibrils or filaments that occur throughout the perikaryon and extend as parallel arrays into the processes. Proplasmic astrocytes occur in grey matter, and as with fibrous astrocytes, their most characteristic feature is the presence of cytoplasmic fibrils. There are fewer fibrils, however, than in fibrous astrocytes. They don't fill the cytoplasm but tend to occur in bundles. The nuclei of protoplasmic astrocytes tend to be round or oval but are less frequently indented than of those of fibrous astrocytes. The karyoplasm shows a fairly even, low density similar to that of fibrous astrocytes and most of the cytoplasmic organelles and inclusions show the same characteristics as their counterparts in fibrous astrocytes (Peters, 1976, and Pannese, 1994).

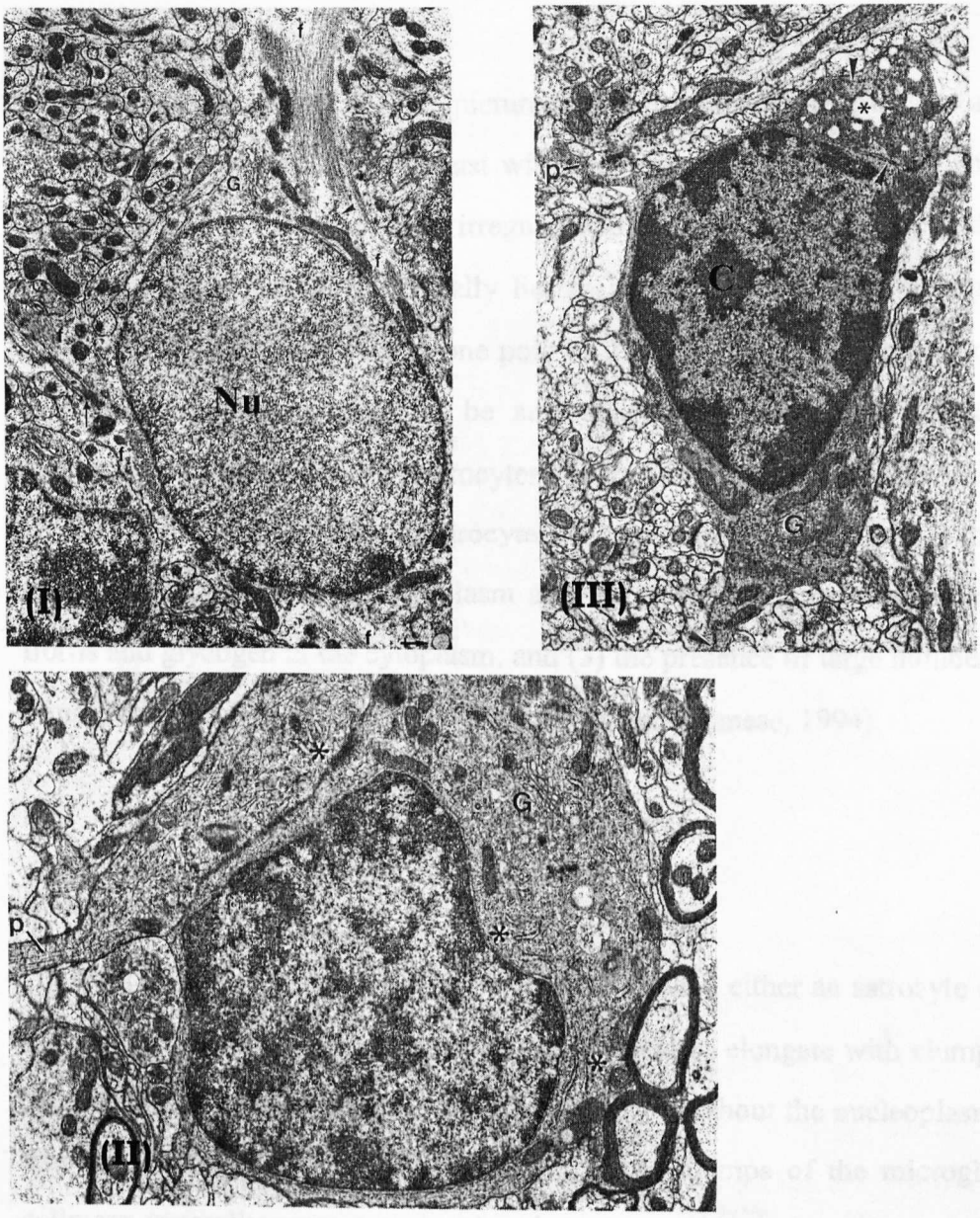

Fig. 1.5 Electron micrographs of macroglial and microglial cells (I) **Fibrous astrocyte**: The karyoplasm exhibits a fairly even, low density except for the thin, condensed rim adjacent to the nuclear envelope. Rat cerebellar cortex, x9500; (II) **Oligodendrocytes:** Dense clumps of chromatin (C) are prominent in the nucleus (Nu) and the cytoplasm is much denser than that of astrocyte. Rat spinal cord, x3100; (III) **Microglia:** The cell outline is irregular and smaller than astrocytes and oligodendrocytes. The chromatin clumps are more prominent and occupy a larger proportion of nuclear volume compared with that of oligodendrocytes. Rat cerebellar cortex, x13500. G=Golgi complex; P=cell process; f=bundles of intermediate filaments; *= granular endoplasmic reticulum (Pannese, 1994)

Oligodendrocytes

Oligodendrocytes (Fig. 1.5II) are pictured under the electron microscope as moderately dense cells that contrast with the rather lucent astrocytes. The nucleus can be round, overall, or irregular and the nuclear chromatin tends to clump. Since the nucleus usually lies in an eccentric position, a large mass of cytoplasm can occur at one pole of the cell, but in most planes of section the nucleus appears to be surrounded by only a thin rim of cytoplasm. Compared with astrocytes, there are certain features that consistently distinguish oligodendrocytes from astrocytes. These are (1) the greater density of both the cytoplasm and the nucleus, (2) the absence of fibrils and glycogen in the cytoplasm, and (3) the presence of large numbers of microtubules in the processes (Peters, 1976, and Pannese, 1994).

Microglia

A microglia cell (Fig. 1.5III) is generally smaller than either an astrocyte or an oligodendrocyte, and its nucleus is usually oval or elongate with clumps of chromatin beneath the nuclear envelope and throughout the nucleoplasm. Compared with oligodendrocytes, the chromatin clumps of the microglia cells are generally more prominent and occupy a larger proportion of the nuclear volume. Hence, the cell often has a darker nucleus than the oligodendrocyte when examined in light microscope preparations stained with basic dyes. The cytoplasm of the microglia cell forms a thin rim around the nucleus, but often extends out in quite broad processes. The cytoplasm of microglia is denser than that of astrocytes, and parallels that of the oligodendrocytes. There are fewer microtubules and none of the glycogen granules and bundle filaments in cytoplasm of microglia (Peters, 1976, and Pannese, 1994).

1.2.3 The effect of culture dimension, 2 or 3 dimensional culture, on cell morphology and cell function

More and more researchers are recognizing the influence of cell culture dimension, two dimensional (2-D) or three dimensional (3-D) culture, on cell growth (Folkman *et al.*, 1975), differentiation, apoptosis (Chen *et al.*, 1997), motility (Ingber *et al.*, 1994), signal transduction (Ishii *et al.*, 2001), gene expression (Folkman *et al.*, 1975), and extracellular matrix (ECM) remodelling. Currently, 3-D culture techniques are being employed because this culture method offers researchers a means to study cell biology under conditions that emulate an *in vivo* environment, which reflects cell-cell and cell-ECM interaction. These interactions might be severely constrained or precluded entirely in 2-D cultures.

More recently, accumulated evidence in the literature has suggested that mechanical tension generated through molecular interactions within the cell is critical for control of cell form and function (Berthiaume *et al.*, 1996, and Chicurel *et al.*, 1998). Tensional forces generated within contractile microfilaments pull inward on the surface membrane and the cell's internal components. These inward-directed forces are resisted by external adhesion to the ECM and to other cells, by internal molecular struts within the cytoskeleton itself and by the surface membrane when stiffened by osmotic pressure. Importantly, the same tensional forces that are balanced by ECM and cytoskeletal struts are also transmitted to the cell nucleus (Chicurel *et al.*, 1998). Tensional forces can be increased by stretching flexible culture substrates (Smith *et al.*, 1997). These forces across integrins are also dependent on matrix rigidity and on its biochemical composition (Choquet *et al.*, 1997). Organotypic slices or spheroids, in which cells are cultured in 3-D natural and synthetic fibre scaffolding, are generally used to form 3-D

matrices. Thus, the tension of cells can be more easily extrapolated to that within the organism *in vivo* by using 3-D matrices than using flat, rigid, monolayer culture.

Effect of culture dimension on cell shape regulation

When cells are plated on coverslips of plastic or glass, single cells exhibit a flattened morphology resulting in a 2-D cell population. By contrast when cells are cultured in 3-D collagen/tissue-derived or cell-derived matrix, each single rounded shape cell is inclined to form spheroids, which leads to a 3-D cell population. Cell control of its shape and structure lies in the balance of forces between external ECM adhesion and internal cytoskeletal struts and cables (Chicurel *et al.*, 1998). If the stiffness of the ECM substrate is greater than that of cell's cytoskeleton, the cell pulls against its ECM adhesions and then the entire cell and nucleus appears flattened or spread. Cell-cell and cell-ECM interactions occur through binding of adhesion molecules (e.g. integrins, selectins) to counter receptors expressed at the surface of cells or by the ECM. In cell-ECM matrix studies (Cukierman *et al.*, 2001, and Yamada *et al.*, 2003), it was reported that the both the focal adhesions and the fibrillar adhesions of fibroblast cells in a 3-D environment are different from that in a 2-D environment. Although 3-D matrices have many of the same plaque proteins as found in focal adhesion, such as paxillin, vinculin and focal adhesion kinase, they lack the $\alpha_v\beta_3$ integrin. Therefore, when comparing cell shapes of fibroblast in 2-D and 3-D environments, cells on 2-D substrates tend to spread onto the substrate in a flattened morphology, whereas cells in 3-D substrates rapidly assume an elongated morphology that tends to mimic shapes of fibroblastic and mesenchymal cells *in vivo*.

Effect of culture dimension on signalling transduction and gene expression

Changes in cell shape and tension force of cells are important because they can cause cells to switch between different genetic programs and have different signalling processes. Differences in signalling transduction and gene expression have been reported in cells suspended in 3-D collagen gels compared with 2-D collagen-coated plastic plates. It was found that the number of ribosomes and mitochondria was less and synthesis of DNA and proteins were decreased in 3-D cultures when compared to 2-D cultures (Ishii *et al.*, 2001). Changing cell shape from flat to round also can shut off growth and turn on differentiation in capillary endothelial cells (Chen *et al.*, 1997) and hepatocytes (Singhvi *et al.*, 1994).

Effect of geometric control on cell life and death

Cell shape was also found to be a critical determinant that switches cells between growth and death and between proliferation and quiescence, regardless of the type of matrix protein or antibody to integrin used to mediate adhesion (Chen *et al.*, 1997). Capillary endothelial cells were cultured on micropatterned substrates that contained ECM-coated adhesive islands of various sizes and shapes. Apoptosis was switched on when cell spreading was restricted by plating on the smallest islands (10μm in diameter). By contrast apoptosis progressively declined when the island size was increased from 20 to 40μm in diameter and at the same time DNA synthesis was concomitantly switched on as cell and nuclear spreading were promoted. After growing the same single cells on multiple, closely spaced adhesive islands of either 3 to 5 μm in diameter to approximate the size of individual focal adhesions, it was found that cell spreading instead of its local ECM contact controlled whether cells would grow or die.

1.2.4 *In vitro* 3-D neuron cell culture models

There have been five methods most commonly employed to produce 3-D brain cell cultures: (1) Organotypic slice cultures: tissue slices are prepared from embryonic or neonatal tissue derived from various species brain and grown on a substrate in media. Organotypic cultures preserve the basic structural and connective organization of their tissue of origin, maintain a high degree of neuronal differentiation, and demonstrate functional synaptic connections (Gähwiler, 1988, and Gähwiler *et al.*, 1997); (2) single cells from a cell line or dissociated from foetal brain dispersed in a rotating vessel or microgravity bioreactors that adhere to one another and eventually form tissue- or organ-like structures (Moscona, 1961, Chatterjee *et al.*, 1994, and Searle, 2004). Numerous morphological and biochemical investigations demonstrated that these 3-D spherical aggregates attain a similar cellular differentiation and maturation to that observed in the tissue *in vivo* (Garber and Moscona, 1972, and Honegger *et al.*, 1979); (3) gel based cell culture: single cells are dispersed in a substrate, such as collagen, or agarose. Gel matrix mimicking ECM can provide a structural support to the cells (O'Connor, 2000, and Ma *et al.*, 2004). 3-D gel matrices provide some degree of structural support, as well as permeability to allow nutrient and waste transport, however, *in vivo*, cells are exposed to complex environments instead of a pure collagen or agarose matrix; (4) stationary or rotating microcarrier cultures: dissociated cells aggregate and adhere around porous circular or cylindrical substrates (Edelman and Keefer, 2005); (5) micromass cultures: small volumes of high concentration cell suspension are cultured in a plastic Petri dish for 2h to form 6-7mm cell islands and cell pellets are then cultured in fresh cell culture medium containing appropriate amounts of nutrients and differentiation factors (Flint, 1983).

1.2.5 3-D neuronal cultures exhibit a more realistic view of the nervous system *ex vivo*

Cumulative evidence has shown that culture environment influences have profound effects on cell structural and functional properties, such as neoplastic properties of tumour cells. Such effects may determine the pharmacological responses of cancer cells to therapeutic drugs (Bjorge *et al.*, 1996). Thus development of 3-D cell culture in neuroscience will have a tremendous effect on the way researchers view cell behaviour *ex vivo*. Many researchers have demonstrated that 3-D neuronal cultures exhibit realistic structural and functional properties.

Recent advances in the literature show that neural progenitor cells, which are isolated from the embryonic or adult central nervous system, can be expanded and differentiate into neurons and glial phenotypes in 3-D collagen gels (O'Connor *et al.*, 2000, O'Shaughnessy *et al.*, 2003, and Ma *et al.*, 2004). In such studies, neuroepithelial cells were isolated from embryonic day 13 (E13) rat cortex and dispersed within type I collagen. Collagen-entrapped neural precursor cells can differentiate into neuron cells, astrocytes, and oligodendrocytes cells and differentiated neurons form synapses and functional neuronal circuits and networks. Immunocytochemistry revealed that neurons were the first cells to differentiate cells as a few neuronal marker- positive cells were detected on the second day. Astrocytes and oligodendrocytes didn't appear until after 10 days in culture. At day 5, most of the cells exhibited cytoplasmic Ca^{2+} oscillations in response to ATP or carbachol, but did not express neurontransmitters (γ-amino butyric acid (GABA) or glutamate). In contrast, about 60% of cells at day 14 responded to both GABA and glutamate. These GABA- and glutamate-responsive cells were neuron-like in morphology.

These data show a developmental progression in 3-D collagen culture.

3-D cell culture *in vitro* can maintain a certain cell density, which is close to the situation *in vivo*. *In vivo* neurons maintain a high density, for example, in human cortex, there are approximately 10^5 neurons per mm^3 and each cell may synapse with 1000 or more distant neurons (Kandel *et al.*, 1991). Conventional cells in 2-D culture systems may not support such high cell density. It was observed that cells in 2-D cell culture are typically grown at low density to promote visibility and each neuron may synapse several hundred times with adjacent neurons. In contrast when cells dispersed in 3-D natural or synthesized matrix, such as collagen gel, the 3-D scaffold can provide a porous matrix with the specific adhesive properties for attachment of neuron cells and process elaboration, and allow nutrient and waste transport. This might eventually yield high-density cell culture (Edelman *et al.*, 2005).

Neurons *in vivo* are surrounded by a network of glial cells, which play many roles, for instance support for neurons to form a functional organ, neuronal nourishment, neurotransmitter uptake and recycling, and axon myelination (Peters, 1976, and Pannese, 1994). Therefore an appropriate ratio of neurons to glial cells resembling *in vivo* conditions should also be considered. Undifferentiated E-18 fetal rat brain neurons are capable of expressing neurofilament (NF) and glials can express glial fibrillary acidic protein (GFAP) (Raju *et al.*, 1981). In 2-D and 3-D cell culture, Searle identified GFAP and NF to determine cellular composition of rat (E18) cerebellum, brainstem, and cerebral cortex by using immunohistochemical analysis (Searle, 2004). It was found that immunoreactivity of glial cells in all brain regions is about 10 times higher than that of neurons in 2-D cell culture. This indicated that monolayer culture favoured the survival and proliferation of glial cells to a much greater extent than neuronal cells and

can't reflect the cellular composition *in vivo*. In contrast, 3-D spheroid culture microenvironment favoured neuronal cell survival and proliferation, which is close to the cellular composition of brain tissue and thus indicated that 3-D cell culture is more representative of *in vivo* condition.

1.2.6 *In vitro* brain tumour invasion model

Brain tumours represent a devastating malignant disease, causing extreme and progressive disability leading to death (Souhami and Tobias, 1998). It is now the most common cause of cancer-related death in children, affecting 3.3 per 100 000 children (Leger *et al.*, 1999). Malignant brain tumours in children under 15-years old account for 23% of brain tumours (Pilkington, 1994). Studying histological sections of human brain tumours can provide little information about the mechanisms underlying local invasion therefore numerous laboratory *in vivo* and *in vitro* models have been developed for the study of brain tumour invasion mechanisms (Engebraaten *et al.*, 1990, and Pilkington *et al.*, 1997). *In vivo* models of brain tumour invasion in laboratory animals have been developed by transplanted tumour or chemically induced primary tumour. However these models are less ideal because they have several disadvantages. For example, transplantable gliomas in rat have shown high metastatic ability (Andersson *et at.*, 1991), whereas intrinsic brain tumours in humans rarely metastasise (Zeltzer *et al.*, 1999).

Due to the limitation of *in vivo* models of brain tumour invasion, a variety of *in vitro* models for study of both cell invasion and migration have been developed, since the invasion behaviour of malignant brain tumours such as medulloblastoma is determined by various factors: receptor mediated

cell-ECM contacts, host-tumour cell interactions and cellular locomotion. The four types of 3-D models most commonly employed to study both tumour cell migration and invasion *in vitro* are: (1) 3-D re-aggregated foetal brain formed as a target invaded by both human and experimental animal brain tumour single cell (Searle, 2004); (2) spherical aggregates of foetal brain cells invaded by tumour aggregates (Terzis *et al.*, 1994, Pilkington, 1997, and Penar *et al.*, 1998). The preparation of tumour material can be multi-cellular spherical aggregates derived from permanent cell lines (Terzis *et al.*, 1994) or biopsy tissue direct from surgery (Engebraaten *et al.*, 1990). (3) single tumour cell invading organotypic brain slices (de Bouard *et al.*, 2002). Organotypic co-culture model was developed by injection of one rodent glioblastoma multiforme cell line into organotypic brain slices; (4) spherical aggregates of tumour cells invading organotypic brain slices (Jung *et al.*, 2002, and Yoshida *et al.*, 2002). Tumour aggregates also were implanted into organotypic slices for development of an organotypic co-culture model.

Ideally, an *in vitro* model of tumour invasion should include a 3-D substrate for tumour that resembles *in situ* brain tissue. Although 3-D spherical aggregates of brain maintain cellular structure and function, the cellular organization of 3-D aggregates can't represent the characteristic properties of brain tissue *in situ*. In contrast, organotypic culture methods not only maintain cellular structure and function, but also provide the original cytoarchitecture that mimic *in situ* brain tissue condition if great care is taken in preparation of the organotypic slices (Gähwiler, 1988). Compared with single tumour cells, tumour spherical aggregates reflect several characteristics of microtumours *in vivo* including diffusion gradients of nutrients and partial pressure of oxygen (Santini and Rainaldi, 1999).

1.3 *IN VITRO* CELL CULTURE MODEL FOR EVALUATING LOCALISATION AND UPTAKE OF NANOPARTICLES

As successful drug delivery systems, drug carriers, such as NPs, should not only safely deliver therapeutic agents to target cells and improve cellular uptake of therapeutic agents, but might also modify their subcellular localisation. 2-D monolayer cell culture models have been widely used with a variety of cell types to investigate intracellular localisation of drug delivery systems, intracellular uptake and retention extent of drug carrier within target cells. Generally, the colloidal and macromolecular carriers are taken up into cells via endocytosis/phagocytosis. Once they are internalized, they will be sorted into endosomal compartments, cytoplasmic, mitochondrial or nuclear based on the surface properties of NPs (Moghimi and Rajabi-Siahboomi, 2000). For intracellular localisation study, NPs are usually labelled with fluorescent dyes, such as fluorescein, rhodamine, or 6-coumarin, and loaded with an electron microscopic marker (e.g. osmium tetroxide or ferritin). LysoTracker (Panyam *et al.*, 2002) and Mitotrackers (Zorov *et al.*, 2004) are used to stain lysosome and mitochondrial compartments respectively. Therefore subcellular localisation of NPs can be visualised by using confocal fluorescence microscopy (McClean *et al*, 1998), transmission electron microscopy (TEM) (Panyam *et al.*, 2003a), or timelapse video microscope (Panyam, 2003b). For intracellular uptake of NP, extent of NP taken up is commonly quantified by flow cytometry, and drug concentration can be measured by HPLC after cells are lysed with 0.05% (wt/vol) Triton X-100 solution (Chawla and Amiji, 2003).

Although the literature indicates that the microenvironment surrounding cells plays an important role in cell growth, differentiation and cellular

function, the use of 3-D cell culture models is scarce in the drug delivery area. Multicellular tumour spheroids were first used to compare antiproliferative effects of free and liposome-encapsulated retinoic acid (Sacks *et al.*, 1992). The difference in antiproliferative effects between retinoic acid and retinoic acid loaded liposome were observed in 2-D monolayer culture versus 3-D spherical aggregates. Retinoic acid and retinoic acid loaded liposome produced similar growth inhibition in 2-D monolayer culture while liposome-encapsulated retinoic acid had an increased effectiveness in 3-D aggregates compared with free retinoic acid. The penetration of different liposomal formulations into prostate carcinoma spheroids was also examined (Kostarelos *et al.*, 2004). This study indicated the surface charge of the liposome has an impact on penetration into tumour spherical aggregates and a delicate balance exists between the strong affinity of delivery systems for the tumour cells and the efficient penetration and distribution within the tumour mass.

Uptake and diffusion of NPs was also examined in *in situ* spleen tissue (Demoy *et al.*, 1999) and brain tissue (Schroeder *et al.*, 1999). In these two studies, tissues were cut into 400μm thick slices after they were removed from rats/mice and then immediately incubated in culture medium containing fluorescent dye labelled NPs. *In vitro* spleen uptake demonstrated that the localisation of NPs in the marginal zone of the spleen was similar to the observations made on spleen frozen sections of intravenously injected mice. It also suggested that information on uptake of NPs by marginal zone macrophages will be lost in 2-D monolayer cells culture because those macrophages are largely lost when preparing classical spleen cell suspensions. Diffusion of NPs in brain tissue block indicated that cell culture dimension have different influence on diffusion of ^{14}C-orotic acid and ^{14}C-orotic acid loaded NPs. It was found that the diffusion of ^{14}C-orotic acid was significantly enhanced in hippocampal slice

preparations after it was loaded into NPs. This significant enhancement of diffusion processes by NPs may be important for drug transport to the neuronal targets after crossing the BBB and can facilitate the pharmacokinetics and pharmacodynamics of drugs.

1.4 POLY (GLYCEROL-ADIPATE) POLYMER

PLGA and PLA are the most widely used polymers in drug delivery systems, but drug incorporation of PLGA and PGA NPs is generally quite low, which leads to large drug wastage during NP preparation and to encapsulating insufficient drug for therapeutic efficacy (Leo *et al.*, 2004, and Govender *et al.*, 1999). Another disadvantage of PLGA and PLA is that an initial high release of drug can be observed in most drugs loaded NPs, which results in a drug concentration near or above the toxic level before it is delivered to the desired site (Shively *et al.*, 1995 and Jeong *et al.*, 2000). With these limitations of PLGA/PLA, we developed a novel biodegradable polymer, poly (glycerol – adipate) (PGA) (Kallinteri *et al.*, 2005). PGA is made with the intention to have a relatively higher drug loading and sustained release of the encapsulated therapeutic agent over a longer period than other polymers currently in use. It has hydrolysable ester bonds in its backbone and side chain. Varied hydrophobic/hydrophilic properties of PGA polymer were achieved by polymer backbone acylated by aliphatic groups (C_8 or C_{18}) of hydroxyl groups with proportion of 40%, 80%, 100%. A scheme of synthesis and structure of PGA are shown in Fig. 1.6. Polymers will be referred to throughout the thesis as X%Cy(Z), where X% is the percentage of acylation, y is the acyl chain length and Z is the average molecular weight of polymer backbone in kDa.

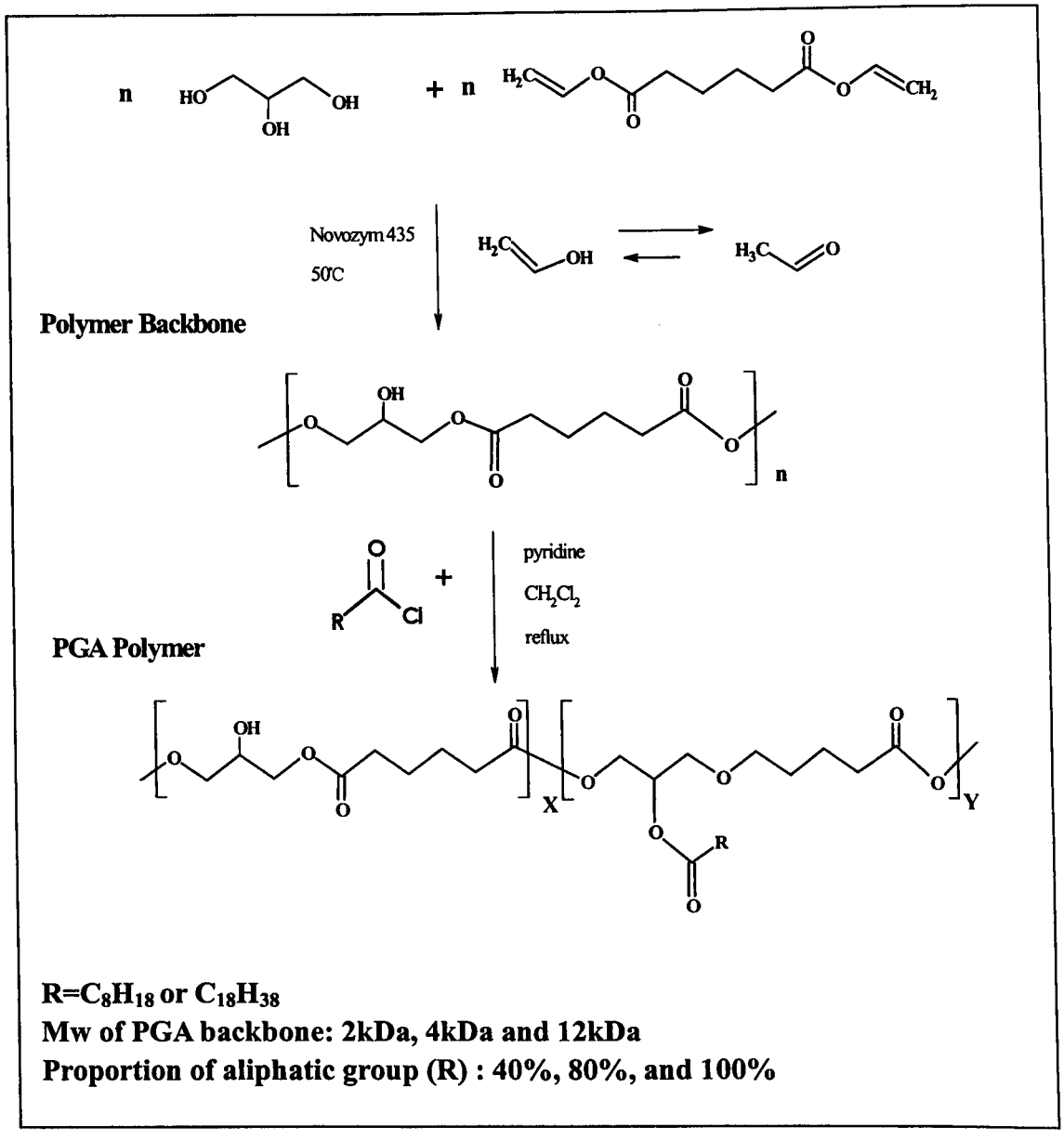

Fig. 1.6 Scheme of synthesis and structure of Poly (glycerol-adipate) polymer used in current work

1.5 AIMS OF THIS PROJECT

The project aim was to investigate uptake, metabolism, and penetration of biodegradable PGA NPs in 2-D and 3-D *in vitro* model systems in order to understand interactions between PGA NPs and normal brain cells and brain tumour cells.

1. *Screen out the suitable PGA polymer and fluorescent dye labelling NPs*: Assess the effect of aliphatic side group, molecular weight of polymer backbone, and hydrophobic/hydrophilic property of fluorescent dye on NP basic physicochemical properties, such as particle size, zeta potential, drug loading and drug entrapment.

2. *Investigate uptake, metabolism and penetration of fluorescent dye labelled NPs in 2-D and 3-D cell culture model systems:* It was expected that penetration of NPs into 3-D cultures may be slow or limited due to their size and rate of diffusion.

3. *Uptake of fluorescent dye labelled NPs in 3-D brain tumour invasion model: co-culture of organotypic brain slice and brain tumour spherical aggregate:* It has been suggested that tumour cells may have higher rates of endocytic activity characteristic than normal cells (Busch *et al.*, 1961, Ghose *et al.*, 1962, and Mego and McQueen, 1965). A tumour invasion model may thus allow *in vitro* evaluation of some aspects of the anticancer therapeutic potential of NPs.

CHAPTER 2

MATERIALS AND METHODS

2.1 MATERIALS

2.1.1 Reagents and buffers

Unless specifically stated, all chemicals used were purchased from Sigma-Aldrich (Poole, UK), water used in investigations was obtained from an ELGA purification system (resistivity 15 MΩcm, Maxima USF ELGA, High Wycombe, UK), while water used in cell culture was of tissue culture grade. Unless specifically mentioned, all fluorescent dyes were purchased from Molecular Probes (Invitrogen, UK). All the reagents used for TEM were from Agar Scientific Ltd. (Essex, UK). All cell culture reagents used were obtained from Invitrogen Life Techonogies Ltd. (Paisley, UK).

N-(2-hydroxyethyl) piperazine-*N'*-(2-ethanesulphonic acid) (HEPES) buffer, adjusted to pH 7.4 with sodium hydroxide, was prepared to the required strength with water. 2-Amino-2-(hydroxymethyl)-1,3-propanediol, hydrochloride (Tri-HCl) was adjusted to pH 7.6 with 1N hydrochloric acid. Paraformaldehyde (PFA) (BHL laboratory Supplies, UK) solution used for biological study was prepared in water at 60°C including 3-4 drops of 5M sodium hydroxide. Poly-D-Lysine (PDL) for biological study was prepared to the required strength with water. 4', 6-diamidino-2-phenylindole, dilactate (DAPI) was dissolved in water to make a 5mg/ml stock solution, which was aliquoted to final working concentration and stored at <= 20°C

for long-term storage and at 2-6°C for short-term storage. LysoTracker Yellow-HCK-123, provided as 1mM stock solution, was prepared by diluting the probe stock solution to concentration at 50nM with HEPES buffer (0.01M, pH 7.4). 3% w/v phosphotungstic acid was adjusted to pH 4.7 with potassium hydroxide.

2.1.2 Polymer and particles

Poly (glycerol-adipate) (PGA) polymer was provided by Dr. G. A. Hutcheon and Dr. S. Higgins, Liverpool John Moores University, U.K as parts of BBSRC grant No 42A/13897 and 42E/19350. The scheme of synthesis and structure of PGA are shown in Fig. 1.6 and more details can be found in the previous published paper (Kallinteri *et al.*, 2005).

P (S/6 % DVB/V-COOH) Mag Microspheres (FITC-labelled magnetic microsphere) was obtained from Bangs Laboratories (Bangs Laboratories, Inc., IN, USA)

Amine-modified polystyrene latex beads (fluorescence red, 0.1μm) were purchased from Sigma-Aldrich (Poole, UK).

2.1.3 Drugs and fluorescent dyes

Dexamethasone Phosphate (DXM-P), Dexamethasone Fluorescein (DXM-FL), Rhodamine B (RB), and Rhodamine B Isothiocyanate (RBITC) were purchased from Sigma-Aldrich (Poole, UK). They were prepared as stock solutions and stored in the fridge: DXM-P was dissolved in water to a final working concentration of 4mg/ml, DXM-FL in HEPES buffer (0.01M, pH7.4) to a final working concentration of 2mg/ml, and RB and RBITC in methanol to final working concentrations of 2mg/ml. Structures of dyes and drugs are given in Fig. 2.1.

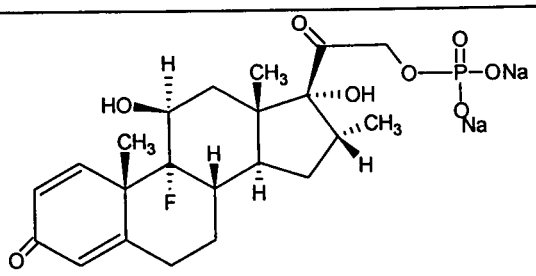

Dexamethasone Phosphate (DXM-P)

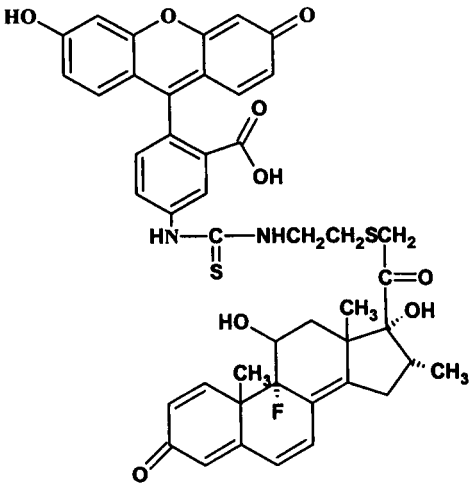

Dexamethasone Fluorescein (DXM-FL)

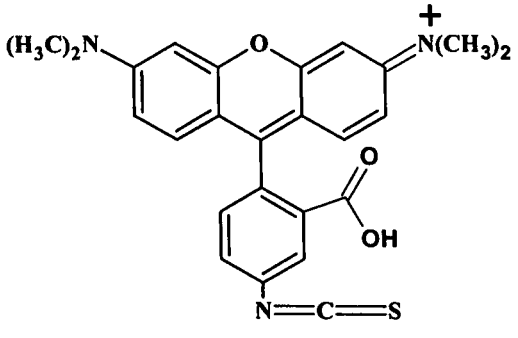

Rodamine B Isothiocyanate (RBITC)

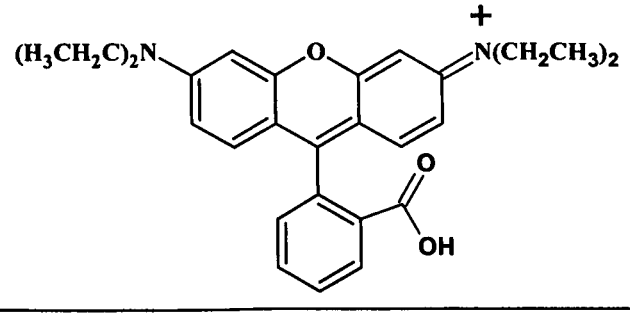

Rodamine B (RB)

Fig. 2.1 Structures of drugs and fluorescence used in current work

2.2 METHODS

2.2.1 Physicochemical characterisation

2.2.1.1 Preparation of drug-free, drug loaded, and fluorescently labelled PGA NPs

PGA polymer was dissolved in acetone at a final concentration of 10 mg/ml. The organic phase including PGA polymer (2ml, 10mg/ml) was added dropwise into aqueous phase with/without drug/ fluorescent dye under magnetic stirring: 1) DXM-P loaded NPs: organic phase was added into water containing DXM-P (1ml, 4mg/ml); 2) fluorescently labelled NPs: PGA was added dropwise into HEPES buffer (7ml, pH7.4, 0.01M) including DXM-FL or RB (1ml, 2mg/ml). RBITC labelled NPs were prepared using the same method as other fluorescent dyes except that RBITC (1ml, 2mg/ml) was dissolved in acetone. The solution was left stirring in a fume hood overnight at room temperature to evaporate acetone.

2.2.1.2 Separation of unincorporated drug/fluorescent dye from drug-loaded or fluorescently labelled NPs

Gel permeation chromatography (GPC) was used for particle clean-up. Sample (4-6ml) was passed through a glass chromatography column (C2.5/40, Pharmacia, bed volume 147ml) packed with Sepharose CL-4B gel (Pharmacia). A peristaltic pump was used to maintain the flow of eluent at 1ml/min, through the column. Fractions, 2ml per tube, were collected by a fraction collector (Pharmacia). Water was the eluent used for all of the

drug-loaded NPs and HEPES (0.01M, pH7.4) was the eluent used for all of the fluorescently labelled NPs.

2.2.1.3 Determination of particle size

Principle of photon correlation spectroscopy

Photon Correlation Spectroscopy (PCS) was used to determine particle size and also gave information on polydispersity of particles. The basic principle of PCS is that a laser beam is passed through a suspension of particles and is scattered by the Brownian motion of particles. The intensity of the scattered light fluctuates with time. Smaller, faster moving particles cause more rapid fluctuations in intensity than larger ones. The fluctuations are assessed by a computer system in a time dependent manner to determine the diffusion coefficient of the particle. The mean particle radius is obtained from the Stokes-Einstein equation.

Method of determination of particle size

Measurements were carried out using PCS (Malvern Instruments Ltd, Malvern, UK), with vertically polarized light supplied by an argon-ion laser (Cyonics). The analysis mode was CONTIN. Samples of the particle suspension were diluted with ultrapure water in a cylindrical glass cell to an appropriate concentration to give 500-600 kcps. The water used for dilution was freshly filtered through a 0.2 μm filter (Sartorius AG, Germany). The sample cell was held in a thermostatically controlled water bath maintained at 25±0.1℃. The laser beam was passed through the sample and the scattered light detected at an angle of 90° by a photomultiplier. The signal was passed to a Malvern 64-channel multibit autocorrelator type K7025 via

an amplifier/discriminator. The autocorrelator was interfaced with a computer system for data analysis. The particle size of each sample was expressed as the mean particle hydrodynamic diameter ± standard deviation of 30 readings.

2.2.1.4 Measurement of particle surface charge

Principle of measurement of particle surface charge

The particle surface charge was measured by Laser Doppler Anemometry (LDA). The principle of measurement of zeta potential is that the particle surface charge influences its velocity in an electrical field. When two laser beams form a crossover through a cell containing a suspension of particles, beams produce interference fringes. The particles interact with these fringes to scatter the light, which oscillation is determined by the particle velocity. The scattered light is detected by a photomultiplier. Then the velocity of the particle is analyzed by a computer.

Method of determination of particle surface charge

Measurements were performed using a Malvern Zetasizer IV (Malvern Instruments Ltd, Malvern, UK) at 20±0.1 ℃. Samples of particles in suspension were appropriately diluted in deionised water to give counts of at least 200cpm. Results are expressed as the mean ± standard deviation of 5 readings.

2.2.1.5 Transmission Electron Microscopy (TEM)

Morphology of the particles was examined using TEM (Jeol Jem 1010 electron microscope, Japan). A sample of particle suspension was diluted with 3% w/v phosphotungstic acid corresponding to a ratio of 1:1 before examination. One drop of sample was placed for 1 minute on a copper grid coated with a formvar carbon film. The excess of sample was drained away with the aid of filter paper. The samples were observed at magnifications ranging between 20 000 and 300 000x, recorded with a Kodak Megaplus digital camera 1.6i, and analysed using the AnalySIS 3.0 software package.

2.2.1.6 Determination of drug/fluorescent dye loading and entrapment efficiency

Drug loading and entrapment efficiency

Drug loading was determined using an indirect method. Firstly, DXM-P solution was scanned from 200 to 400nm to determine the λ_{max} on a Agilent spectrophotometer (Agilent 8453, Germany). Secondly, 100μg /ml stock of DXM-P solution was made up accurately in a volumetric flask. Then it was diluted to give solutions of 0.5, 1, 2, 4, 6, 8, 10μg/ml. The absorbance of each solution was measured at the λ_{max} on Agilent spectrophotometer. The amount of drug which has not been incorporated was measured and the amount of incorporated drug was calculated from the initial amount of drug by subtraction.

The % w/w drug loading was calculated, to describe the weight of drug loaded into the particles as a function of the total weight of particles.

$$\text{Percentage of drug loading (\%w/w)} = \frac{\text{mass of actual drug in the NPs}}{\text{mass of polymer used in formulation}} \times 100$$

Another important expression is the entrapment efficiency which indicates extent of drug loss to the external phase.

$$\text{Entrapment efficiency (\%)} = \frac{\text{mass of actual drug in NPs}}{\text{mass of initial amount of drug}} \times 100$$

Fluorescent dye loading and entrapment efficiency

Fluorescent dye labelling was determined by a direct method: Freeze-dried fluorescently labelled PGA NPs were dissolved in acetone/methanol (2:1 ratio). The fluorescence of the solution was measured at excitation and emission wavelengths of 554nm and 575nm respectively, with slit widths set at 5nm (Hitachi F-4500 fluorescence spectrophotometer, Hitachi Scientific Instruments, Finchampstead, UK). The amount of fluorescent label was calculated by a using standard curve of fluorescent dye in HEPES buffer (0.01M, pH 7.4). Fluorescent dye loading and entrapment efficiency were calculated using the same equations as described above except using an amount of fluorescent dye instead of drug.

2.2.2 NP preparation for biological study

For all experiments of NP in biological study, NPs were coated with 0.1% Polysorbate-80 and passed through a syringe filter (0.2μm, Vivascience, Gemany) to sterilize the NP suspension.

2.2.3 Routine cell culture

2.2.3.1 Cell types

DAOY cell line

DAOY cell line was established in 1985 from a solid mass tumour removed from the posterior fossa of a four-year-old male and diagnosed as desmoplastic cerebellar medulloblastoma (Jacobsen *et al.*, 1985). DAOY cells also have been widely used in laboratory studies of medulloblastoma.

U937 cell line

U937 cell line was derived from a patient with generalized histiocytic lymphoma (Sundstrom and Nilsson, 1976). Usually U937 cells are rounded, small, non-adherent cells and display many monocytic characteristics.

2.2.3.2 Monolayer cell culture

DAOY cells (American Type Culture Collection, Manassas, USA) were maintained on Minimum Essential Medium (MEM) supplemented with 15% Foetal Bovine Serum (FBS), 200mM L-glutamine, 0.1mM non-essential

Amino Acids, 1.0mM sodium pyruvate, and 7.5% sodium bicarbonate solution at 37°C and 5% CO_2.

U937 cells were a generous gift from School of Biomedical Sciences (University of Nottingham, Nottingham, UK) and cultured in Dulbecco's Modified Eagle Medium (DMEM) supplemented with 15% FBS, and 200 mM L-glutamine at 37°C and 5% CO_2.

Mixed foetal rat brain cells were dissociated from the whole brain of E-18 Wistar rats (animal house, University of Nottingham) according to the method described previously by Searle (Searle, 2004). After whole brains were rapidly removed and immersed in ice-cold Hank's Balanced Salt Solution (HBSS) including 10mM HEPES, brain tissues were gently minced into small pieces using a scalpel. The tissue fragments were incubated with 2.5% trypsin (2ml) (Worthington Biochemical Corporation, NJ, USA) and HBSS (3ml) in 5% CO_2 incubator at 37°C. After 45 min of incubation, the action of trypsin was halted by transferring the tissue fragments into 20% heat inactivated Newborn Calf Serum (NCS) in PBS (pH 7.4, 10mM) buffer. Then individual cells were gently dissociated from tissue fragments by using a glass Pasteur pipette, cultured at a density of 1×10^6 cells/well or 0.5×10^6 cells /well in a 24-well tissue culture plate and maintained on MEM supplemented with 10% NCS, 200mM L-glutamine, and 7.5% sodium bicarbonate solution at 37°C and 5% CO_2.

Both DAOY and U937 cell lines were subcultured every 7 days at a 1:50 split ratio. DAOY cells were detached from substratum using trypsin-EDTA. Multicellular rat brain preparations were cultured for 1-2 days after dissociation.

2.2.3.3 Aggregate culture

DAOY aggregates

DAOY cells were grown in monolayers and detached from the substratum as described above. The DAOY aggregates were formed using rotation methods: the individual cells (2ml, 1×10^6 cells/ml) were cultured in DAOY culture medium in 25 ml screw top culture flasks (Scientific Laboratory Supplies, UK) and maintained at a constant rotation of 70 rev/min on an orbital shaker (Cole-Palmer, USA) at 37°C. Cultures were observed and medium was exchanged at 24 h of culture.

Mixed foetal rat brain aggregates

Primary mixed brain aggregates, in which individual cells were dissociated from E-18 rats, were prepared and cultured as described previously in DAOY aggregates except mixed foetal brain aggregates were maintained on MEM supplemented with 10% NCS culture medium.

2.2.3.4 Organotypic brain slice culture

Organotypic slice culture has been widely used to study the properties of synaptic transmission between monosynaptically coupled cell pairs because it preserves high neuronal connectivity (Gähwiler *et al.*, 1997). There are two widely used methods for the culture of organotypic slices, the roller-tube method (Gähwiler *et al.*, 1997) and the air-medium interface method (Stoppini *et al.*, 1991). After brain was removed from rat, the tissue is chopped into sections of 100-400μm in thickness and subsequently washed in a balanced salt solution to allow tissue debris and potentially

toxic substances to diffuse away. The next step involves attaching the slices to a substrate. Both the roller-tube method and the air-medium interface method used similar tissue culture medium. The difference between these two methods is how the cultures are embedded and maintained. In *roller-tube methods*, the brain slice is embedded in either a plasma clot or in a collagen matrix on glass coverslips and then undergoes continuous slow rotation. In *air-medium interface method*, slices are placed at the air-medium interface either on Transwell or Millicell semiporous membranes and kept stationary during the entire culture process. The air-medium interface method is preferable for the repeated observation of live cells.

Considering that cultures grown by the air-medium interface method are prepared easily and can be observed during all stages of cultures, the air-medium interface method was used in organotypic slice culture in this thesis. Organotypic brain slices were prepared from 2-day-old Wistar rats. After brain was rapidly removed and immersed in ice-cold HBSS containing 10mM HEPES, cortices were cut into 400μm thick and cerebella were chopped into 300μm thick slices with a tissue chopper (0.4μm in pore size, 30mm in insert size, Mcllwain Tissue Chopper, Mickle Laboratory Engineering Co., Ltd., UK) under sterile conditions in a laminar flow hood. Three slices were then laid down on a Millicell-CM membrane insert (Millipore, Carrigtwohill, Co. Cork, Ireland), and the insert was placed in individual wells of 6-well plates. 1ml of medium was added to the bottom of culture plate (Fig. 2.2). Slices were cultured in the same culture medium as mixed foetal brain cells in monolayer at 37°C with a 5% CO_2 incubator, and half medium was changed every other day.

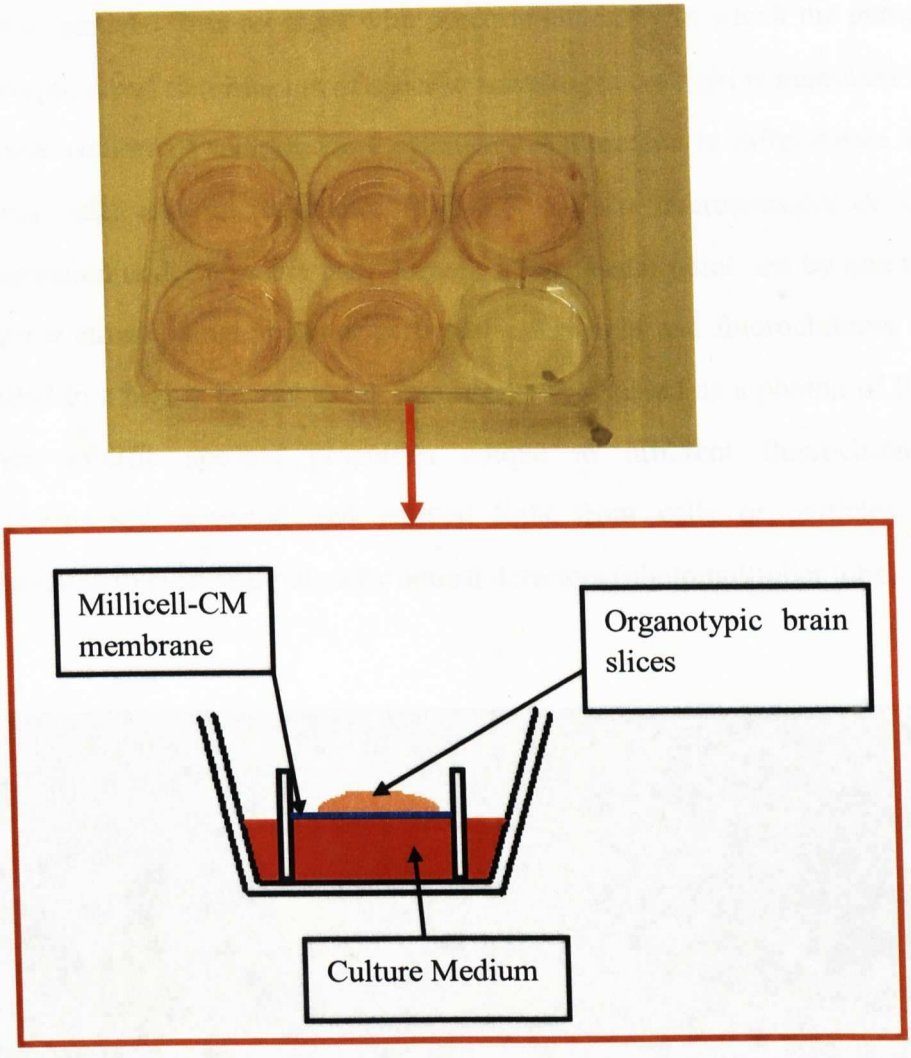

Fig. 2.2 Techniques used for culturing organotypic slices: Brain slices (400μm), dissected from P2 Wistar rats, were laid down on a small piece of porous and transparent Millicell-CM membrane, and the membrane placed in the 6-well plates. Medium was added to the bottom of the culture plate. Cultures were kept in a 5% CO_2 incubator at 37°C.

2.2.4 Flow cytometry

Principle of flow cytometry

One unique feature of flow cytometry is that it measures fluorescence per cell or particle. This contrasts with spectrophotometry in which the percent absorption and transmission of specific wavelengths of light is measured for a bulk volume of sample. Flow cytometry is a method to differentiate and count cells and microparticles (Fig. 2.3). When microparticles or cell suspension under pressure pass through a laser beam point one by one in a narrow stream, single cells or particles scatter light and fluorochromes are exited to a higher energy state. This energy is released as a photon of light with specific spectral properties unique to different fluorochromes. Subsequently, scattered and emitted light from cells or particles are converted to electrical pulses by optical detectors (photomultiplier tube).

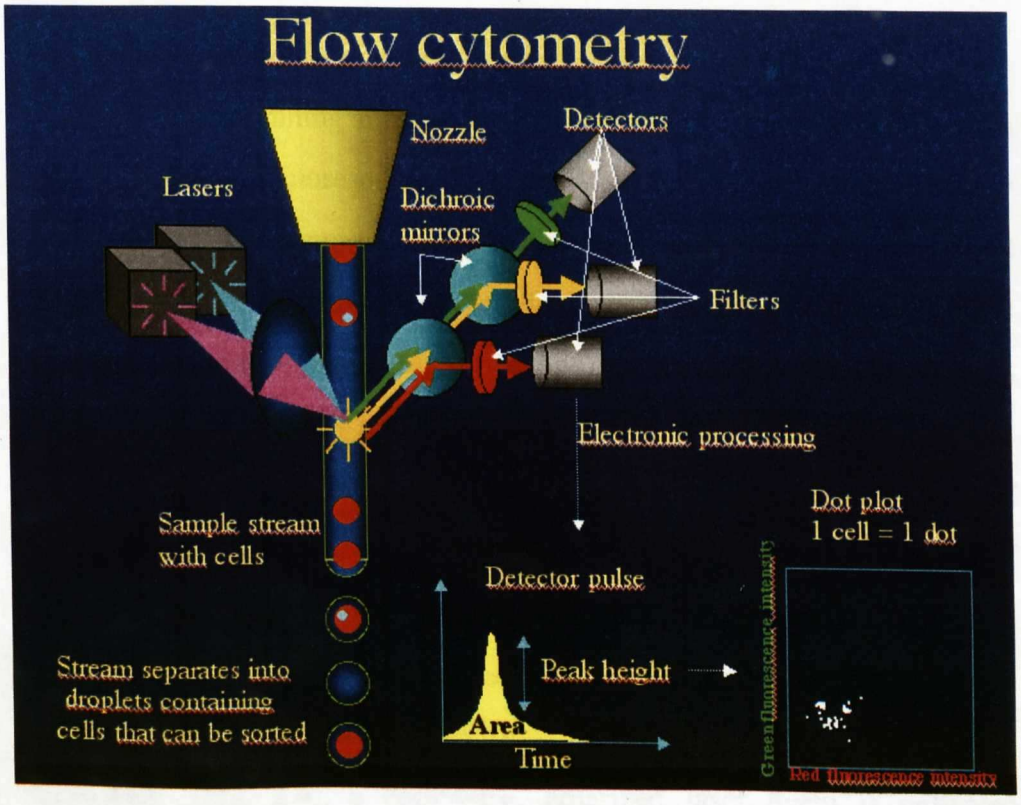

Fig. 2.3 Principle of flow cytometry (website image1)

Method of measuring fluorescently labelled NPs within cells

Following the incubation time for NP uptake or retention, the cells were washed three times with PBS, resuspended in fresh culture medium and placed in an incubator for 30 min for recovery of cell membrane. After washing twice with cold PBS, cells were transferred into tubes and immediately placed on ice. The intracellular fluorescence intensity was determined on a Beckman Coulter EPICS XL-MCL flow cytometry (Beckman Coulter Limited, Buckinghamshire, UK) using XL SYSTEM II™ software. Approximately 5 000 event cells were evaluated for forward and side scatter characteristics to determine the trend of RBITC labelled NP taken up by cells. Forward scatters correlates with the cell volume, while side scatter correlates with the amount and type of cytoplasmic granules.

2.2.5 Microscopic studies

Principle of confocal laser scanning microscopy

Confocal laser scanning microscopy (CLSM) exhibits several advantages over conventional fluorescence microscopy. CLSM rejects light not only from out of focus sample plane but also light scattered from the optical instrument itself, resulting in increased contrast and fine detail of samples detected. Another important advantage of confocal microscopy is enhancement of optical (z) axial resolution and producing optical sections through a three dimensional (3-D) specimen. By moving the focal plane of the instrument step by step through the depth of the specimen, a series of optical sections can be recorded, which allows one to visualize cells and tissues in 3-D. The basic principle of confocal microscopy is: In the confocal epi-fluorescence mode of a single beam scanning optical microscope (Fig. 2.4), a collimated, polarized laser beam is deflected

stepwise in the x- and y-direction by a scanning unit (not shown) before it is reflected by a dichroic mirror (beam splitter) so as to pass through the objective lens of the microscope, and focused onto the specimen. The emitted, longer-wavelength fluorescent light collected by the objective lens passes through the dichroic mirror (transparent for the longer wavelength) and is focused into the confocal aperture to eliminate all the out-of-focus light, i.e., all light coming from regions of the specimen above or below the plane of focus. Therefore, the CLSM not only provides excellent resolution within the plane of section (0.25 mm in the x- and y-directions), but also yields similarly good resolution between section planes (0.3 mm in the z-direction).

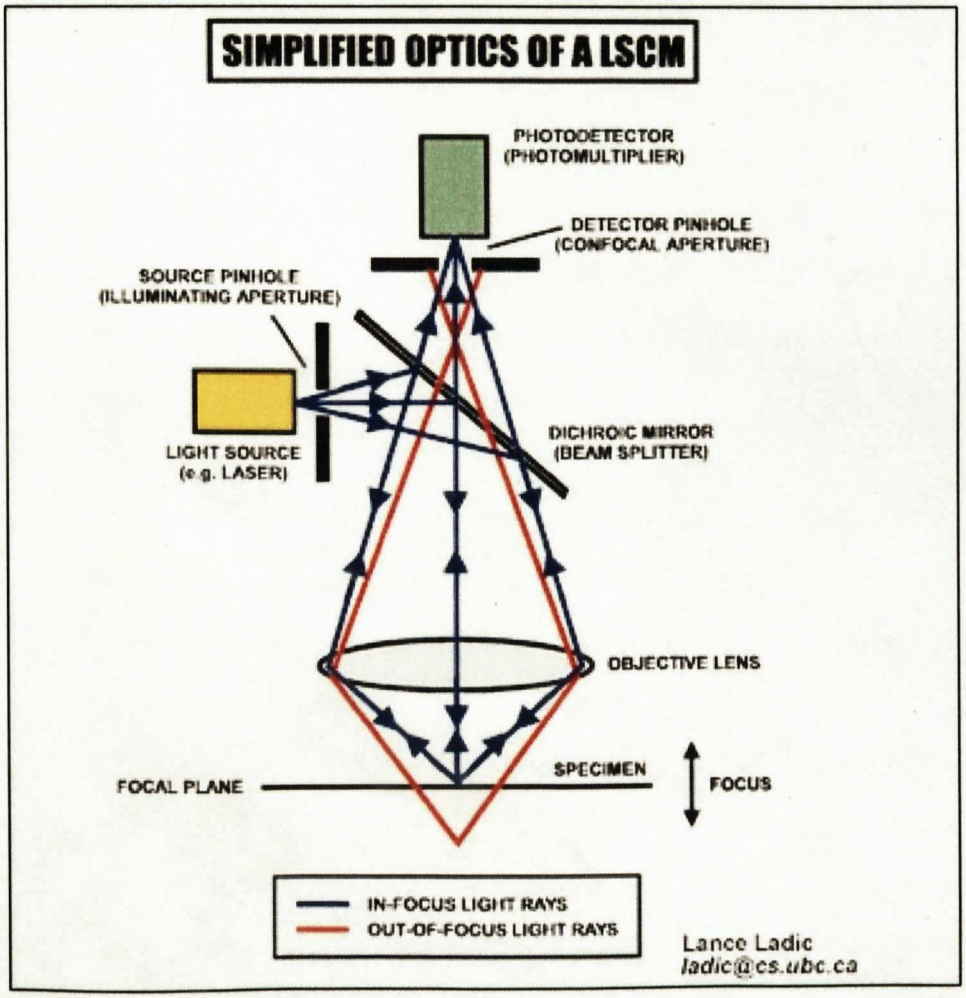

Fig. 2.4 Principle of confocal laser scanning microscopy (Website image

Method of microscopic studies

Confocal laser scanning fluorescence microscopy (Leica SP2 MP, Leica Microsystems Ltd, UK) was mostly used to investigate metabolism and distribution of NPs in different cell culture dimension models. For microscopy studies, monolayer cells, aggregates, slices, and co-culture samples were incubated with DAPI (300nM) for 30 min after samples were fixed. Samples subsequently were rinsed with PBS / Tris-HCl three times and visualized and imaged under a Leica SP2 MP confocal microscope using 476nm filter (Lyso Tracker), 488nm filter (fluorescein), 543nm filter (RBITC), and UV laser (DAPI).

CHAPTER 3

PHYSICOCHEMICAL CHARACTERISATION OF POLY (GLYCEROL-ADIPATE) NANOPARTICLES

3.1 INTRODUCTION

Biodegradable and biocompatible NPs have been investigated as an effective drug delivery system, which can deliver the drug to a target site and increase the therapeutic value while minimizing side effects. Following i.v. administration, particle size as well as surface properties could influence distribution of NPs *in vivo*, since these parameters are key factors influencing NP uptake by the MPS. Generally, a small size (< 200nm) and a hydrophilic surface are needed in order to reduce opsonization reactions and clearance by MPS. A successful NP system also needs to have a high drug loading and entrapment efficiency to reduce the amount of carrier required for treatment and minimise wastage of drug.

To overcome some problems of lower drug loading and faster drug release associated with polymers currently in use, a novel biodegradable polymer, PGA, is being developed by our research group. A range of hydrophobic/hydrophilic properties were obtained by varying the average molecular weight of the polymer backbone and the substitution ratio of the aliphatic group (Fig. 1.6). In this chapter, the particle size and surface charge of NPs have been studied in order to examine the influence of acylated aliphatic group on NP physicochemical characteristics. The percentage of drug loading and entrapment efficiency was also studied to investigate

interaction between NPs and therapeutic agent. DXM-P was used as a drug because we are interested in delivering drug to brain and corticosteroid can alleviate the oedema caused by brain tumours.

3.2 METHODS

3.2.1 Preparation of drug-free, and DXM-P loaded PGA NPs (see 2.2.1.1)

3.2.2 Measurement of particle size and surface charge (see 2.2.1.3 and 2.2.1.4)

3.2.3 Determination of DXM-P loading and entrapment efficiency (see 2.2.1.6)

3.2.4 TEM (see 2.2.1.5)

3.3 RESULTS

3.3.1 Particle size

PCS was carried out to measure the mean hydrodynamic diameter and polydispersity of DXM-P loaded and drug free PGA NPs. The results obtained for PGA NPs are shown in Table 3.1. The mean size of NPs produced by the nanoprecipitation method was in the range 160nm-270nm with a relatively narrow particle size distribution. In the absence of drug, not all of the polymers could form NPs, especially polymer with 80% substitution of aliphatic group. However, all polymers could form NPs when they encapsulated DXM-P. For DXM-P loaded NPs, it was shown that particle size decreased slightly compared with drug free NPs. The average particle size of DXM-P loaded NPs is related to the average molecular weight of polymer backbone and type of aliphatic group. Particle size of NPs formed by polymer with 2kDa backbone slightly increased with an increase in the substitution of aliphatic groups. In polymers with 6kDa backbone, there was no difference in particle size between polymers with 40% and 80% substitution. In addition, it was found 100% C_{18} (12) NPs had a smaller particle size instead of an increased size. For the influence of type of aliphatic group on the particle size, it was shown that the particle size of NPs formed by polymers with C_{18} substitution was larger than that formed by polymers with C_8 substitution.

Polymer Type	Particle size±S.D. (nm) [polydispersity]	
	Empty NPs	DXM-P loaded NPs
40%C_8(2)	213.7 ± 0.8 [0.027]	164.1 ± 0.9[0.075]
80%C_8(2)	-[a]	221.9 ± 1.5[0.168]
100%C_8(2)	-	254.0 ± 4.4[0.221]
40%C_{18}(2)	250.1± 11.6[0.126]	239.8±12.7[0.527]
80%C_{18}(2)	-	244.8 ± 5.7[0.217]
100%C_{18}(2)	227.0 ± 7.9[0.213]	316.1±16.5[0.258]
40%C_8(6)	-	207.8 ± 0.4[0.039]
80%C_8(6)	-	207.2± 3.4[0.122]
100%C_8(6)	276.4 ± 3.5[0.193]	251.9 ± 4.9[0.225]
40%C_{18}(6)	232.0 ± 23.6[0.133]	226.7 ± 1.0[0.121]
80%C_{18}(6)	246.3 ± 23.3[0.076]	229.4 ± 4.4[0.104]
100%C_{18}(6)	225.3 ± 0.9[0.065]	232.5 ±13.4[0.090]
40%C_8(12)	191.0 ± 2.0[0.111]	184.4 ± 4.8[0.090]
80%C_8(12)	-	225.1 ± 5.5[0.102]
40%C_{18}(12)	212.7 ± 20.6[0.139]	211.0 ± 3.6[0.154]
80%C_{18}(12)	-	256.3 ± 1.9[0.135]
100%C_{18}(12)	244.4 ± 2.1[0.095]	224.0 ± 2.4[0.077]

a: "-" represents no NPs formed and aggregation observed

Table 3.1 Particle size of DXM-P loaded/free PGA NPs : NPs were formed using the nanoprecipitation method. NP suspension was diluted with ultrapure water to an appropriate concentration to give 500-600 kcps. Particle size was the mean hydrodynamic diameter and measured by Photon Correlation Spectroscopy. The particle size of each sample is expressed as the mean particle hydrodynamic diameter ±standard deviation of 30 readings.

3.3.2 DXM-P loading studies

The results of DXM-P loading are illustrated in Table 3.2 and Fig. 3.2. For C_8 acylated polymers, an increase in DXM-P loading from 1.82% up to 7.89% was seen with an increase in the number of substitution of aliphatic side groups from 40% to 100%. It would be expected that drug loading of polymers with C_{18} aliphatic group have the same increasing trend, but 100% C_{18} polymer incorporating DXM-P was obviously lower than that of 80% C_{18} polymers, some even lower than 40% C_{18} polymers. From the results of drug entrapment efficiency as shown in Table 3.2, the entrapment efficiency was higher in comparison to previous work using PLGA or PLA polymers (Chasteigner *et al.*, 1996 and Govender *et al.*, 1999). Entrapment efficiency had same increasing trend as percentage of drug loading. Entrapment efficiency values increased from 3.00% to 39.48%, which indicated relatively low drug wastage during preparation.

Polymer Type	DXM-P loading (%w/w)	Entrapment Efficiency (%)
40%C_8(2)	1.820	9.100
80%C_8(2)	1.995	9.975
100%C_8(2)	5.590	28.00
40%C_{18}(2)	-	-
80%C_{18}(2)	0.600	3.000
100%C_{18}(2)	2.695	13.47
40%C_8(6)	1.855	9.275
80%C_8(6)	2.130	8.200
100%C_8(6)	7.350	36.75
40%C_{18}(6)	4.065	20.32
80%C_{18}(6)	7.485	37.42
100%C_{18}(6)	4.165	20.82
40%C_8(12)	5.460	27.30
80%C_8(12)	7.895	39.47
40%C_{18}(12)	7.800	39.00
80%C_{18}(12)	7.460	37.30
100%C_{18}(12)	2.105	10.52

Table 3.2 Drug loading and entrapment efficiency of PGA NPs : Amount of DXM-P was encapsulated in PGA NPs was determined using an indirect method and expressed as percentage of drug loading and entrapment efficiency. Drug loading (%) describes the weight of drug loaded into the particles as a function of the total weight of particles. Entrapment efficiency indicates extent of drug loss to the external phase.

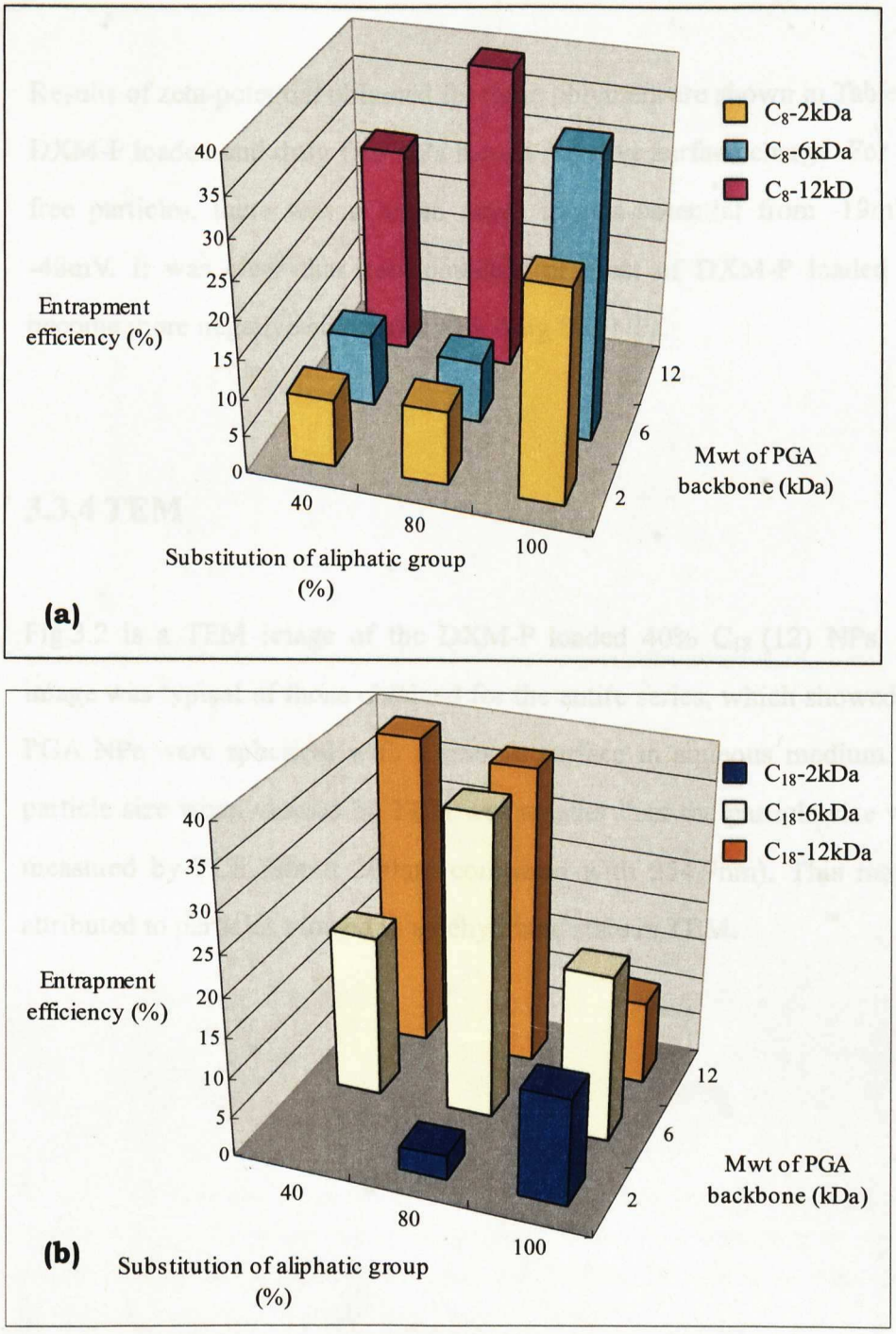

Fig. 3.1 Entrapment efficiency of PGA NPs with different aliphatic group and different percentage of substitution (a) PGA polymer substituted with C_8 aliphatic group; (b) PGA polymer substituted with C_{18} aliphatic group

3.3.3 Surface charge

Results of zeta-potential obtained for these polymers are shown in Table 3.3. DXM-P loaded and drug free NPs have a negative surface charge. For drug free particles, there was a broad range in zeta-potential from -19mV to -48mV. It was clear that zeta potential of most of DXM-P loaded NPs become more negative compared with drug free NPs.

3.3.4 TEM

Fig.3.2 is a TEM image of the DXM-P loaded 40% C_{18} (12) NPs. This image was typical of those obtained for the entire series, which showed that PGA NPs were spherical with a smooth surface in aqueous medium. The particle size when viewed by TEM was smaller than the particle size when measured by PCS (about 200nm compared with 254.9nm). This may be attributed to particles viewed in a dehydrated state in TEM.

Polymer Type	Zeta-potential ± S.D. (mV)	
	Empty NPs	DXM-P loaded NPs
40%C_8(2)	- 18.4 ± 0.7	- 28.8 ± 1.1
80%C_8(2)	-	-46.7 ± 0.5
100%C_8(2)	-	-47.3 ± 1.3
40%C_{18}(2)	-	-35.3 ± 0.6
80%C_{18}(2)	- 32.4 ± 2.7	-35.7 ± 2.6
100%C_{18}(2)	- 40.7 ± 3.1	-32.3 ± 3.0
40%C_8(6)	-	- 29.0 ± 1.1
80%C_8(6)	-	-48.7 ± 0.9
100%C_8(6)	-47.5 ± 0.7	-44.0 ± 1.5
40%C_{18}(6)	-32.4 ± 4.3	-46.3± 0.9
80%C_{18}(6)	- 34.7± 1.6	-43.3± 2.1
100%C_{18}(6)	- 39.7 ± 3.3	-49.5± 0.7
40%C_8(12)	-34.0 ± 1.4	-32.0 ± 1.0
80%C_8(12)	-	-29.9 ± 1.0
40%C_{18}(12)	-25.9 ± 3.3	- 34.5± 4.3
80%C_{18}(12)	-	-48.0± 5.0
100%C_{18}(12)	-	-44.6± 1.1

a: "-" represents no NPs formed and aggregation observed

Table 3.3 Surface charge of PGA NPs: NPs were formed using a nanoprecipitation method. NP suspension was appropriately diluted in deionised water to give counts of at least 200cpm and measured by using Malvern Zetasizer Ⅳ. Results are expressed as the mean ±standard deviation of 5 readings.

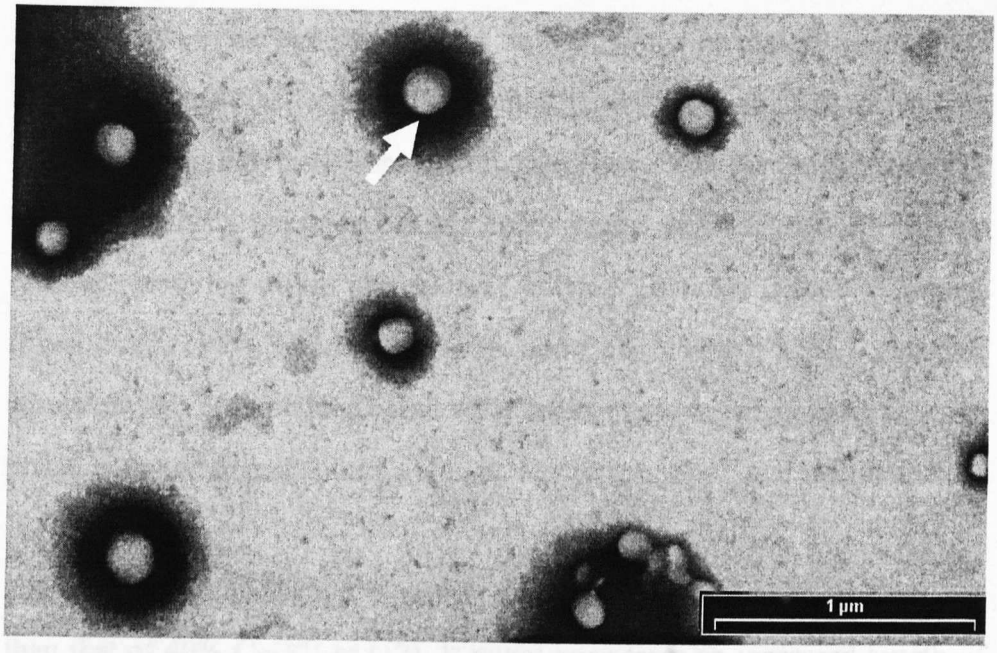

Fig. 3.2 Transmission electron micrograph of DXM-P loaded 40%C_{18}-12kDa PGA NPs (arrow). Scale bar: 1μm

3.4 DISCUSSION

3.4.1 Particle size

Firstly, the possible mechanism of NP formation will be described because it is the key factor to understand the results of particle size. Basically, NP formation is associated with complex interfacial hydrodynamic phenomena and the "diffusion-stranding" process between two unequilibrated liquid phases (Fessi *et al.*, 1989, and Galindo-Rodriguez *et al.*, 2004). This technique involves the addition of polymer dissolved in a water miscible solvent into an aqueous solvent under magnetic stirring. The rapid diffusion of solvent into the aqueous phase together with the increased interfacial surface area created by the turbulence causes a decrease in the interfacial

tension between the two phases. This results in polymer molecules grouping together and then the formation of small droplets of organic solvent without the need for high force mechanical mixing. The solvent then diffuses further into the aqueous phase and water concurrently diffuses into the solvent droplets, resulting in the formation of polymer particles from the droplets (Fessi *et al.*, 1989, Wehrl *et al.*, 1995, and Chorny *et al.*, 2002,). Thus NP formation can be explained based on aqueous phase-organic phase, aqueous phase-polymer, organic phase-polymer, and polymer-polymer interactions.

For drug free PGA NPs, the particle size of 40%C_8 (2) or (12) is smaller than that of 40% C_{18} (2) or (12). It might arise from an increased length of polymer side chains, which can influence the viscosity of organic phase (Galindo-Rodriguez *et al.*, 2004). When 40% C_{18} polymer dissolved in acetone, a more viscous organic phase is obtained because increased length of polymer side chains could lead to a greater volume of polymer chains per unit volume of solvent. The higher viscous organic phase could provide a higher mass transfer resistance. Thus the diffusion of polymer-solvent phase into the external aqueous phase is reduced and larger NPs are formed. In contrast, when 40% C_8 polymer dissolved in acetone, it has a relatively lower viscosity of organic phase, which increases the distribution efficiency of the polymer-solvent phase into the external phased leading to formation of smaller NP. An increased viscosity of organic phase might be used to explain the reason that particle size of 100% C_{18} (12) NPs are larger compared with that of 100% C_{18} (6) NPs. Some polymers can't form NPs, which might be because different polymer properties have a different effect on the interaction of acetone-polymer and NP formation process. But it is not the only reason explaining whether NPs will occur because many factors have an effect on NP formation

A slight decrease of particle size in DXM-P loaded NPs compared with drug

free NPs was observed, which might indicate that DXM-P could play a role in NP formation procedure. Normally, interfacial turbulence may be promoted by various factors, such as solute transfer out of the phase of higher viscosity, steep concentration gradients near the interface and interfacial tension sensitive to solute concentration. Govender *et al.* found that drug free PLGA NPs prepared in pH 9.3 buffer solution were significantly smaller than those prepared in water pH 5.8 (Govender *et al.*, 1999). The author attributed it to the greater ionization of carboxyl groups at higher pH. DXM-P has a steroid ring, which is highly lipophilic, and is water soluble due to the presence of the phosphate group. During NP formation stage, it was assumed that acetone diffuses from the organic phase into the water and carries with it some PGA polymer chains which are still in solution. As acetone diffuses further into the water, the associated PGA polymer chains deposit in the aqueous phase. At the same time, the steroid ring of DXM-P also could bind to the polymer chains through hydrophobic interaction, while the hydrophilic group, phosphate group, protruded into the surrounding medium. Thus interfacial tension and turbulence could be significantly decreased leading to DXM-P loaded NPs formation.

3.4.2 DXM-P loading studies

Generally, physicochemical properties of NPs, surface area of NPs and physicochemical properties of drug influence drug incorporation efficiency. The percentage of DXM-P loading and entrapment efficiency was apparently influenced by average molecular weight of polymer backbone and acylated aliphatic group with different length (C_8 or C_{18}). These are opposite to reports from Fonseca *et al* (Fonseca *et al.*, 2002) and Görner *et.al.* (Görner *et al.*, 1999). Görner *et al.* using a series of PLA with

different molecular weight examined the influence of molecular weight on the incorporation of lidocaine and found the same entrapment efficiency. Fonseca *et al.* reported paclitaxel incorporation was independent of molecular weight and composition of the copolymers of PLGA. The opposite results may be attributed to different properties between PGA polymer and PLGA/PLA. The higher molecular weight of polymer backbone, the more hydrophobic the segments in PGA polymer, which leads to stronger interaction between polymer and polymer, or polymer and drug and thus more drug was encapsulated into NPs. This could explain the increase in drug loading with an increase of molecular weight of polymer backbone. It was also found that drug loading of NPs produced by polymer with C_8 slightly increased when molecular weight of polymer backbone is less than 12kDa while a clear increase was observed when the molecular weight of backbone was 12kDa. This resulted in a 300% increase for 40% C_8 and a 400% increase for 80% C_{18}. The difference in increase rate might also indicate 12kDa is a critical point for molecular weight of backbone affecting the hydrophobic property of PGA polymer. The hydrophobic property of PGA polymer was also dependent on the percentage of acylated aliphatic groups in polymer backbone. In Table 3.2, it was found that although there is a doubling in amount of aliphatic groups from 40% C_8 (2) to 80% C_8 (2), or from 40% C_8 (6) to 80% C_8 (6), the increase of amount in percentage of drug loading is slight, 9% increase for the 2kDa polymer backbone and 15% for the 6kDa polymer. However the difference in percentage of drug loading from 80% C_8 to 100% C_8 polymer was marked, showing a 181% increase for the 2kDa polymer backbone and 245% increase for the 6kDa polymer, and drug loading in 80% C_8 (12) NPs is about 1.5 times higher than in 40% C_8 (12). These difference in drug loading indicated C_8 chains were exerting a weaker influence on the hydrophobic property of PGA polymer as percentage of substitution was increased. Drug loading of 40% C_8 NPs is lower since their particle sizes are smaller than

that of 80% C_8 and 100% C_8 NPs , which results in a larger surface area for drug loss into the aqueous phase during nanoprecipitation. A higher percentage of drug loading in 100% C_8 NPs could be because of its higher percentage of substitution, which leads to entangled acylated aliphatic chains provided more free space available to accommodate the drug. The hydrophobic property of PGA polymer also increased with an increase of the length of acylated aliphatic chains. Comparing drug loading between NPs formed by polymer with C_8 chains and NPs substituted with C_{18} aliphatic chains, it was shown that the drug loading in a series of NPs substituted with C_{18} chains is much higher than that of NPs formed by polymer with C_8 chains. This could be due to the longer carbon chains and hence greater lipophilicity of C_{18} chains than C_8 chains which increased interaction between polymer and drug and reduce the loss of drug into aqueous phase. This would be in agreement with the finding of Yamakawa *et al.* (Yamakawa *et al.*, 1992) and Govender *et al.* (Govender *et al.*, 1999). The lower drug loading in 100% C_{18} NPs was possibly attributed to decreased solubility of polymer in acetone, which leads to a greater aggregation of polymer chains and hence most of drug was lost because of absorbtion on the aggregates during NP formation.

3.4.3 Surface charge

As seen in Fig. 1.6, there are two functional groups on the end of polymer backbone: on average, one is a hydroxyl group (-OH), and another is a carboxyl group (-COOH). Thus the negative charge of drug free NPs mainly arises from the presence of ionised carboxyl groups on the NP surface, as reported previously for drug free PLGA and PLA NPs (Stolnik *et al.*, 1995b, and Govender *et al.*, 2000). It is shown in Table 3.3 that the surface charge

became more negative with an increase of percentage of acylated aliphatic group. Taking account of structure of PGA polymer, there could be molecular hydrogen bonding through interactions between pendant hydroxyl groups and carboxyl groups on the end of polymer backbones. When 40% hydroxyl groups on PGA polymer backbone were acylated by aliphatic groups, it could have more chance of having a pendant hydroxyl group (-OH) and have less space obstacle caused by acylated aliphatic groups. The pendant hydroxyl group thus had an enhanced chance to form hydrogen bonds with carboxyl groups on the end of other polymer backbones. This resulted in few ionised carboxyl groups located on the surface of NPs. On the contrary, pendant hydroxyl group acylated by aliphatic chains had a reduced opportunity to form hydrogen bonds with an increase of acylation of polymer backbones because the influence of the obstacle caused by C_8 or C_{18} was larger. When most or all of pendant hydroxyl groups were substituted by aliphatic chains, most of ionised carboxyl groups could appear on the NP surface. Apart from hydrogen bonds being formed between polymer and polymer, intrapolymer-hydrogen bonds also played a role in the surface charge of NPs. In addition, more negative surface charge also due to the ionic property of carboxyl group. Carboxyl groups could be ionised during NP formation, which leaded to carboxyl groups having a preference to be in the aqueous phase. This effect would become stronger when the more hydrophobic the core of the PGA NPs became.

From Table 3.3, it is illustrated that surface charge become more negative after DXM-P was incorporated into NPs. For instance, 40% C_8 (2) NPs had a significant increase of negative charge, -28.8±1.1 mV, on the surface in comparison with empty particles, -18.4±0.7 mV. The apparent increase of negative charge on DXM-P loaded 40% C_8 (2) NPs was probably due to the preferential surface localisation of drug (Allen *et al.*, 1999, and Heinsman *et al.*, 2001). Since DXM-P is an alkaline drug (pH, 7.5-9.0), it is negatively

charged in water. In contrast, there was little difference in zeta potential between some of DXM-P loaded NPs (80%C_{18} (2), 100%C_8 (6), and 40%C_8 (12)) and drug free NPs. This could suggest that most of DXM-P were encapsulated inside the NPs, not on the surface because more phosphate groups were needed to be accommodated if the polymer was increasingly acylated.

3.5 SUMMARY

This chapter has examined NP size, surface charge, drug loading and entrapment efficiency to have a deeper understanding the influence of composition of PGA polymer on properties of PGA NPs and interaction between NPs and drug.

The influence of composition of PGA polymer on NP properties

PGA polymer is composed of glycerol and adipate at 1:1 ratio with a pendant hydroxyl group acylated by different length aliphatic chains (C_8 or C_{18}). Its hydrophilic/hydrophobic properties were modified by varying the molecular weight of polymer backbone and percentage of substitution of aliphatic chains. In the particle size study, a transmission electron micrograph demonstrated NPs were spherical and discrete in the nanometer size range. The mean hydrodynamic diameters and polydispersity indices confirmed that all NPs are in the sub-micrometer size range with a relatively narrow particle size distribution. Based on the principle of NP formulation and structure of PGA polymers, particles are influenced by molecular weight of polymer backbone, percentage of substitution of aliphatic groups, and length of aliphatic chains since these parameters influence properties of

PGA polymer, which results in effects on the diffusion rate of acetone into the aqueous phase and hence the size of NPs.

The nanoprecipitation technique is mostly used to incorporate water insoluble drugs into PLGA/PLA NPs because it suffers from the drawback of a poor incorporation of water soluble drugs due to the loss of drug into aqueous phase during manufacturing. Generally, the drug loading of water soluble drugs is very low, such as procaine hydrochloride, 0.27 %w/w (Govender *et al.*, 2000), even for some water insoluble drugs, drug loading is also lower compared with PGA NPs (1.82%w/w-7.8%w/w). The drug loading value of most water insoluble drugs in PLA or PLGA are: indomethacin, 2% w/w (Fessi *et al.*, 1989) or 5.8%w/w (Magenheim *et al.*, 1993), and dexamethasone, 0.9% w/w (Fessi *et al.*, 1989) and itraconozole, 4.1%w/w (Chasteigner *et al.*, 1996). After drug loading studies, it was found that polymer backbone and its side chains have an influence on drug loading and entrapment efficiency. When the molecular weight of polymer backbone was below 12 kDa and polymer was acylated by C_8 chains, they exerted a weak influence on drug loading and entrapment efficiency. On the contrary, NPs can have a higher drug loading and less drug wastage during preparation when molecular weight of polymer backbone is 12 kDa or polymer were substituted by C_{18} chains.

The zeta potential study showed that NPs had a negative surface charge and that the surface became more negative with an increased percentage of substitution of aliphatic groups. It also showed that the molecular weight of polymer backbone and length of aliphatic groups didn't have any influence on the amount of ionised carboxyl groups on the surface of NPs.

The influence of drug on particle size and surface charge

As shown in Table 3.1, particle size of DXM-P loaded NPs was slightly smaller than that of drug free NPs. This could be attributed to the ionization of DXM-P, which makes the solubility parameter of drug-water close to the parameter of polymer-acetone and decreases concentration gradients near the interface between PGA solution and aqueous phase. This resulted in rapid diffusion of acetone into aqueous phase and thus led to smaller NPs.

After DXM-P was incorporated into NPs, the zeta potential of some NPs become more negative while some remain unchanged, which might be due to the amount of DXM-P absorbed on the surface of NPs. It is suggested that the position of DXM-P in NPs had an obvious influence on the surface charge of NPs.

Considering the physicochemical characteristics of series of DXM-P loaded NPs, 40%C_{18} (12) polymer was chosen for routine NP preparation due to its higher drug loading and entrapment efficiency, relatively hydrophilic surface and sub-micrometer size. In the following studies, we have investigated the interaction of PGA NPs and hydrophobic fluorescence as a drug model and its release profile in order to proceed with a quantitative analysis of NP behaviour in cells.

CHAPTER 4

PHYSICOCHEMICAL PROPERTIES OF FLUORESCENTLY LABELLED NANOPARTICLES AND *IN VITRO* RELEASE STUDIES

4.1 INTRODUCTION

Understanding the kinetics of cellular and tissue uptake, intracellular distribution and retention of NPs (Panyam *et al.*, 2003a and 2003b) is important because most drug and macromolecular agents, whose site of action is within the cells, need to be delivered into cells or subcellular compartments for therapeutic effect. For many of these applications, fluorescence is used extensively to label NPs during preparation so that NP uptake and distribution can be visualized by either confocal or fluorescence microscopy or quantified by flow cytometry. Due to the wide range of materials and production methods used, the physical properties of fluorescently labelled NP including hydrophobicity, surface charge, and particle size distribution could vary.

NPs as colloid particles in a dispersion medium always show Brownian motion and hence may adhere to one another and form flocculates and aggregates successively increasing size in high salt concentrations or under conditions of physiological ionic strength. The stability of a NP suspension is thus determined by the interaction between the particles during such a

collision. To maintain the stability of a NP suspension, repulsive forces must be dominant in the whole system, which can be achieved by one of two fundamental mechanisms: steric or electrostatic stabilization (Everett, 1988). Steric stabilization can offer several distinct advantages over electrostatic stabilization, such as relative insensitivity to the presence of electrolytes (Napper, 1989). Non-ionic surfactants, such as poloxamers and polysorbates, are widely used as stabilizers providing steric stabilization for drug formulation vehicles. Many studies have shown that polysorbate-80 coated polybutylcyanoacrylate NPs can also be transported across the blood brain barrier (Kreuter *et al.*, 2002, 1997, and 2001, and Ramge *et al.*, 2000) and polysorbate-80 is thus a particularly appropriate choice of stabiliser for this work.

Drug delivery systems aim to deliver the drug at a specific site and also give a controlled drug release rate over an extended duration or at a specific time during treatment. Targeted delivery of therapeutic agents can be achievable by modifying the surface properties of drug delivery systems, resulting in enhancement of therapeutic efficacy and lowering of toxic effects (Solaro *et al.*, 2003). Controlled release over an extended duration can be highly beneficial to drugs, which are rapidly metabolized and eliminated from body after administration (Uhrich *et al.*, 1999)

The aim of the following studies was to identify suitable fluorescent labelling techniques for NPs, which would be suitable for studies in confocal /fluorescent microscopy and flow cytometry. Particle size, surface charge and fluorescent dye loading were examined. DXM-FL, RB and RBITC were used for encapsulation in NPs. DXM-FL was chosen because it has similar structure of DXM-P. RB and RBITC as long-wavelength light-emitting dyes are more photostable than fluorescein labelling reagents. Moreover, spectra of RBITC are not affected by changes in pH above 3

(Brismar *et al.*, 1995). The effect of varying the concentration of polysorbate-80 on the adsorption of serum protein on the surface of NPs and the on the colloidal stability of the dispersion were studied. Finally, *in vitro* drug release was also determined.

4.2 METHODS

4.2.1 Preparation of fluorescently labelled PGA NPs (see 2.2.1.1)

4.2.2 Measurement of particle size and surface charge (see 2.2.1.3 and 2.2.1.4)

4.2.3 Determination of fluorescent dye loading and entrapment efficiency (see 2.2.1.6)

4.2.4 Interaction of surfactant coated NPs with serum and NP stabilisation

The stabilization of polysorbate-80 was monitored by measuring the turbidity of NP suspension coated with polysorbate-80 as a function of the electrolyte concentration. The critical flocculation point was taken as the electrolyte concentration at which a dramatic increase in the turbidity was first detected. Each NP suspension (0.15ml) coated with different

concentration of polysorbate-80 (0.01%, 0.1%, and 0.5%) was incubated with an equal volume of DAOY cell culture medium including 15% FBS for 5 min. This mixed solution (0.3ml) was then added to 1.0 ml of Na_2SO_4 solutions of varying concentration (0, 0.01, 0.025, 0.05, 0.1, 0.25, 0.4, 0.45, 0.5, 0.55, 0.6 M). Mixed solutions were placed in a horizontal water bath for 15min, and turbidity was measured at a wavelength of 564 nm using an Agilent spectrophotometer.

4.2.5 *In vitro* release study

Release study using a fixed shaking speed

In vitro fluorescent dye released from PGA NPs was performed in HEPES buffer (0.1M, pH4.5 or pH7.4) and DAOY cell culture medium using dialysis bags on a shaker stand with shaking speed of 50 rpm in a water bath at 37 °C. The details were as follows: RBITC labelled NP suspension (1ml, about 4mg/ml) or free RBITC (1ml, 2μg/ml) coated with 0.1% polysorbate-80 and 1ml of HEPES buffer/DAOY cell culture medium were added in dialysis bag, and then placed in a beaker with HEPES buffer/DAOY cell culture medium (15ml). The 15ml eluate was removed from the beaker and an equal volume of fresh HEPES buffer/DAOY cell culture medium was added at regular time intervals. The quantity of RBITC was measured fluorometrically at λ_{Ex}=554nm, λ_{Em}=575nm.

Release study using different shaking speed

In vitro release study of RBITC from NPs was investigated using the same protocol as above except that the NP suspension was dialysed against HEPES buffer (0.1M, pH 7.4) with three shake speeds (25 rpm, 50rpm, and 100rpm) for 24h.

4.3 RESULTS

4.3.1 Physicochemical properties of fluorescent dye labelled NPs

Aimed at choosing a suitable fluorescence probe for evaluating PGA NPs in cell cultures, particle size, surface charge, and fluorescent dye loading were examined for DXM-FL, RB, and RBITC with various initial loading amounts. Table 4.1 illustrated the influence of the initial amount of fluorescent dye on the fluorescent dye incorporation and entrapment efficiency. In all cases, it was showed that fluorescent dye loading and entrapment efficiency was affected by the initial amount of fluorescent dye, which illustrated a proportional relationship between initial amount and fluorescent dye loading. Incorporation of DXM-FL, RB, and RBITC was in the range from 0.02-0.04%, 0.003-0.029%, and 0.007-0.19%, respectively. Entrapment efficiency of DXM-FL decreased from 0.64%-0.43% with an increase in the initial amount of dye. Entrapment efficiency of RB changed slightly with various initial amount, which was around 2%, while a significant increase in entrapment efficiency of RBITC from 4.8%-17% was observed with an increase of the initial amount of dye used.

As estimated by laser light scattering, the mean particle size of DXM-FL labelled NP, RB labelled NPs, and RBITC labelled NPs were in the range 165-203nm, 179-197nm, and 164-185nm, respectively (Table 4.1). RB and RBITC labelled NPs had relatively narrow particle size distribution while particle size distribution of DXM-FL labelled NPs was comparatively broad. Particle size of DXM-FL labelled NPs has an apparent increase with increasing amounts of initial dye. RB or RBITC labelled NPs showed only

	Initial amount of fluorescent dye (μg)	Particle Size. nm ± S.D	Poly-dispersity	Zeta-potential mV ± S.D.	Loading amount of fluorescent dye (μg)	Actual fluorescent dye loading (%w/w)	Entrapment Efficiency (%)
DXM-FL	500	165.0±1.0	0.266	-58.5±1.4	3.21	0.02	0.64
	1000	172.5±2.4	0.239	-59.0±0.5	5.92	0.03	0.59
	2000	203.6±1.0	0.256	-52.1±1.1	8.68	0.04	0.43
RB	30	179.5±13.6	0.159	-56.0±2.7	0.60±0.3	0.0031±0.002	2.0±1.1
	50	183.4±13.3	0.151	-50.8±7.3	1.78±0.6	0.0089±0.003	3.6±1.1
	100	189.7±4.7	0.173	-55.9±0.6	2.37±0.8	0.012±0.004	2.4±0.8
	250	197.8±7.0	0.173	-54.5±3.6	5.64±1.5	0.029±0.008	2.3±0.6
RBITC	30	185.7±5.9	0.240	-49.3±0.1	1.43±0.5	0.007±0.002	4.8±1.5
	50	164.8±8.7	0.138	-53.8±1.8	3.59±0.1	0.018±0.001	7.2±0.3
	100	171.1±10.1	0.169	-56.6±0.1	16.24±5.1	0.081±0.03	16.2±5.1
	250	175.6±6.1	0.150	-52.1±0.7	37.47±9.8	0.190±0.05	17.2±1.7

Table 4.1 Physicochemical properties of fluorescently labelled PGA NPs: NPs were formed using a nanoprecipitation method. NP suspension was diluted with HEPES buffer to an appropriate concentration to give 500-600 kcps. Particle size was mean hydrodynamic diameter and measured by PCS. Zeta-potential was measured by using Malvern Zetasizer IV. Values are means ± s.d., n=3

a slight increase in particle size with initial dye amount. As shown in Table 4.1, all fluorescently labelled NPs exhibited a net negative charge with similar zeta potential values ranging from -49.3 to-59.0 mV.

Compared with data from all of fluorescent dyes labelled NPs, RBITC was chosen as suitable fluorescence labelling NPs for biological studies because RBITC labelled NPs had smaller and more consistent particle sizes, and relatively higher dye loading. However RBITC has the disadvantage of binding to proteins.

4.3.2 The effect of non-ionic surfactant on stability of the NP suspension

Fig. 4.1 shows the interaction of polysorbate-80 coated NPs with serum proteins and the effect of this interaction on the colloidal stability of the dispersion after addition of electrolytes. Turbidity of NP dispersion was decreased with an increasing of concentration of polysorbate-80. The turbidity of surfactant coated NP suspension was lower than that of non-coated NP suspension before the critical flocculation point (CFPT) and was higher than the control sample (only polysorbate-80 in Na_2SO_4). It was also found that turbidity of naked NPs in the absence of serum was significantly higher than that of serum conditioned. When NPs were coated with polysorbate-80, CFPT was found to be at a relatively higher concentration of the electrolyte in 0.1% or 0.5% polysorbate-80 coated NP suspension compared with 0.01% coated NP suspension. The 0.1% and 0.5% polysorbate-80 coated NPs flocculated at the same sodium sulfate concentration (0.45 mol dm^{-3}). NPs coated with 0.01% polysorbate-80 flocculated at 0.4 mol dm^{-3}. It was interesting that flocculation wasn't

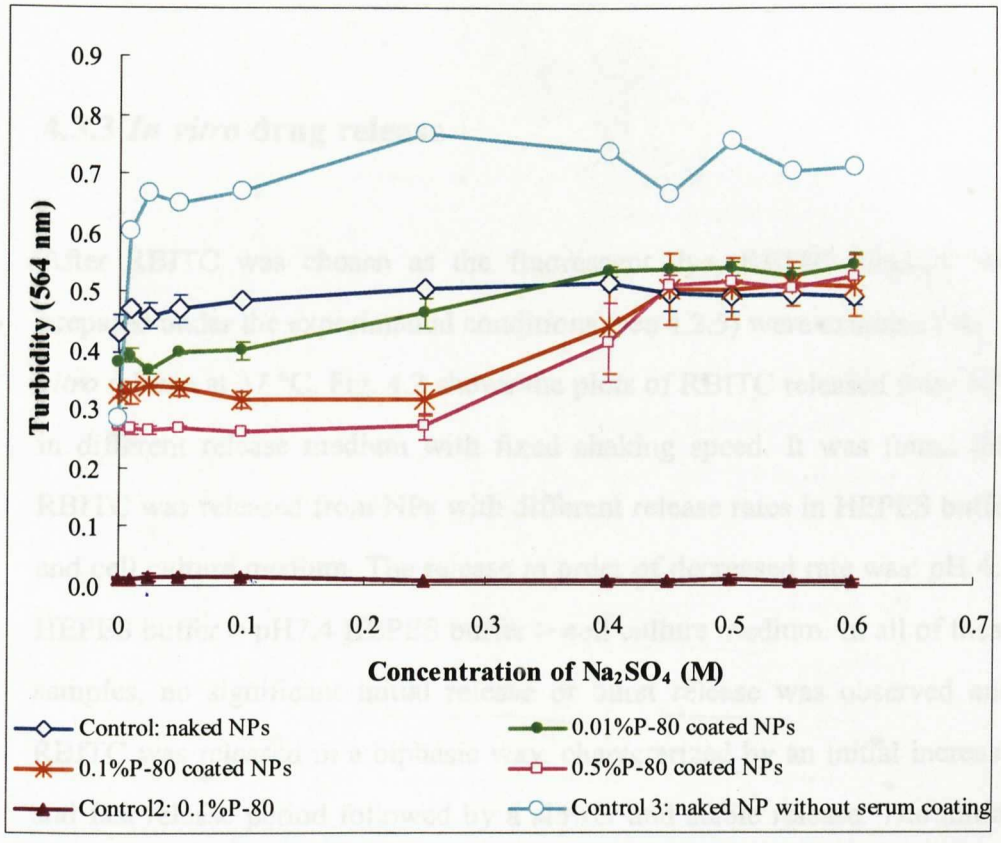

Fig. 4.1 Critical flocculation concentration of polysorbate-80 coated /uncoated PGA NPs assessed by turbidity method The polysorbate-80 coated /uncoated NPs were incubated with an equal volume of serum for 5 min (expect Control 3). The excess serum proteins were not removed in order to mimic physiological conditions. Serum conditioned/serum untreated NP suspensions were then added to a series of sodium sulfate concentration and incubated for 15 min at 37 °C. Values are mean ± s.d. (n=3).

observed to occur in uncoated NPs suspension after incubation with serum while flocculation can be found in the suspension of naked NPs without incubating with serum.

4.3.3 *In vitro* drug release

After RBITC was chosen as the fluorescent dye, RBITC labelled NPs prepared under the experimental conditions (see 4.2.5) were examined for *in vitro* release at 37 °C. Fig. 4.2 shows the plots of RBITC released from NPs in different release medium with fixed shaking speed. It was found that RBITC was released from NPs with different release rates in HEPES buffer and cell culture medium. The release in order of decreased rate was: pH 4.5 HEPES buffer > pH7.4 HEPES buffer > cell culture medium. In all of these samples, no significant initial release or burst release was observed and RBITC was released in a biphasic way, characterized by an initial increase and fast release period followed by a slower and stable release. The initial RBITC released from NPs in 1day was 28.6%, 13.9%, and 4.3% in pH4.5 and pH7.4 HEPES buffer, and cell culture medium respectively. After this initial release, RBITC was released in a continuous way for 17 days only reaching 42%, 27.5%, and 12.5% for RBITC labelled NPs in pH4.5 and pH7.4 HEPES buffer, and cell culture medium respectively. Free RBITC was used as control to reflect the diffusion rate of RBITC through the dialysis bag. It was observed that 70% of RBITC diffused into HEPES buffer in 4h and 82% diffused into cell culture medium in 4 days.

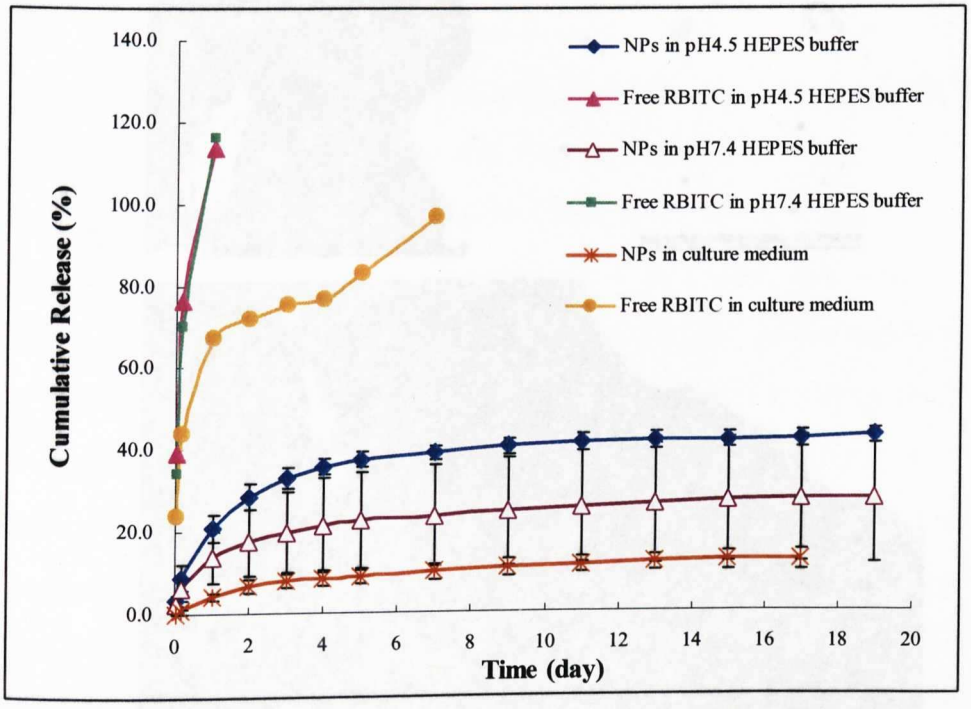

Fig. 4.2 *In vitro* release profile of RBITC labelled NPs in HEPES buffers and cell culture medium Equal volume of RBITC labelled NPs suspension and release medium were put into dialysis bags, and then dialyzed in sink conditions in release medium with fixed shaking speed. Values are mean ± s.d. (n=3).

PAGES
MISSING
IN
ORIGINAL

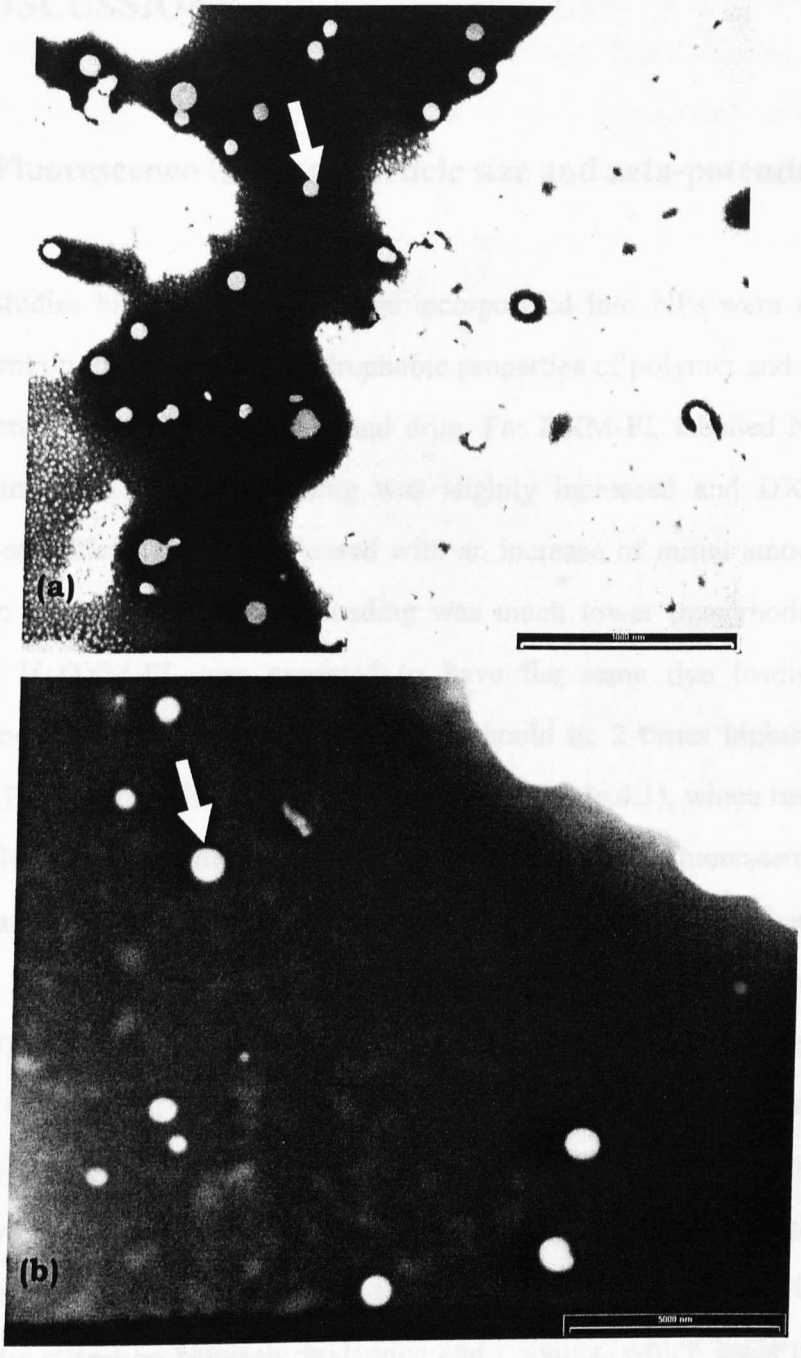

Fig. 4.3 Transmission electron micrographs of release profile of RBITC labelled NPs. RBITC labelled NPs (white arrow) and equal volume HEPES buffer (pH 7.4, 0.1M) were loaded into dialysis bag and then dialysis in HEPES buffer (pH 7.4, 0.1M) with various shaking speeds. (a) before RBITC release; Scale bar: 1000nm ; (b) After 24h in a release experiment with shaking speed at 25 rpm, Scale bar: 5000nm

4.4 DISCUSSIONS

4.4.1 Fluorescence loading, particle size and zeta-potential

Many studies have shown that drugs incorporated into NPs were mostly dependent on the hydrophilic/hydrophobic properties of polymer and drugs, and interaction between polymer and drug. For DXM-FL labelled NPs, it was found that DXM-FL loading was slightly increased and DXM-FL entrapment efficiency was decreased with an increase of initial amount. It was also shown that DXM-FL loading was much lower than rhodamine loading. If DXM-FL was expected to have the same dye loading as rhodamine, the initial amount of DXM-FL should be 2 times higher than that of RB or 10 times higher than that of RBITC (Table 4.1), which resulted in significant wastage during NP formulation. The lower fluorescent dye incorporation of DXM-FL was mostly attributed to its physicochemical property. DXM-FL (Fig. 2.2) can be dissolved and ionized in HEPES buffer (pH >7.4) and the DXM-FL thus would tend to diffuse from the organic phase to the external HEPES buffer during the process of NP formation. Although RB is also water soluble, RB like RBITC (Fig. 2.2) has a positively charged group in its structure, which would neutralize negative charge caused by carboxyl groups on the structure. This would result in an electrostatic attraction between rhodamine and polymer, which leads to an increased affinity between RB/RBITC and PGA polymer, and hence enhancing rhodamine loading into NPs. Apart from the water-soluble property of DXM-FL, higher molecular weight (MW: 840.98) also had an effect on DXM-FL loading. For rhodamine labelled NPs, it was illustrated that RBITC loading was about 2-8 times higher than RB loading when using the same initial mass (Table 4.1). This discrepancy was mainly due to the difference in hydrophobic/hydrophilic property: RB is very soluble in

HEPES buffer while RBITC is very sparingly soluble in HEPES buffer. It has been documented by a number of investigators that nanoprecipitation method is mostly suitable for compounds having a hydrophobic property, which could enhance affinity of drug with polymer (Barichello *et al.*, 1999, and Fonseca *et al.*, 2002). The hydrophobic nature of RBITC was higher than that of RB, which resulted in an enhanced interaction between hydrophobic segments of PGA polymer and RBITC. The stronger interaction and hydrophobic nature of RBITC would decrease RBITC diffusion from the organic phase to the external HEPES buffer, leading to a relative higher loading efficiency.

The fluorescently labelled NPs prepared by the nanoprecipitation method exhibited a similar particle size and surface charge (Table 4.1). These findings were attributed to lower dye loading and also indicated that most of the fluorescent dye was encapsulated in the core of polymer matrix and little was adsorbed on the NP surface. The study of surface charge of DXM-FL, RB, and RBITC labelled NPs shows that these NPs had a high negative zeta potential like DXM-P loaded NPs. According to the structure of DXM-FL, RB, and RBITC, no negative charge was observed. All of these suggested that higher negative charge of DXM-P modified NPs was not due to drug on surface. Finally, on the basis of particles, zeta-potential, drug loading and entrapment efficiency, RBITC was considered as a suitable fluorescent dye to evaluate PGA NPs using fluorescence microscope and flow cytometry.

4.4.2 Interaction of surfactant coated PGA NPs with serum proteins and colloidal stability

The investigation on stability of polysorbate-80 coated PGA NPs showed differences in the turbidity of NP suspensions with different concentrations of polysorbate-80 coating before CFPT occurred (Fig.4.1). These may arise from the differences in particle size and refractive index, and slight variation in the concentration of NP suspensions (Stolnik *et al.*, 1995a). The difference in turbidity is most probably due to increased particle size following incubation in serum, because of the hydrophobic segments of amphiphilic proteins adsorbed onto the NP surface (Brash, 1996 and Riley *et al.*, 1999). As polysorbate-80 surface coverage of NPs increased with an increase of polysorbate-80 concentration, the amount of serum protein adsorbing to the NPs decreased. The higher turbidity of uncoated NP in the absence of serum was due to NP aggregation because large aggregation can be observed after incubation with sodium sulfate.

The steric barrier of colloidal drug carrier not only prevents uptake by the reticuloendothelial system but ensures that NPs do not form agglomerates *in vivo* or *in vitro*. To examine the ability of polysorbate-80 in providing an effective steric barrier, flocculation studies were also performed at the same time thus mimicking physiological conditions. The coated NPs were stabilized by the presence of serum and flocculation only occurred at high electrolyte concentration (Fig. 4.1). It is well known that flocculation is a consequence of segmental attraction that occurs when the solvency of the dispersion medium is slightly decreased below that of a θ-solvent for the stabilising moieties of polysorbate (Napper, 1989). The SO_4^{2-} anion is thought to be unhydrated in aqueous solution. It exerts a strong destructive effect on the structure of hydrogen bonding between the water and

polysorbate chains (Tadros *et al.*, 1980, Napper, 1989, and Riley *et al.*, 1999). With an increase of concentration of SO_4^{2-} anion, the stabilising moieties of polysorbate became more dehydrated, chain-chain interaction became attractive and flocculation occurred. Incubation of uncoated NPs in the presence of serum was found to enhance their colloidal stability. It was most probably due to protein adsorbed on the naked particle surface, providing a steric barrier in the form of "loop" or "tails" (Riley *et al.*, 1999). However stability induced by serum proteins was not able to prevent flocculation occurring with a small increase in polysorbate-80 coated NP suspension in sodium sulfate concentration. Under the stress generated by a Brownian collision, sufficiently attached stabilizing polysorbate chains can move laterally on the surface of NPs while weakly-anchored stabilizing chains might detach from the NP surface, which would lead to bare patches on the surface of NPs created, resulting in decrease in stability (Napper, 1989). On the basis of stability studies, it was concluded that NPs coated with 0.1% and 0.5% polysorbate-80 were found to be stable under conditions mimicking the physiological environment.

4.4.3 *In vitro* release studies

Before studying the interaction of PGA NPs with cells, the RBITC release profile was studied to ensure that the RBITC estimated in cells was mainly due to the uptake of NPs rather than uptake of RBITC released from NPs during incubation. In addition, RBITC labelled NPs were also studied in HEPES buffer of different pH to observe the release behaviour of RBITC under physiological conditions relevant to extracellular conditions and lysosomal compartments. When NPs were incubated in various release media, it can be seen that different NP environments did affect the release

profile of RBITC. These differences were attributed to the properties of polymer and RBITC. As PGA polymer was composed of glycerol and adipate (1:1 ratio) with ester bonds in its back bone and side chains (Fig. 1.6), it was expected that PGA NPs were sensitive to pH and hydrolysis by enzymes and RBITC was released faster in lower pH HEPES buffer and cell culture medium. However, RBITC release from NPs was slower in cell culture medium than that in HEPES buffer (pH 7.4). This could be due to the properties of RBITC, in which isothiocyanate moiety can react with an amino group on serum protein to form a stable thiourea resulting in an increase in the average molecular weight of RBITC. Generally, the release is controlled by the partition coefficient of drug between continuous and dispersion phases (Sasaki *et al.*, 1984, and Washington, 1990). As described in release study methodology (see 4.2.5), NP suspension and an equal volume of release media were added into the dialysis bag. Once RBITC diffused out from NPs, RBITC could bond with serum proteins, which may result in slower diffusion of RBITC across membrane than that of unbound RBITC. The effect of molecular weight on the membrane diffusion of RBITC into sink was also confirmed by a control sample. It showed that free RBITC took a longer time diffusing across the dialysis bag in cell culture medium than in HEPES buffer.

In many of NPs produced using polyesters, such as PLGA and PLA, after samples were immediately placed in the release media 20%-50% of drug is released within several hours before the release rate reaches a stable profile (Peracchia *et al.*, 1997, Cascone *et al.*, 2002, and Sant *et al.*, 2005). Initial high release of drug is considered as a negative effect because it may lead to a drug concentration near or above the toxic level *in vivo* before it is delivered to the target site (Shively *et al.*, 1995 and Jeong *et al.*, 2000). A burst release was not observed in any of the RBITC labelled NP samples and release rate was slow and continuous. Although a burst release can be

caused by the NP manufacture process, geometry of NP, drug loading distribution in the NP, and properties of polymer and drugs (Huang *et al.*, 2001), in this case, the drug and PGA polymer properties were thought to be the main factor minimizing an initial high RBITC release. PGA polymer became more hydrophobic with an increase of substitution of fatty acids ($-C_{18}H_{38}$), which could depress the initial penetration of HEPES buffer or cell culture medium into the core of NP matrix. This would lead to a decrease in hydrolyzing ester bonds of PGA polymer, producing pores within the NP matrix and hence maintaining the structure of NP matrix in an intact form. Lower porosity and relatively intact matrix could reduce diffusion of RBITC from NPs. Breitenbach *et al* decreased the hydrophilicity of PLA-PVA microspheres by decreasing PVA, which led to a significantly decreased burst release of FITC labelled dextran (Breitenbach *et al.*, 2000). Apart from the composition of PGA polymer, RBITC, which is hydrophobic, also played a role in preventing RBITC burst release and giving a slow and continuous release rate. Hydrophobic PGA NP would be expected to become increasingly hydrophobic when RBITC is incorporated into the polymer matrix with consequent increased difficulty of water penetration into the core of NP matrix (Vihola *et al.*, 1998).

Because of the slow and continuous release rate of PGA NPs and different release rate in HEPES buffer with different pH and cell culture medium, it thus was deduced that RBITC released from NPs might be due to NP degraded as surface erosion mainly controlling the release kinetics coupled with RBITC diffusion. It was assumed that varying shaking speed would result in different release rate of RBITC from NPs. To confirm this hypothesis, *in vitro* release of RBITC labelled NPs were carried out in pH 7.4 HEPES buffer with a shaking speed varying from 25 rpm to 100rpm. It was found that the shaking speed (Table 4.2) didn't affect the RBITC release rate. In addition, the appearance of NP (Fig. 4.3) didn't change before and

after RBITC release. NP size became a little larger after NPs were replaced in release media for 24h than NPs without dialysis, which might be due to penetration of small amount buffer into NPs causing swelling. Although all of data seemed not to be in agreement with the hypothesis, considering the release study in different release media and TEM images, it might be deduced that RBITC release rate was mainly controlled by the rate of porosity formation in the NPs matrix combined with drug diffusion. The intact appearance of NPs might be due to the hydrophobicity of PGA NPs and relative short incubation time of PGA NPs with HEPES buffer. This resulted in decreased penetration rate of HEPES buffer into the NP matrix and few pores produced within the NP matrix, which were not visible under TEM.

4.5 SUMMARY

To investigate interaction of PGA NPs and brain tumour cells/normal cells, the physicochemical properties of two types of fluorescent dye labelled NPs, surfactant concentration, and *in vitro* release of fluorescently labelled NPs were examined.

Firstly, three fluorescent dyes, DXM-FL, RB, and RBITC, were used to label PGA NPs and then compare their properties including surface charge, fluorescent dye loading, and entrapment efficiency. It was found that NPs had highest loading efficiency for RBITC and lowest efficiency for DXM-FL. Table 4.1 also illustrated that all of fluorescently labelled NPs had similar particle size and surface charge. The discrepancy in fluorescent dye loading could be attributed the surface charge on the dye structure and hydrophobic/hydrophilic property of fluorescent dyes. The similar particle

size and surface charge was due to the low dye entrapment into NPs. The similar surface charge also suggested that it was mainly due to ionized carboxyl groups on the PGA polymer and that most of dye was distributed in the core of NP matrix. Based on the physicochemical properties of fluorescent dye labelled NPs, RBITC was chosen to label NPs.

Secondly, it is well known that NP aggregation and plasma proteins adsorbed on the surface of NPs are regarded as key factors for determination of *in vivo* organ distribution after intravenous injection. To minimize plasma protein adsorption and stabilize the NP, various concentrations of polysorbate-80 were used to study the stability of surfactant coated NPs under physiological conditions. It was shown that adsorption of serum proteins on the NP surface decreased with an increased concentration of polysorbate-80 and CFPT occurred at 0.45 mol dm^{-3} for 0.1% and 0.5% polysorbate-80 coated NPs, later than that of 0.01% coated NPs (Fig. 4.1). It was concluded that high concentration coated NPs were found to be stable under conditions mimicking the physiological environment. Thus, 0.1% polysorbate-80 was chosen to stabilize NPs

Finally, 0.1% polysorbate-80 coated RBITC labelled NPs was used to examine RBITC release *in vitro* with different dialysis media and shaking speed. The results (Fig.4.2 and Table 4.2) showed that RBITC release was slow and continuous and a burst release was not observed. It was also suggested that release rate was mainly controlled by the rate of porosity formation on the NP matrix based on the TEM work and release study in different release media.

CHAPTER 5

ASSESSMENT OF RHODAMINE B ISOTHIOCYANATE LABELLED NPS IN TWO DIMENSIONAL CELL CULTURE

5.1 INTRODUCTION

Brain tumours represent a devastating malignant disease, causing extreme and progressive disability leading to death (Souhami and Tobias, 1998). It is the second most common cause of cancer-related death in children, affecting 3.3 per 100 000 children (Leger *et al.*, 1999). Medulloblastoma is a malignant, invasive, embryonal tumour and the principle, infra-tentorial, posterior fossa tumour of children with an annual incidence of 0.5 per 100,000 children less than 15 years old (Rorke *et al.*, 1983). The essential clinical treatments of medulloblastoma are both radiotherapy and chemotherapy and adjuvant non-surgical treatment (Gilbertson *et al*, 2004). High dose therapy, chemotherapeutic agents in medulloblastoma, such as dibromodulcitol, and carboplatin, have major side effects, including granulocytopenia (Schuler *et al.*,1992) anaemia, leucopenia, thrombocytopenia (Castello *et al.*, 1990, and Borsi *et al*, 1996). One approach to overcome undesirable side effects of those chemotherapeutic agents includes the use of biodegradable polymeric nanoparticles for tumour targeted drug delivery. It is well known that most solid tumours show enhanced vascular permeability and enhanced permeability and retention effects for lipid and macromolecular agents (Duncan *et al.*, 1998, Monsky *et al.*, 1999, and Maeda, 2000). Thus, using NPs as a drug delivery method

could improve the selectivity of treatment and reduce systemic side effects by enhanced delivery of therapeutic agents to the desired medulloblastoma cells.

Generally, NPs of varying sizes may induce a foreign body reaction when introduced into the body. This reaction is mediated by the cells of MPS leading to NP systems being rapidly removed from the blood circulation. Mediated by the serum opsonins, this clearance process has been shown to be correlated with particle surface properties (Stolnik *et al.*, 1995a). Therefore, surface modification of NPs extends their circulation half-lives *in vivo* mainly by coated with hydrophilic and non-ionic polymers (Stolnik *et al.*, 1995a). So far Poly (ethylene oxide), polysorbates and poloxamers have been widely used for this purpose. The protective nature of these surfactants is attributed to forming a protective hydration shell around the particles surface, impairing interactions with approaching opsonins as well as phagocytic cells (Torchilin *et al.*, 1995)

As a good drug delivery system, it should not only deliver therapeutic agents to the target site with maximum uptake by target cells but also minimize therapeutic related side-effects by lower uptake of drug delivery system by the normal tissue cells. With this aim, intracellular uptake of RBITC labelled PGA NPs by the DAOY cell line, a human medulloblastoma, and retention of RBITC labelled NPs within DAOY cells were evaluated in this chapter. Since RBITC labelled NPs were stabilized by polysorbate-80, phagocytosis was also studied by incubating NPs with U937, a macrophage cell line, and the extent of phagocytic uptake was determined using flow cytometry. Finally, normal mixed foetal brain cells were also used to examine intracellular uptake of RBITC labelled NPs using flow cytometry.

5.2 METHODS

5.2.1 Routine 2-D monolayer cell culture (see 2.2.3.2)

5.2.2 Cellular NP uptake studies

DAOY cells

DAOY cells were plated at a density of 1 × 10^6 cells per 25 cm^2 tissue culture flask and allowed to attach for 24h. To study the effect of concentration of NPs and incubation time on cellular NP uptake, cells were incubated with a series of doses of NP (50, 100, 200, and 500 μg) per 0.5 × 10^6 cells for 2h or incubated in growth medium including 200μg NPs per 0.5 × 10^6 cells for different incubation time (from 15min to 24h). The cells were washed three times with PBS. Subsequently, the cells were detached by trypsin-EDTA for flow cytometry experiments. DAOY cells, used for microscopy studies, were prepared using the same procedure as above except that cells were seeded on PDL coated glass coverslip at 75,000 cells/ml per well in 24-well plates. After cells were washed three times with PBS, cells were fixed in 1% fresh prepared PFA and observed under a fluorescence microscope.

U937 cells

RBITC labelled NP taken up by U937 was carried out using the same method as described in DAOY cells except that U937 cells were washed with PBS by a centrifugation method.

Normal mixed rat brain cells

Mixed foetal rat brain cells were seeded at 0.5×10^6 cells/ml per well in 24-well plates. For study of the effect of incubation time on NP uptake, cells were incubated with growth medium including 200μg NPs for different incubation time. After cells were washed three times with PBS, cells were harvested by trypsin-EDTA and treated for flow cytometry study or were fixed in 1% freshly prepared PFA for microscopy study. Both methods are described below.

5.2.3 Metabolism of RBITC labelled NPs in DAOY cells

Retention of RBITC labelled NPs within DAOY cells

After a 2h incubation period in the presence of RBITC labelled NPs as described in 5.2.2, DAOY cells in monolayer culture were rinsed three times with PBS, replaced with fresh warmed medium in the absence of NPs and placed in incubator for various time (1-4h). At the end of the incubation period, the cells were then washed three times with PBS and culture medium containing free RBITC and NPs was collected. Cells were detached using Trypsin-EDTA and treated for flow cytometry. The amount of RBITC and NPs were measured using an ultracentrifugation method. For microscopy study, cells were fixed in 1% freshly prepared PFA.

Ultracentrifugation to quantitate free RBITC and RBITC labelled NPs in DAOY cell culture medium

DAOY culture medium containing free RBITC and NPs was collected and then centrifuged by using a Beckman L-8 60M Ultracentrifuge at 40,000rpm (142,500 ×g) for 1h at 4°C. The supernatant containing free RBITC or NPs was measured fluorometrically at λ_{Ex}=554nm, λ_{Em}=575nm.

5.2.4 Flow cytometry (see 2.2.4)

5.2.5 Microscopic Studies (See 2.2.5)

5.3 RESULTS

5.3.1 Investigation of RBITC labelled NP taken up by different cell types

5.3.1.1 Investigation of uptake of RBITC labelled NPs into different cell types by confocal microscopy

Confocal microscopy was employed to visualize the interaction of fluorescently labelled NPs and different cell types in RBITC labelled NP uptake studies. Fig. 5.1 shows confocal images of different cell types (DAOY cells, mixed brain cells, and U937 cells) incubated with RBITC labelled NPs for 2h. RBITC labelled NPs were endocytosed by DAOY cells and mixed brain cells. The spherical bright red fluorescent spots could be observed in discrete areas surrounding the nucleus. It should be noted that as the size of NPs are below 200nm in diameter, individual NPs would appear very small under confocal microscopy. The large dots are therefore collections of a large number of NPs. The confocal fluorescence micrograph of U937 cells appears to show a surface location of NPs. There are many small dots and some large red fluorescent spots. The latter almost certainly indicate an intracellular location, but appearing near the cell surface due to the large nucleus in these cells.

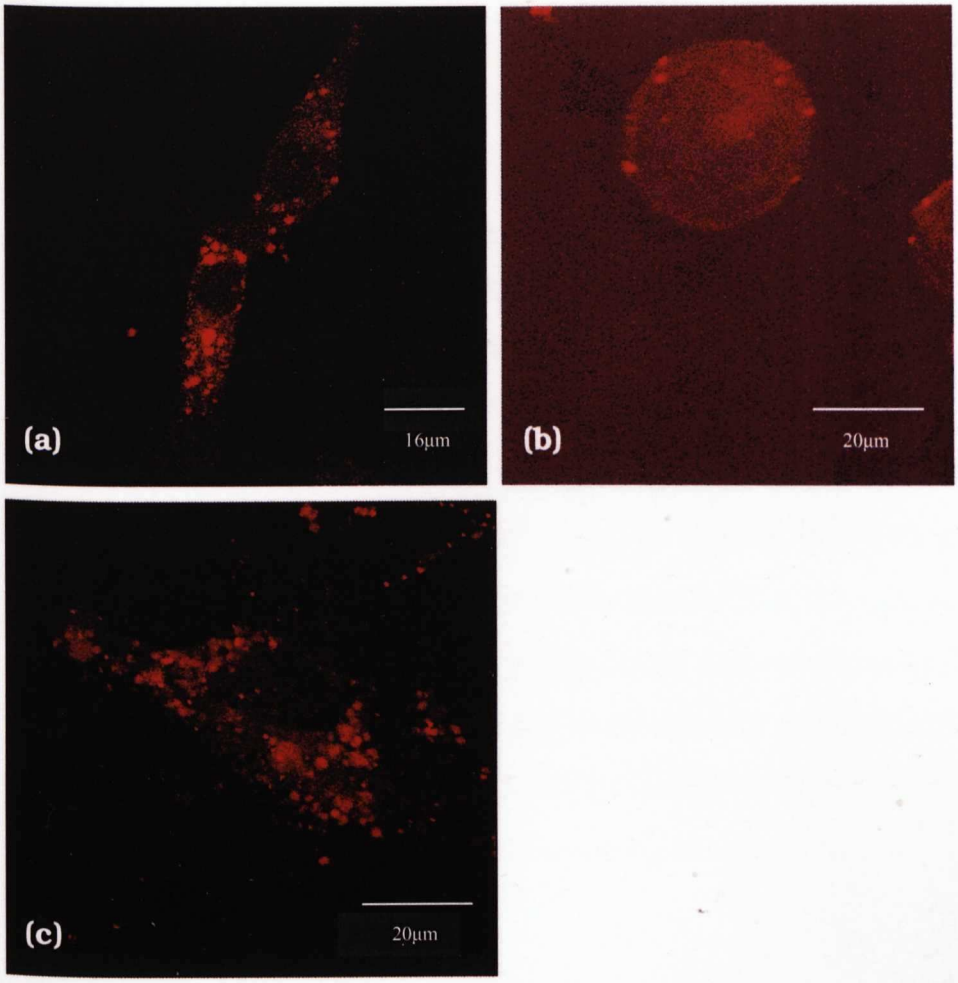

Fig. 5.1 Confocal maximum fluorescence intensity fluorescence micrographs demonstrating uptake of RBITC labelled NPs by cells. Cells were incubated with NPs (4mg/ml, 50μl) for 2h and then observed under confocal fluorescence microscopy. (a) DAOY cells, a medulloblastoma cell line; (b) U937, a human hematopoietic monocytic cell line; (c) mixed foetal brain cells. It was shown that fluorescently labelled NPs were taken up by DAOY cells and mixed foetal brain cells. NPs also were strongly associated with U937 cells, some of which were endocytosed. The location of the remainder is unclear.

5.3.1.2 Flow cytometry investigation of uptake of RBITC labelled NPs by different cell types

Dose-dependent uptake of RBITC labelled NPs by cells

Quantitative evaluation of cellular uptake of fluorescently labelled NPs was performed using flow cytometry. Flow cytometry is a means of measuring certain physical and chemical characteristics of cells or particles as they travel in suspension one by one past a laser beam. Thus flow cytometry can measure fluorescence intensity of every single cell or particle. As shown in Fig. 5.2, the cellular level of mean fluorescence intensity (MFI) progressively increased with dose of RBITC labelled NPs and did not reach saturation in DAOY cells and U937 cells. To confirm that MFI mainly resulted from cellular uptake of fluorescently labelled NPs, the same amount of free RBITC as that released from NPs in DAOY cell culture medium with 2h incubation time was also used. It was found that MFI of free RBITC was also increased with dose equivalent to RBITC labelled NPs but its MFI was much lower compared with MFI of fluorescently labelled NPs.

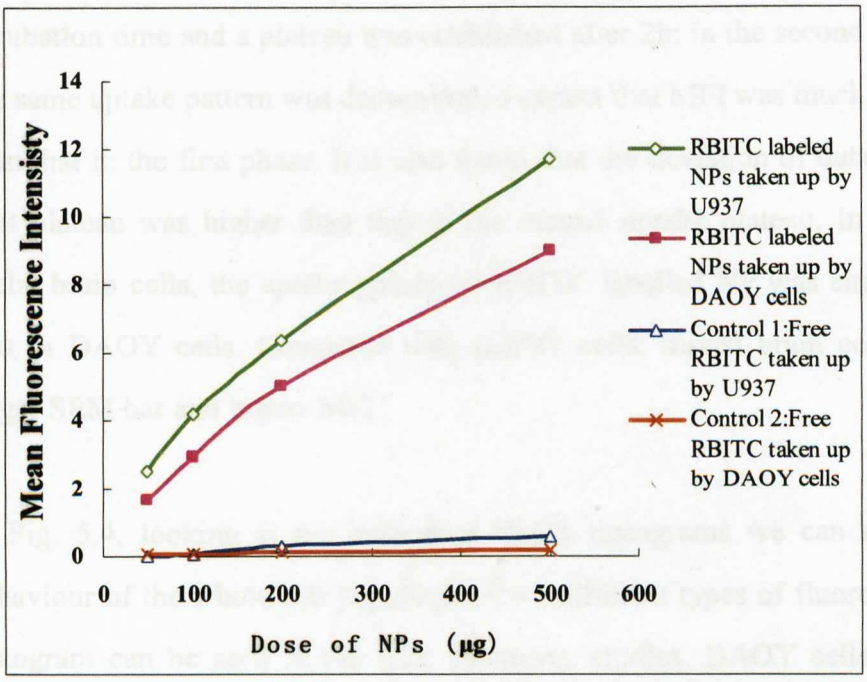

Fig. 5.2 Dose dependent uptake of RBITC labelled NPs by cells in monolayer culture. DAOY and U937 cells were incubated with different concentration of NPs for 2h. It was shown that intracellular MFI was mainly due to the uptake of NPs instead of free RBITC released from NPs during incubation time; MFI increased with dose of NPs for both cell types. Amount of free RBITC incubated with cells was equal to that of RBITC released from RBITC labelled NPs in DAOY cell culture medium with 2h incubation time. Values are mean ± SEM (n=3)

Time-dependent uptake of RBITC labelled NPs by cells

Fig. 5.3 shows that RBITC labelled NPs was also dependent on the incubation time. Studies of flow cytometry in DAOY cells show a biphasic-uptake. In the first phase, the MFI increased sharply within 2h of incubation time and a plateau was established after 2h; in the second phase, the same uptake pattern was demonstrated expect that MFI was much higher than that in the first phase. It is also found that the deviation of data in the first plateau was higher than that in the second uptake plateau. In mixed foetal brain cells, the uptake pattern of RBITC labelled NP was similar to that in DAOY cells. Compared with DAOY cells, mixed brain cells had larger SEM bar and higher MFI.

In Fig. 5.4, looking at the individual FACS histograms we can see the behaviour of the whole cell population. Two different types of fluorescence histogram can be seen in the flow cytometry studies. DAOY cells had a narrow and single peak in each incubation time. In contrast, mixed brain cells had a broad peak and shape of peak which changed with incubation time.

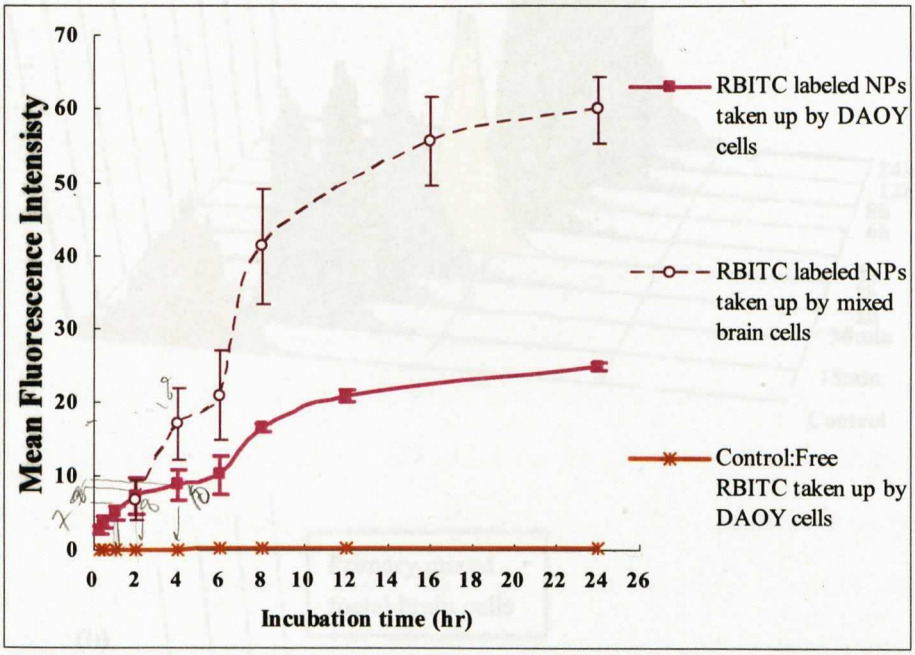

Fig. 5.3 Time dependent uptake of RBITC labelled NPs by cells in monolayer culture. DAOY and mixed brain cells were incubated with 200 µg/ml /well dose for different time intervals. It was shown that MFI increased with incubation time. NPs uptake was dependent on the cell types. Mean ± SEM (n=3), $p < 0.05$

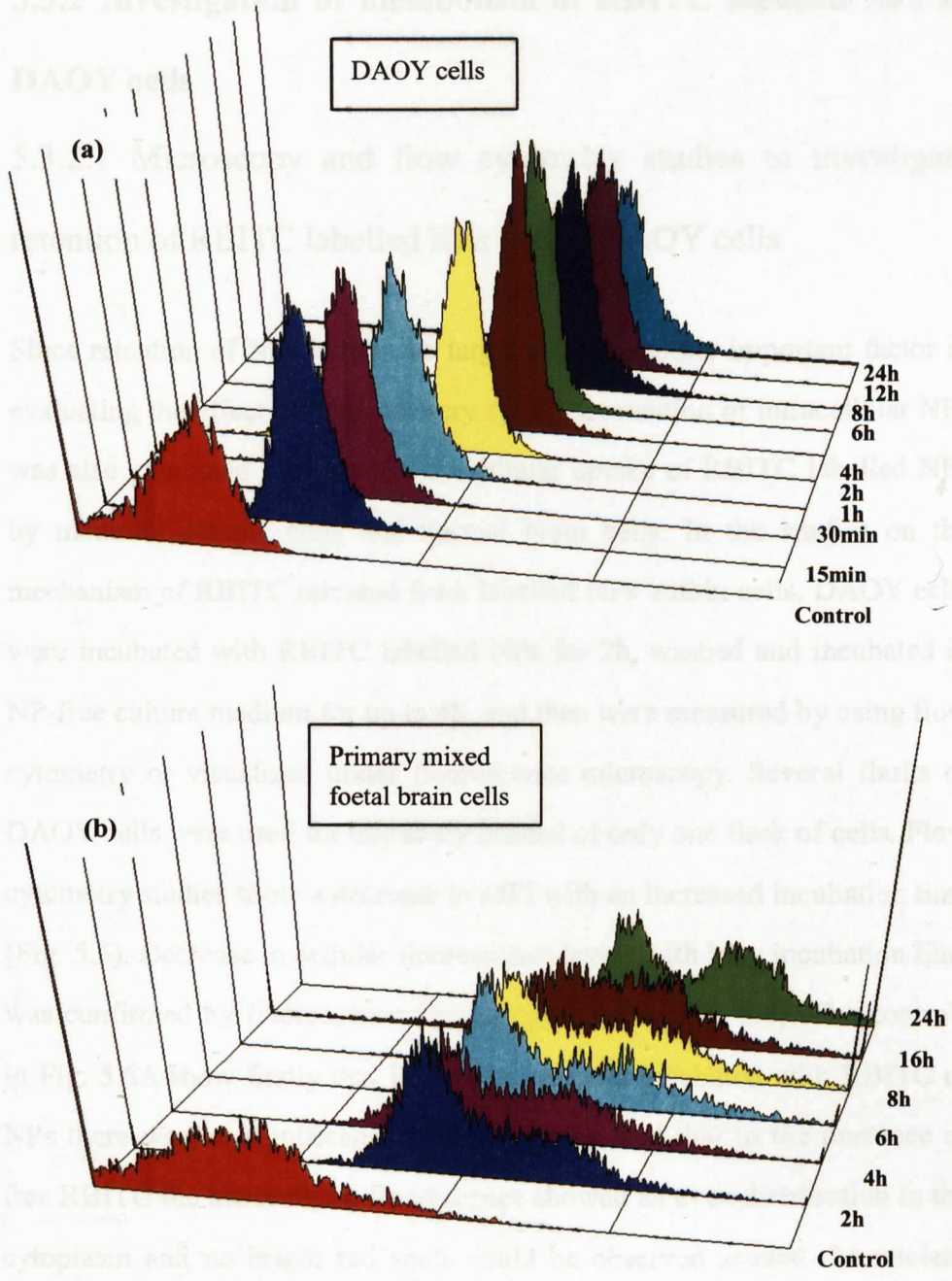

Fig. 5.4 Fluorescence histograms showing time-dependent uptake of RBITC labelled NPs by different types of cells: Cells were incubated with 200 μg/ml /well dose for different time intervals. These intracellular fluorescence histograms represent one experiment to illustrate the raw data summarized in Fig.5.3. (a) DAOY cells; (b) Primary mixed foetal brain cells. **X-axis**: intracellular fluorescence; **Y-axis**: cell number; **Z-axis**: incubation time with RBITC-labelled NP suspension; Control sample: cells incubated with fluorescence-free culture medium

5.3.2 Investigation of metabolism of RBITC labelled NPs in DAOY cells

5.3.2.1 Microscopy and flow cytometry studies to investigate retention of RBITC labelled NPs within DAOY cells

Since retention of NPs within the target cells is another important factor in evaluating the effect of drug delivery systems, retention of intracellular NPs was also examined after studies on cellular uptake of RBITC labelled NPs by medulloblastoma cells and normal brain cells. In the studies on the mechanism of RBITC released from labelled NPs within cells, DAOY cells were incubated with RBITC labelled NPs for 2h, washed and incubated in NP-free culture medium for up to 4h, and then were measured by using flow cytometry or visualized under fluorescence microscopy. Several flasks of DAOY cells were used for this study instead of only one flask of cells. Flow cytometry studies show a decrease in MFI with an increased incubation time (Fig. 5.5). Decrease in cellular fluorescence levels with long incubation time was confirmed by fluorescence microscopy studies (Fig. 5.6). The controls in Fig. 5.6A show firstly that in DAOY cells not incubated with RBITC or NPs there was no significant autofluorescence, and that in the presence of free RBITC the intracellular fluorescence showed an even distribution in the cytoplasm and no bright red spots could be observed around the nucleus after 2h incubation. After 2h incubation time of cells with medium containing NPs, an even distribution of red fluorescence in cytoplasm and some bright red spots in the periphery of cytoplasm were seen (Fig. 5.6c). The cellular levels of even red fluorescence in the cytoplasm decreased with time and the red fluorescence spots migrated to a perinuclear location and then decreased in fluorescence intensity (Fig. 5.6d and e). After 4h of washing time, most of RBITC delivered by NPs had diffused out of the cells.

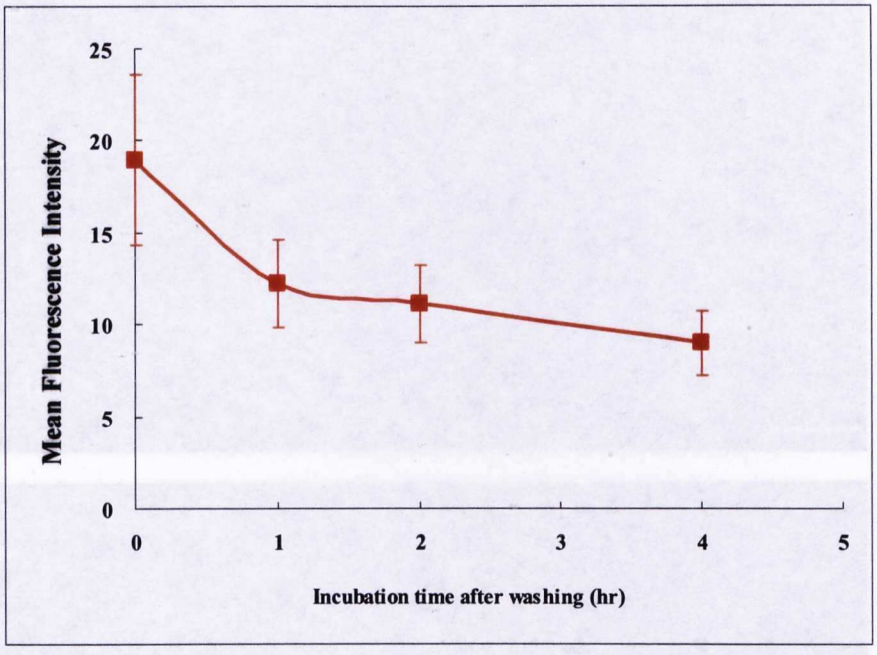

Fig. 5.5 Retention study of RBITC labelled NPs within DAOY cells using flow cytometry. Cells were washed and incubated with NP-free culture medium for different times after incubation with culture medium containing NPs for 2h. Intracellular fluorescence intensity was measured by flow cytometry. Values are mean ± SEM (n=3).

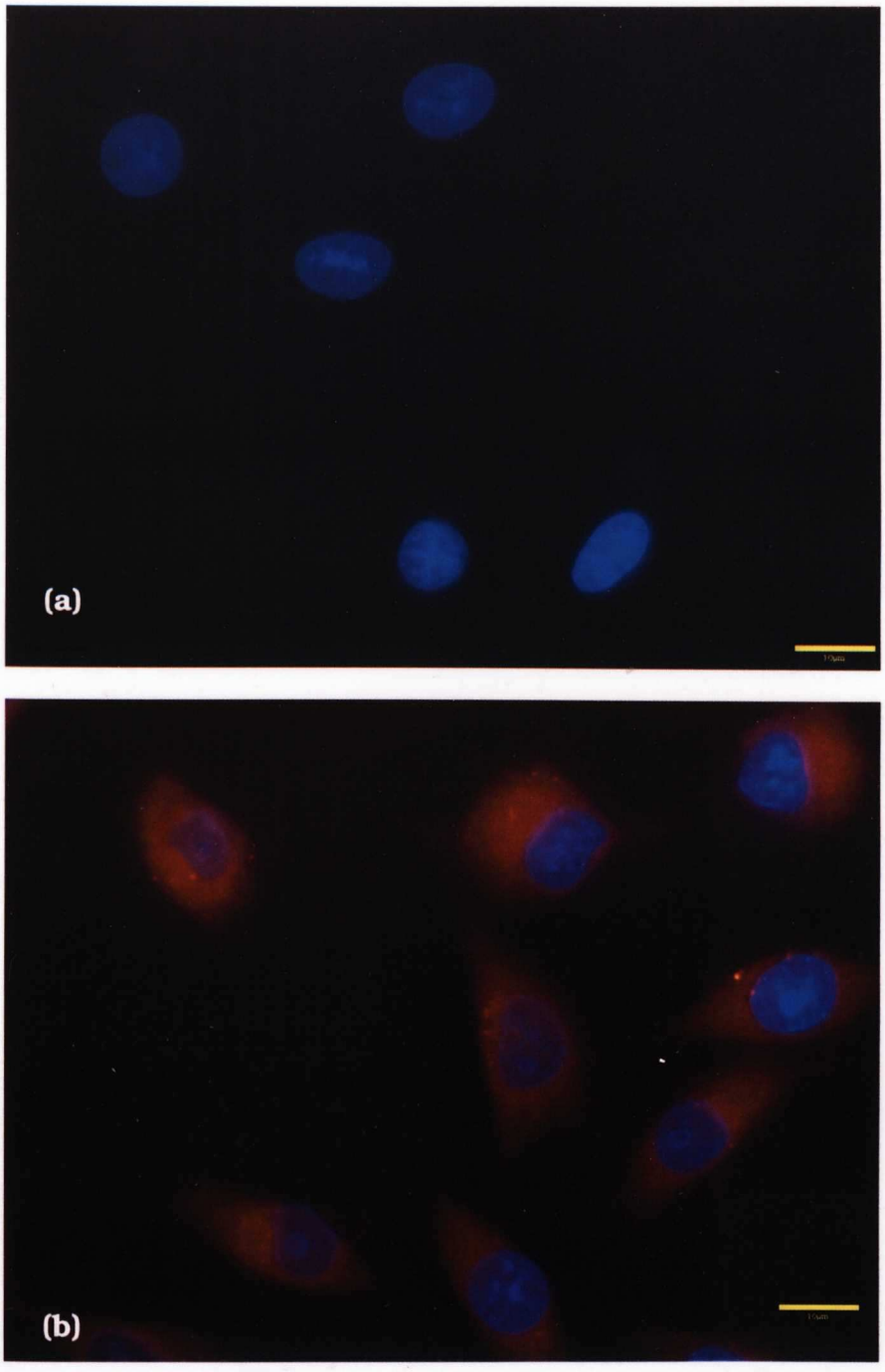

Fig. 5.6A Time series fluorescence micrographs showing the retention of RBITC labelled NPs within DAOY cells. (a) cells were incubated with culture medium without NPs and only stained with DAPI; (b) cells were incubated with culture medium containing free RBITC solution; Scale bar: 10μm.

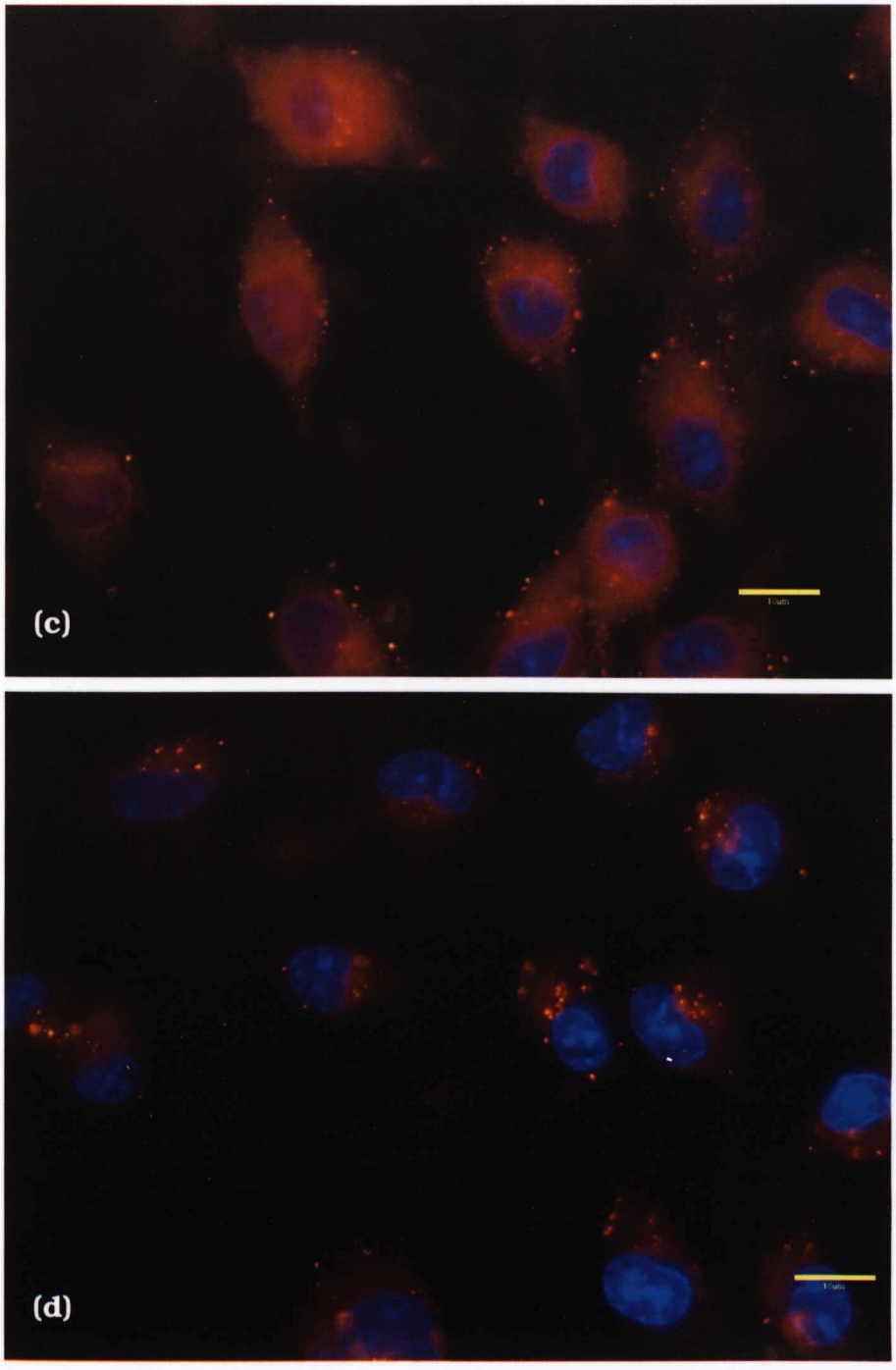

Fig. 5.6B Time series fluorescence micrographs showing the retention of RBITC labelled NPs within DAOY cells. Cells were incubated with culture medium containing RBITC labelled NPs for 2h, then washed and incubated with NP-free culture medium for different time (c) 0h after washing; (d) 2h after washing. Scale bar: 10μm.

5.3.2.2 Ultracentrifuge method to study metabolism of RBITC labelled NPs within DAOY cells

To have a detailed understanding of RBITC labelled NP metabolism and transport, DAOY cell culture medium was also examined to determine drug release using an ultracentrifugation method. After the drug loading period, cells were washed and incubated with NP-free culture medium. For a study of cellular retention of NPs, MFI was measured using flow cytometry (see 5.2.1). At the same time, cell culture medium possibly containing NPs and free RBITC was ultracentrifuged and analyzed to study the release rate of RBITC from NPs and NP transport in DAOY cells. RBITC and RBITC labelled NPs were separated by ultracentrifugation based on the different size and density. Due to the small size of NPs, a high speed centrifugation was necessary. Only the upper supernatant was collected and measured because the NPs were too small to sediment fully. To define the separation efficiency, two types of control were used: one was a culture medium containing 0.4 μg free RBITC and another was cell culture medium containing 800 μg RBITC labelled NPs. The mean data of three separate experiments are shown in Table 5.1.

Incubation time after washing (h)	**Fluorescence**		
	(-) ultracentrifugation	**(+) ultracentrifugation**	**(%) decrease**
1	3.6 ± 0.3	2.8 ± 0.5	21.5 ± 9.6
2	4.8 ± 0.3	4.0 ± 0.5	15.7 ± 6.5
4	5.8 ± 1.4	4.9 ± 1.3	15.0 ± 2.7
Control 1	66.9 ± 9.9	51.7 ± 6.8	22.1 ± 8.0
Control 2	167.0 ± 8.4	72.5 ± 12.0	56.8 ± 5.2

Control 1: DAOY cell culture medium containing free RBITC (0.1μg/ml, 4ml)

Control 2: DAOY cell culture medium containing RBITC labelled NPs (200μg/ml, 4ml)

Values are mean ± SEM (n=3)

Table 5.1 Ultracentrifugation method demonstrating mechanism of RBITC labelled NPs uptake and transported within DAOY cells

Fluorescence data of both control samples showed an obvious decrease after cell culture medium was centrifuged. NPs were not completely separated and only 56.8% NPs were precipitated. 22.1% of free RBITC settled in the bottom of centrifugation tube after 1h of ultracentrifugation time. Data of control samples therefore suggested that 43.2% NPs and 77.9% free RBITC were in the upper layer supernatant after growth medium was ultracentrifuged. Samples of 2h and 4h incubation time after washing had a similar decrease in level, about 15% of fluorescence decreased after ultracentrifugation, while decrease level in sample of 1h incubation time after washing were 1.4 times higher than in samples of either 2h or 4h incubation time after washing.

The relationship between the total amount of RBITC, RBITC diffusing from cytoplasm, and RBITC loaded in NPs can be described by the following equations derived in appendix II:

$$D_0 = \frac{W_c - 0.42W_0}{0.36} \qquad (1)$$

$$P_0 = \frac{0.78W_0 - W_c}{0.36} \qquad (2)$$

Where W_0: the total amount of RBITC in mixture growth medium before ultracentrifugation

D_0: the amount of RBITC diffusing from DAOY cells in mixture growth medium before ultracentrifugation

P_0: the amount of RBITC encapsulated by NPs in mixture growth medium before centrifugation

W_c: the total amount of RBITC in supernatant after ultracentrifugation

Table 5.2 shows the results of NPs recycled into growth medium and free RBITC diffusing into cell culture medium calculated from the data in Table 5.1 using these equations. It was found that a small amount of NPs recycled to the culture medium only in the first 1h of incubation time after washing but not at the later incubation time. So recycled NPs only accounted for 12.7% of total NPs taken up by DAOY cells. There were 39.8%, 66.7% and 86.6% RBITC released from NPs after 1h, 2h, and 4h of incubation time after washing, respectively.

Incubation time after washing (h)	RBITC labelled NP recycled (%)*	Free RBITC release (%)**
1	12.7 ± 3.3	39.8 ± 17.9
2	0	66.7 ± 16.7
4	0	86.6 ± 27.5

* (% w/w) RBITC labelled NP recycled= amount of RBITC inside NPs in supernatant ×100/amount of RBITC inside NPs in DAOY cells after 2h of incubation time.

** (%w/w) free RBITC release = amount of free RBITC in supernatant ×100/ amount of RBITC in DAOY cells after 2h of incubation time.

Values are mean ± SEM (n=3)

Table 5.2 Ultracentrifugation method showing endocytosis of RBITC labelled NPs by DAOY cells

5.4 DISCUSSION

5.4.1 Cellular uptake of RBITC labelled NPs by cells in 2-D monolayer culture

Generally, colloidal and macromolecular carriers are taken up into cells either by phagocytosis, by pinocytosis, or by receptor mediated endocytosis. Once those carriers attach on the plasma membrane, the lipid bilayer of cell membrane invaginates forming free cytoplasmic vesicles around colloidal or macromolecular carriers. The vesicle fuses with early endosome, which is slightly acidic pH (pH ≈6.0-6.8), and then traverses to the perinuclear cytoplasm and becomes a late endosome and fuses with primary lysosomes to become a secondary lysosome compartment, which has a lower pH (pH ≈4.5-5) and about 40 acid hydrolases (Avers *et al*, 1976, and Mellman *et al*, 1996), and thus digests colloid or macromolecular carriers. After 2h of incubation time, it was observed that big bright red fluorescent spots were located in the perinuclear region of cells (Fig. 5.1a and c), which is the location of the lysosome within cells (Brown, 1974). This strongly suggested that RBITC labelled NPs were sorted into lysosome compartments.

Flow cytometry studies showed that RBITC labelled NP uptake by DAOY cells and brain cells was dependent on dose of NPs and incubation time. It also showed that there were two plateaus in uptake by DAOY cells and mixed brain cells had similar uptake stages as DAOY cells had (Fig. 5.3). This suggested that cellular uptake of NPs was primarily mediated by a specific endocytosis process due to their saturable uptake pattern.

To give some explanation of this complex pattern of uptake, we need to consider the processes involved in endocytosis in more details. Endocytosis are complex processes, which involve vesicles forming and invaginating into cytoplasm, material being sorted into and digested in lysosome, internalized membrane, membrane-bound ligands and some molecules recycled back to the cell surface of origin and degradative structures evolving into residual bodies. Membrane recycling is a closely related process involved in maintenance of surface area and volume of the entire cell as well as of various intracellular compartments on the protein transport pathway (Van Deurs *et al.*, 1989). Evidence has accumulated that a number of physiological ligands and cell surface receptors are rapidly recycled from the endosomal system (Anderson *et al.*, 1982; Goldstein *et al.*, 1985; and Hopkins, 1983, 1986) and few via secondary lysosome and Golgi complex (Muller *et al.*, 1983, and Van Deurs *et al.*, 1989). The Golgi complex is a way-station in the cell through which some proteins are modified chemically and wrapped in a membrane before exiting the cell. One of the packaged structures produced at the Golgi membranes is the primary lysosome (Avers, 1976). This means that membrane and digestive enzymes of endososome-lysosome system are transported from the Golgi complex to the endosomes-lysosomes. Thus the different range in deviation of NP uptake and two saturation stages of NP uptake could be attributed to cells being at different stages, which might affect the rates of membrane recycling, the amount of lysosomes produced in the cells, distribution of lysosomes in the cytoplasm, and mature stages of lysosomes, which influence the number and type of digestive enzymes in lysosomes.

The MFI of mixed foetal brain cells was about 2 times higher than DAOY cells. The explanation of this discrepancy is most likely due to differences in cell types. For instance, in liver, roles and properties of lysosomes appreciably differ between hepatocytes and Kupper cells, both of which are

cell types with quite prominent populations of lysosomes (Holtzman, 1989). The relatively larger deviation of cellular uptake in mixed foetal brain cells was mostly due to differences between different cell types within the brain cell population.

Flow cytometry studies of free RBITC uptake showed that the contribution of RBITC to the MFI was very low and only accounts for 1% of overall intracellular fluorescence intensity. Combining with the microscopy studies, it confirms that the MFI of DAOY and mixed brain cells was mainly due to the cellular uptake of RBITC labelled NPs.

Since light is scattered by cells providing some information regarding the morphology of cells when individual cells pass through detector point, two different types of histogram were observed in flow cytometry studies (Fig. 5.4). DAOY cells having a narrow peak was because they are single type of cell, which has a homogeneous morphology while mixed brain cells were dissociated from foetal rat brain tissue and consist of neurons and supporting cells with various sizes. Flow cytometry studies also indicated for the mixed brain cells that different cells within the population had different rates and capacities for NP uptake. In contrast, the cell lines were quite homogenous in the rate of NP uptake.

Confocal fluorescence micrographs of U937 cells appeared to show NPs adsorbed on the cell surface. However, dose-dependent uptake studies showed MFI of U937 was increased with an increase of NP concentration. This suggested that RBITC labelled NPs were in fact taken up by these cells.

5.4.2 Investigation of metabolism of RBITC labelled NPs in DAOY cells

As discussed in studies of NP uptake, NPs were taken up by DAOY cells, probably sorted into the lysosome compartment, and were then degraded allowing RBITC released from NPs to diffuse into the cytoplasm. Thus fluorescence micrographs (Fig. 5.6A) of DAOY cells cultured in cell culture medium containing free RBITC represented RBITC diffusion into cytoplasm via the plasma membrane. The time-series fluorescence images of cells incubated with NP showed intracellular fluorescence intensity level decreased with incubation time of cell with fresh culture medium. The MFI was about 42% and 52% lower 2h and 4h after washing, respectively compared with 0h after washing. Considering the fluorescence micrograph of 0h after washing, it was suggested that most NPs could be degraded within 2h and that free RBITC diffusion into external culture medium via cell membrane was fast.

The previous experiments demonstrated that after uptake of NPs, fluorescence disappeared from the cells. We wished to quantitate the level of fluorescence released and to ascertain whether the released fluorescence was free drug or NP. Isothiocyanate groups of RBITC react with an amino group on the protein in DAOY cell culture medium. This results in a gradient suspension of free RBITC after ultracentrifugation. Thus free RBITC was used as one of controls in this study to quantitate the fluorescence lost from the upper supernatant due to precipitation of protein bonded RBITC after ultracentrifugation if released fluorescence was free RBITC. RBITC labelled NP suspension also used as another control was because the size of NP is too small to effectively separate even if a high speed centrifugation was used. Table 5.1 showed that there are about 7% different in fluorescence

between 1h after washing and 2h after washing but no difference was observed in samples of 2h after washing and 4h after washing. These suggested that 7% difference in fluorescence was due to the loss of NPs from upper supernatant after ultracentrifugation. It was also found that there was about 15% decrease in fluorescence in samples of 2h after washing and of 4h after washing. Considering all of the samples, it suggested that this 15% decrease in fluorescence was caused by the disappearance of free RBITC from upper supernatant. Thus it could be deduced: 1) that initially a high cytoplasmic level of dye in the first 1h incubation with NP-free culture medium was present presumably due to digestion of NPs and release of fluorescence via the lysosomal membrane, 2) that some NPs were recycled into the extracellular medium during the first 1h after washing, and 3) that recycled NPs were re-taken up by DAOY cells in the following 1h or 3h incubation time in the NP-free culture medium. It also suggested that fluorescence in the medium mostly resulted from free RBITC, which was released from NPs and then diffused out of cells via the plasma membrane. It is noted in the literature that cell membrane cycles between the cell surface and intracellular endocytic compartments (Steinman *et al.*, 1976, Gibbs *et al.*, 1984, and Van Deurs *et al.*, 1989). Steinman *et al.* reported that for macrophages with a fixed endocytic rate, endocytosing 3.1% of their surface area per minute, no cell shrinkage or increase in total surface area of intracellular vacuoles was observed within a 3h period. They therefore concluded that both endocytosis and exocytosis are proceeding simultaneously (Steinman *et al.*, 1976).

Table 5.2 shows that few NPs were recycled into growth medium and also confirmed that recycled NPs were re-taken up by DAOY cells with longer incubation time. The cumulative percentage of RBITC in culture medium was increased with an increase of incubation time with fresh culture medium. The drop in MFI (Fig. 5.5) closely matched the increased

appearance of the RBITC in the culture medium. Around 87% RBITC measured in the culture medium after 4h incubation time suggested that NPs were quickly degraded intracellularly. This is very different from the NPs incubated with cell culture medium where RBITC release was very slow (see Chapter 4). This was because NPs appear to be sorted into lysosome compartments after they were taken up by cell. The low pH and presence of enzymes in the lysosome compartments would accelerate degradation of the ester bonds of the PGA polymer and cause the fast release of RBITC intracellularly.

5.5 SUMMARY

To evaluate PGA NPs as a useful delivery system for brain tumour therapy, cellular uptake, intracellular distribution, retention and metabolism of RBITC labelled NPs have been examined in DAOY cells (medulloblastoma), and U937(macrophage) cell lines, and mixed foetal brain cells in 2-D cell culture.

Uptake of RBITC labelled NPs in DAOY cells, mixed foetal brain cells and U937 cells

Microscopy studies demonstrated that NPs were taken up by DAOY cells, mixed foetal brain cell, and U937 cells. The intracellular position of NPs suggested that NPs were sorted into lysosome compartments after they were taken up by cells. Flow cytometry studies showed cellular uptake of NPs were dependent on the incubation time and dose of NPs. Flow cytometry and time series NP uptake in DAOY cells indicated that NP uptake was probably mediated by specific endocytic process. The higher cellular uptake

of NPs in mixed foetal brain cells reflected different kinetics of cellular uptake of NPs between DAOY cells and mixed foetal brain cells.

Retention and metabolism of RBITC labelled NPs in DAOY cells

Results from studies in this chapter suggested that after uptake, a small fraction of NPs recycle back to the outside of cell, whereas most of NPs entered later endosomes and secondary lysosomes. Recycled NPs were re-taken up in the following 2h incubation time. Comparing the intracellular release of fluorescent dye from NPs with release of fluorescent dye from NPs in cell culture medium, it was found that intracellular release of RBITC was about 30-40 times faster in cells than that in cell culture medium. The rapid decrease of MFI suggested poor intracellular fluorescent dye retention when pre-loaded cells were incubated with NP-free medium. However it should be realized that a constant presence of NPs next to or near cells and NP concentration outside the cells may reduce the rate of elimination of drug from cells.

As many researchers reported that cell culture dimension had an influence on the cell, such as shape and growth pattern of single cell or one group cells, signal transmission between cells, and so on, in the following chapter cellular uptake of NPs will be examined in DAOY aggregates, mixed brain aggregates and brain slice culture.

CHAPTER 6

EVALUATING UPTAKE OF RHODAMINE B ISOTHIOCYANATE LABELLED NANOPARTICLES IN THREE DIMENSIONAL CELL CULTURE

6.1 INTRODUCTION

Traditionally, cells are predominantly cultured using 2-D tissue culture methods. Nowadays, more and more researchers are realizing the limitations of 2-D cell culture because cells *in vivo* are exposed to a 3-D tissue, in which cell-cell and ECM interactions, and multiple cell types exist. In the living animal, neurons arise with a tree-like series of branches, the dendrites and nerve fibre or axon. The axon may be short (a few tens of micrometres) or long (several metres in large animals) (Brown, 1991). Moreover, neurons maintain a high density, for example, in human cortex, there are approximately 10^5 neurons per mm^3 (Kandel *et al.*, 1991).

Conventional cells in 2-D culture systems are typically grown at low density to promote visibility, which may not support such extensive growth. In contrast, 3-D cell culture methods offer a distinct advantage over a conventional 2-D cell culture model. Use of 3-D culture systems allow for the introduction of 3-D matrices of natural and/or synthetic fibre scaffolds, which may eventually emulate the architecture and environment of neurons *in vivo*. In addition, neurons are a type of cell whose normal function is

highly dependent on its interaction with other cells. Over many decades researchers found that glial cells play an important role during neuronal growth. Glial cells can influence proliferation and differentiation of neurons (Levitt *et al.*, 1980), and secrete diffusible factors that trophically support neurons (Banker, 1980; Selak *et al.*, 1985).

Investigations of differences in the properties of cells in 2-D versus 3-D cell culture were first made by cancer researchers. They found that the fundamental differences are related to integrin signaling (Pouliot, 2000, and Lefevre *et al.*, 2001), cell polarity (Lefevre *et al.*, 2001), and apoptosis, which have a profound influence on neoplastic properties of tumour cells and thus lead to different responses of cancer cells towards therapeutic drugs between 2-D and 3-D cell culture (Lefevre *et al.*, 2001, and Sahai *et al*, 2003). Compared with antiproliferative effects of retinoic acid loaded liposomes in 2-D and 3-D tumour cell culture, it was found that retinoic acid loaded lipsomes had enhanced antiproliferative effectiveness in 3-D culture compared to in 2-D cell culture (Sacks *et al.*, 1992)

Although a variety of systems have been developed to mimic physiological 3-D environments (Cukierman *et al.*, 2002), a recent approach involves using tissue- or cell culture-derived 3-D matrices for analyzing the behaviour of migratory cells (Cukierman *et al.*, 2001). The logic behind this approach is that cells don't normally encounter a pure collagen matrix. On the contrary, they exist in complex environments comprised of multiple molecules and various types of cells. Recent findings indicated that cells respond differently from tissue-or cell culture derived 3-D matrices compared to pure collagen gels or flat tissue culture substrates (Cukierman *et al.*, 2001).

The cell culture dimension not only plays an important role in cell morphology and function but also could influence uptake of drug delivery systems by target cells (Sacks *et al.*, 1992) and penetration of drug delivery systems to the target cells (Kostarelos *et al.*, 2004). So far few references in the field of drug delivery area have been found using 3-D cell culture models to evaluate drug delivery systems. In this chapter, uptake of RBITC labelled NPs was studied in 3-D cell culture model. Normal and malignant brain aggregates, and organotypic brain slices were used as three-dimensional cell culture method.

6.2 METHODS

6.2.1 Routine culture of spherical aggregates and organotypic slices (see 2.2.3.3 and 2.2.3.4)

6.2.2 Cellular uptake of RBITC labelled NPs

Aggregates

After both DAOY aggregates and mixed neonatal brain aggregates were prepared by a rotation method (see 2.2.3.3), the growth medium was replaced with fresh culture medium containing NP suspension (200μg NPs/0.5 $\times 10^6$ cells) and incubated for a range of times (from 2hr to 24hr). At the end of the incubation period, aggregates were washed three times with PBS and incubated with trypsin-EDTA (1ml) at 37°C for 15min to allow aggregates to detach. Individual cells were then gently dissociated from

aggregates by using a glass Pasteur pipette and then prepared for flow cytometry.

For microscopy investigation, both DAOY aggregates and mixed foetal brain aggregates were incubated with NP suspension (200 μg/ 0.5 $\times 10^6$ cells) in growth culture medium for 4h, 8h, and 24h or 48h. 30min before the end of incubation time, aggregate suspension (0.3ml) and fresh growth medium (0.7ml) was transferred into a well with a PDL coated coverslip in 24-well plates to allow cells to attach onto the coverslip. The cells were rinsed three times with PBS and fixed in 1% freshly prepared PFA.

Organotypic brain slice

Maintaining cerebral cortex on culture medium for 14 days, NP (200μg) suspension was added directly on the top of slices and incubated with slices for 24h. LysoTracker Yellow (50nM) was added to each sample 1h before the end of incubation time. Cerebral cortex slices were washed three times with PBS and fixed in 1% freshly prepared PFA for microscopic study.

6.2.3 Immunohistochemisty

Liver from adult Wistar rat was used as positive and negative control. After liver tissue was rapidly removed from the rat, it was frozen in liquid nitrogen-cooled isopentane, and then cut into 20 μm thick sections using a Leica Cryostat (Leica CM3050 S, Bucks, UK). After brain cerebral cortex slices were incubated with RBITC labelled NPs and LysoTracker (50nM), slices were washed with Tris-HCl buffer (10mM, pH 7.6) three times. Live cryostat-cut sections and brain cerebral cortex slices were fixed in the

Periodate-lysine-paraformaldehyde fixative of McLean and Nakane (McLean and Nakane, 1974) for 20min at room temperature and then were processed for immunohistochemistry. Both sections were hydrated in Tris-HCl buffer, rinsed in 0.025% Triton-X100 in Tris-HCl, blocked with 10% Normal Horse Serum (10% Normal Horse Serum and 1% Bovine Serum Albumin (BSA) in Tris-HCl), and incubated overnight with mouse anti-rat CD11B primary monoclonal antibody (1:200 in Tris-HCl including 1% BSA, Autogen Bioclear Ltd., Wilts, UK) at 4°C. The sections were generally washed with Tris-HCl and subsequently incubated with fluorescein horse anti-mouse IgG(H+L) secondary antibody (1:1000 in Tris-HCl with 1% BSA, Vector Laboratories, USA) for 1h at room temperature. Sections then were washed extensively in Tris-HCl and deionied water, and prepared for fluorescence microscope study.

6.2.4 Flow cytometry (see 2.2.4)

6.2.5 Microscopic studies (see 2.2.5)

6.2.6 Calculation of penetration of NPs into spherical aggregates and slices

After Aggregates and slices were incubated with NPs for 2h or 24h, they were visualized under confocal fluorescence microscopy in the z-dimension. MFI of each optical slice in z-dimension was calculated using LCS Lite 2.61.1537 (Leica Microsystems, Lecia, UK). Then the penetration of NPs

was calculated as follows:

$$\text{Penetration (\%)} = \frac{\text{Optical slice number where MFI rises rapidly above background}}{\text{Number of optical slices in z-dimension}} \times 100$$

6.2.7 TEM study

After organotypic brain cerebral cortex slices were cultured for 14 days, they were incubated with 200μg ferritin-loaded NPs for 24h and 48h, and were rinsed with PBS three times. The slices were fixed in 2% PFA and 3% glutaraldehyde in 0.1M cacodylate buffer for 1hr and then were postfixed in 1% osmium tetroxide for 1h. The slices were dehydrated in a graded series of ethanol solutions (60%, 80%, and 100%). They were then soaked in a mixture of 100% 1,2-Epoxypropane and Agar embedding resin at a 1:1 ratio overnight at 4°C, after which they were soaked three times in fresh neat Agar resin for 2h. The slices were placed in embedding wells with fresh neat Agar resin, and wells were placed in a vacuum oven at 60°C for at least 48h for polymerization of the resin. The polymerized blocks were cut into thin sections (80-100nm thick). Then sections were placed on formvar-coated copper grids, stained with an aqueous solution of 2% uranyl acetate for 15 min, washed briefly in water, stained with Reynolds lead citrate for 5 min, and finally washed in water before visualization. Samples were imaged under TEM (JEOL JEM100) with magnifications ranging from 20,000 to 300,000x.

6.3 RESULTS

6.3.1 Uptake of RBITC labelled NPs by DAOY and mixed foetal brain spherical aggregates

6.3.1.1 DAOY and mixed foetal brain spherical aggregate culture

After dissociation of foetal whole brain or harvesting DAOY monolayer cells, cell suspensions were seeded at 1×10^6 cells/ml in rotation culture (see 2.2.3.3). These cultures formed as spherical aggregates within 24h (Fig. 6.1 (a) and (b)). To visualize aggregates under the confocal microscope, mixed foetal brain aggregates were transferred into a 24-well plate with PDL coated coverslips after 1 day of culture by the rotation method, and then cultured for 24h in a 24-well plate (Fig. 6.1 (c)).

As can be seen in Fig 6.1, the aggregates were well formed and individual cells could still be distinguished in the periphery of the aggregates. Mixed foetal brain aggregates appeared larger in size and denser with less translucence under a light microscope than DAOY aggregates. Mean diameters were 120μm for mixed foetal brain aggregates and 100μm for DAOY aggregates. When mixed foetal brain aggregates were cultured in a 24-well plate for 24h, some cells on the edge of aggregate grew onto the PDL coated coverslip, in which the shape of single cells could be clearly seen, and cells in the middle of aggregate stayed within the spheroid shape.

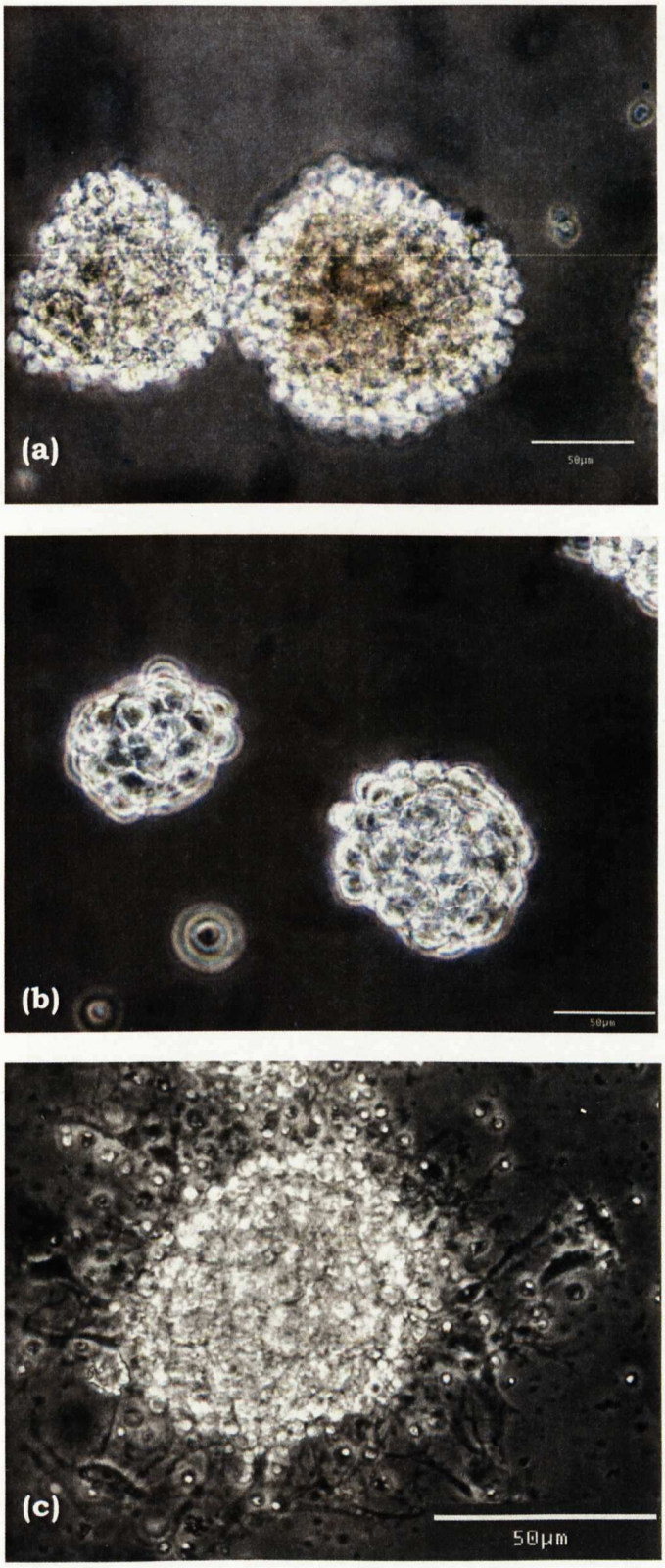

Fig. 6.1 Phase-contrast micrographs illustrating the aggregates formed by the rotation method. (a) mixed foetal brain aggregates grown for 1day; (b) DAOY aggregates grown for 1 day; (c) mixed foetal brain aggregates cultured in a 24-well plate with PDL coated coverslip for 1 day after aggregates grown by the rotation method for 1day. Scale Bar: 50μm

6.3.1.2 Localisation and intracellular distribution of RBITC labelled NPs in mixed foetal brain spherical aggregates

As shown in Fig.6.2, most of the red fluorescence was colocalised with LysoTracker Yellow, so the yellow fluorescence surrounding the nucleus changed into orange fluorescence. It also shows that some red fluorescence dots, which did not associate with yellow fluorescence dots, far way from nucleus and were therefore in the interstitial compartment (white circle).

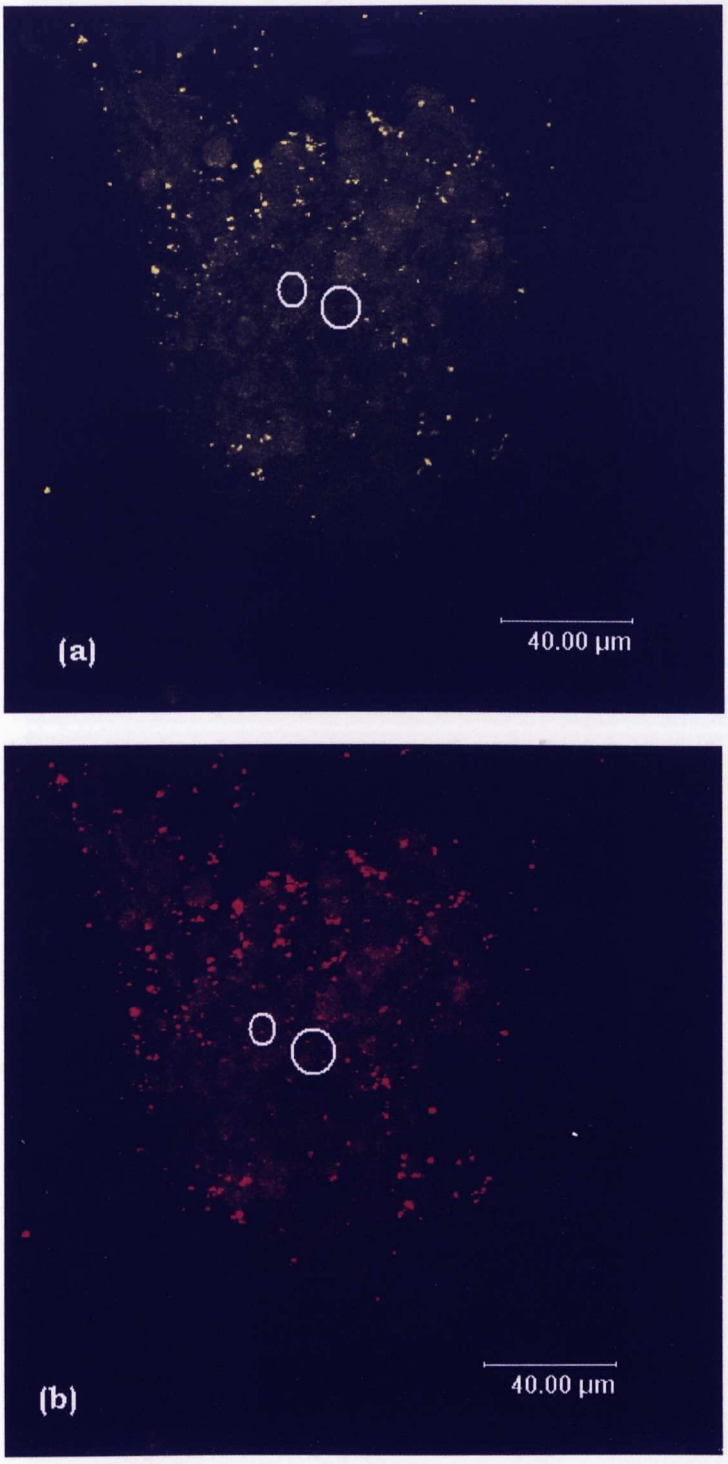

Fig. 6.2A Confocal images showing localisation of RBITC labelled NPs within mixed foetal brain aggregates: (a) yellow fluorescence from LysoTracker, a marker for lysosome; (b) red fluorescence from NPs. As can be seen, the majority of NPs were taken up by brain cells and into lysosome compartment and few NPs were localized in the interstitital compartment (white circle).

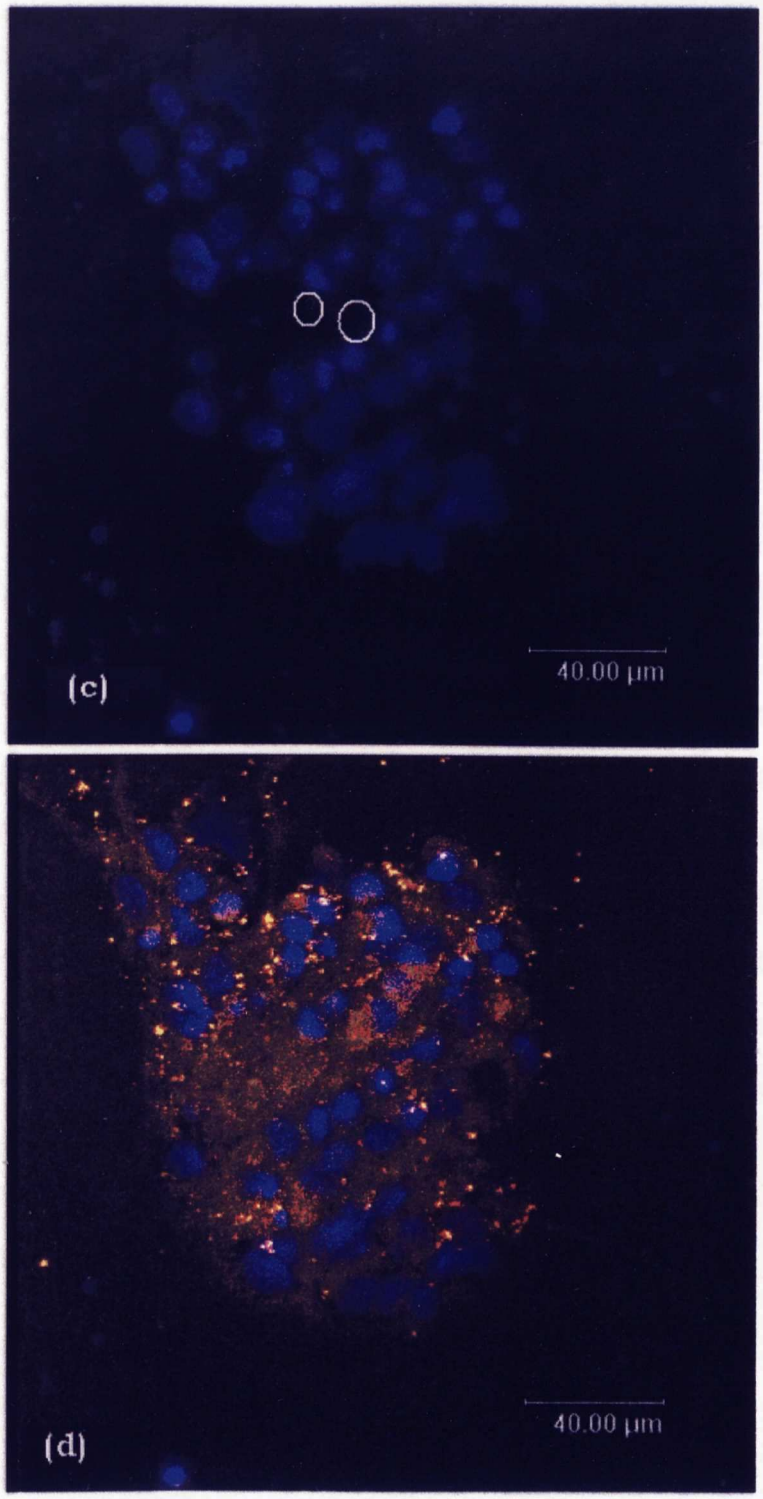

Fig. 6.2B Confocal images showing localisation of RBITC labelled NPs within mixed foetal brain aggregates: (c) blue fluorescence from DAPI, a marker for nuclei; (d) co-localisation of red with yellow and blue fluorescence. As can be seen, the majority of NPs were taken up by brain cells and into lysosome compartments.

6.3.1.3 Time-dependent uptake of RBITC labelled NPs by aggregates using flow cytometry

Viability of cells dissociated from mixed foetal brain aggregates or DAOY aggregates was studied before the flow cytometry technique was used for measurement of RBITC labelled NP taken up by aggregates. After individual cells were gently dissociated from aggregates, equal volumes of individual cell suspension were immediately mixed with 0.4% trypan blue before they were assessed by light microscopy. The viabilities of individual cells were 98%-100%. Individual cell suspensions were then transferred into a 25 cm^2 tissue culture plate and cultured at 37°C and 5% CO_2 for 24h. As shown in Fig. 6.3 and Fig. 6.4, individual DAOY cells and brain cells appeared to retain a high level cellular integrity after trypsin treatment and mechanical dissociation. All DAOY cells (Fig. 6.3) attached on the tissue culture plate were flat in shape and the clear cellular outlines could be seen. Foetal brain cells (Fig. 6.4) also re-attached onto the tissue culture plate on the following day. Glial cells showed bipolar flat shape and spread well. Several neurons grew on the surface of flat-shaped glial cells.

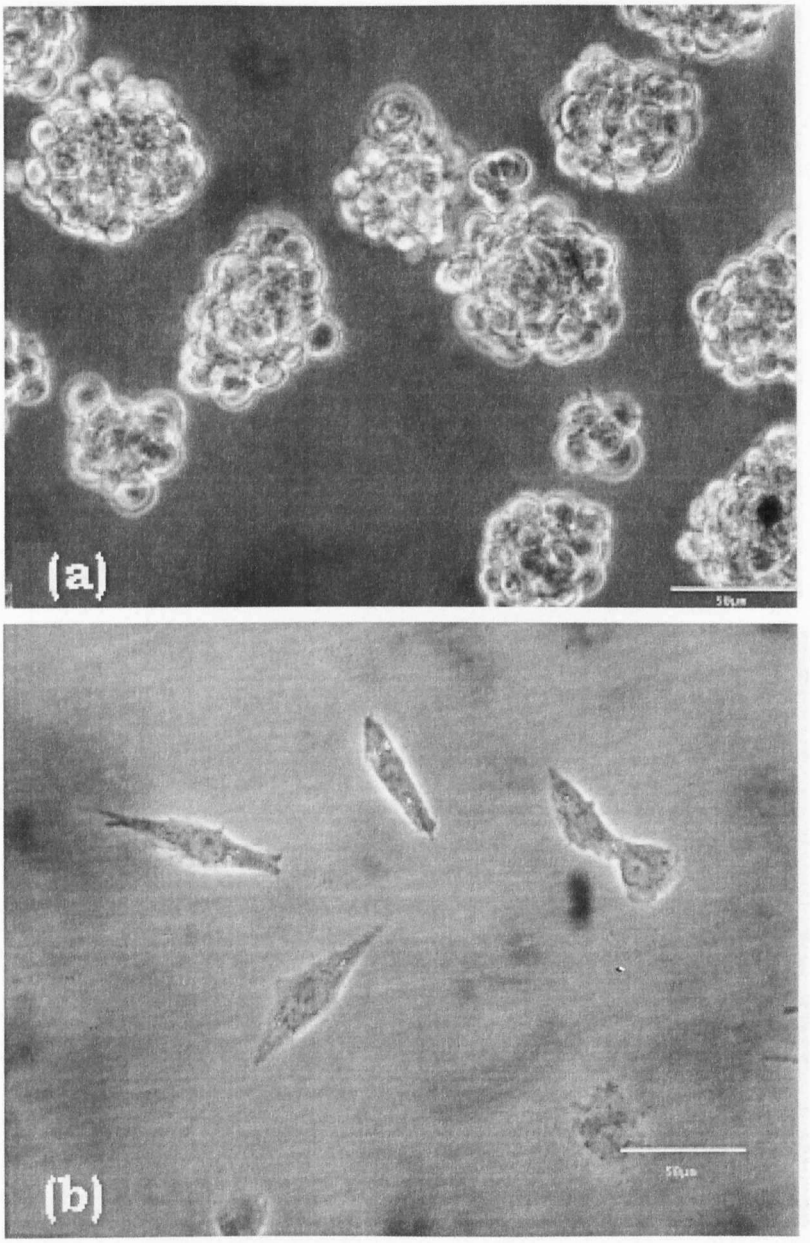

Fig. 6.3 Phase-contrast micrographs demonstrating viability of DAOY cells for flow cytometry study: DAOY aggregates were dissociated into individual cells after treatment with trypsin-EDTA and then the cell suspension was cultured in a tissue culture plate at 37°C and 5% CO_2 for 24h. (a) DAOY aggregates; (b) individual DAOY cells. As shown, the DAOY cells were flat and spread well on the following day. Scale bar: 50μm.

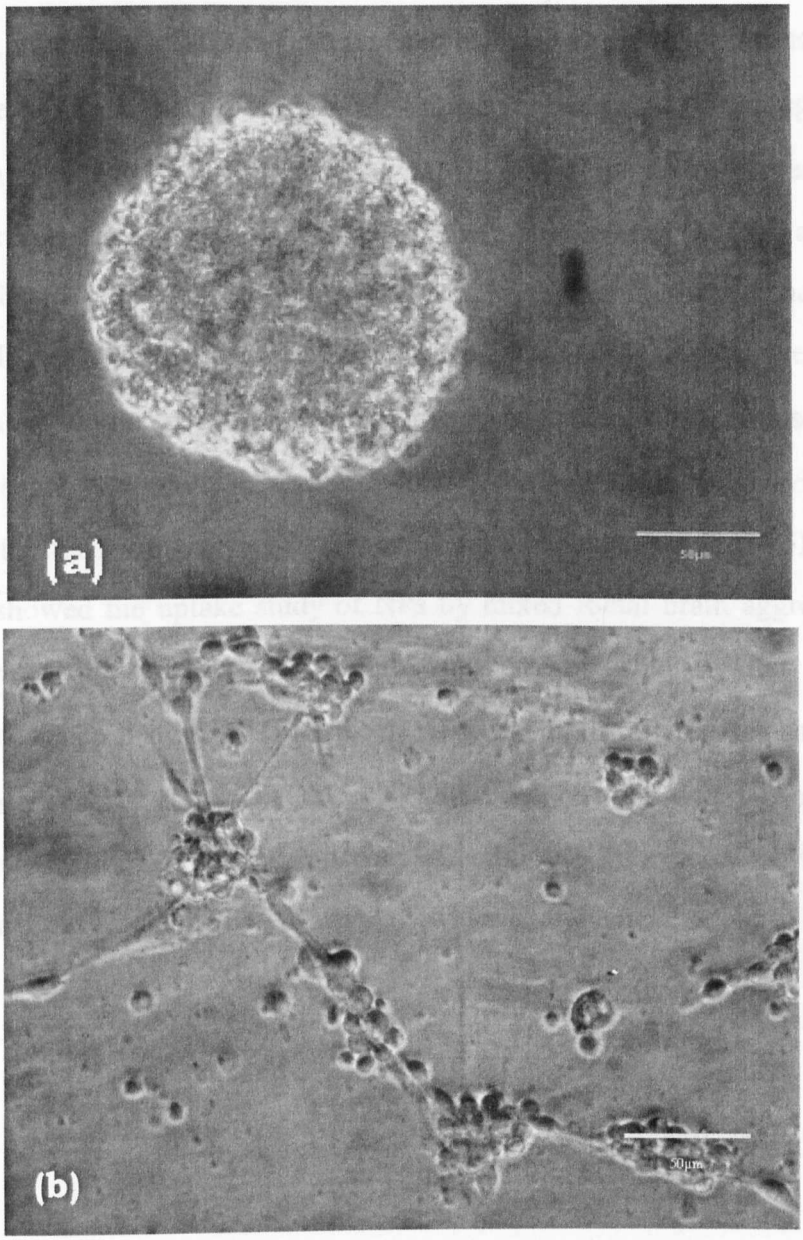

Fig. 6.4 Phase-contrast micrographs demonstrating viability of mixed foetal brain cells for flow cytometry study: Mixed foetal brain aggregates were dissociated into individual cells after treatment with trypsin-EDTA and then the cell suspension was cultured in a tissue culture plate at 37°C and 5% CO_2 for 24h. (a) mixed foetal brain aggregates; (b) individual foetal brain cells. As shown, glial cells were flat and spread well, and neurons aggregated on glial cells as substrate on the following day. Scale bar: 50μm.

After aggregates were incubated with RBITC labelled NP suspension for various times, they were dissociated into individual cells and then immediately assayed by flow cytometry. In the cellular uptake study (Fig. 6.5), intracellular MFI in both types of cell in 3-D culture increased with an increase of incubation time. In the uptake study of DAOY aggregates (Fig. 6.5A, and Fig. 6.6), intracellular MFI reached its plateau after 6h. The fluorescence histogram of the control sample of DAOY aggregates incubated with fluorescence-free cell culture medium was a narrow and single peak. The narrow peak was because DAOY aggregates were formed from a single population of homogeneous cells. In contrast, DAOY aggregate samples incubated with NP suspension showed broader distributions with varying peaks and shoulders over time. Fig. 6.5B and Fig. 6.6 showed the uptake study of NPs by mixed foetal brain aggregates. As shown, MFI reached a maximum and entered plateau after 16h. The fluorescence histogram (Fig. 6.5B) of foetal brain aggregates sample was broader than that of DAOY aggregates, which was due to foetal brain aggregates formed by several types of cells. The fluorescence histogram at other times also appeared to have a broader character.

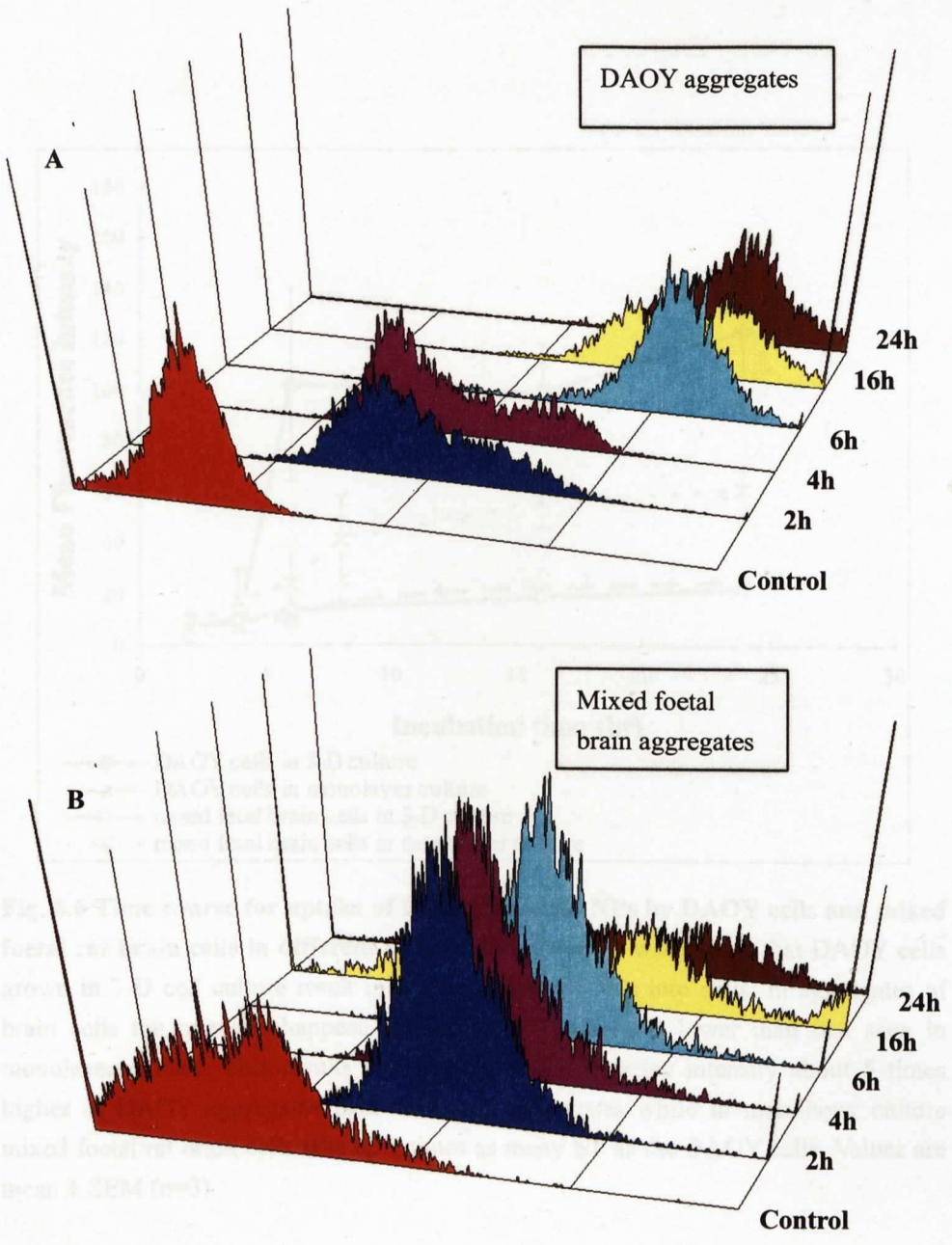

Fig. 6.5 Fluorescence histograms showing RBITC labelled NPs taken up by aggregates: After aggregates were incubated with NP suspension for various times, they were dissociated into individual cells and immediately assayed by flow cytometry. These intracellular fluorescence histograms are from one experiment which illustrates the raw data summarized in Fig. 6.6. (a) DAOY aggregates; (b) Mixed brain foetal brain aggregates. **X-axis**: intracellular fluorescence; **Y-axis**: cell number; **Z-axis**: incubation time with NP suspension; Control sample: aggregates incubated with fluorescent dye free culture medium

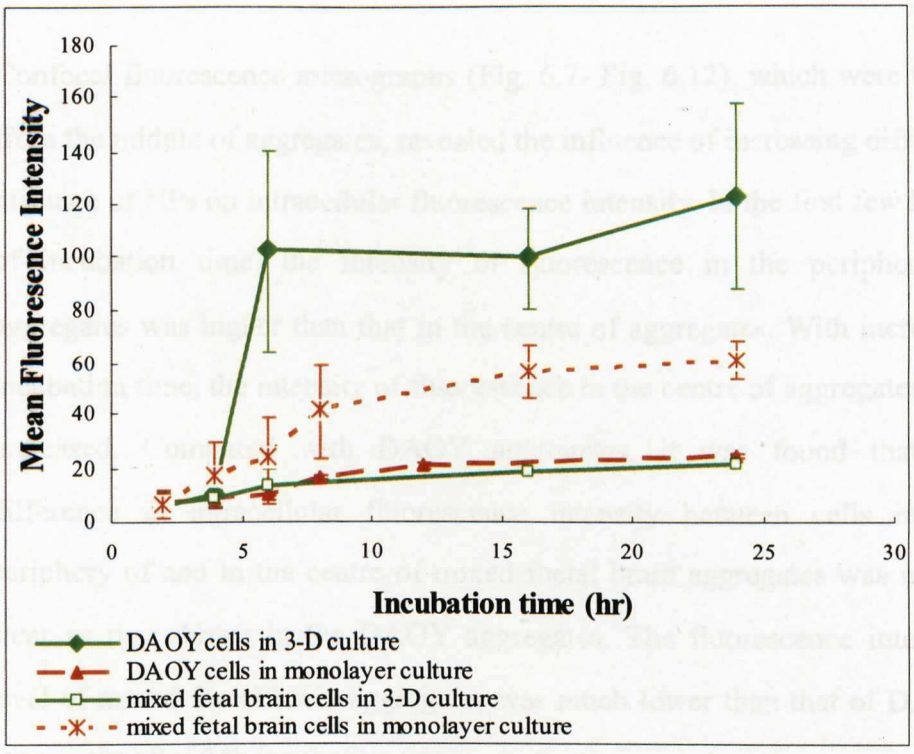

Fig. 6.6 Time course for uptake of RBITC labelled NPs by DAOY cells and mixed foetal rat brain cells in different culture dimension. It was shown that DAOY cells grown in 3-D cell culture result in a great uptake of NPs into cells. In aggregates of brain cells the opposite happens, uptake in 3-D culture is lower than that seen in monolayer culture. This results in intracellular fluorescence intensity about 5 times higher in DAOY aggregates than brain cell aggregates while in monolayer culture mixed foetal rat brain cells take up 2 times as many NP as the DAOY cells. Values are mean ± SEM (n=3).

6.3.1.4 Time-dependent uptake of RBITC labelled NPs by aggregates using confocal fluorescence microscope

Confocal fluorescence micrographs (Fig. 6.7- Fig. 6.12), which were taken from the middle of aggregates, revealed the influence of increasing diffusion distance of NPs on intracellular fluorescence intensity. In the first few hours of incubation time, the intensity of fluorescence in the periphery of aggregates was higher than that in the centre of aggregates. With increased incubation time, the intensity of fluorescence in the centre of aggregates was increased. Compared with DAOY aggregates, it was found that the difference in intracellular fluorescence intensity between cells in the periphery of and in the centre of mixed foetal brain aggregates was not as clear as that shown in the DAOY aggregates. The fluorescence intensity level of mixed foetal brain aggregates was much lower than that of DAOY aggregates after 24h incubation time.

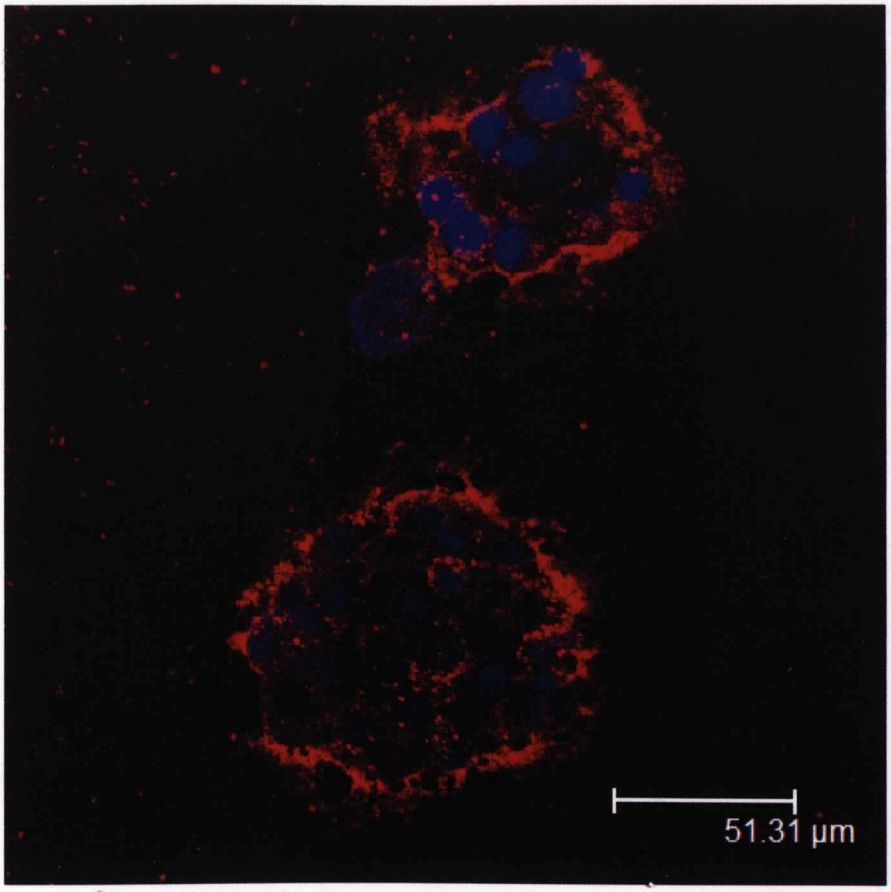

Fig. 6.7 One of confocal images taken from the middle of aggregates demonstrating diffusion distance of RBITC labelled NPs in DAOY aggregates after 4h incubation: DAOY aggregates were incubated with NPs for 4h, aggregates were transferred into a 24-well plate with PDL coated coverslip 30 min before the end of incubation time. As shown, most of NPs were localized on the surface of aggregates and few NPs were taken up by cells in the centre of the aggregates.

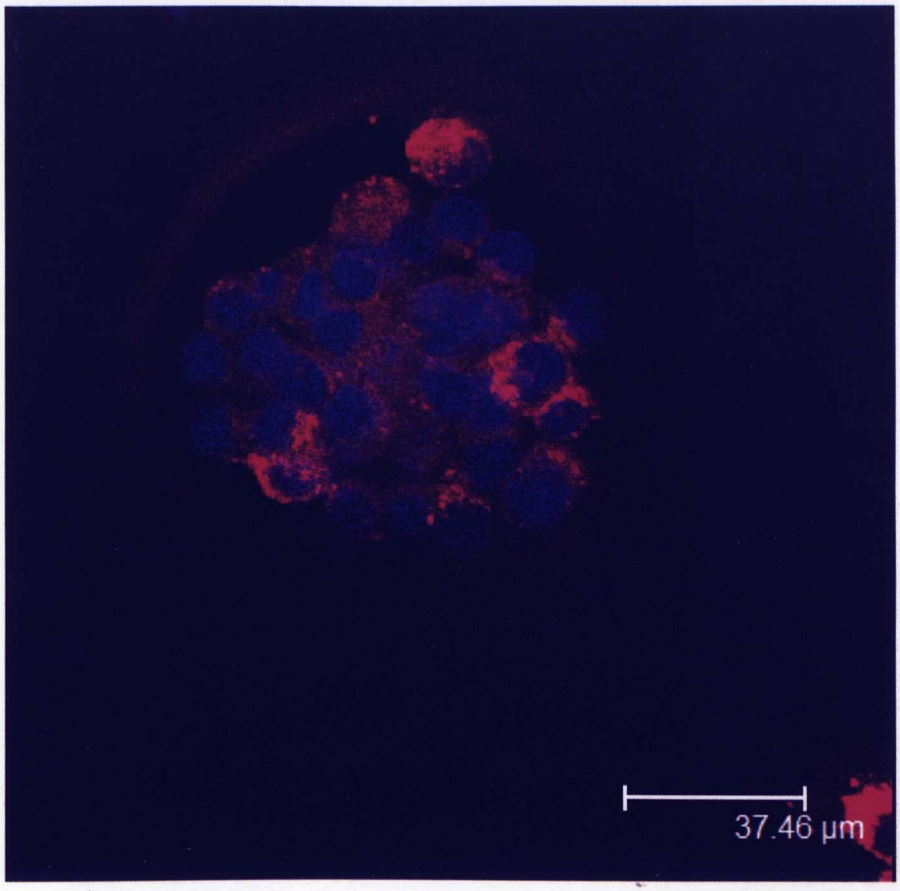

Fig. 6.8 One of confocal images taken from the middle of aggregates demonstrating diffusion distance of RBITC labelled NPs in DAOY aggregates after 6h incubation: DAOY aggregates were incubated with NPs for 6h, aggregates were transferred into a 24-well plate with PDL coated coverslip 30 min before the end of incubation time. As shown, most NPs diffused into the whole DAOY aggregates.

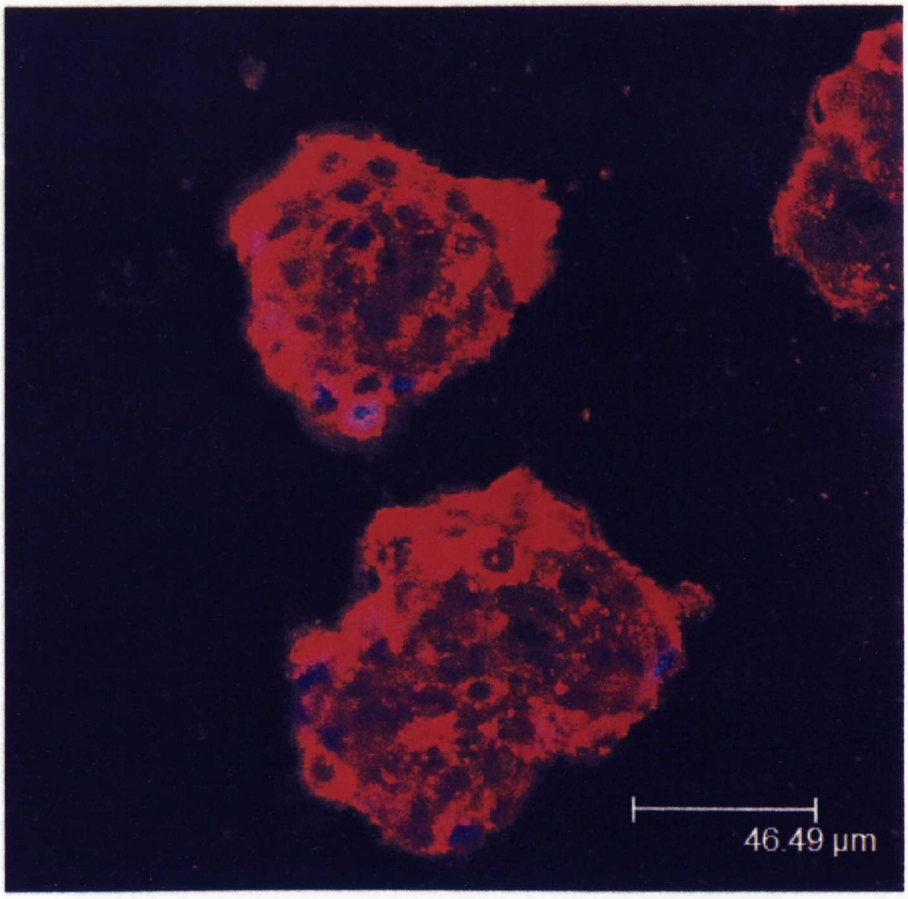

Fig. 6.9 One of confocal images taken from the middle of aggregates demonstrating diffusion distance of RBITC-labelled NPs in DAOY aggregates after 24h incubation: DAOY aggregates were incubated with NPs for 24h, aggregates were transferred into a 24-well plate with PDL coated coverslip 30 min before the end of incubation time. As shown, intracellular fluorescence intensity increased and cells on the surface of aggregates had very high fluorescence intensity.

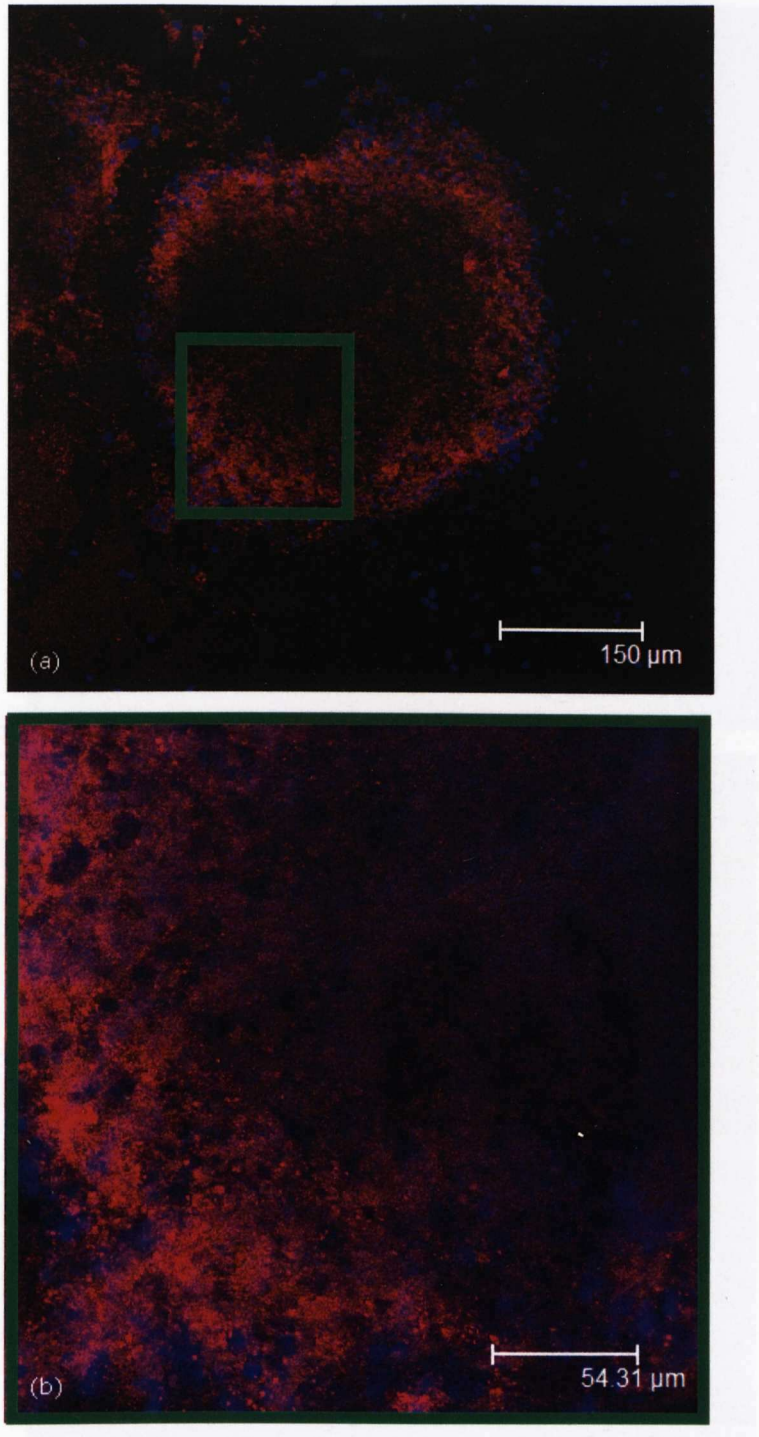

Fig. 6.10 One of confocal images taken from the middle of aggregates demonstrating diffusion distance of RBITC labelled NPs in mixed foetal brain aggregates after 4h incubation: mixed foetal brain aggregates were incubated with RBITC labelled NPs for 4h, aggregates were transferred into a 24-well plate with PDL coated coverslip 30 min before the end of incubation time. (a) fluorescent image of aggregate with low magnification; (b) one part of aggregate taken from (a) with high magnification. As shown, most NPs were taken up by cells on the surface of aggregates and few NPs were taken up by cells in the centre of aggregates.

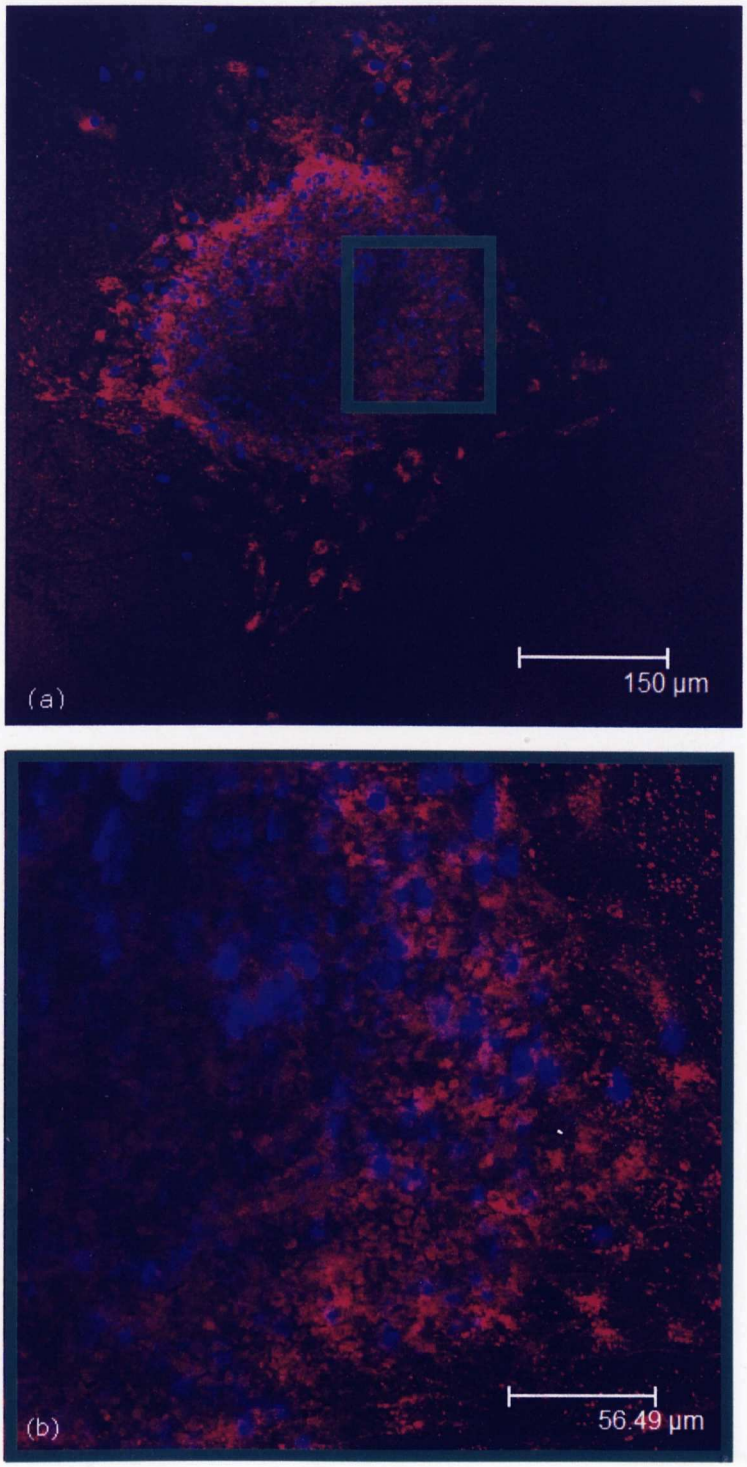

Fig. 6.11 One of confocal images taken from the middle of aggregates demonstrating diffusion distance of RBITC labelled NPs in mixed foetal brain aggregates after 6h incubation: mixed foetal brain aggregates were incubated with NPs for 6h, aggregates were transferred into a 24-well plate with PDL coated coverslip 30 min before the end of incubation time. (a) fluorescent image of aggregate with low magnification; (b) one part of aggregate taken from (a) with high magnification. As shown, most NPs were taken up by cells on the surface of aggregates and few NPs were taken up by cells in the centre of aggregates.

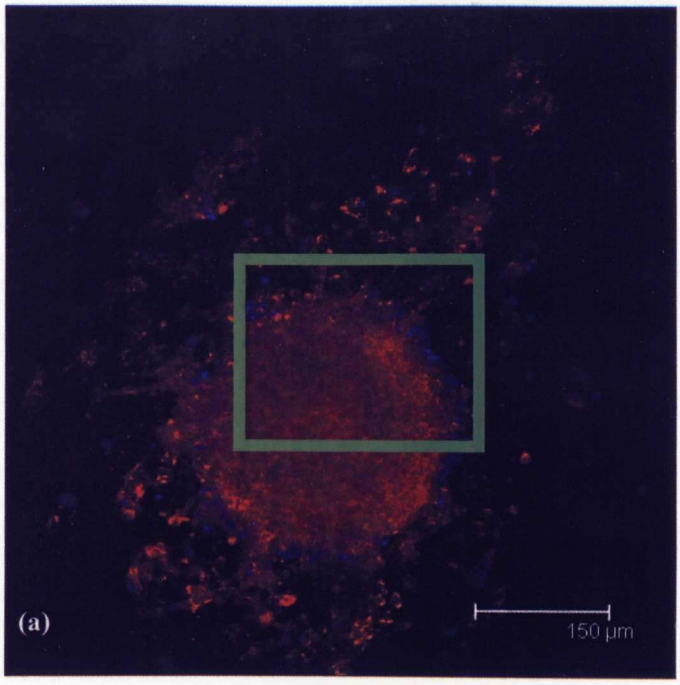

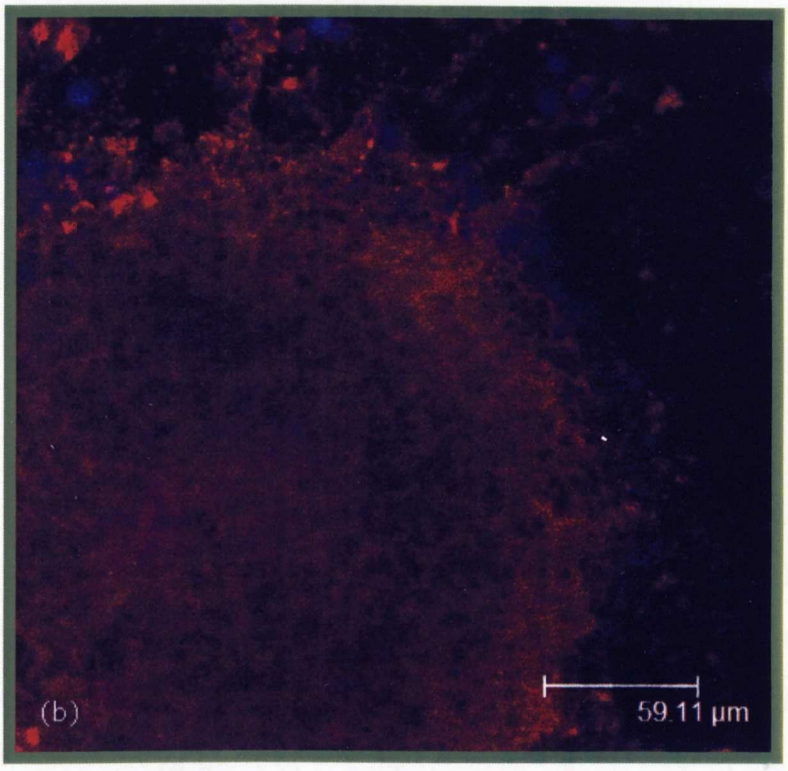

Fig. 6.12 One of confocal images taken from the middle of aggregates demonstrating diffusion distance of RBITC-labelled NPs in mixed foetal brain aggregates after 24h incubation: mixed foetal brain aggregates were incubated with RBITC labelled NPs for 24h, aggregates were transferred into a 24-well plate with PDL coated coverslip 30 min before the end of incubation time. (a) fluorescence image of aggregate with low magnification; (b) one part of aggregate taken from (a) with high magnification. As shown, fluorescence intensity of some cells on the surface of aggregates decreased, while cells in the middle of aggregates increased.

6.3.1.5 Penetration investigation of RBITC labelled NPs in mixed foetal brain aggregates

Fig. 6.13 and Fig. 6.14 show the penetration of RBITC labelled NPs in mixed foetal brain aggregates. In this study, two types of aggregates were used. One type of aggregate was formed by a rotation method, transferred and cultured in a 24-well plate for 24h, and then incubated with fluorescently labelled NPs for 24h. Another type of aggregate was formed spontaneously without any mechanical forces, in which high concentrations of individual cells were cultured in a 24-well plate after foetal brains were dissociated into individual cells which then reformed themselves into aggregates. This type of aggregate was cultured for 24h and then incubated with NP suspension for 2h. For the latter type of aggregates, confocal fluorescence micrograph (Fig. 6.13A) indicated that the inner structure (blue fluorescence) of aggregate was more loosely organized than that of aggregates formed by a rotation method (Fig. 6.14A). Individual cells (Fig. 6.13A) both in the periphery of aggregates and in the inner region of aggregate can still be discerned. The distance between two individual cells in the inner region of the spontaneously formed aggregate was greater compared with the cells in the periphery of aggregates. The DAPI fluorescence image also demonstrated there were no cells in some areas in the centre of these aggregates. The gallery of fluorescence images (Fig. 6.13B) showed that most of red fluorescence can be seen in the middle of the spontaneously formed aggregates (from 4.396μm to 10.990μm in Z-dimension) and few NPs in the bottom of the aggregates (from1.099μm to 3.297μm in Z-dimension). Using the penetration equation (see 6.2.6) it was calculated that most of NPs diffused into 30-80% of aggregates.

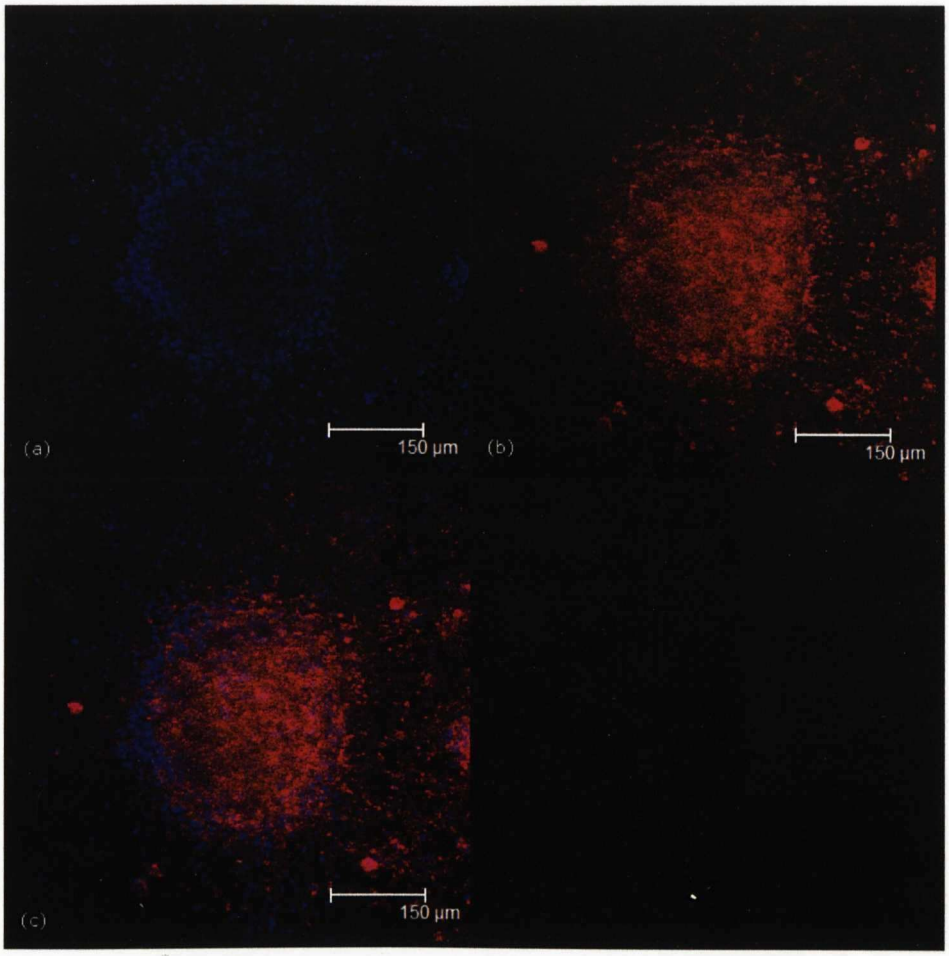

Fig. 6.13A Confocal image demonstrating the influence of structure of interstitial compartment within mixed foetal brain aggregates on penetration of NPs. The aggregates formed spontaneously when high concentration of cells were used during 2-D monolayer cell culture and incubated with RBITC labelled NP suspension for 2h. This is one of confocal images from Fig. 6.13B. (a) blue fluorescence from DAPI; (b) red fluorescence from RBITC labelled NPs; (c) co-locolization of (a) and (b). It shows the relatively loose inner structure compared with aggregates formed by rotation method (Fig. 6.14A) and even distribution of red fluorescence in the inner region of the aggregate.

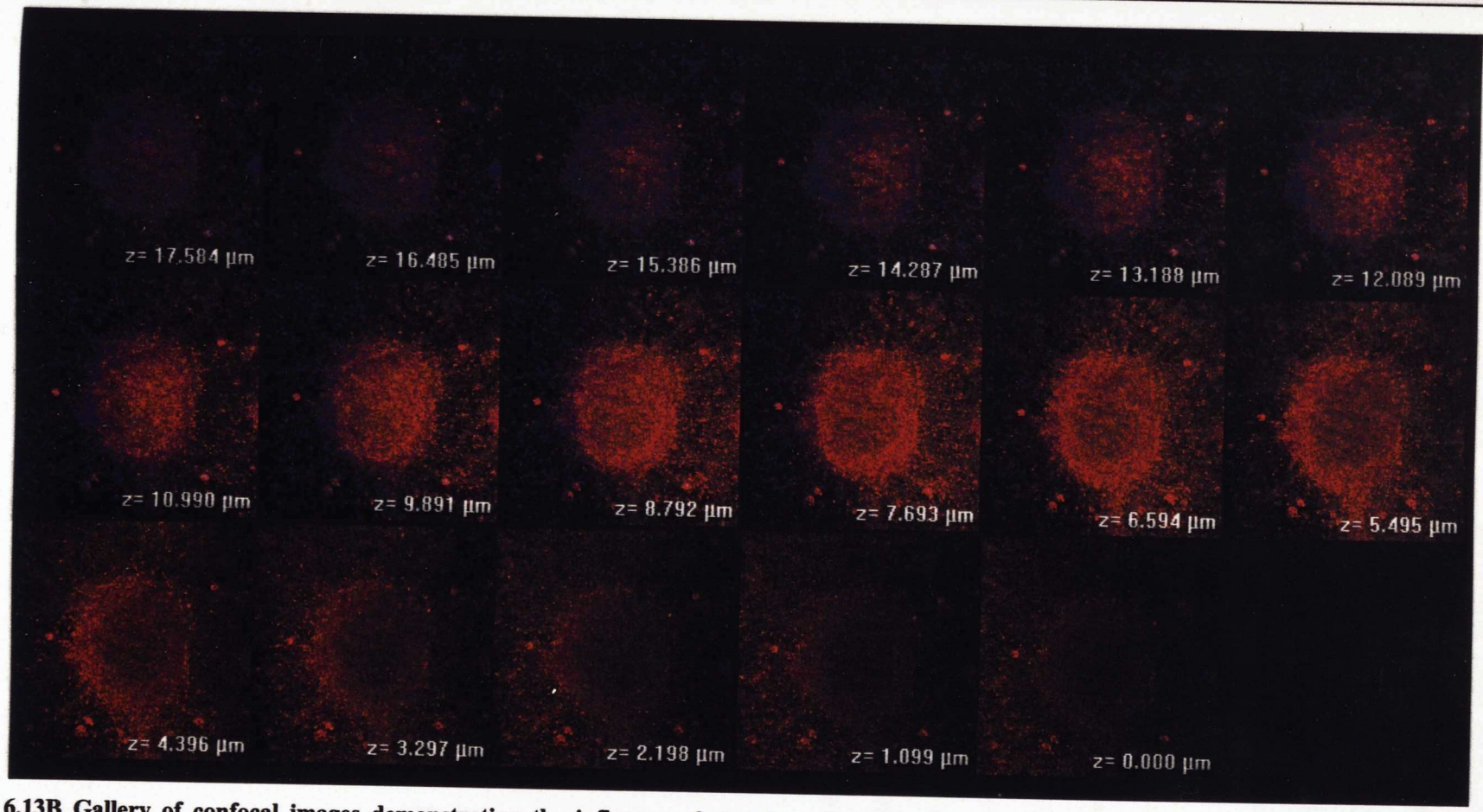

Fig. 6.13B Gallery of confocal images demonstrating the influence of structure of interstitial compartment within mixed foetal brain aggregates on penetration of NPs. The spontaneously formed aggregates when high concentration of cells was used during 2-D monolayer cell culture incubated with RBITC labelled NP suspension for 2h (x20). It shows most NPs penetrated into the middle of the aggregate and few NPs at the bottom of the aggregate after 2h incubation time. (see video 6.1). Z: z-dimension scan.

For aggregates formed by the rotation method, confocal fluorescence images (Fig. 6.14A) show that aggregates were completely formed and became well rounded with highly compacted cells. Individual cells in the periphery of aggregate still could be discerned while cells in the inner region of aggregate couldn't be distinguished. The distribution pattern of red fluorescence in the inner region of aggregates was different from that of aggregates formed spontaneously: red fluorescence in the sample of spontaneously formed aggregates was almost uniformly distributed; while in the sample of aggregate formed by the rotation method, it was found that the red fluorescence intensity in some areas was higher than that of other areas. The gallery of fluorescence images showed that most NPs were localized in the middle of aggregates (from5.861μm to11.723 μm in Z-dimension) and a few NPs penetrate through whole aggregates after 24h incubation time. Based on the penetration equation (see 6.2.6), it was calculated that most of NPs penetrated into 25-50% of aggregates.

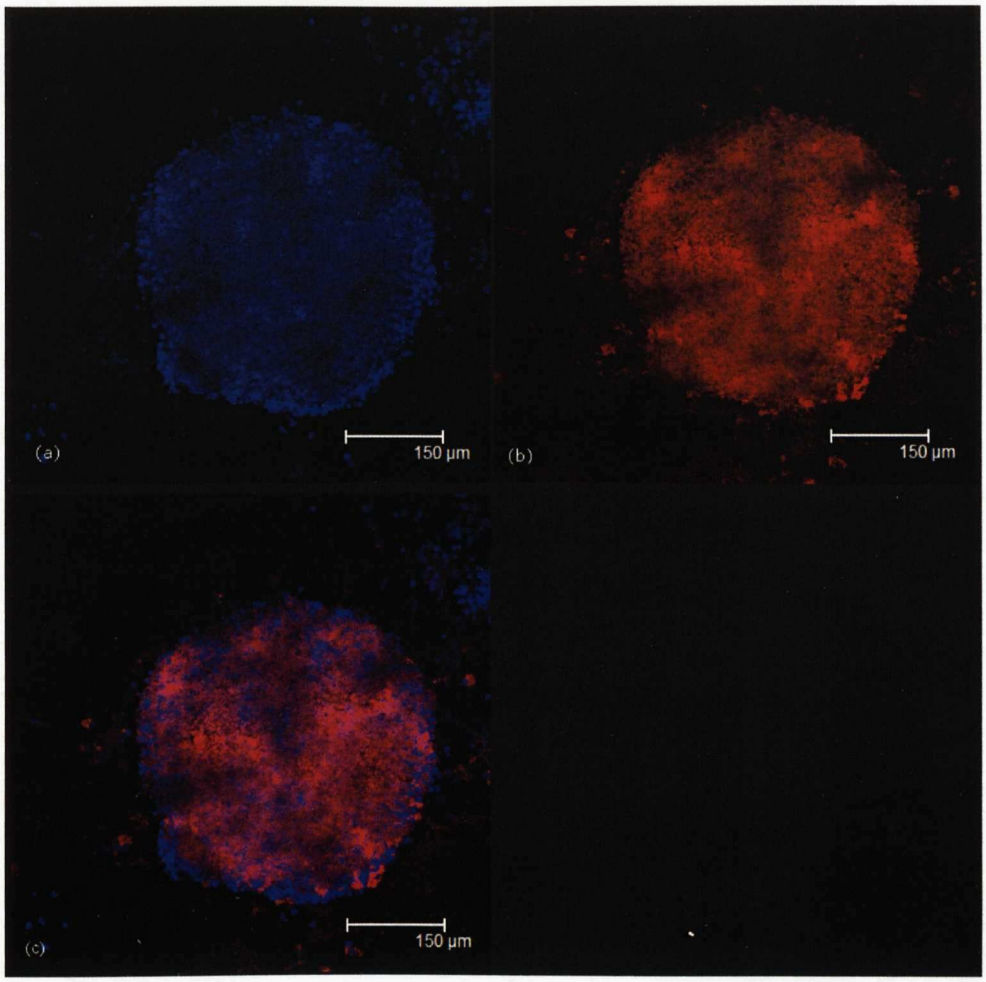

Fig. 6.14A Confocal images demonstrating the influence of structure of interstitial compartment within mixed foetal brain aggregates on penetration of NPs. The aggregates were formed by **rotation method**, cultured in a 24 well plate for 24h, and then incubated with NPs for 24h. This is one of confocal images from Fig. 6.14B. (a) blue fluorescence from DAPI; (b) red fluorescence from RBITC labelled NPs; (c) co-locolization of (a) and (b). It shows that aggregates have a relatively compact inner structure and uneven distribution of red fluorescence in the inner region of aggregates.

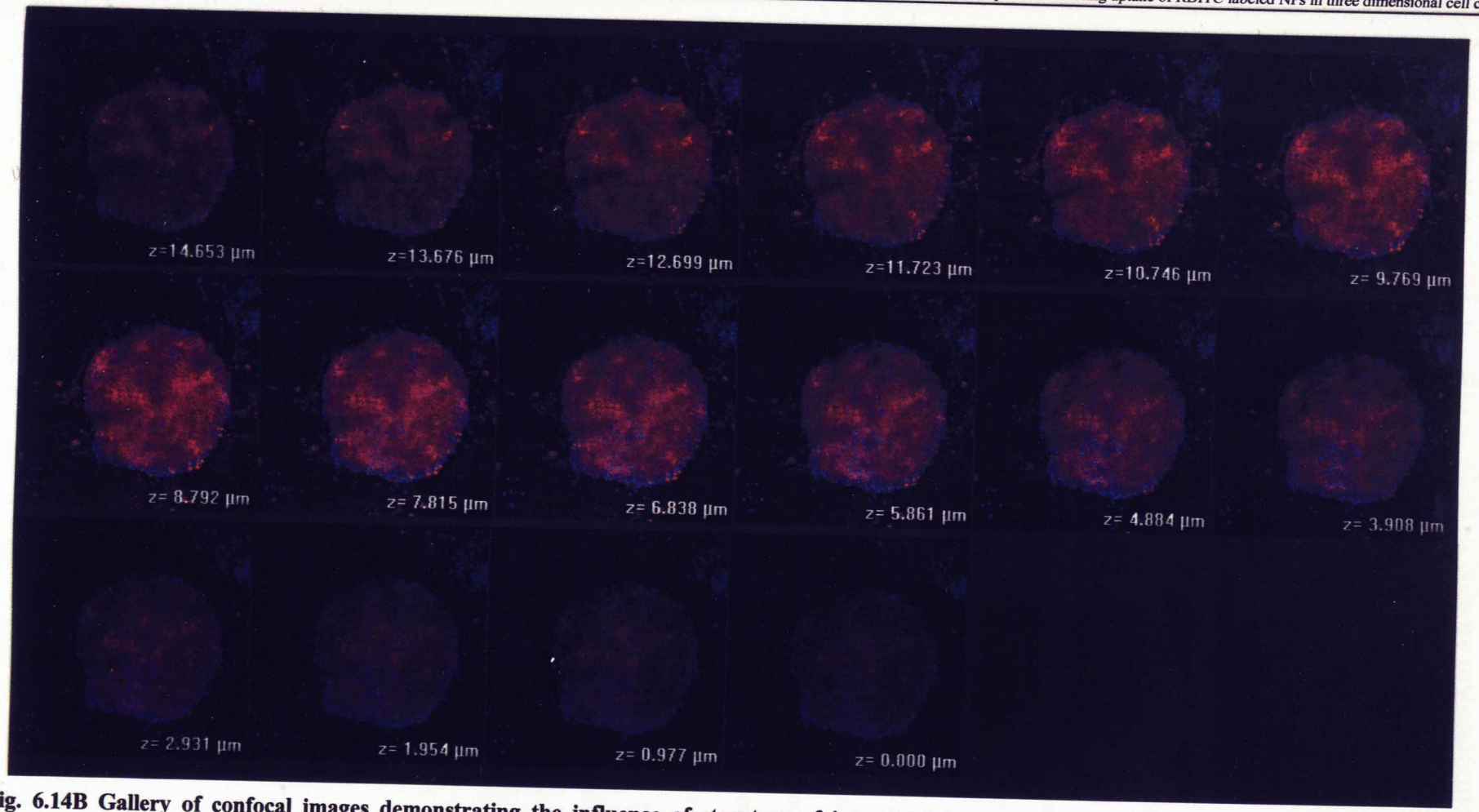

Fig. 6.14B Gallery of confocal images demonstrating the influence of structure of interstitial compartment within mixed foetal brain aggregates on penetration of NPs. The aggregates were formed by **the rotation method**, cultured in a 24-well plate for 24h, and then incubated with NPs for 24h (x20). It shows that few NPs penetrate into whole aggregates and most of them are in the middle of aggregates after 24h incubation time. (see video 6.2) Z: z-dimension scan

6.3.2 Uptake of RBITC labelled NPs by organotypic rat brain slices

6.3.2.1 Organotypic brain slice culture

After brain cerebral cortex was dissected from 2-day neonatal rat brain, slices (400μm thick) cut from the cerebral cortex were cultured for 14 days (see 2.2.3.4). After 48h, culture viability was assessed using a light microscope. As shown in Fig. 6.15, cell outgrowth was evident as neurites extending from the edge of the cerebral cortex slices after 48h culture. A TEM image (Fig. 6.16) also confirmed the culture viability. Neonatal cerebral cortex slices appeared densely packed with cells of varying size and morphology. Large mononuclear cells had a large dense nucleus and cytoplasm filled with organelles. The nucleus was ellipsoidal and occupied most of the cell body. Cellular and organelle integrity appeared to have remained after 14 days in culture. All these data indicate that the method used in our work was successful in maintaining and growing cerebral cortex slices from 2-day neonatal rats.

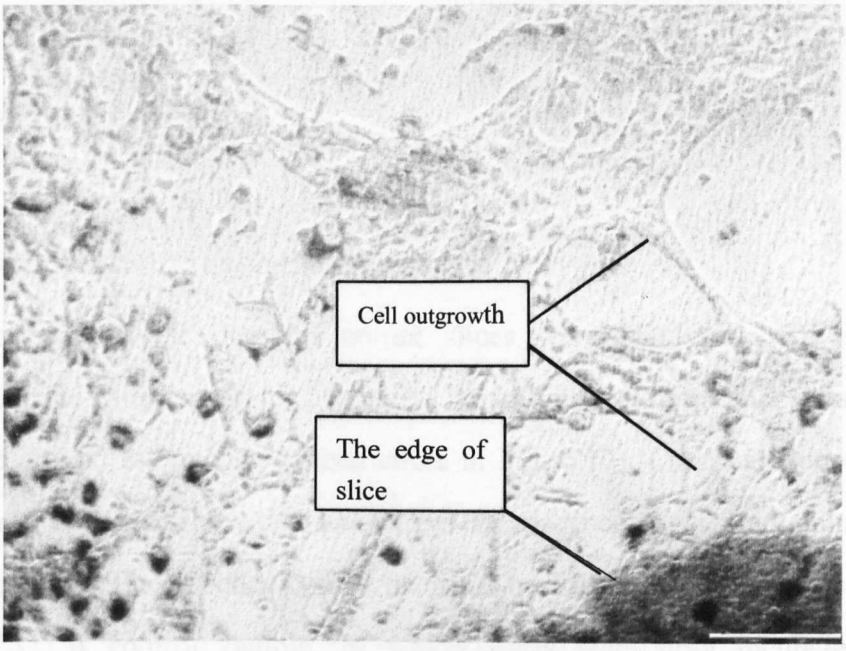

Fig. 6.15 A phase-contrast micrograph showing culture viability of brain cerebral cortex slices. As shown, cell outgrowth at the edge of brain slice is present. Scale bar: 50μm.

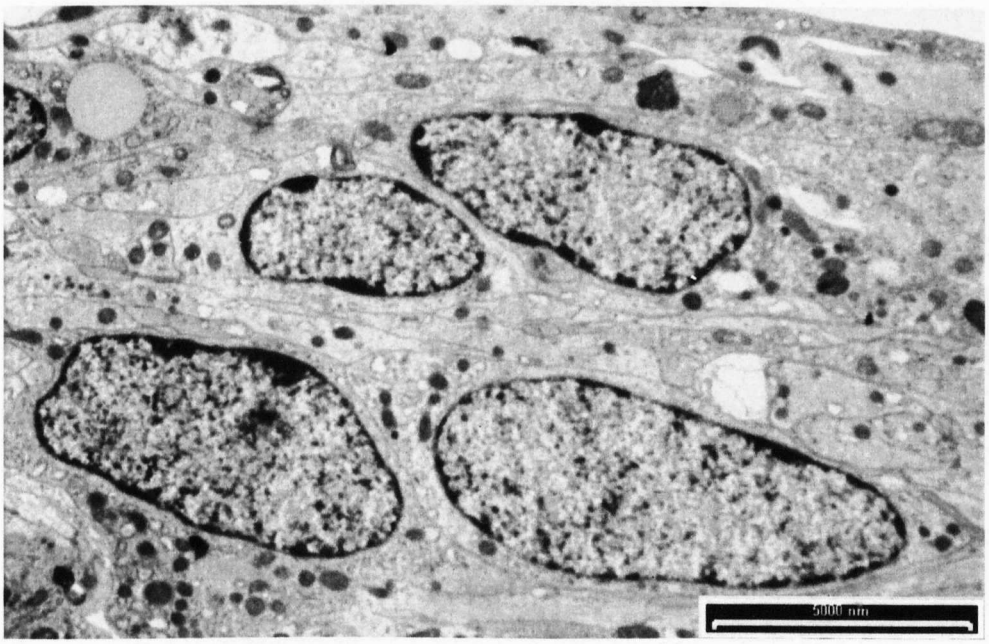

Fig. 6.16 A TEM image of a neonatal rat cerebral cortex slice showing that cells remained viable after 14-day culture. Scale bar: 5000nm

6.3.2.2 Localisation of RBITC labelled NPs in organotypic cerebral cortex slices

Confocal fluorescence microscopy

After organotypic cerebral cortex slices were incubated with RBITC labelled NP suspension for 24h, some larger orange fluorescence dots can be seen around the nucleus (green circle in Fig. 6.17). Confocal fluorescence micrographs also show that several red fluorescence dots are not colocalised with yellow fluorescence dots in the same position (see pink squares in Fig. 6.17A). A control sample, in which slices were only incubated with LysoTracker Yellow, showed very little yellow fluorescence around the nucleus (Fig. 6.18).

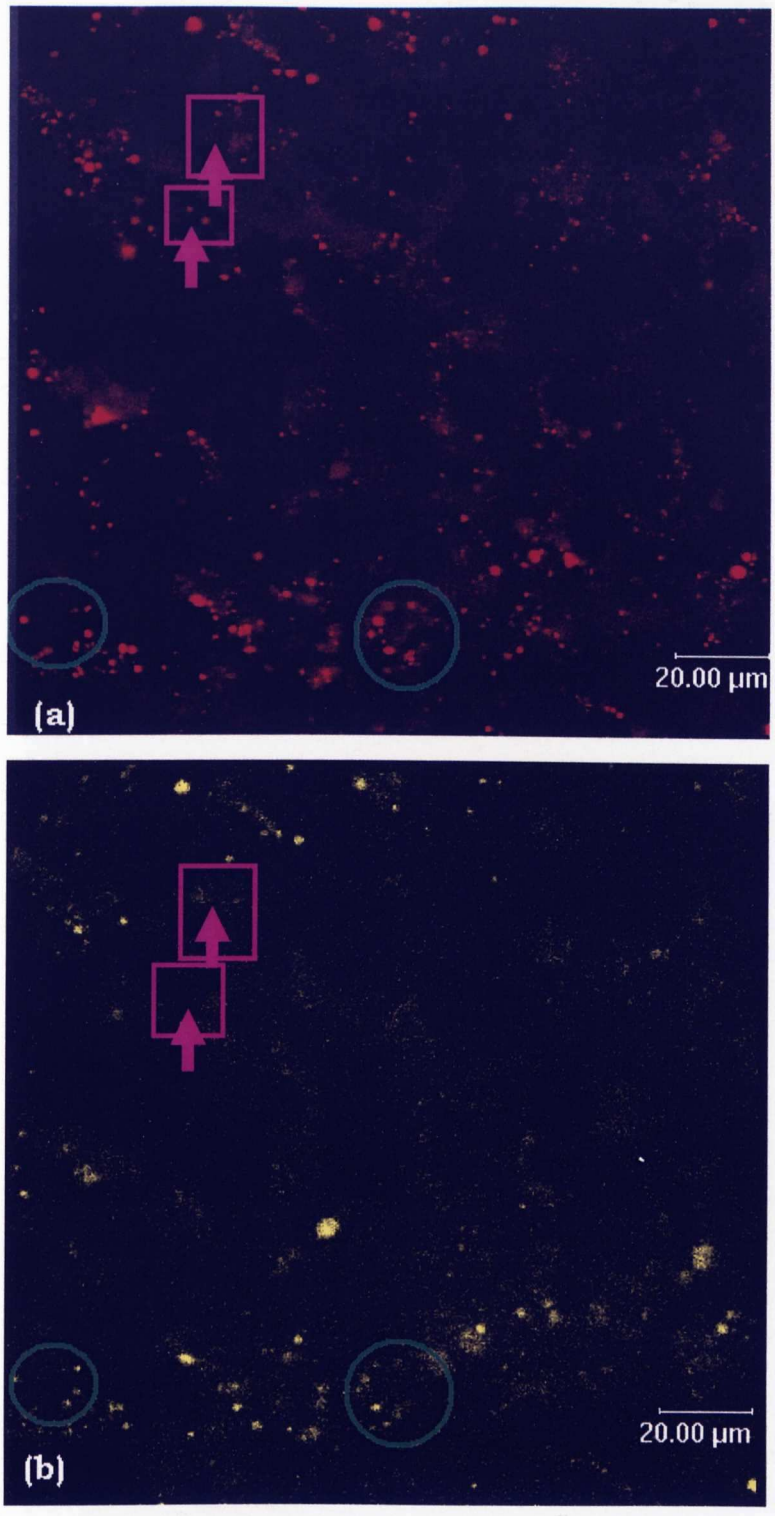

Fig. 6.17A Confocal images of RBITC labelled NPs taken up by organotypic rat cerebral cortex slices: slices were incubated with NPs suspension (200µg, 4.0mg/ml) for 24h. (a) red fluorescence from NPs; (b) yellow fluorescence from LysoTracker Yellow. As can be seen, the majority of NPs were taken up by brain cells and sorted into the lysosomal compartment (green circle) and few NPs are localized outside of cells (pink square and arrow).

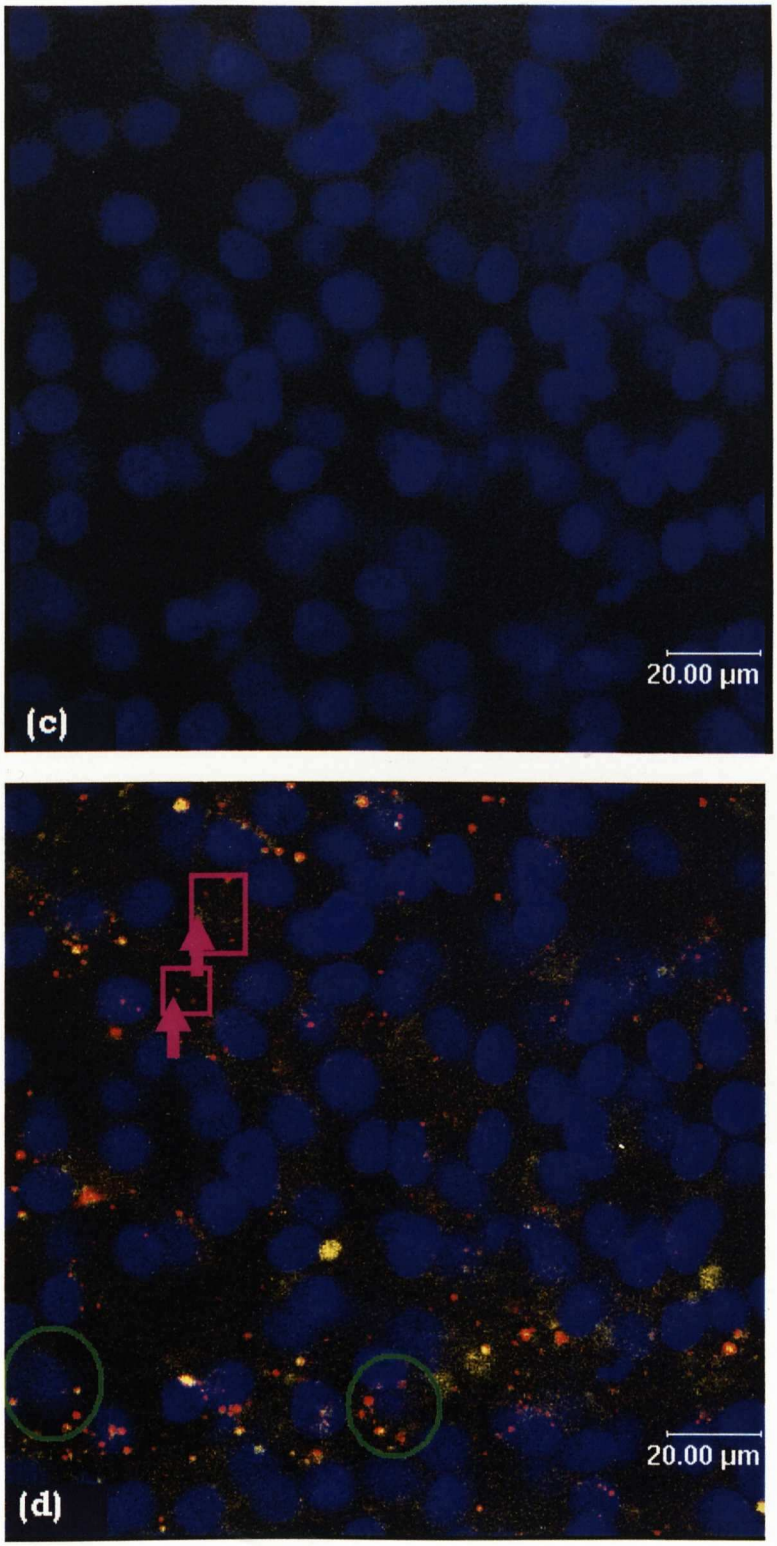

Fig. 6.17B Confocal images of RBITC labelled NPs taken up by organotypic rat cerebral cortex slices: slices were incubated with NPs suspension (200µg, 4.0mg/ml) for 24h. (c) blue fluorescence from DAPI; (d) combined picture of red with yellow and blue fluorescence. As can be seen, the majority of NPs were taken up by brain cells and sorted into the lysosomal compartment (green circle) and few NPs are localized outside of cells (pink square and arrow).

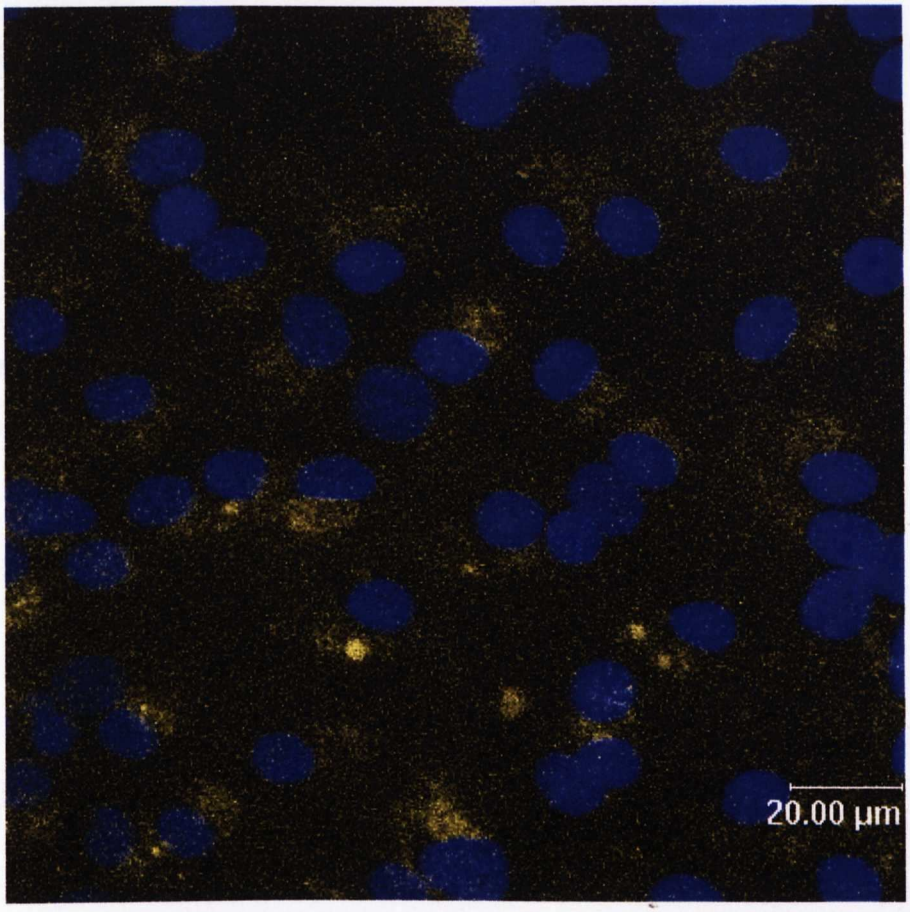

Fig. 6.18 A confocal image of control organotypic cerebral cortex slices: slices were incubated with 50nM LysoTracker Yellow for 2h. As can be seen, LysoTracker Yellow appears as very small yellow fluorescence dots in many cells showing their characteristic location around nucleus.

TEM

Ferritin is an electron-dense protein having a diameter of 8-12nm and was thus loaded into NPs for microscopy investigation using electron microscopy. Fig. 6.19 shows the TEM images of ferritin only, NPs without ferritin loading and ferritin loaded NPs. It shows that ferritin was visible under TEM without contrast agents as individual, small, uniform sized electron-dense particles (Fig. 6.19a). The NPs without ferritin loading required negative staining with 3% w/v phosphotungstic acid to be visualized under TEM while ferritin loaded NPs could be visualized without any staining (Fig. 6.19b and c). It was clearly demonstrated that ferritin clusters in the centre of NPs.

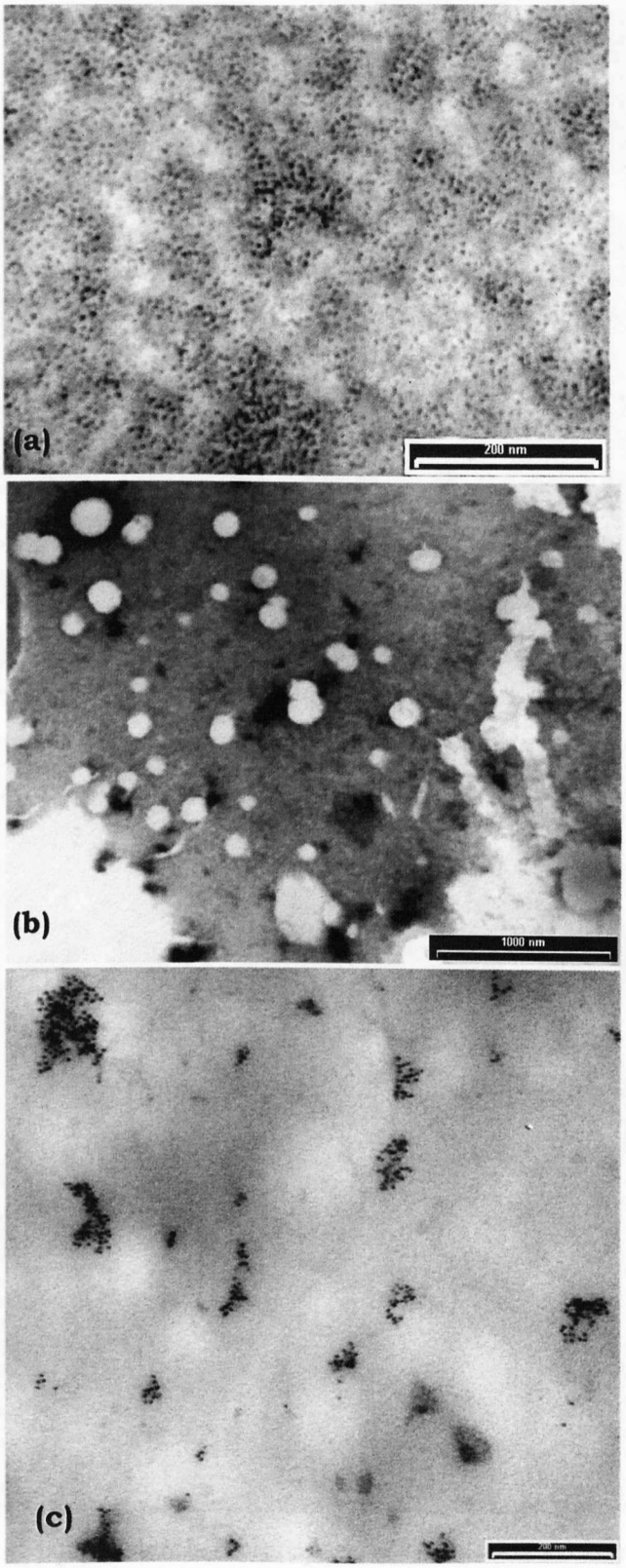

Fig. 6.19 TEM images of control and Ferritin loaded NPs. (a) 2% w/v horse spleen ferritin solution only, scale bar: 200nm; (b) NPs without ferritin loading, scale bar: 1μm; (c) ferritin loaded NPs, scale bar: 200nm. NPs without ferritin loading were visualized following negative staining with 3% w/v phosphotungstic acid. Ferritin solution only and Ferritin loaded NPs were visualized without any staining.

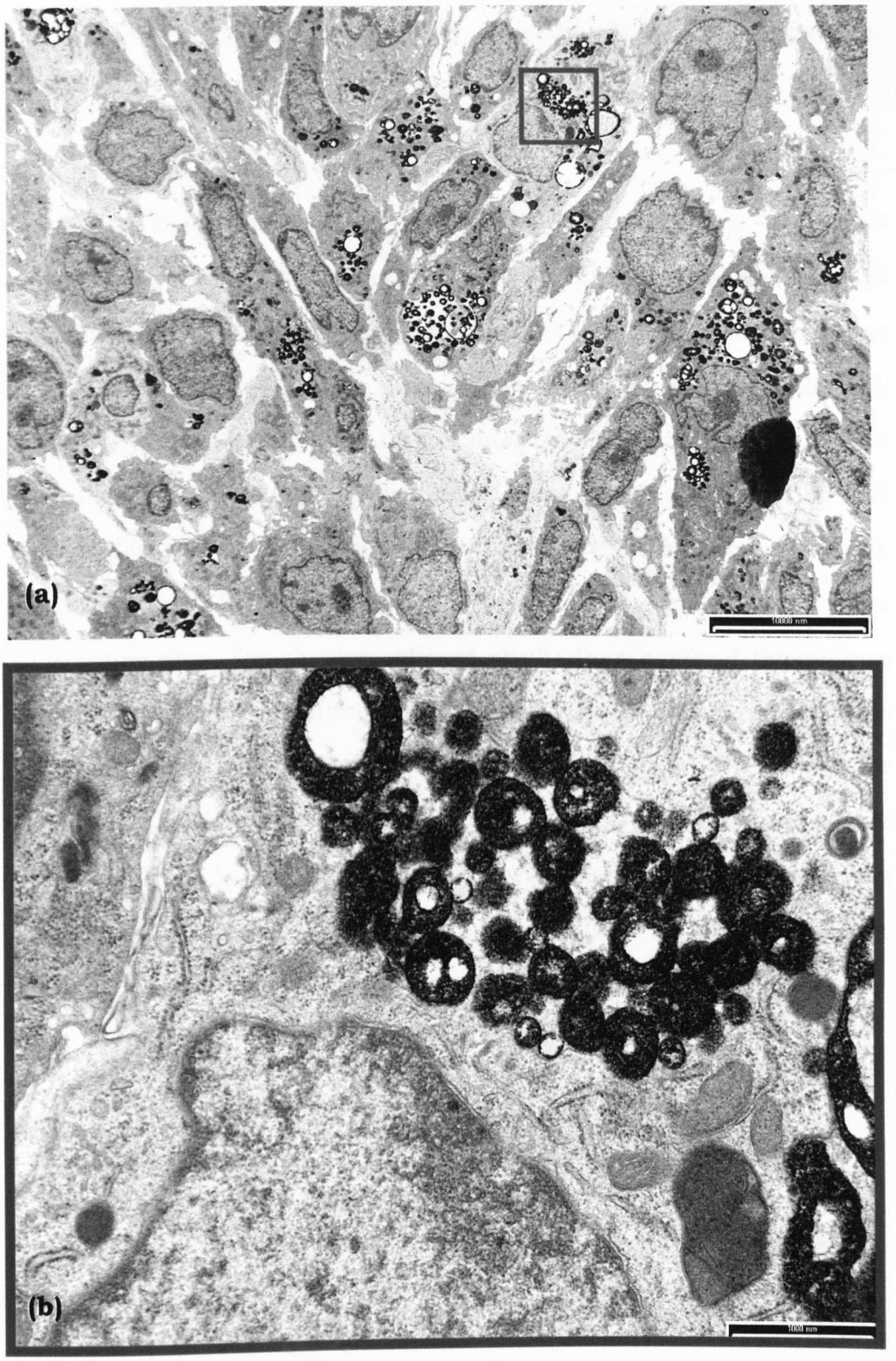

Fig. 6.20 TEM images showing localisation of ferritin loaded NPs within cells in organotypic cerebral cortex slices. (a) NPs presented in the lysosome compartment scale bar; 10000nm; (b) NPs presented in lysosomes at higher magnification, scale bar: 1000nm. Control cerebral cortex slice sample seen Fig. 6.16.

6.3.2.3 Penetration of RBITC labelled NPs in organotypic cerebral cortex slices

Fig. 6.21 shows the penetration of RBITC labelled NPs in organotypic cerebral cortex slices by using confocal fluorescence microscopy. Although the thickness of slices changes from about 400μm to 26μm after slices were cultured for 14 days, the slice culture didn't spread as a monolayer and still retained a three-dimensional organization. It was found that most NPs localized in about 5μm to 10μm depth of slices, which account for 20-35% of the thickness of slices according to the penetration equation (see 6.2.6), and only few NPs penetrated to the bottom of the slices after 24h of incubation time. The above mentioned results from confocal fluorescence images were further confirmed by TEM study (Fig. 6.22). Fig. 6.22 shows cells in the top 1 or 2 layers of slices didn't take up any NPs because the distinct dark colour of ferritin can't be distinguished within the intracellular compartments. As the scan of slices in z -dimension increased, it was found that most NPs were taken up by the cells in the middle of slices. There was no evidence of uptake into cells at the bottom of the slices.

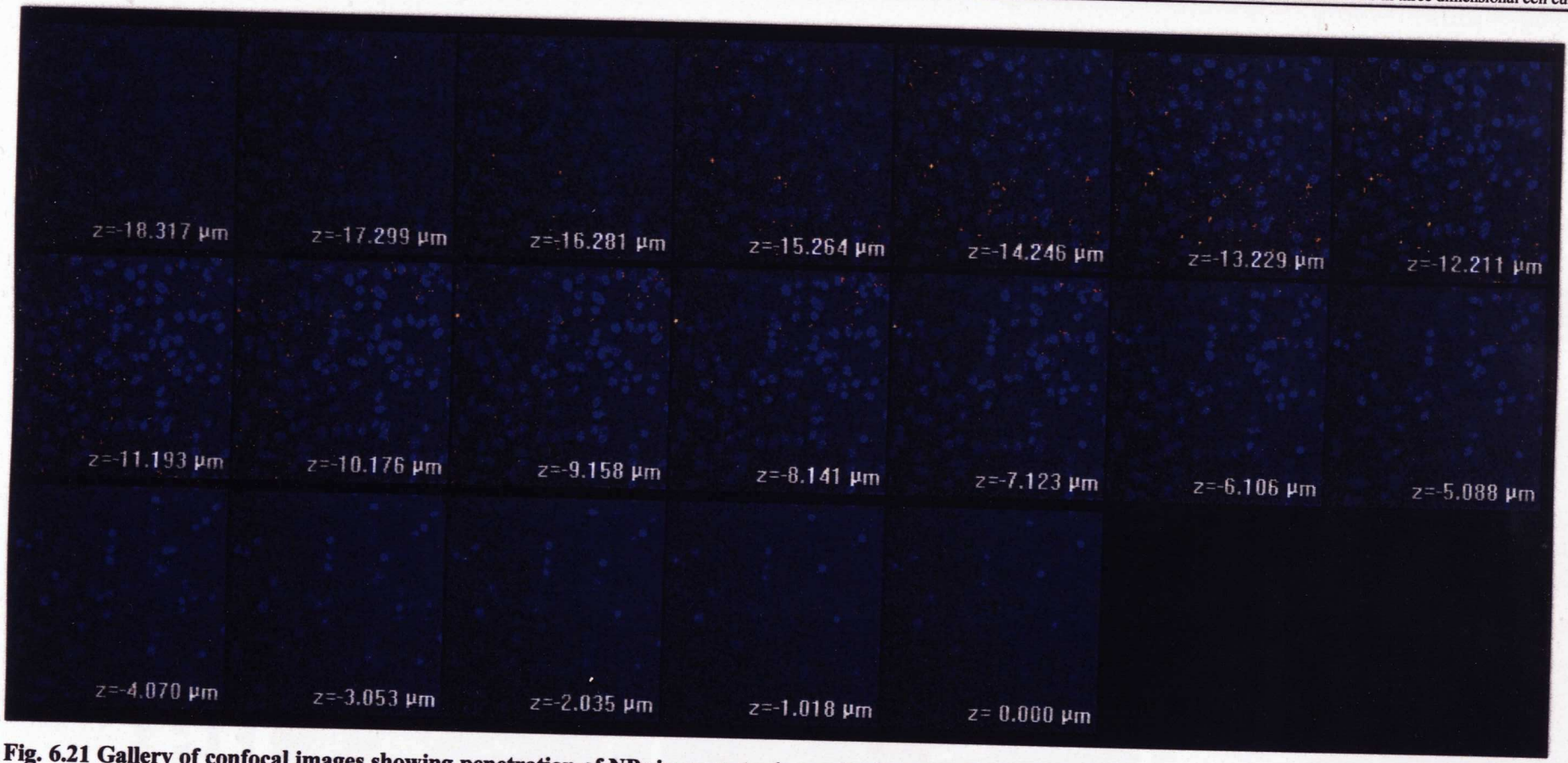

Fig. 6.21 Gallery of confocal images showing penetration of NPs in organtypic cerebral cortex slices after slices were incubated with NPs for 24h. As shown, most NPs localised in the top and middle of slices. (whole scan seen video 6.3). Z: z-dimension scan

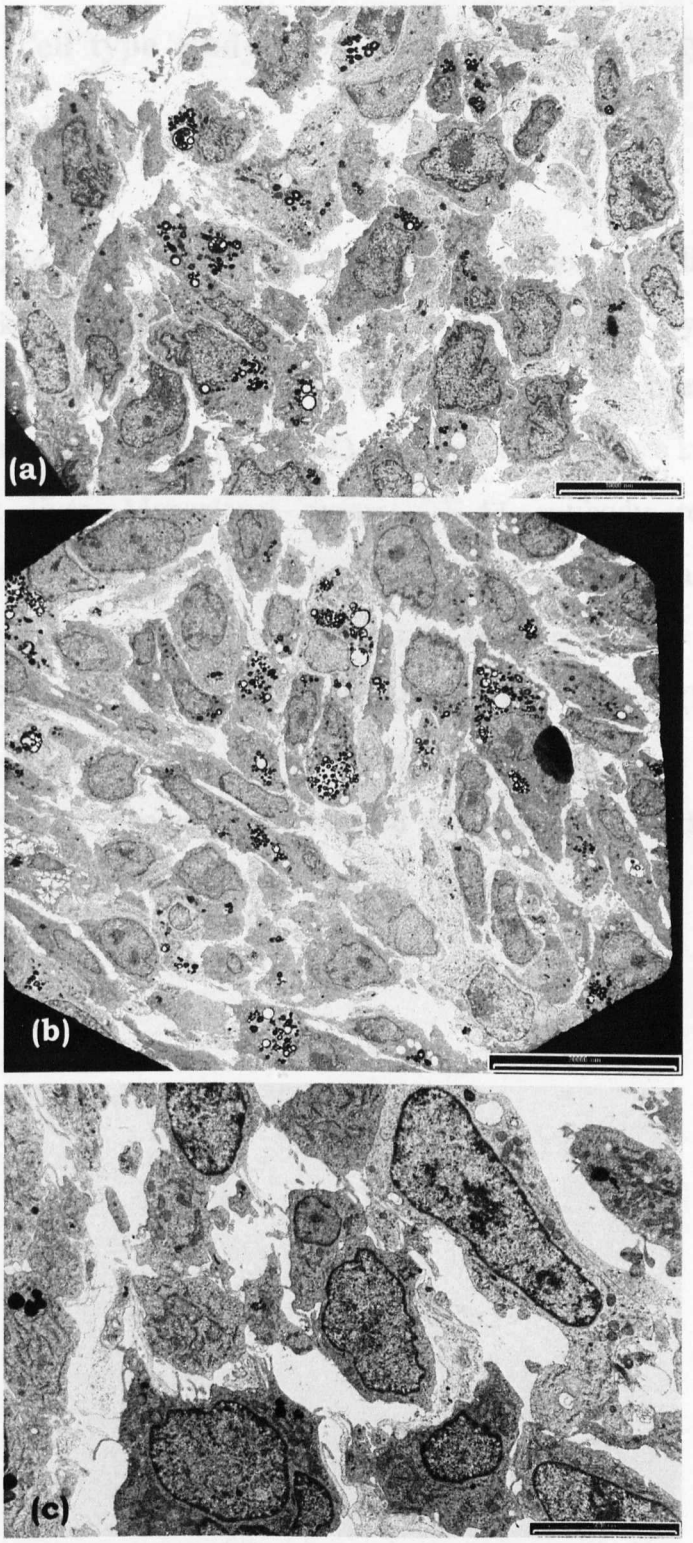

Fig. 6.22 TEM images showing the penetration of NPs in organotypic cerebral cortex slices. Slices were incubated with ferritin loaded NP suspension for 24h and then observed under TEM. (a) the top/the surface of slices, scale bar: 10000nm; (b) middle of slices, scale bar: 20000nm; (c) the bottom of slices, scale bar: 2000nm. As shown, most NPs were taken up by the cells in the middle of slices.

6.3.3 Cell type study of NP uptake in organotypic cerebral cortex slices

Fig. 6.23a is a Hematoxylin & Eosin stained section of rat liver. The section is pink and homogeneous, and cells are separated by empty spaces indicating sinusoidal spaces from where the blood has been washed away. Visible vein on the left of Fig.6.23a also was regarded as a key characteristic of rat liver. Monoclonal mouse OX-42 antibody recognises most macrophages including resident peritoneal and activated macrophages, and Kupffer cells (manufacturer's instruction, Autogen Bioclear Ltd, UK). There is no OX-42 staining on the negative control of liver slice (Fig. 6.23b). In a positive control section, several cells closing to the veins show relatively brighter green fluorescence compared with background indicating they are stained by OX-42 monoclonal antibody (Fig. 6.23c).

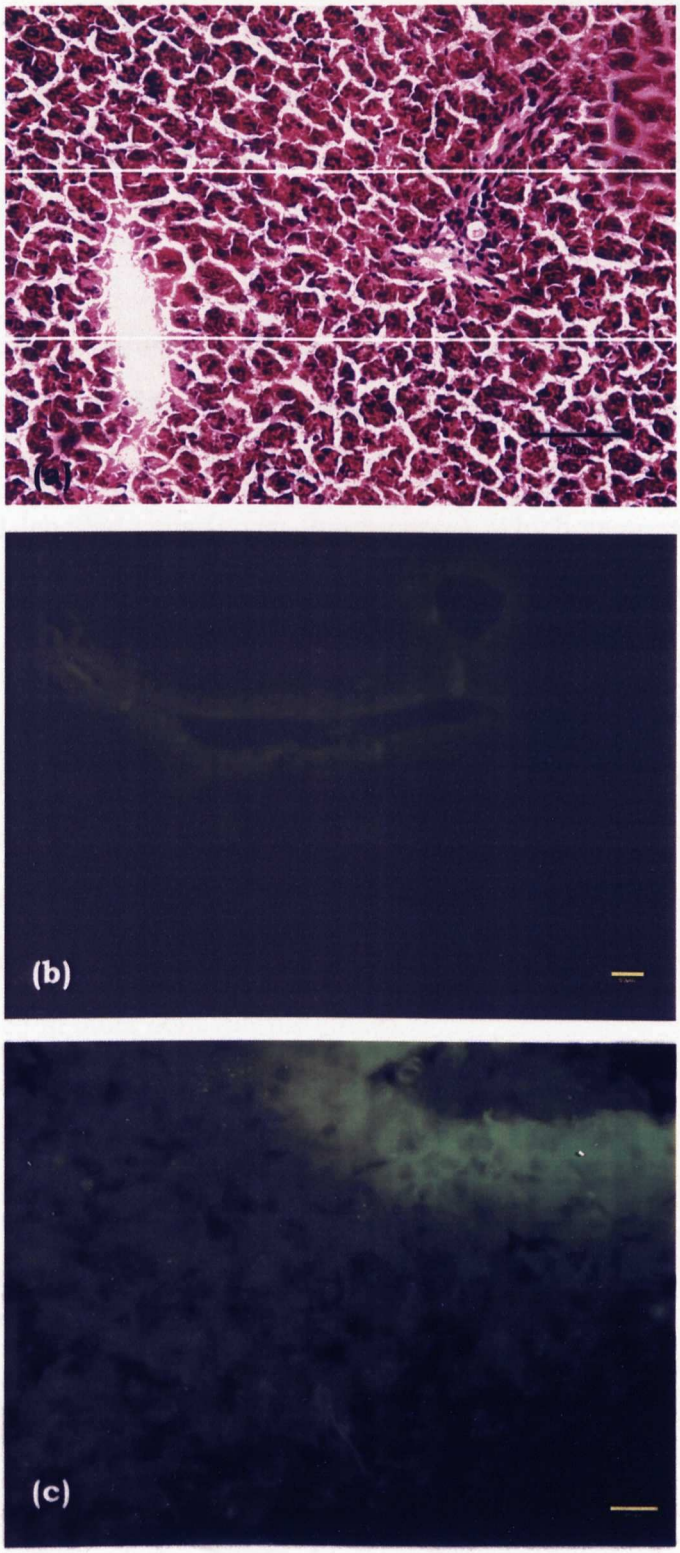

Fig. 6.23 Micrographs illustrating rat liver as control sample for immunohistological staining study. (a) a Hematoxylin & Eosin staining micrograph showing features of rat liver; Scale bar: 50μm; (b) a negative control: liver slices without monoclonal mouse OX-42 antibody staining, Scale bar: 100μm; (c) a positive control: liver slice with OX-42 monoclonal antibody staining. Scale bar: 100μm

Fig. 6.24a demonstrates that normal cerebral cortex slice gives some green fluorescence background of autofluorescence. Fig. 6.24b shows that microglia or macrophages still exist in the normal cerebral cortex slice after 14 days culture.

Fig. 6.25 illustrates the population of macrophages in organotypic slice culture incubated with NP suspension is similar to the control sample. It also shows that only a few orange fluorescence dots localized intracelluarly in OX-42 labelled cells (green fluorescence), which suggested that not many NPs were recognized and taken up by brain macrophages or microglial.

Fig. 6.26 shows confocal fluorescent micrograph of both DXM-FL labelled NPs (green fluorescence) and polystyrene latex beads (red fluorescence) incubated with cerebral cortex slices. As shown, red and green fluorescence can be seen around the nucleus and there are few colocalisation (yellow fluorescence) within cells (white square). Some more colocalisation can be observed in other cells (purple circle).

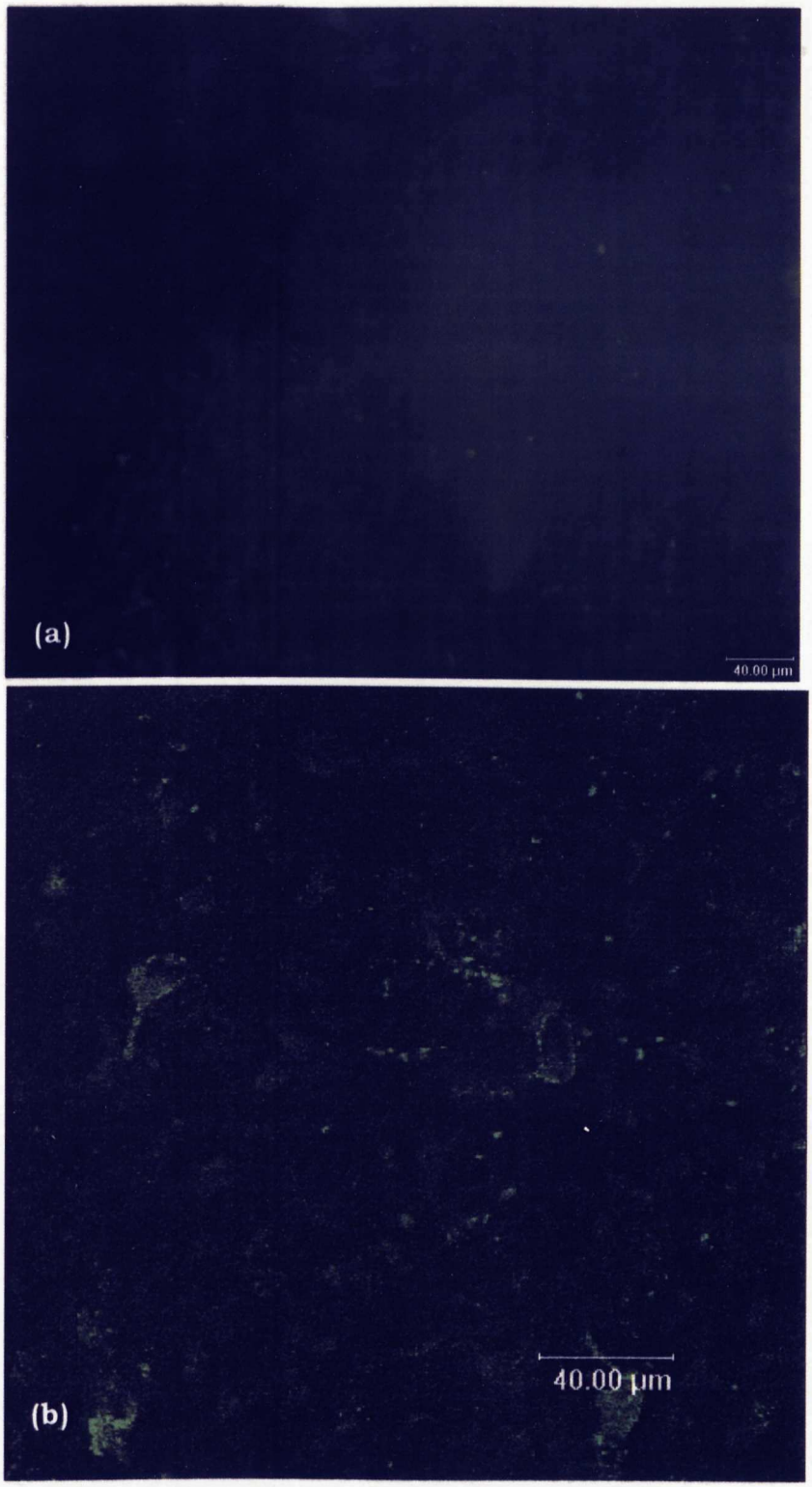

Fig. 6.24 Confocal fluorescence micrographs demonstrating OX-42 staining macrophages in cerebral cortex slices without adding NPs. (a) cerebral cortex slices without OX-42 labelling; (b)cerebral cortex slice with OX-42 labelling. It was shown that microglia or microphages still exist in the normal cerebral cortex slices in 14-day cultures.

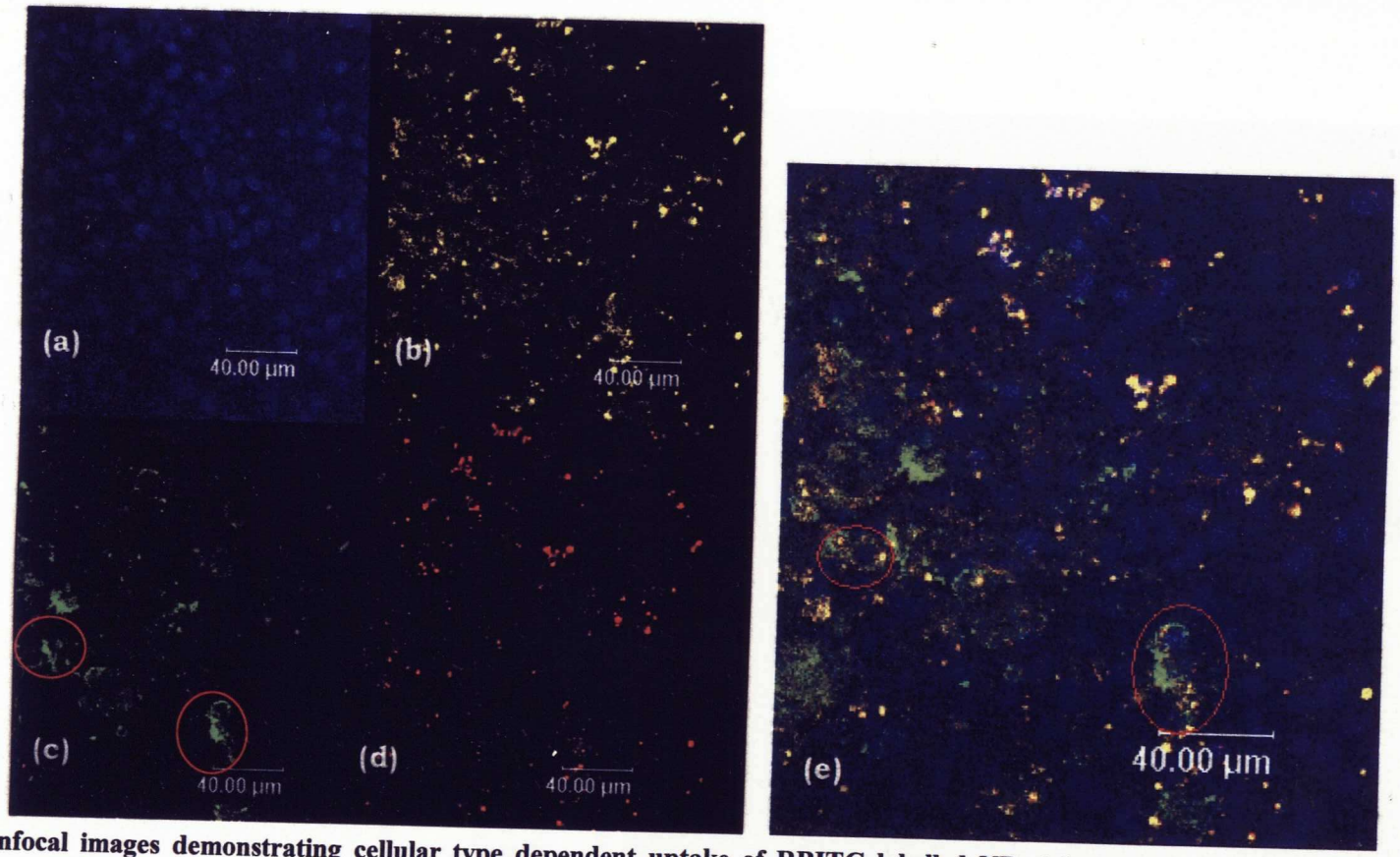

Fig. 6.25 Confocal images demonstrating cellular type dependent uptake of RBITC labelled NPs taken up by organotypic rat cerebral cortex slices: Immunochemical staining was carried out after slices were incubated with RBITC labelled NPs suspension (200µg, 4.0mg/ml) for 24h. (a) blue fluorescence from DAPI; (b) yellow fluorescence from LysoTracker; (c) green fluorescence from monoclonal mouse OX-42 antibody, which labels macrophage cells; (d) red fluorescence from NP; (e) combined image of (a), (b), (c) and (d). As can be seen, few NPs were taken up by microglia.

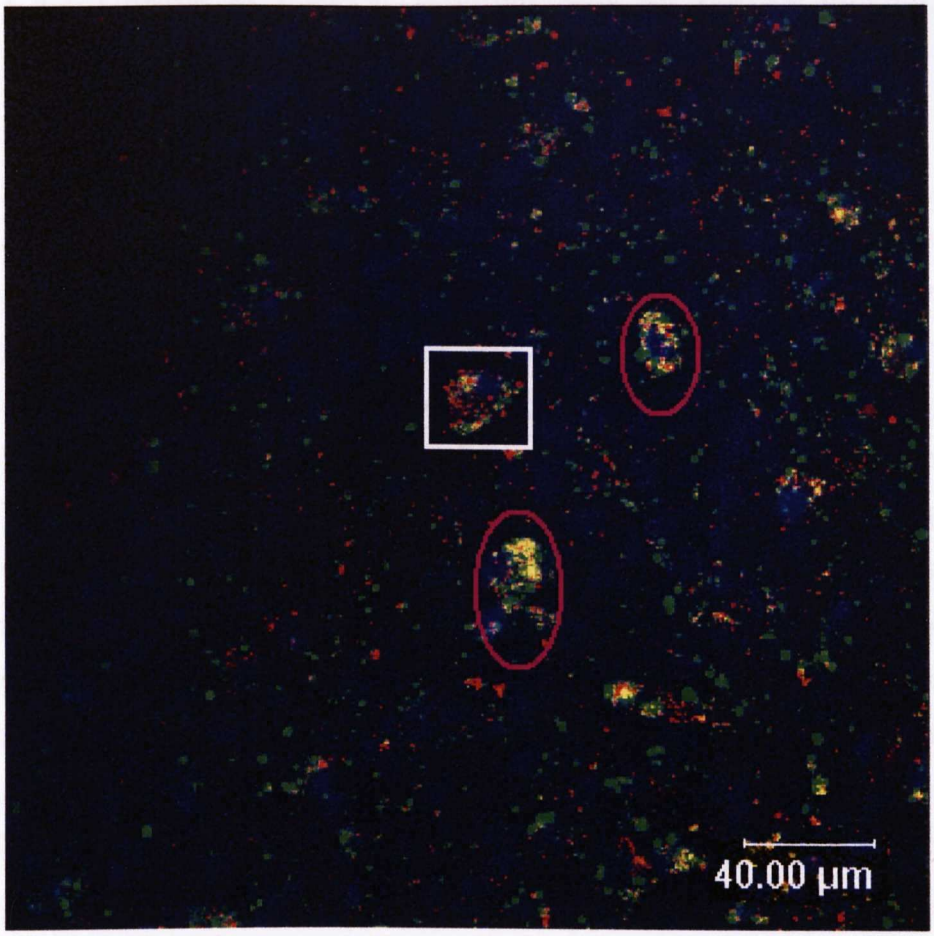

Fig. 6.26 Confocal fluorescence micrograph showing uptake of DXM-FL labelled PGA NPs and polystyrene latex beads by cerebral cortex slices. Equal amount of DXM-FL labelled PGA NPs and polystyrene latex beads was added onto cerebral cortex slices and then incubated for 24h. **Red fluorescence** came from polystyrene latex beads; **Green fluorescence** from DXM-FL labelled PGA NPs; **Blue fluorescence** came from DAPI; **Yellow fluorescence** indicated co-localisation of red and green fluorescence. It was shown that both types of particles were taken up by brain cells and they were sorted into same (purple circle) or different intracellular compartments (white square). Several cells accumulated huge amount of polystyrene latex beads and few DXM-FL NPs (white square)

6.4 DISCUSSION

6.4.1 Uptake of RBITC labelled NPs by DAOY aggregates and mixed foetal brain cell spherical aggregates

In the previous chapter, uptake of RBITC labelled NPs by cells was evaluated in monolayer culture. It was found that some large red fluorescent dots surrounded the nucleus of the cell, which indicated NPs may be present in late endosomes and lysosomes. Due to 3-D cell culture models more closely resembling an *in vivo* environment, NPs could also possibly be localized in the ECM. To determine whether the NPs were localized in lysosomes or in interstitial compartments, mixed foetal brain aggregates were incubated with NPs in the presence of LysoTracker Yellow, a marker freely permeating cell membranes and typically concentrated in acidic organelles in living cells. The LysoTracker Yellow, which is colourless at neutral pH, has a yellow fluorescence at the acidic pH. Confocal fluorescence micrographs (Fig. 6.2) illustrated that most NPs were taken up by brain cells and sorted into lysosome compartments as seen by the colour change of LysoTracker dye from yellow to orange colour. Only a few NPs were localized in the ECM.

By checking the viability of individual cells after they were dissociated from aggregates, the uptake of RBITC labelled NPs by DAOY and brain cell aggregates was studied by using flow cytometry and confocal microscopy. It was found that all of the DAOY cell samples in 2-D monolayer culture had a narrow and single MFI peak (Fig. 5.4b) while all of DAOY samples except the control showed a broader distribution peak in 3-D cell culture (Fig 6.5A). For the uptake study using primary mixed brain cells, the MFI peak was broader in 2-D monolayer culture (Fig. 5.4a) than that in 3-D spherical aggregate culture (Fig. 6.6B) before 6h of incubation time. With increased incubation time, the peak shape changed to the opposite way: the peak became broader in 3-D aggregate culture than that in 2-D monolayer culture. The differences in the MFI peak reflected the influence of cell

culture dimension on the diffusion distance and extent of access of NPs into the aggregates. In 2-D monolayer culture, NPs are in contact with all cells and access of NPs to each cell is not limited by diffusion distance. However, in 3-D spherical aggregates, most of the fluorescently labelled NPs would be taken up by cells close to the aggregate periphery with fewer NPs penetrating into the centre of the aggregates during the first several incubation hours. With increasing incubation time, uptake at the periphery would become saturated, allowing an increased uptake in the centre of the aggregate. This hypothesis of different diffusion distance of NPs in aggregates was confirmed by a direct observation of aggregates by confocal fluorescence microscopy (Fig. 6.7- Fig. 6.12). Fig. 6.7 and Fig. 6.10 showed that the intensity of fluorescence in the aggregate periphery was higher and concentrated around the cell nucleus while the intensity of fluorescence in the centre of aggregate was lower. Brighter fluorescence could be seen in only a few cells in the middle of aggregates. With increased incubation time, the intensity of fluorescence in the middle of the aggregate became higher, which led to brighter red fluorescence seen in most of cells (Fig. 6.8 and Fig. 6.11). After the aggregates were exposed to the NP suspension for 24h, NPs were taken up by all of the cells in the aggregates. It was also found that fluorescence intensity in cells localized in the periphery of aggregates was much higher than the rest of cells in the aggregates (Fig. 6.9 and Fig. 6.12).

Apart from the influence of distribution distance of NPs on NP intracellular uptake, the characteristics of the cell itself also played an important role on NP uptake. Aggregates consist of actively proliferating cells in the periphery and quiescent, intact and viable cells in the inner regions. Aggregate organization and thickness of proliferation cell layers differ significantly in different cell types (Sutherland *et al.*, 1988). As shown in Fig. 6.6, the intracellular MFI of mixed foetal brain aggregates was similar to that of DAOY aggregates in the first 4h of incubation time. The MFI of these two types of aggregates showed different trends after 6h of incubation time. Uptake of NPs by DAOY aggregates increased sharply with increased incubation time while uptake of NPs by mixed foetal brain aggregates showed only a slight increase. This resulted in MFI of DAOY aggregates

about 5 times higher than that of mixed foetal brain aggregates. Although there were slight differences in fluorescence intensity between the two types of aggregates in the first 4h of incubation time, confocal fluorescence images (Fig. 6.7 and Fig. 6.10) revealed distinctly different uptake patterns of NPs. From routine observation in aggregate culture, it was seen that the morphology of DAOY aggregates appeared smaller and less dense with greater translucence under a light microscope compared with mixed foetal brain aggregates. Therefore it was expected that the smaller size and less compact structure of DAOY aggregates could lead to faster and deeper penetration of NPs in ECM. On the contrary, Fig. 6.7 showed the fluorescence of some cells in the periphery of DAOY aggregate was relatively high and concentrated around the nucleus of the cells, suggesting lots of NPs were taken up by cells and most NPs did not broken down inside the lysosomes. As shown in Fig. 6.10b, Fig. 6.11b and Fig. 6.12b, the fluorescence intensity of cells, which were close to outside of brain aggregates or in the middle of brain aggregates, was lower and fluorescent dye was more evenly distributed, suggesting that NPs were degraded and RBITC was released into the cytoplasm. The observed differences might be due to the differences in the susceptibility of cells to the surface properties of NPs, recovery rate of cell membrane, and proliferative activity.

Fig. 6.6 also suggested the influence of cell culture dimension on the uptake of NPs by DAOY cells and mixed foetal brain cells. It was found that DAOY cells grown in 3-D cell culture resulted in a massive uptake of NPs into cells. In aggregates of brain cells the opposite happens, uptake in 3-D culture was lower than that seen in monolayer culture. This resulted in intracellular fluorescence intensity about 5 times higher in DAOY aggregates than mixed brain aggregates while in monolayer culture mixed brain cells took up 2 times as many NP as the DAOY cells. Recent studies have reported that mechanical tension generated between ECM and the cytoskeleton plays an important role in the regulation of cell growth, differentiation, cell signal transduction and gene expression (Chicurel *et al.*, 1998). Because the cytoskeleton is viscoelastic, slight mechanical effects can influence ion channel activity, transmembrane receptor localisation at

the plasma membrane of cells, and gene transcription (Janmey, 1998). In addition, in contrast to 2-D substrate, cytoskeletal organization in 3-D ECM has less mechanical stress. The higher uptake of NPs by DAOY cells in 3-D culture compared with corresponding 2-D culture might be due to the influence of stress-induced changes in the geometry of the cytoskeleton on increased activity and number of membrane receptors, and localisation of these receptors at the plasma membrane of cells. Apart from different physical and chemical stresses between 2-D cell culture and 3-D cell culture, the cells in aggregates are also exposed to a non-uniform distribution of oxygen and nutrients. This may lead to aggregates having actively proliferating cells in the periphery of the aggregate and numerous quiescent, intact and viable cells in the inner regions while 2-D cell culture only have actively proliferating cells. In addition, the cell culture dimension also affects the composition of 3-D cell cultures. In the study of the role of dimensionality in medulloblastoma invasion (Searle, 2004), Searle found 2-D monolayer culture conditions favoured survival and proliferation of glial cells to a much greater extent than neuronal cells. On the contrary, 3-D cell cultures favoured the survival and proliferation of neuronal cells compared with that of glial cells and was close to the cellular composition of brain tissue *in vivo*. Co-localisation confocal fluorescence images (Fig.6.2) demonstrated some cells took up lots of NPs while few NPs were taken up by some other cells, suggesting that uptake of NPs by mixed foetal brain aggregates was dependent on cell type. The lower amount of NPs taken up by mixed foetal brain cells in 3-D culture compared with that in 2-D substrate could be attributed to the influence of geometry on cell behaviour and cellular composition of aggregates.

When developing a drug delivery system, at least three factors must be considered: (1) the rate of release of therapeutic agents from the drug delivery system; (2) the amount of drugs released from the drug delivery system; (3) the extent of drug and drug delivery system distribution in the target organ. The first two factors have been investigated in the previous chapters, which showed a continuous and relatively slow release rate of RBITC from NPs (see 4.3.3), therefore the penetration extent of RBITC

labelled NPs was studied in the 3-D spherical aggregate model. Confocal fluorescence micrographs (Fig. 6.13 and Fig. 6.14) indicated that the inner structure of aggregates and migration rate of cell could have an effect on the penetration of RBITC labelled NPs. It was shown that the penetration distance of NPs in spontaneously formed aggregates and aggregates formed by the rotation method was 30-80%, 25-50% of the whole aggregate thickness, respectively, after 2h and 24h incubation time (Fig. 6.13B). Generally, the movement of macromolecules within the 3-D cell culture model is determined by the structure and composition of the interstitial compartment. Due to the loose inner organization of cells in spontaneously formed aggregates, NPs should be able to move faster and penetrate deeper within aggregates within a short time than that with aggregates formed by the rotation method.

6.4.2 Uptake of RBITC labelled NPs by organotypic slices

3-D cell aggregates have a well defined structure, which maintains the complex 3-D network of cell-cell and cell-matrix interactions, but it still has its limitations. It cannot completely replace the testing of biological mechanisms *in vivo* because of interorgan chemical communication. However the tissue structure of individual organs may be investigated *in vitro*. Many studies have shown that the different cell types, cytoarchitecture of the tissue, connections between cells and neuronal properties are largely preserved in organotypic brain slice cultures (Gähwiler *et al.*, 1988, and Bahr *et al.*, 1995). Thus uptake of NPs was also investigated in organotypic cerebral cortex slice cultures for an improved understanding of the interaction between NPs and cells in a tissue. Firstly, localisation of NPs was studied using organotypic slice cultures to check whether NPs are taken up by cells and enter into endosomes and secondary lysosomes in these more densely packed cultures. LysoTracker Yellow was again used as later endosome and lysosome tracer. After organotypic cerebral cortex slices were incubated with RBITC labelled NP suspension for 24h, some larger orange

fluorescence dots could be seen around the nucleus (green circle in Fig. 6.17), which indicated most NPs enter into lysosome, and only a few NPs localised outside of cells (see pink square in Fig. 6.17). A control sample, in which slices were only incubated with LysoTracker Yellow, showed very little yellow fluorescence around the nucleus (Fig. 6.18). Compared with confocal fluorescent image of slices incubated with NPs, it could be deduced that NP uptake increased the prominence of the compartment size of lysosomes and large intracellular yellow fluorescence dots in Fig. 6.17 was due to lysosomes full of NPs.

The above results of NP localisation in cerebral cortex slices were then followed by using TEM to confirm localisation of NPs within cells. Compared with the control slice sample (Fig. 6.16), Fig. 6.20a confirmed the results from confocal fluorescence images, which indicated NPs were sorted into secondary lysosome or later endosome compartment within cells. More information about the localisation of NPs was obtained using TEM. Most NPs have been sorted into lysosome compartments, which are positioned close to the nucleus. Lysosomes had varied sizes from 0.2 μm to 1.2μm. The different size of lysosome compartments containing ferritin loaded NPs might be due to a variety of digestive activities and a wide array of NPs in various stages of the intracellular uptake pathway when slices were fixed. After NPs were sorted into lyososomes (Fig. 6.20b), it was not possible to clearly distinguish NPs within the cellular compartments because only clusters of electron-dense ferritin particles can be distinguished. This might be due to most of NPs having been degraded within the lysosome compartment after a 24h incubation time.

Once NPs were incubated with aggregates and slices, they faced a range of possibilities: 1) some NPs were taken up by cells in the periphery of aggregates or cells on the top layer of slices; 2) some NPs were recycled back to the ECM after they were taken up by cells; 3) some NPs were bound to fixed elements in ECM; 4) some NPs localised in ECM reached cells and were taken up by surrounding cells; 5) some NPs diffused out from aggregates or slices and entered into the cell culture medium. Comparing

the penetration of NPs in mixed foetal brain aggregates whether aggregates were formed by the rotation method or spontaneously formed, penetration of NPs was faster than in organotypic cerebral cortex slices. The percentage penetration of NPs in the z-dimension in aggregates formed spontaneously, or formed by the rotation method, and in organotypic slices were 35-80%, 25-50%, and 20-35%, respectively. This might be mainly due to differences in the structure of interstitial compartment among these cell culture models. To simplify the number of possibilities faced by of NPs, the discussion here only refers to penetration of some NPs in ECM.

Firstly, ECM has an effect on viscosity of extracellular space (ECS) leading to different penetration of NPs in 3-D cell culture model. Fick's second law gives the most general equation describing NP penetration in the ECM: $\frac{\partial c}{\partial t} = D\frac{\partial^2 c}{\partial x^2}$, where C is the concentration of NPs; x is the position; t is time; D is NP diffusion coefficient through ECM. Fick's second law states that the rate of change of concentration in a volume element within ECM is proportional to the NP diffusion coefficient, which describes how individual NPs diffuse through tortuous ECM. The relation between penetration media and NP diffusion coefficient is given by the Stokes-Einstein equation as:

$D = \frac{RT}{6\pi r \eta N_A}$, which states that the NP diffusion coefficient is the inverse of the viscosity of the penetration media (η). ECS of the brain is a major channel for intercellular communication, nutrient and metabolite trafficking and drug delivery (Hrabětová and Nicholson, 2004). The channels of ECS are filled with ionic solution, closely resembling cerebrospinal fluid in composition, and macromolecules of ECM, predominantly proteoglycans and glycosaminoglycans (Margolis and Margolis, 1993, and Novak and Kaye, 2000). Secondly, ECM also plays a role in controlling the width of intercellular gaps. The large endogenous molecules and drug carriers are likely to be more sensitive to the width of intercellular gaps (Nicholson and Tao, 1993). The studies also indicated that the transport of charged molecules is influenced by the negative charge

associated with the ECM (Novak and Kaye, 2000). The effective viscosity of the medium in the interstitial spaces is increased by the presence of ECM (Hrabětová and Nicholson, 2004). Therefore composition of ECM is an important factor influencing NPs penetration. On one hand, the complex 3-D ECM affects the distribution and function of physiologically occurring factors. These biological effectors, for example hormones and growth factors, fundamentally control cell growth, differentiation and death. On the other hand, types of cell and development stage of cells could influence ECM organization and bring about its degradation because ECM such as collagens and proteoglycans is synthesized and processed intracellularly. It was found that cells in mature connective tissue devote a large proportion of their metabolic energy to proteoglycan (Hay *et al.*, 1991). Not only culture conditions and microenvironment, but also the three-dimensional architecture of the cells can influence ECM expression (Enam *et al.*, 1998). Matrix assembly, disassembly and reassembly of collageous matrices are dynamic processes which occur when a cell or a tissue undergoes growth, repair, or regeneration. Although aggregates appeared to maintain a high level of integrity of intracellular compartments and cell membrane after enzymatic treatment and mechanical dissociation (Searle, 2004), stimulation resulting from enzymatic treatment and mechanical dissociation might change cell signaling between cells. This could lead to a series of changes in remodelling ECM organization and composition. While in organotypic brain slices, the basic features of tissue organization are already present at the time of dissection, and the original ECM organization and composition could correspond to their location in situ after long term *in vitro* culture (Gähwiler, 1988). Thus, differences in composition and organization of ECM between aggregates and organotypic slices lead to different effects on the viscosity of ECS, width of intercellular gaps, and adsorption rate of NPs on the component of ECM. These resulted in the different penetration of NPs in 3-D cell culture models.

6.4.3 Cell type study of NP uptake in organotypic cerebral cortex slices

The localisation and penetration of NPs in mixed foetal brain aggregates and organotypic cerebral cortex slices also suggested RBITC labelled NPs were taken up selectively by particular cell types. Macrophages are widely distributed and play important roles in many tissues, such as recognition and clearance of damaged and senescent cells, invading particles, and macromolecular ligand (Gordon, 1995). Immunohistochemistry was used to investigate: (1) whether brain macrophages or microglia still exist in cerebral cortex after long time culture; (2) whether PGA NPs would be taken up by those macrophages. The monoclonal antibody OX-42 was used as a marker because it recognizes most macrophages including resident peritoneal and activated macrophages. It could recognize brain macrophages and microglia because OX-42 can recognize the complement C3bi receptor, which is expressed by both brain macrophages and microglia (Perry *et al.*, 1985, Robinson *et al.*, 1986, and Perry *et al.*, 1988). Its immunoreactivity is localised uniformly on the plasma membrane. It was expected that some brain macrophages and microglia could be found in our slice culture model (Fig. 6.24) based on Milligan's study (Milligan *et al.*, 1991). Milligan *et al.* reported that brain macrophages disappeared completely after the third postnatal week and microglia exhibited a gradual increase in number. The microglia cells remain in the adult central nervous system, constituting the resident macrophage population. As shown in Fig. 6.27 a few macrophages or microglial cell can be detected and only a few polysorbate-80 coated PGA NPs were taken up by macrophages or microglia. These might be due to the stabilisation of NPs by polysorbate-80. When uncoated NPs are administered intravenously, apart from particle size, their hydrophobic surface could adsorb blood components, opsonizing antibodies (IgG) and certain complement fragments (C3b, C3d and C4b). These opsonins can trigger phagocytosis by binding to specific cell-surface receptors on the macrophages and result in NPs being cleared from circulation (Taylor *et al.*, 2005). In contrast, polysorbate-80 is a non-ionic surfactant and has

hydrophobic and hydrophilic moiety in its structure. The hydrophobic moiety adsorbs on hydrophobic NP surface and hydrophilic regions hydrogen bond with water molecules, forming a protective hydration shell and thus reducing opsonisation, which acts as a bridge between NPs and phagocytes. Thus, after the NP suspension was incubated with polysorbate-80, PGA NP surface properties such as surface charge and surface hydrophobicity/hydrophilicity are altered. The steric stabilisation provided by polysorbate-80 conferred a relative "invisibility" to RBITC labelled NPs, which leads to relative lower immunoactivity of slices and uptake of NPs by macrophages. Polysorbate-80 coated polybutylcyanoacrylate NPs preferentially adsorbed apolipoprotein E on their surface, which can be recognized by brain cells, especially endothelial cells (Kreuter, 2001).

To confirm the results mentioned above, carboxylate-modified polystyrene latex beads, average size 100nm, were also investigated in organotypic slices. Polystyrene beads are known to be avidly taken up by macrophages (Illum *et al.*, 1986a). It is found that only a few cells accumulated a huge amount of polystyrene latex beads while other cells only took few polystyrene latex beads (Fig. 6.26). Cells containing a huge amount of polystyrene latex beans also took up a certain amount of DXM-FL labelled NPs. Among those several cells, it was demonstrated some polystyrene latex beads were sorted into the same intracellular compartments as DXM-FL labelled PGA NPs as evidenced by the change from red/green fluorescence into yellow fluorescence and some polystyrene latex beads were localised in the different intracellular compartments. Thus, those several cells were deduced as brain macrophages or microglia. The polystyrene latex bead study might also be looked on as evidence supporting the results obtained from the immunohistochemical staining study.

6.5 SUMMARY

In this chapter, uptake of fluorescently labelled NPs has been investigated in DAOY aggregates, mixed foetal brain aggregates and organotypic cerebral cortex slice cultures. Observation of routine culture under light microscope and TEM images confirmed that aggregates and organotypic slices were grown in a healthy condition and could maintain a histological similarity to *in vivo* tissue.

The influence of cell culture dimension on localisation and intracellular uptake of RBITC labelled NP:

In investigating interactions between NPs and cells, a suitable *in vitro* model as drug delivery target tissues is needed. Firstly, *in vitro* studies of NP distribution and intracellular localisation were carried out in 2-D (see chapter 5) and 3-D cell culture model in order to compare the effect of cell culture dimension on NP uptake. Those studies showed there was no difference in intracellular localisation between the 2-D cell culture model and the 3-D culture model. Confocal fluorescent micrographs demonstrated that NPs were sorted into lysosomes in DAOY and mixed brain cells in monolayer culture, DAOY and mixed foetal brain aggregates, and organotypic slices. Confocal microscopy studies in spherical aggregates and organotypic slices also illustrated that a few NPs were located in ECM during the process of NP uptake. Secondly, quantitative evaluation of NP uptake was performed by using flow cytometry following disaggregation of 2-D and 3-D cell cultures. Intracellular uptake of NPs was dependent on the incubation time and NP concentration. Flow cytometry studies also showed cell culture dimension had an obvious influence on the uptake of NPs by cells grown in 2-D and 3-D culture models. It was found that uptake of NPs by DAOY aggregates was about 6 times higher than that of DAOY cells in monolayer culture while mixed brain cells had an inverse pattern of NP uptake, in which uptake of NPs by brain cells in monolayer culture was about 2 times higher than by mixed brain aggregates. 2-D monolayer culture

could therefore lead to an incorrect characterization of the physiology of cells from the drug delivery viewpoint. However, recent studies showed the distribution of proliferating or quiescent cells within spherical aggregates, antigen expression, pH and pO_2 gradients closely parallel those *in vivo* (Sutherland, 1988). Aggregate models could therefore supply crucial information that may help us shape future research into drug delivery systems.

The influence of ECM on penetration of NPs in 3-D cell culture models:

Penetration of NPs through tissue was evaluated in three different 3-D cell culture models: 1) aggregates which formed spontaneously by using a higher individual cell concentration; 2) aggregates formed by a rotation method; 3) organotypic cerebral cortex slices. These three culture models were chosen because structure of ECM as well as components of ECM can influence the penetration of NPs during NPs uptake process. Confocal micrographs illustrated the aggregates formed spontaneously had a relatively looser structure than aggregates formed by the rotation method, and organotypic slices had a more compact structure than spherical aggregates. Thus the penetration of NPs in aggregates was faster and deeper than that in organotypic slices.

Uptake of NPs by organotypic slices

Finally, an immunohistochemical staining method was used to study interaction between NPs and brain macrophages and microglia because localisation and penetration studies suggested NP uptake was cell type dependent. Confocal micrographs indicated only a few NPs were taken up by brain macrophages or microglia, which was mainly due to the stabilisation of particles by polysorbate-80. Polystyrene latex beads were also used in following study to confirm the results found in immunohistochemical staining method. It was found that abundant polystyrene beads were only accumulated in several cells and these cells contained only a few PGA NPs. It was also found that polystyrene latex

beads and PGA NPs were sorted into different lysosome compartments.

Studies of NP uptake suggested that a 3-D cell culture model may increase the probability that conclusions drawn for a specific cell function and delivery system may be more easily extrapolated to that function within the organism *in vivo*. In the next chapter, DAOY aggregates, and organotypic cerebral cortex and cerebellum slices were chosen to develop a medulloblastoma invasion model and evaluation of uptake of NP in this realistic brain tumour tissue culture model.

CHAPTER 7

EVALUATION OF RHODAMINE B ISOTHIOCYANATE LABELLED NANOPARTICLES IN A TUMOUR AGGREGATES AND ORGANOTYPIC BRAIN SLICES CO-CULTURE MODEL

7.1 INTRODUCTION

Invasion is defined as the destruction of host cell ECM and active translocation of tumour cells through the ECM and is not simply due to expansion of tumour by growth or a passive distribution of tumour cells (Kaczarek *et al.*, 1999). Neoplastic cell migration and invasion can take several different forms (Bolteus *et al.*, 2001): 1) diffuse individual cell infiltration of brain, which is characteristic of glioma; 2) pseudoinvasion via vascular basal laminae, which is seen most frequently in malignant tumours, such as medulloblastoma; 3) consecutive waves of tumour cells displacing normal brain substance ("Roman army" movement), which is seen particularly in medulloblastoma; 4) leptomeningeal spread, which commonly occurs in gliomas and meningiomas. Thus invasion of tumour cells into normal tissue is a complicated process and invasion follows a three-step model (Pilkington, 1994, MacDonald *et al.*, 1998, and Bellail *et al.*, 2004): tumour cells 1) detach from the growing primary tumour mass; 2) adhere to the ECM via specific receptors; and 3) locally degrade ECM of adjacent cells and migrate into adjacent host tissue.

In order to study the invasive phenotype, suitable model systems are required. Numerous laboratory *in vivo* and *in vitro* models of brain tumour invasion have been developed to study the mechanism of tumour invasion and improve clinical therapeutic efforts. *In vivo* models of brain tumour invasion are usually set up by either a transplanted rat brain tumour or a chemically induced primary tumour in animals. Development of animal models is limited by several disadvantages, such as a long latent period between administration of carcinogen and overt signs of neural neoplasia together with the relatively low incidence of intracranial neoplasms (Pilkington, 1994 and 1997). Therefore, *in vitro* models have been widely developed. The following brain tumour invasion models are commonly used as *in vitro* models: 1) 3-D spherical foetal brain aggregates or organotypic slice invaded by single brain tumour cells (Searle, 2004); 2) spherical brain tumour aggregates invading 3-D spherical host aggregates (Pilkington, 1997, Penar *et al.*, 1998, and Terzis *et al.*, 2004). The model of organotypic slices invaded by 3-D spherical tumour aggregates has seldom been used. It was found that the invasion of malignant brain tumour such as medulloblastoma is mediated through various factors, which include receptor mediated cell-substratum contacts, cell-cell interaction and cellular migration.

Uptake of RBITC labelled NPs have been studied in DAOY cells and brain cells in monolayer cultures and 3-D cultures. Those studies indicated that cell culture dimension played an important role in the uptake and penetration of NPs. Thus the invasion model design is important because cell culture microenvironment has an effect not only on the invasive behaviours of brain tumour cells but may also have an effect on the NP uptake behaviour of brain tumour cells and normal brain cells. An optimal model to study tumour cell invasion may be an organotypic model, since the interaction between tumour cells and host tissue and interaction between NPs and brain tumour cells/normal brain cells are similar to the *in vivo*

situation. Medulloblastoma arises in the cerebellum and brainstem but not the cerebral cortex *in situ* (Chang *et al.*, 1969 and Nystrom *et al.*, 1972), therefore organotypic cerebellum and cerebral cortex slices were chosen as host tissues. DAOY aggregates were created from re-aggregation of single DAOY cell suspensions in flasks in a rotation culture system. In the following chapter, the development of co-culture models of tumour aggregates and host tissue are described. This model was then used to study the uptake of RBITC labelled NPs.

7.2 METHODS

7.2.1 A co-culture model of tumour aggregates and an organotypic brain slices

To accurately evaluate drug delivery systems *in vitro*, we are developing a co-culture model of tumour aggregates and organotypic brain slices. On day 1, cerebral cortex slices and cerebellum slices were dissected from P2 rat brains and cultured as described in 2.2.3.3. On day 3, DAOY monolayer cells were seeded as subconfluent in 25 cm^2 tissue culture flask. Culture medium was replaced with fresh culture medium (5ml) including FITC labelled magnetic microspheres (40μl, 1%w/v) on the following day. After 24h of incubation of DAOY monolayer cells with magnetic microspheres, DAOY cells were harvested and cultured in 25 ml screw top culture flasks for 24h to form DAOY aggregates (as described in 2.2.3.3). On day 6, DAOY aggregates (2μl), ranging in size from 200μm to 300μm, was gently added on the surface of each slice. The co-culture model of DAOY aggregates and organotypic brain slices were cultured for another 2 days, 4 days, or 6 days. The culture technique was shown in Fig. 7.1.

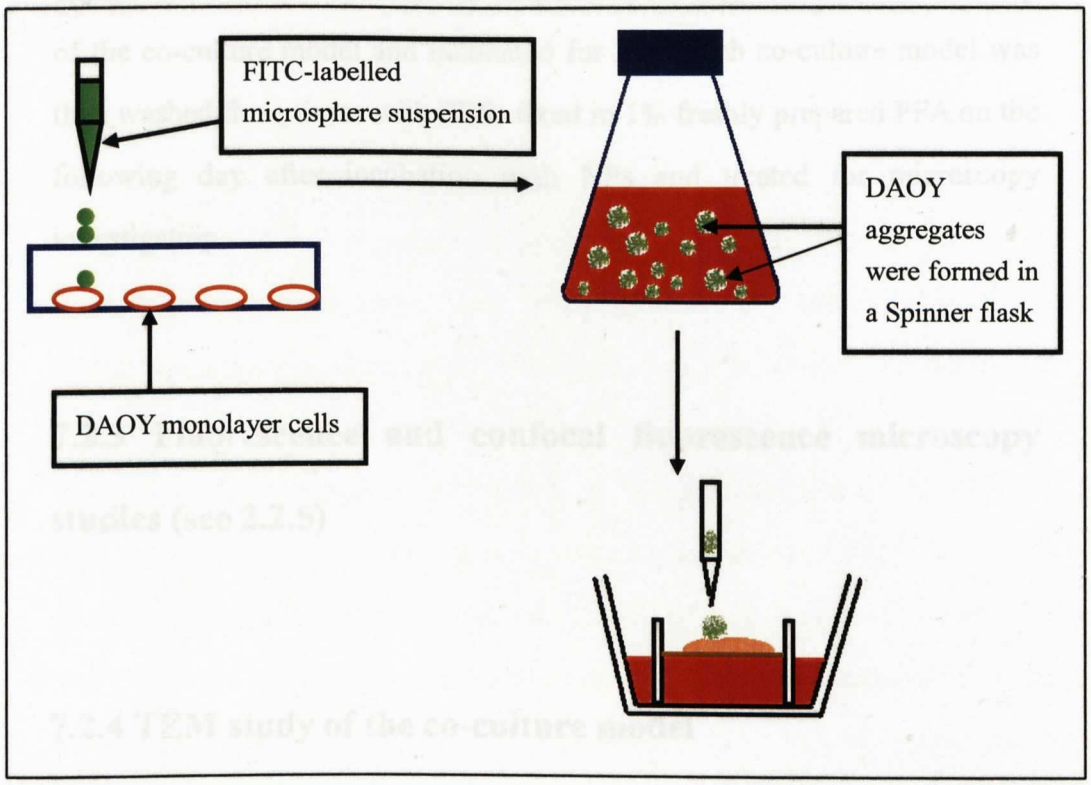

Fig. 7.1 Techniques used for culturing a co-culture model of DAOY aggregates and organotypic brain slices: After DAOY monolayer cells were incubated with FITC labelled microspheres (40µl, 1%) for 24h, cells were harvested and cultured in a Spinner flask for 24h to form aggregates. DAOY aggregate suspension (2µl) was gently added on the surface of brain slices on the following day. Then the co-culture models were maintained in 5% CO_2 incubator at 37°C for 2 days, 4 days, or 6 days.

7.2.2 RBITC labelled NPs taken up by the co-culture model

When DAOY aggregates were added onto the surface of organotypic brain slices, they were cultured for 2 days, 4 days or 6 days. To investigate NP uptake by co-culture models, NP suspension (200μg) was added on the top of the co-culture model and incubated for 24h. Each co-culture model was then washed three times with PBS, fixed in 1% freshly prepared PFA on the following day after incubation with NPs and treated for microscopy investigation.

7.2.3 Fluorescence and confocal fluorescence microscopy studies (see 2.2.5)

7.2.4 TEM study of the co-culture model

After DAOY aggregates and organotypic slices were co-cultured for 2 days, 4 days, or 6 days, they were processed into polymerization resin blocks and sections using the same procedure as described in 6.2.6.

7.3 RESULTS

7.3.1 Identifying DAOY cell in monolayer and spherical aggregate culture with FITC labelled magnetic microspheres

Fig. 7.2 shows the morphology of DAOY cell in monolayer culture and in 3-D spherical aggregate culture after taking up FITC labelled magnetic microspheres. This represents the morphology of individual DAOY cells invading into brain tissue after adhesion between tumour cells. FITC labelled magnetic microspheres were taken up by DAOY cells in monolayer culture and localised in lysosomes after 24h incubation (Fig. 7.2a and b). Then DAOY aggregates were formed spontaneously from the above mentioned DAOY cell in monolayer culture. As shown in Fig. 7.2c and d, DAOY aggregates were well formed, individual cells still could be seen in the periphery of the aggregate and cells in the centre of aggregates were darker under phase-contrast microscopy compared with DAOY aggregates without FITC labelled magnetic microspheres (Fig. 6.1). However DAOY aggregates accumulated with magnetic microspheres were not of uniform size and often clumped together over time in culture (Fig. 7.2d). This might be due to a few residual magnetic micropheres absorbed on the cell surface, which changed the surface charge property of DAOY cells.

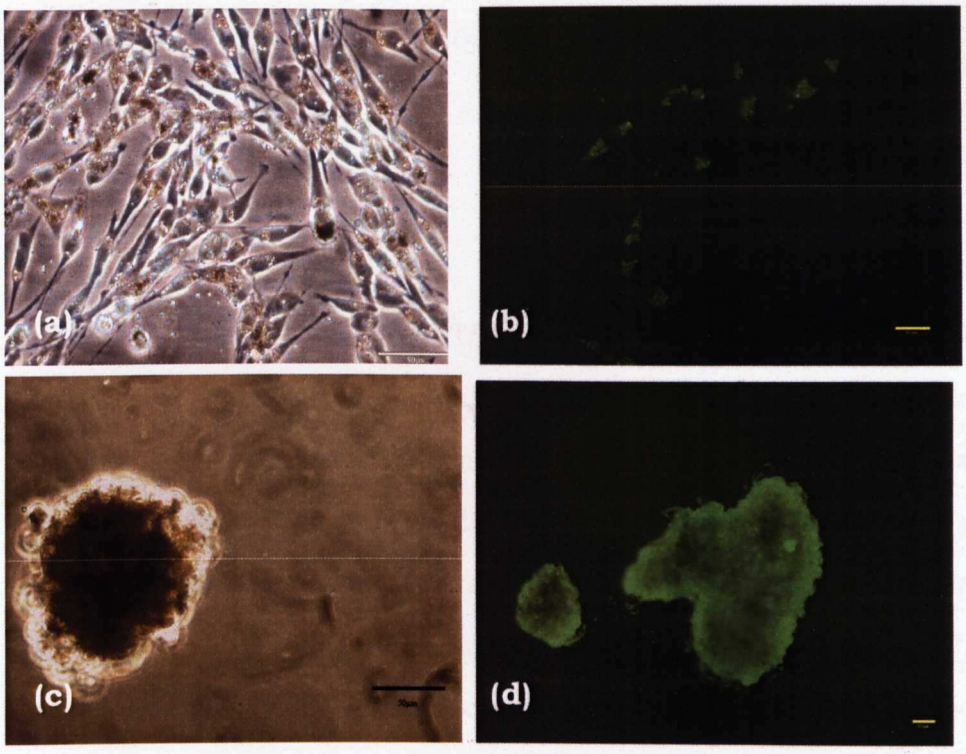

Fig. 7.2 Images of DAOY cells marked with FITC labelled magnetic microspheres in monolayer and aggregate culture. DAOY cells in monolayer were incubated with culture medium including FITC labelled magnetic micropheres for 24h and were harvested to form spherical aggregates by using the rotation method. Aggregates were cultured for 24h. (a) a phase-contrast micrograph showing DAOY cells in monolayer culture with accumulated microspheres; Scale bar: 50μm; (b) a fluorescent micrograph demonstrating microspheres taken up by DAOY cells in monolayer.; Scale bar: 20μm; (c) a phase-contrast micrograph illustrating DAOY aggregates formed from (a) using rotation method after 16h; Scale bar: 50μm; (d) a fluorescent micrograph (c) after 24h; Scale bar: 50μm; It shows that microspheres were taken up by DAOY cells in monolayer, and aggregates were formed well, but aggregates clumped together with longer incubation time.

7.3.2 The co-culture model of DAOY aggregates and organotypic cerebellum slices

7.3.2.1 Evaluation of the co-culture model using fluorescence microscopy

Fluorescence microscopy

After DAOY cells containing FITC labelled magnetic microspheres had formed spherical aggregates, they were added onto the top surface of organotypic brain slices and then were co-cultured for 2, 4, or 6 days. Finally invasion results were observed using fluorescence microscopy and TEM. Fluorescence images illustrated trends in the invasive behaviour of DAOY aggregates over time *in vitro* with cerebellum slices (Fig. 7.3-7.5). Individual DAOY cells invaded cerebellum slices over time *in vitro* by varying amounts and distances: 1) individual DAOY cells started to invade cerebellum slices over 2 days. It was shown that only one single DAOY cell appearing green fluorescence in image (red arrow) was found in host tissue and it had invaded over a relatively short distance, 210μm, from the DAOY aggregate margin (Openlab 3.1.7 package, Improvision, UK); 2) invasion of individual DAOY cells into slices appeared more clearly after 4 days co-culture time with a longer invasion distance. Most individual DAOY cells reached 109μm to 136μm and a few DAOY cells were up to 427μm away from the DAOY aggregate margin after 4 days co-culture time. 3) after 6-day incubation, DAOY cells had massively invaded the cerebellum slices. The invasion distance of most cells was within 455μm and some of the DAOY cells reached 972μm away from the aggregate margin.

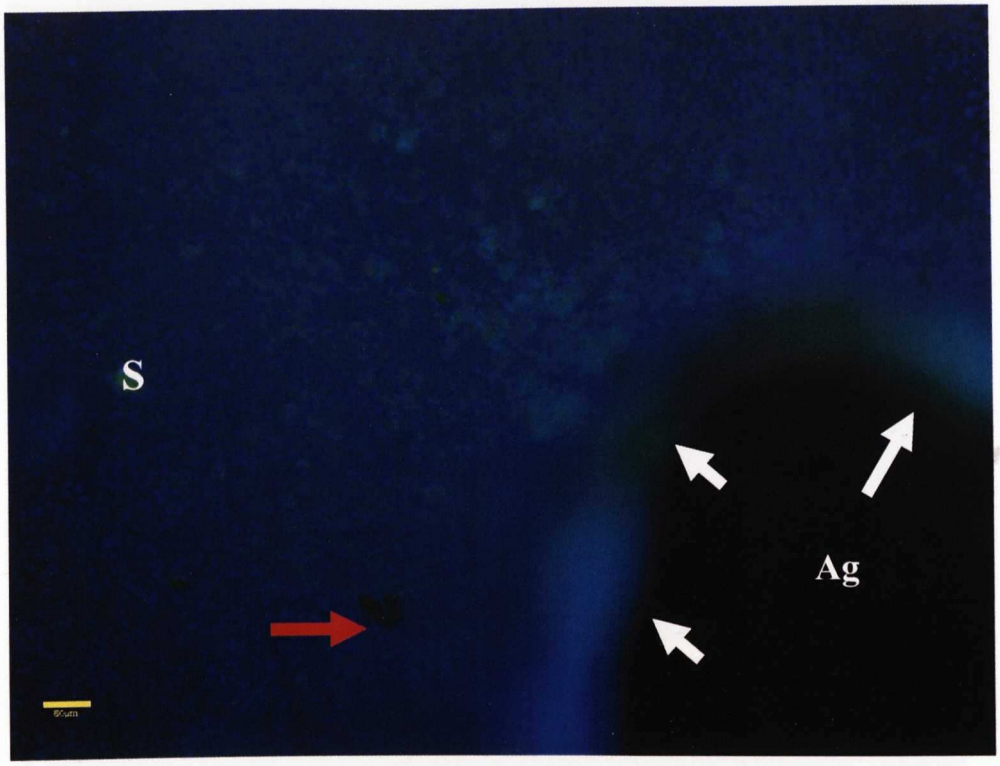

Fig. 7.3 A fluorescence micrograph showing co-culture of DAOY aggregates (Ag) and organotypic cerebellum slices (S) for 2 days. DAOY aggregates containing FITC labelled magnetic microspheres were added onto the surface of slices and they were co-cultured for 2 days. **Green or dark green fluorescence** was from FITC labelled magnetic micropheres; **blue fluorescence** was from DAPI. It was shown that one single DAOY cell appearing dark green (red arrow) in the image was found in the host tissue slice within a relatively short distance of invasion from the DAOY aggregate margin (white arrow) (210μm, Openlab 3.1.7 package, Improvision, UK); Scale bar: 50μm. Scale bar: 50μm

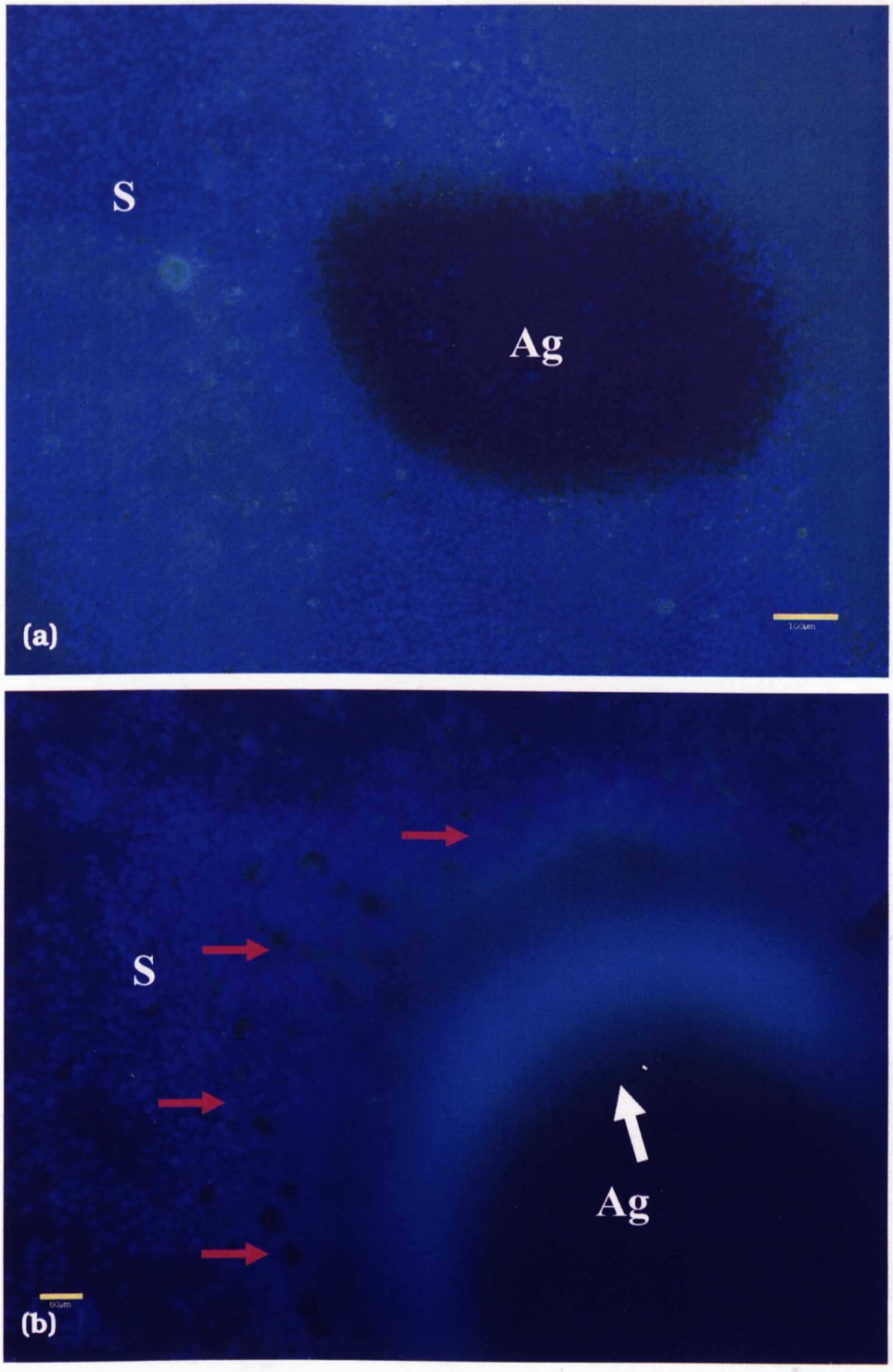

Fig. 7.4 Fluorescence micrographs showing co-culture of DAOY aggregates (Ag) and organotypic cerebellum slices (S) for 4 days. (a) lower magnification, scale bar: 100μm; (b) higher magnification, scale bar: 50μm. **Green or dark green fluorescence** was from FITC labelled magnetic microspheres; **blue fluorescence** was from DAPI. It was shown that DAOY aggregate invasion occurred and invading individual DAOY cells (red arrow) typically reached 109μm to 136μm but some DAOY cells were up to 427μm away from the DAOY aggregate margin (white arrow) after 4 days co-culture time.

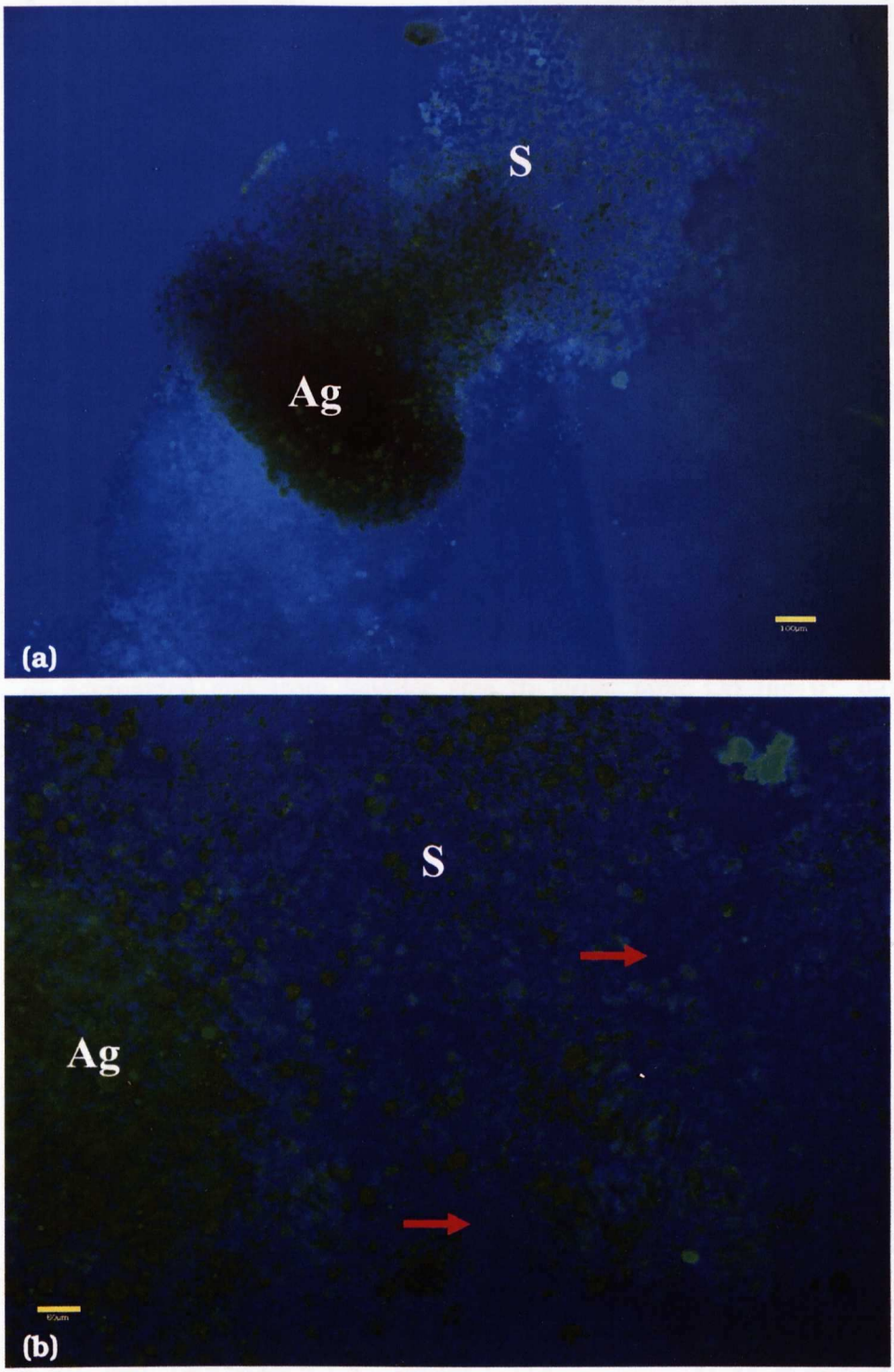

Fig. 7.5 Fluorescence micrographs showing co-culture of DAOY aggregates (Ag) and organotypic cerebellum slices (s) for 6 days. (a) lower magnification, scale bar: 100μm; (b) higher magnification, scale bar: 50μm. **Green or dark green fluorescence** was from FITC labelled magnetic microphores; **blue fluorescence** was from DAPI. Massive tumour cell invasion could be observed. The invasion distance of most DAOY cells (red arrow) was within 455μm but some of DAOY cells reached up to 972μm.

Confocal fluorescence microscopy

The same samples were also observed under the confocal fluorescence microscope because the confocal fluorescence microscopy enables the collection of a series of images through organotypic cerebellum slices, which can provide more information about the invasion behaviour of DAOY aggregates in inner slices. The movies 7.1-7.3 illustrate the whole scanning processes of co-culture model from the top to the bottom for 2 days, 4 days or 6 days co-culture time. A series of z-dimension scans in the margin of DAOY aggregates illustrated that aggregates progressively spread into the cerebellum slices over a 2-day co-culture time. At days 2 and 4, green fluorescence gradually spread from middle of aggregate into the edge of aggregated and from smaller size to larger size. On the 6^{th} day of co-culture, green fluorescence spread wasn't as clear as that on 2-day and 4-day co-cultures.

7.3.2.2 Evaluation of the co-culture model using TEM

A second way of ascertaining the invasive properties of the co-culture model was visualizing the co-culture model under TEM. Fig.7.8 - Fig.7.10 demonstrate the process of DAOY aggregates invading into cerebellum slices. To compare DAOY aggregate invasion over time, three areas were commonly chosen: 1) whole image of co-culture model with lower magnification; 2) area right under DAOY aggregate; 3) area close to the brain/tumour border. After 2 days of co-culture, a firm attachment of DAOY aggregates to the cerebellum slice was observed. The cerebellum slice kept much of its organotypic structure at the border between DAOY aggregate and cerebellum slice. A few single DAOY cells infiltrated the cerebellum slice (Fig. 7.8a and b), but no DAOY single cells were observed in the area, which was close to the brain/tumour border (Fig. 7.8c). With longer co-culture time, DAOY aggregate invaded the cerebellum slice and normal brain slices were destroyed at the brain/tumour border. In addition to many DAOY single cells invading the cerebellum slices, some DAOY cells were also discerned at the bottom of cerebellum slice (Fig. 7.9 a and b, and Fig. 7.10 a and b). DAOY single cells could also be seen in the area close to the brain/tumour border (Fig. 7.9 c and Fig. 7.10 c).

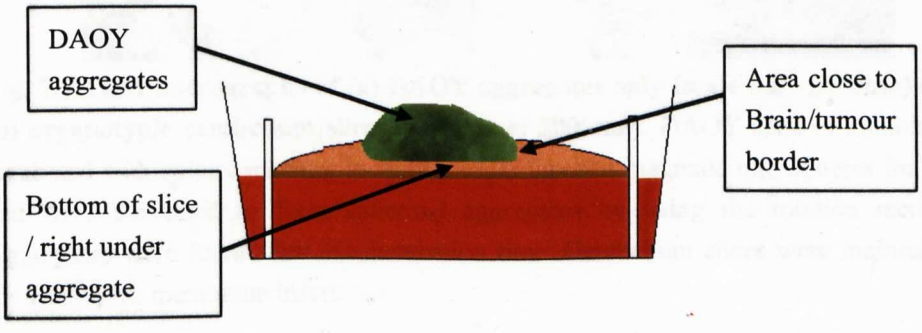

Fig. 7.6 Image demonstrating the area of TEM image taken from the co-culture model

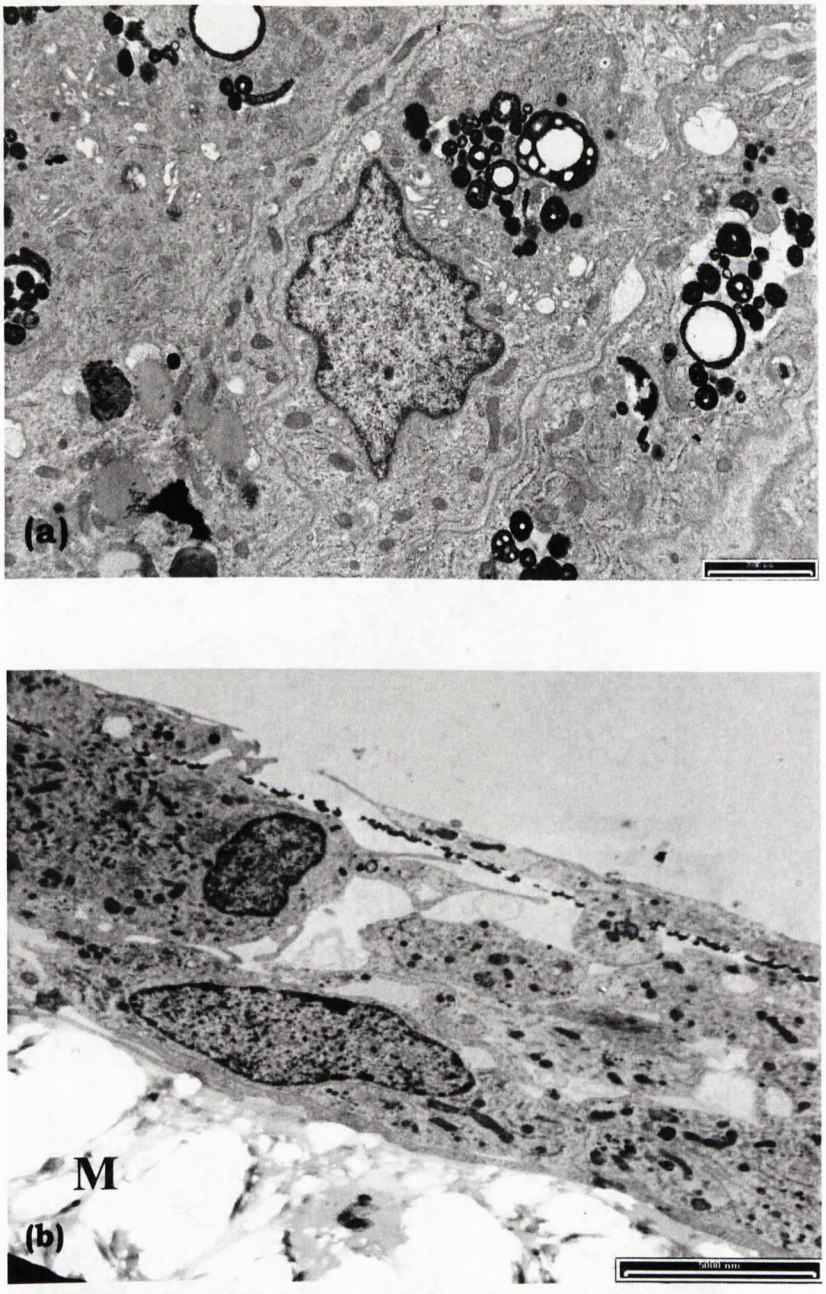

Fig. 7.7 TEM micrographs of (a) DAOY aggregates only (scale bar: 2000nm) and (b) organotypic cerebellum slices (scale bar: 5000nm). DAOY cells in monolayer incubated with culture medium including FITC labelled magnetic microphores for 24h and were harvested to form spherical aggregates by using the rotation method. Aggregates were fixed after 24h incubation time. Cerebellum slices were maintained for 4 days. M: membrane insert.

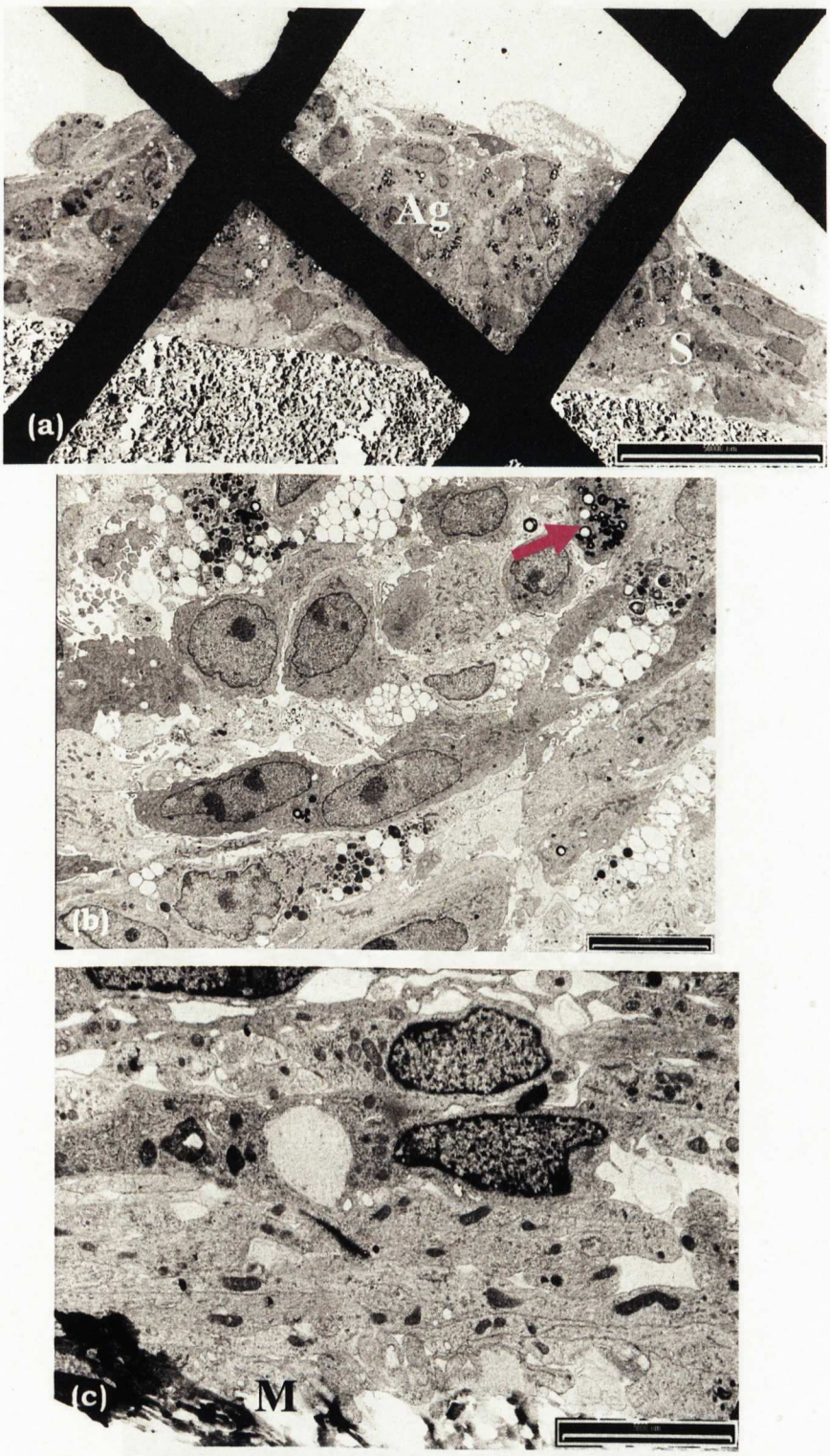

Fig. 7.8 TEM micrographs of DAOY aggregate (Ag) and cerebellum slice (S) co-cultured for 2 days. (a) a 2-day co-culture model with lower magnification; scale bar: 50,000nm; (b) area of the slice just right under the DAOY aggregate with high magnification. scale bar: 10,000nm; (c) area of the slice close to the brain/tumour border with high magnification; scale bar: 5,000nm. As shown, DAOY aggregate attached on the slice and individual cells (purple arrow) invaded into slice. No DAOY cells were observed in the area close to the brain/tumour border. M: membrane insert.

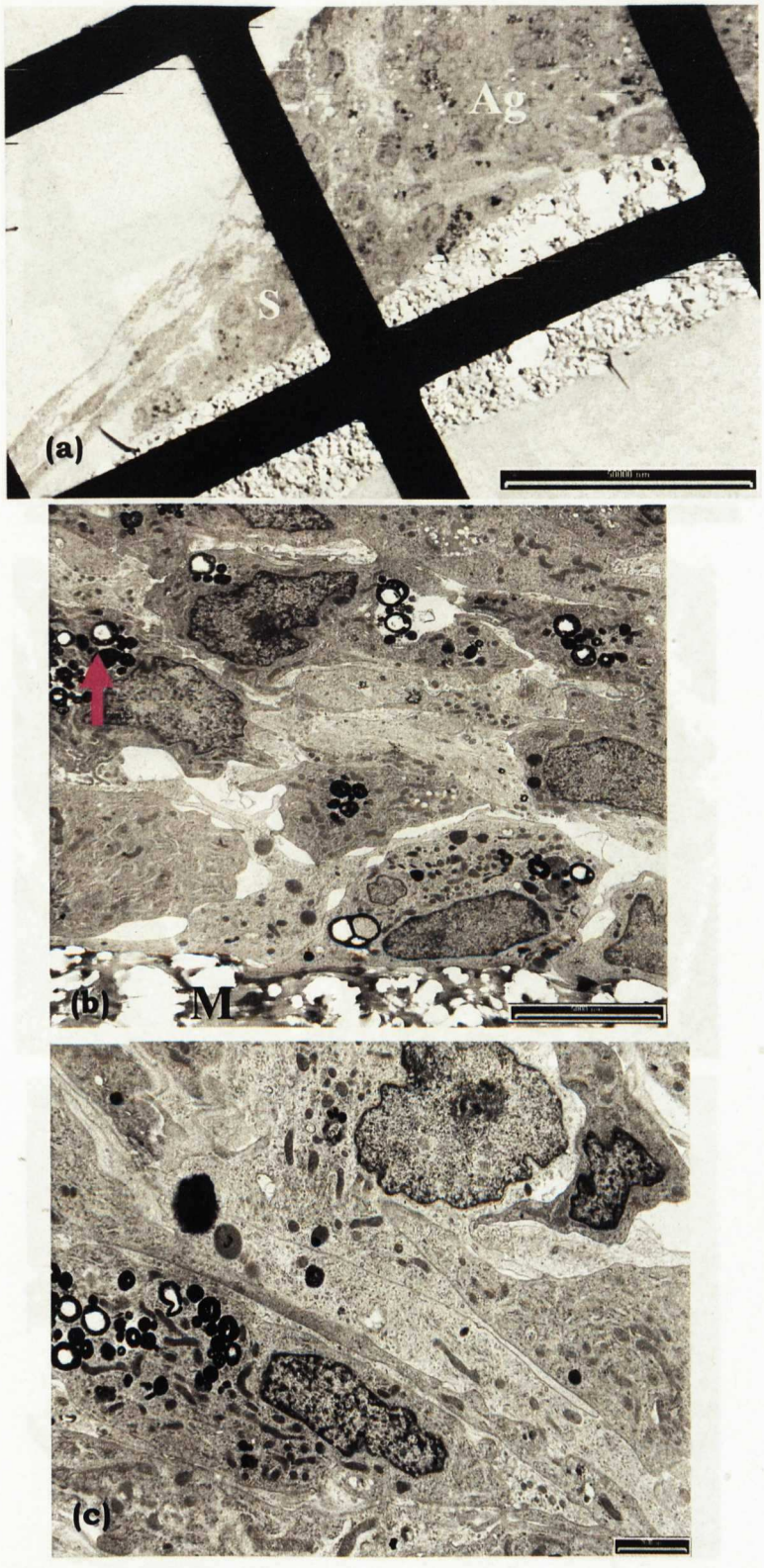

Fig. 7.9 TEM micrographs of DAOY aggregate (Ag) and cerebellum slice (S) co-cultured for 4 days. (a) a 4-day co-culture model; scale bar: 50,000nm; (b) area of the slice right under the DAOY aggregate with high magnification; scale bar: 5,000nm; (c) area of the slice close to the brain/tumour border with high magnification; scale bar: 2,000nm. It was shown that DAOY cells (purple arrow) invaded into the bottom of the slice and the area close to the brain/tumour border. M: membrane insert.

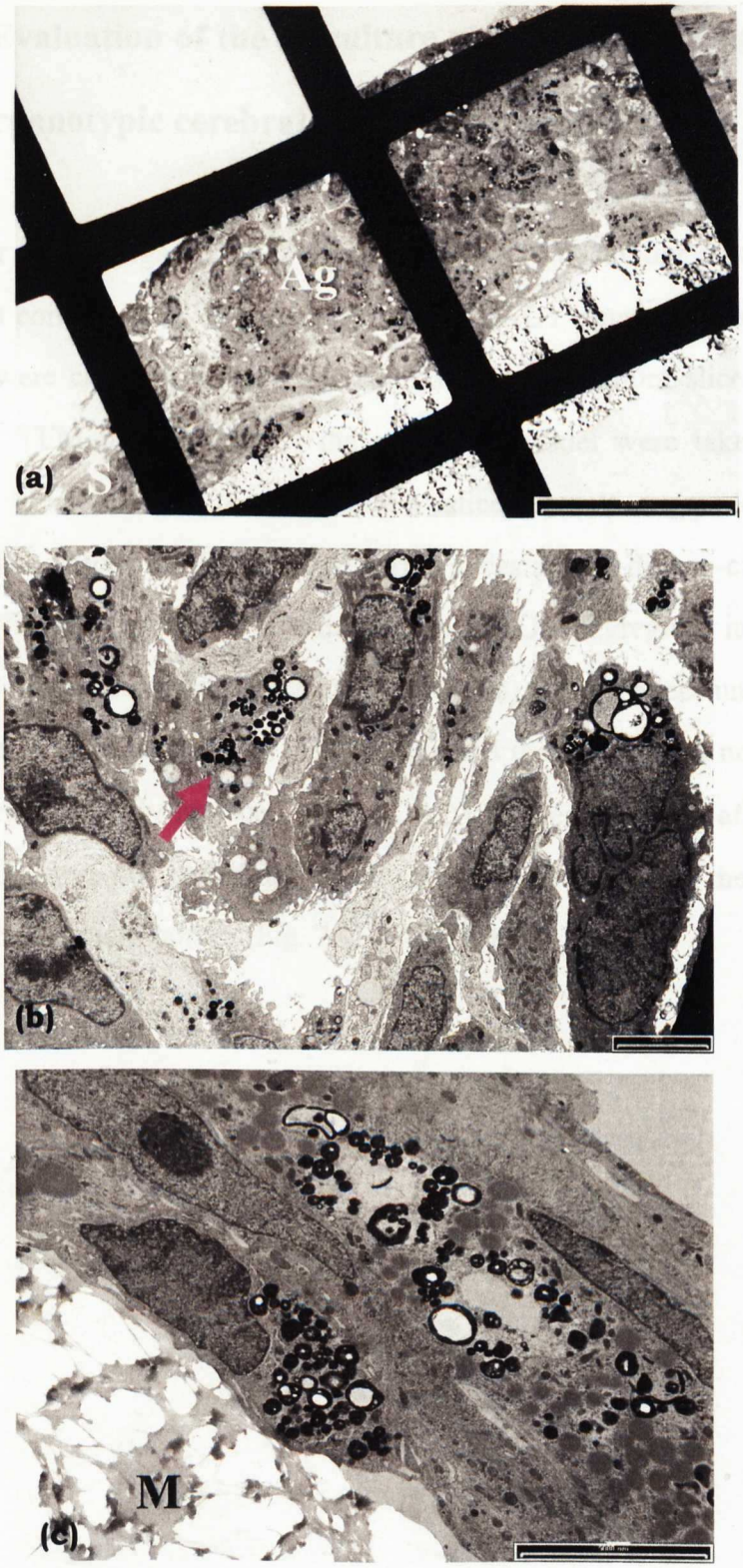

Fig. 7.10 TEM micrographs of DAOY aggregate (Ag) and cerebellum slice (S) co-cultured for 6 days. (a) a 6-day co-culture model; scale bar: 50,000nm; (b) area of the slice right under the DAOY aggregate with high magnification; sale bar: 5,000nm; (c) area of the slice close to the brain/tumour border with high magnification; scale bar: 5,000nm It was shown that DAOY cells (purple arrow) invaded into the bottom of the slice as well as the area close to the brain/tumour border.. M: membrane insert.

7.3.3 Evaluation of the co-culture model of DAOY aggregates and organotypic cerebral cortex slices using TEM

In order to investigate DAOY aggregate invasive behaviour in organotypic cerebral cortex slices, co-culture models of DAOY aggregates and cerebral cortex were cultured in the same condition as cerebellum slice co-culture models. TEM micrographs of the co-culture model were taken to show similar areas as for the cerebellum slice co-culture model. DAOY aggregates attached to the cerebral cortex slices after 2-day co-culture (Fig. 7.11). With an increase of co-culture time, DAOY aggregates invaded into cerebral cortex slices (Fig. 7.12a and Fig. 7.13a). Cortex slices under DAOY aggregate were destroyed by DAOY cells and the majority of normal brain cells were gradually replaced by the DAOY aggregate. Even after a 6-day co-culture time, no DAOY individual cells could be found in the area close to the brain/tumour border (Fig. 7.11 b-Fig. 7.12b).

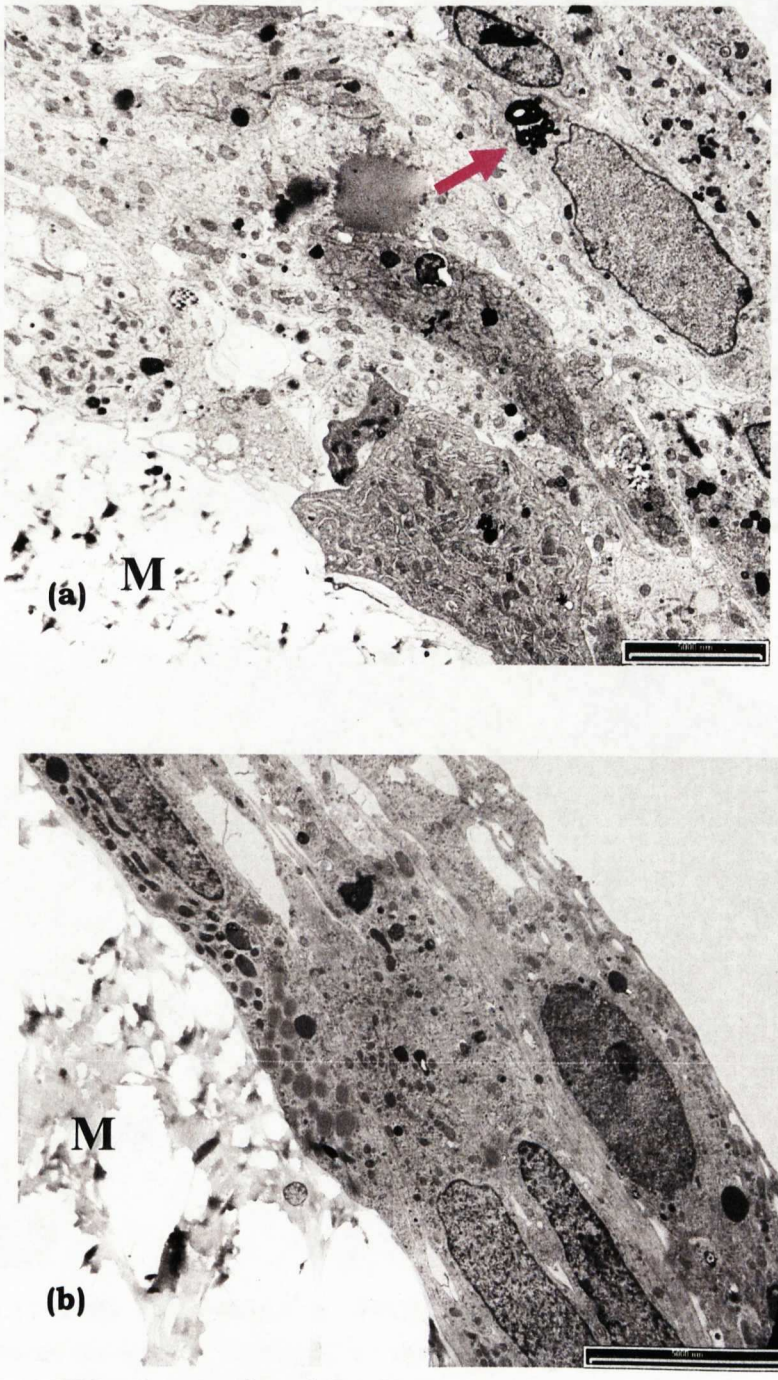

Fig. 7.11 TEM micrographs of DAOY aggregate and cerebral cortex slice co-cultured for 2 days. (a) area of the slice right under DAOY aggregate; scale bar: 5,000nm; (b) area of the slice close to brain/tumour border; scale bar: 5,000nm. It was shown that the DAOY aggregate attached on the slice and individual cell (purple arrow) invaded into the slice. No DAOY cells were observed in the area close to the brain/tumour border. M: membrane insert.

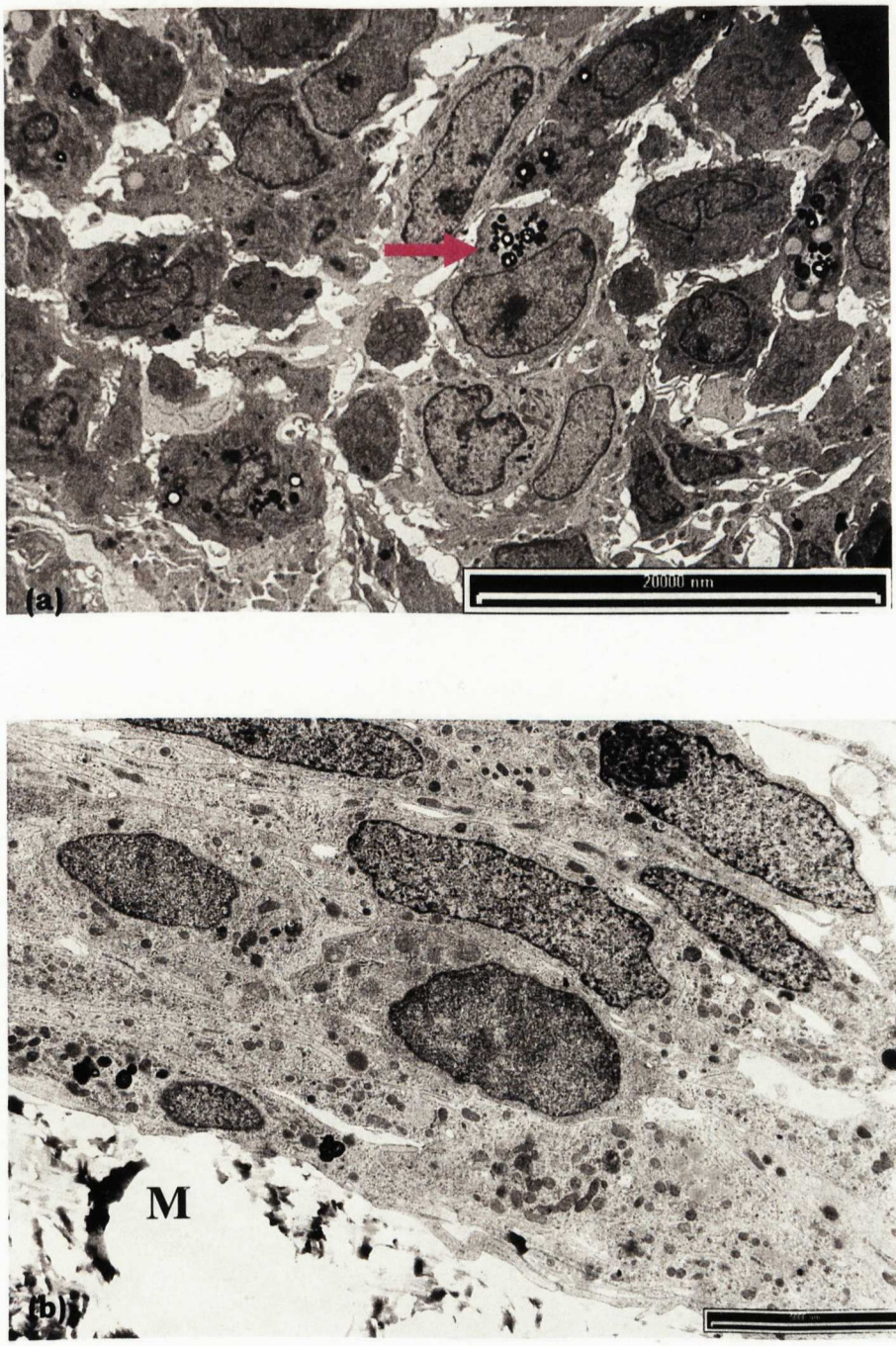

Fig. 7.12 TEM micrographs of DAOY aggregates and cerebral cortex slice co-cultured for 4 days. (a) area of the slice just under DAOY aggregates; scale bar: 20,000nm; (b) area of the slice close to brain/tumour border; scale bar: 5,000nm. It was shown that DAOY cells (purple arrow) invaded into the bottom of the slice but no DAOY cells were observed in the area close to the brain/tumour border. M: membrane insert.

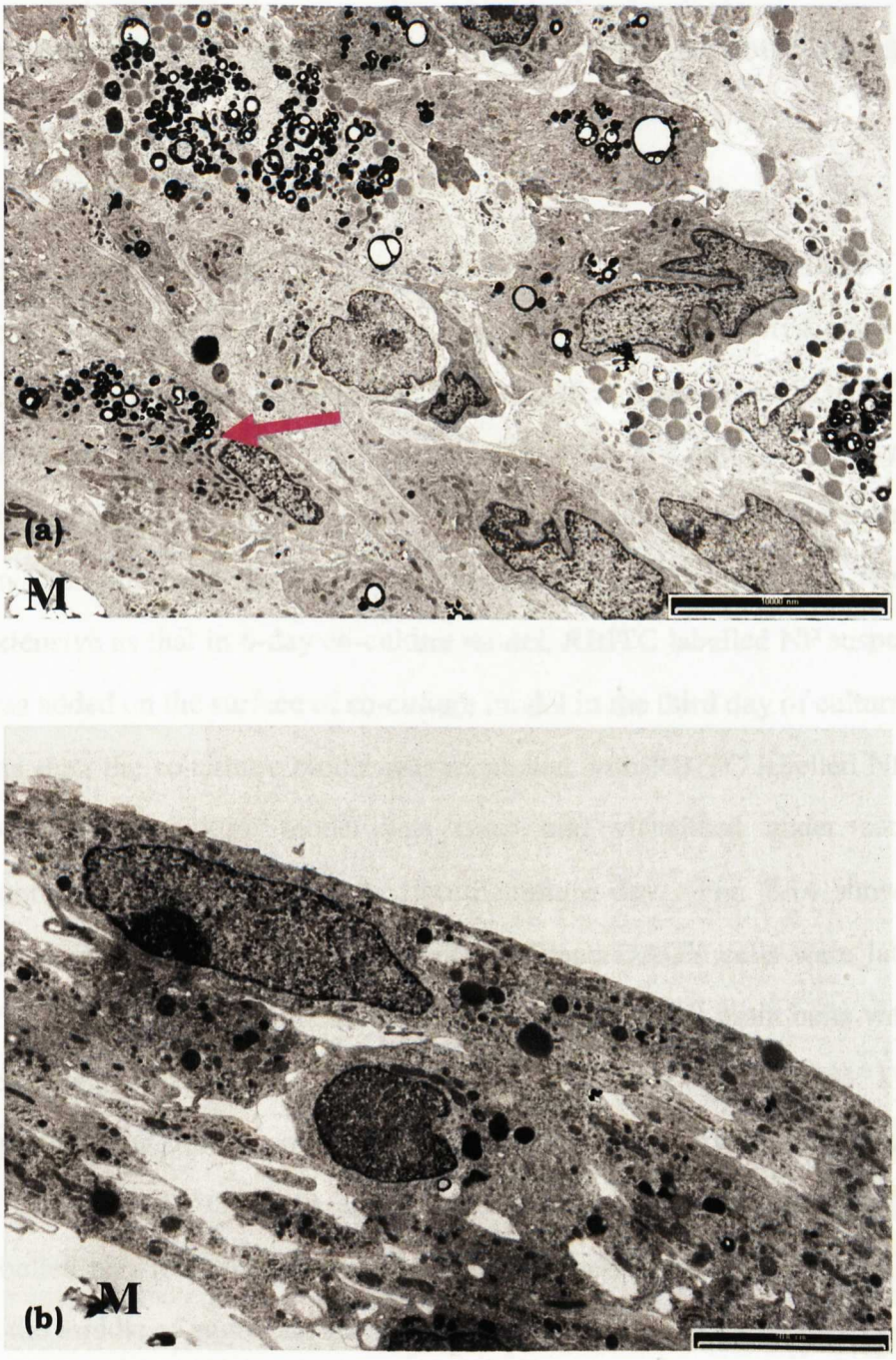

Fig. 7.13 TEM micrographs of DAOY aggregate and cerebral cortex slice co-cultured for 6 days. (a) area of the slice under the DAOY aggregate; scale bar: 10,000nm; (b) area of the slice close to brain/tumour border; scale bar: 5,000nm. It was shown that DAOY cells (purple arrow) invaded into the bottom of the slice but no DAOY cells were observed in the area close to the brain/tumour border. M: membrane insert.

7.3.4 Microscopic investigation of RBITC labelled NPs in tumour aggregates and organotypic cerebellum slices co-culture model

Fluorescence microscopy and TEM studies ascertained that DAOY cells invaded into cerebellum slices and massive invasion occurred after 6-day co-culture time. To clearly understand the different response of DAOY cells and normal brain cells to RBITC labelled NPs, a 4-day co-culture model was chosen to carry out NP uptake study because not only DAOY aggregate invasion into cerebellum slice occurred but the invasion pattern was not as extensive as that in 6-day co-culture model. RBITC labelled NP suspension was added on the surface of co-culture model in the third day of culture time and then the co-culture model was incubated with RBITC labelled NPs for 24h. The co-culture model was fixed and visualized under confocal fluorescence microcope on the fourth culture day. Fig. 7.14 shows the uptake of NPs by the co-culture model. Since DAOY cells were labelled with FITC labelled magnetic microspheres and normal brain cells weren't, cells with green and blue (DAPI) fluorescence represented DAOY aggregates or DAOY single cells and brain cells had only blue fluorescence. It shows that DAOY cells on the edge of aggregates took most of RBITC labelled NPs (red fluorescence) and few NPs were taken up by DAOY cells in the middle of aggregate and normal brain cells (Fig. 7.14).

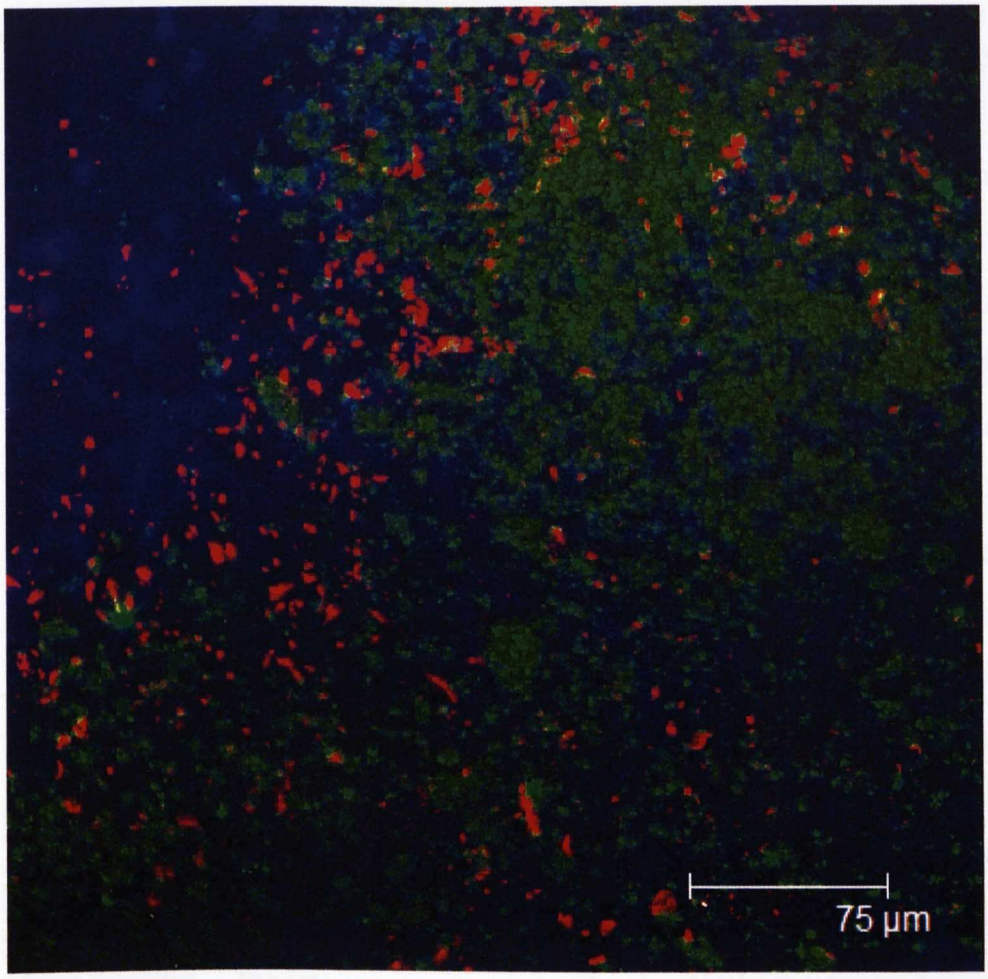

Fig. 7.14 Confocal micrograph demonstrating RBITC labelled NPs taken up by 4-day co-culture model of DAOY aggregates and organotypic cerebellum slices. RBITC labelled NPs culture medium (4mg/ml, 50µl) was added on the top of co-culture model and incubated with co-culture model for 24h after DAOY aggregates and slices were co-cultured for 3 days. Red fluorescence was from RBITC labelled NPs; Cells containing green (from FITC labelled magnetic microspheres) and blue (from DAPI) fluorescence represent DAOY cells; Normal brain cells had only blue fluorescence. It was shown that DAOY cells take up most NPs and few NPs were internalized by normal brain cells.

7.4 DISCUSSION

7.4.1 Assessment of the co-culture model of tumour spherical aggregates and organotypic brain slices

Several *in vitro* invasion models have investigated the role of dimensionality and brain regional specificity on DAOY cells and DAOY aggregate invasive behaviour (Searle, 2004). The greatest invasion of DAOY aggregates into cerebellum aggregates occurred over 48 hours co-culture time and the invasion of DAOY aggregates couldn't be observed in cerebral cortex aggregates after 48 hours, which led to the expectation that DAOY aggregates would also invade organotypic cerebellum slices. Fluorescence and confocal fluorescence microscopy, and TEM studies confirmed that DAOY aggregates invaded into adjacent cerebellum slices (Fig. 7.3-7.10 and movie 7.1-7.3). Based on the commonly reported invasion mechanism (Liotta, 1986, Pilkington, 1994, and Bolteus *et al.*, 2001), it was deduced that the microenvironment created by brain cells in organotypic slices and DAOY aggregates resulted in DAOY cell invasion. In order to invade into the brain slices, DAOY aggregates might stimulate normal cellular elements of the brain to produce and secrete ECM components, which may contribute to DAOY cell adhesion to the matrix. It has been reported that hyaluronan and many other ECM components are upregulated to facilitate primary brain tumour migration and invasion *in vitro* (Demuth and Berens, 2004). Following DAOY cells adhesion to and migration on the ECM components, local matrix might be degraded by DAOY cell-associated proteinases. Several proteases are thought to be involved in the degradation of ECM components of host cells, including matrix metalloproteinases (MMPs), serine proteinases, cysteine proteinases, glycosidases (Rooprai and

McCormick, 1997). Among these, MMPs are viewed as a major factor affecting tumour invasion (Pilkington, 1994, Béliveau *et al.*, 1999, Bellail *et al.*, 2004, and Demuth and Berens, 2004). The MMPs constitute a multigene family of >25 secreted and cell surface enzymes that process or degrade various pericellular substrates (Sternlicht and Werb, 2001). Several studies address that MMPs are over expressed in classic and desmoplastic medulloblastomas (Ozen *et al.*, 2004) and in gliomas (Demuth and Berens, 2004). During the process of invasion of brain tumour cells, cross-talk between brain cells and DAOY cells also played a critical role because ECM components producing, cell adhesion molecules and proteases expression, and cell are interactive. Cell-cell communications, which are important in growth control and differentiation, are in part accomplished by gap junctions and second messengers (Goodenough *et al.*, 1996). Decreased gap junction formation may result in fewer inhibitory signals leading to the promotion of uncontrolled cell division and differentiation (Ruch, 1994).

Microscopy studies were used to investigate the invasion behaviour of aggregates. DAOY aggregates as a unit adhered to adjacent cerebellum slices and gradually destroyed and invaded normal cerebellum slice from the tumour/ brain border. Terzis *et al.* reported a similar invasion pattern of DAOY aggregates after 7-day co-culture of DAOY aggregates and normal whole brain aggregates (Terzis *et al.*, 1994). Individual DAOY cells spread widely to invade almost the whole cerebellum slices over a relatively long distance after 6 days of co-culture (Fig. 7.5). All of these results suggest this organotypic co-culture tumour invasion model is similar to the invasive behaviour of medulloblastoma *in vivo* (Bolteus *et al.*, 2001)

TEM studies showed that DAOY aggregate invasion into cerebral cortex slices occurred, but DAOY cell invasion was relatively limited compared

with the co-culture model of DAOY aggregates and cerebellum slices. The tumour microenvironment consists of neoplastic cells, host cells and ECM (Mareel *et al.*, 1990). The microenvironment created by cerebellum and DAOY aggregates differed from the corresponding microenvironment created by cerebral cortex slices and DAOY aggregates, resulting in the different invasion patterns observed. Tumour invasion is a complicated process, governed by molecular cross-talk between DAOY cells and DAOY cells, DAOY aggregates and normal brain cells, and DAOY cells and normal brain cells; types and amount of lytic enzymes produced by DAOY aggregates and DAOY cells; fine regulation of adhesion to and detachment from ECM (Mareel *et al.*, 1993). Histological differences between cerebellum slices and cerebral cortex slices result in biological differences. This could influence regulatory factors (growth and invasion) being produced and destroyed and the concentration of nutrients, resulting in a change in the culture environment (Fidler, 1991, and Mareel *et al.*, 1993). Variability of brain slices in cell surface molecules, production of growth factors and growth inhibitors could modify adhesion properties of DAOY cells (Wikstrand *et al.*, 1991 and Peyrl *et al.*, 2003) and affect DAOY aggregate invasion and adhesion of DAOY cells in the periphery of DAOY aggregates (Finn *et al.*, 1997). Culture microenvironment could affect the production of growth factors (Smits *et al.*, 1996) and MMP's (Bodey *et al.*, 2000a and b) by DAOY cells, which could affect local ECM degradation created by culture environment and subsequent DAOY aggregate and cell invasion.

Since medulloblastoma arises in the cerebellum and brainstem but not the cerebral cortex *in situ* (Kleihues *et al.*, 2000) and Searle's study also indicated that DAOY aggregates didn't attach to brain cortex aggregates (Searle, 2004), it was therefore expected that DAOY cell would not invade organotypic cerebral cortex slices. However, TEM results were different

from previous reports suggesting that DAOY aggregates only invaded into cerebellum slices not into cerebral cortex. As mentioned in previous chapters, cell culture dimension played a critical role in cyto-architecture of regional brain cultures, in turn affecting types of brain cell, ratio between each brain cell, composition of ECM, and subsequent invasive behaviour of DAOY cells. Several co-culture models have been used to investigate the role of dimension on medulloblastoma invasion including: 1) co-culture of DAOY single cells and brain monolayer cells from cerebellum or cerebral cortex; 2) co-culture of DAOY single cells and spherical aggregates dissociated from different part of brain, and 3) co-culture DAOY aggregates and regional brain aggregates (Searle, 2004). Searle reported that invasion occurred in the first two culture models but not in the third one. Very little is known about the mechanisms involved in medulloblastoma cell invasion so far, therefore the discrepancy results between ours and Searle's could be attributed to the difference in culture model resulting in different culture histology and microenvironment that were created by tumour cells and regional brain cells (Fidler, 1991).

7.4.2 Microscopic investigation of RBITC labelled NPs in the co-culture model of tumour aggregates and organotypic cerebellum slices

Since NP taken up by DAOY aggregates was 5 times higher than that by mixed whole foetal brain aggregates (Fig. 6.6), results of NP uptake study was in accordance with uptake study in study of 3-D aggregates. The massive uptake of NPs by DAOY cells in the periphery of DAOY aggregate compared with in the middle of DAOY aggregate could possibly be attributed to the "fried egg" pattern of the co-culture model. With increased

co-culture incubation time, DAOY cells in the periphery of aggregate invaded into cerebellum slice while DAOY aggregates in the middle still kept a spherical shape. Once NP suspension was added from the top of the co-culture model, the brain slice and DAOY cells in the periphery of aggregates had more chance and longer incubation time with NP suspension than DAOY cells in the middle of aggregate, which resulted in maximum uptake of NPs by DAOY cells that invaded brain slices and brain cells. Although NPs taken up by DAOY cells in this co-culture model could be lower than that *in vivo*, it could still reflect the NP uptake ratio of brain tumour cells to brain cells. Thus it is suggested that culture models of 3-D spheroids and organotypic slices would be useful tools to quantitate and determine the pattern of NPs uptake by target cells *in vitro*. It was also indicated that PGA NPs may be more preferentially distributed in the brain tumour tissue, which lead to better therapeutic benefit by localising the drug in the vicinity of the cancer cells and reducing side-effects.

7.5 SUMMARY

In this chapter the cyto-architecture and histology of the co-culture model of tumour cells and organotypic slices were investigated to develop an *in vitro* brain tumour invasion model system and evaluate PGA NPs as a drug delivery system in this invasion model.

Since medulloblastoma arises in the cerebellum and brainstem but does not develop or metastasise into the cerebral cortex (Kleihues *et al.*, 2000), DAOY aggregates were co-cultured with cerebellum and cerebral cortex for varying periods to investigate and develop an *in vitro* medulloblastoma invasion model for further evaluation of NP uptake and cellular distribution.

In a study of the co-culture model of DAOY aggregates and cerebellum slices, fluorescence microscopy and TEM studies demonstrated DAOY aggregates attached and invaded as a unit into slices. In addition, DAOY single cells in the periphery of aggregates detached from DAOY aggregates and gradually replaced normal brain cells over time. After 6 days of co-culture, the invasive distance from the DAOY aggregate margin of some DAOY single cells could reach to 972μm. In cerebral cortex studies, TEM studies showed converse results compared with Searle's work. DAOY aggregates attached and invaded into slices with relative limited invasion of DAOY single cells. This difference was attributed to the different culture dimensionality of brain cells, which led to differences of tumour growth microenvironment.

The ultimate aim of this study was to develop an *in vitro* 3-D brain tumour invasion model and evaluate PGA NPs as a drug delivery system. In the study of NP uptake by co-culture model, a 4-day co-culture model of organotypic cerebellum slices and DAOY aggregates was chosen because invasion of DAOY cell had occurred but DAOY cells hadn't invaded into whole slices. Confocal micrographs illustrated that DAOY cells took up most of the NPs but few NPs were distributed into brain cells, which corresponds with results of NP uptake in DAOY and brain aggregates.

All of the results presented in this chapter suggest that this novel 3-D *in vitro* model system of regional medullobostoma invasion could be used to effectively evaluate the selectivity of a drug delivery system between tumour cells and brain cells, which reflect the effective therapeutic benefits and side-effects derived from a drug loaded delivery system.

CHAPTER 8

CONCLUSIONS AND FUTURE PROGRESS

8.1 CONCLUSIONS

Through the years, numerous novel drug-delivery systems have been developed and a large number of formulations are helping patients. Although the advances made to date are impressive, there are still a number of questions facing us today needed to be answered, for instance, 1) how the behaviour of drug delivery systems in the tissue after they leave the circulation; 2) how the precision of targeting of drug delivery system is; 3) how quickly the drug delivery system can reach the target sites after leaving circulation. To effectively answer these questions, suitable cell culture models are required in the drug delivery area. 2-D cell culture has been widely used to study cellular uptake of drug delivery systems, but its disadvantage limits the probability of extrapolating the behaviour of drug delivery systems *in vivo*. It is difficult to determine tissue penetration and cellular uptake of drug delivery systems in animal models. A suitable cell culture model which is more complex than a 2-D culture is therefore necessary, and ideally the culture should be as similar as possible to tissue in vivo to ensure that valid conclusions may be drawn.

Thus a series of biodegradable PGA polymers were synthesised with aim to have a realistic drug loading and release profile for therapeutic use. Uptake and penetration of PGA NPs were then investigated in an *in vitro* 3-D brain tumour invasion model. By understanding both the physicochemical and biological evaluation of PGA NPs it was hoped that the anticancer

therapeutic potential of PGA NPs *in vivo* could be investigated and deduced by this *in vitro* tumour invasion model.

Particle size, surface charge, and surface characteristics (hydrophobicity/hydrophilicity) are particularly important in relation to particle sequestration by the MPS system (Douglas *et al.*, 1987), cellular uptake and intracellular trafficking (Labhasetwar *et al.*, 1998). A successful NP system may also need to have a high loading capacity to reduce the quantity of the carrier required for administration. Initial physicochemical investigation into drug/fluorescent dye loading ability of PGA NPs and the properties of the drug/fluorescent dye loaded NPs indicated an improved performance for PGA NPs compared with PLGA or PLA NPs, reflecting the superior affinity of drugs, especially hydrophilic drugs. Although DXM-P is a hydrophilic drug and has a lower drug loading (1.82%w/w-7.8%w/w), its drug loading was higher than that of water soluble drug encapsulated by PLGA NPs or even higher than some hydrophobic drug entrapped by PLGA NP (0.2%-5.8%) (Fessi *et al.*, 1989, and Magenheim *et al.*, 1993). It was apparent that the nature of polymer and drug or fluorescent dye affect the incorporation of drug into NPs, particle size and surface charge (see chapter 3 and 4, and Kallinteri *et al.*, 2005). By comparing physicochemical properties of a range of drug/fluorescent loaded NPs, it was decided to adopt 40% C_{18} (12) polymer and RBITC for biological studies.

The results obtained from the stabilization of NP suggested that naked NPs were unsuitable for effective study of particle behaviour in a cell culture model. A possible solution was to coat NPs with nonionic surfactants, polysorbate-80, at various concentrations. Success was achieved by using high concentrations (0.1% and 0.5%) of polysorbate-80. Thus, the NP possessed sufficient potential to prevent interparticle aggregation and to reduce opportunity of NP recognition by the MPS.

The release studies of RBITC labelled NPs in various media were shown to have a slow and continuous release rate and no burst release. This was a consequence of the presence of increased substitution of fatty acids ($-C_{18}H_{38}$), yielding more hydrophobic NPs that could depress the initial penetration of release media into the core of NP matrix. In addition, the release studies were further investigated in DAOY cells grown in monolayer culture. It indicated a dynamic endocytosis and exocytosis process of NPs by DAOY cells, and a faster RBITC release from NPs intracellularly (see section 5.2). The clinical view suggests that slow and continuous release in physiological conditions to allow the drug delivery system to reach its intended site, followed by fast release intracellularly, and re-take up of NPs by cells will be beneficial. Drugs delivered like this will have a greater chance of being successfully delivered to the target cell while minimizing the drug related side-effects (Shively *et al.*, 1995 and Jeong *et al.*, 2000).

Since cell culture dimension has an effect on cell shape, signal transduction and ECM remodelling, it was hypothesised that cell culture dimension could also have an influence on the NP uptake by host cells and tumour cells within cell culture model. This hypothesis was proved as a different rate of uptake of particles was observed in 2-D monolayer culture and 3-D spherical aggregates. By comparing NP uptake by brain cells and tumour cells in 2-D and 3-D cell culture, it was found that the 3-D cell culture microenvironment favoured uptake by DAOY cells while the 2-D cell culture favoured uptake by brain cells (see chapter 6). Recent literature suggests that 3-D cell culture is more representative of the *in vivo* situation than 2-D monolayer cell culture. Therefore the demonstration of the uptake of NPs implies that 3-D cell culture model could be a more effective way to quantitate uptake of drug delivery systems by host cells and target cells than a 2-D cell culture model.

One property of evaluation of NPs in 3-D cell culture model that requires further exploration is the influence of the culture model on the penetration of NPs. The results obtained from three types of cell culture models demonstrated that the penetration of NPs into 3-D cell culture model was relatively faster than that expected and suggested that penetration was affected by the structure of the interstitial compartment, e.g. the volume faction of ECS occupied tissue and viscosity of the medium in the interstitial spaces (Hrabětová and Nicholson, 2004). Although the ECS has an effect on the penetration of NPs, it also should consider the influence of particle size and its surface charge, which could interact with the macromolecules of ECM. Therefore, some aspects of physicochemical properties of NPs affecting the rate of diffusion of NP in 3-D cultures models can be progressed in future work. It is hoped that various diffusion rate could be achieved by modifying NP properties.

Another matter that requires in-depth testing is selective uptake of NPs by cells. The study of NP uptake by macrophages (U937) revealed the potential of NP taken up by macrophages. Based on this result, it was thus expected that NPs was also taken up by brain macrophages or microglial cells. However, immunohistochemistry images showed most NPs taken up by other types of cells while only a few NPs taken up by brain macrophages or microglia. The most likely explanation of these results is stabilisation of NPs via polysorbate-80. Previous studies confirmed that apolipoprotein E was absorbed on the surface of poysorbate-80 coated PBCA NPs and then particles seem to mimic LDL particles, internalized through LDL receptor-mediated endocytosis (Kreuter, 2001). There are several LDL receptors are shown to be expressed in the brain tissue (Chung and Wasan, 2004). Thus the explanation of selective uptake of NPs was cells in brain slices with accumulated PGA NPs having one or several types of LDL receptors. From the study of selective uptake, it showed the priority of 3-D

cell culture model, which can provide information from a variety of directions. It is very difficult to obtain those informations from 2-D cell culture model.

The development of an *in vitro* tumour invasion model has enabled the aim of this study to be largely fulfilled, in that the effective evaluation of a drug delivery system *in vitro* has been taken a stage further. Electron and fluorescence microscopy analyses revealed that DAOY spherical aggregates attached and invaded into cerebellum slice from 2 days and that DAOY aggregates attached to cerebral cortex slice within 2 days but the invasion of DAOY cells was limited even after 6 days. The difference in invasion behaviour of DAOY cells to cerebral cortex between this co-culture model and model reported in literature (Searle, 2004) might be due to different culture models resulting in different culture environment created by tumour cells and regional brain cells (Fidler, 1991). However, the invasion behaviour of DAOY cells to organotypic cerebellum has a similar pattern as that *in vivo*. This, therefore, suggested that the co-culture model of DAOY spherical aggregates and organotypic cerebellum slice can be used as a representative model to study the behaviour of NPs. The next stage was to begin to investigate the uptake of NPs in this co-culture model. Confocal micrographs demonstrated that tumour cells had higher rates of NP uptake than normal host cells, which indicated that such co-culture tumour invasion model has a greater chance to evaluate anticancer therapeutic potential of drug delivery systems *in vitro*.

8.2 FUTURE PROGRESS

Culture dimensionality had been shown to affect the morphology and microenvironment of tumour and brain cells in 2-D and 3-D, which resulted in different selectivity and uptake extent of NPs. In the 3-D co-culture model, the preparation of tumour material came from a permanent cell line. Use of cell lines may not reflect the original in situ characteristics of the tumour due to phenotypic selection and changes in culture. In contrast, biopsy spheroids maintain the same DNA ploidy as the original tumour hence reflecting the genetic instability (Bjerkvig *et al.*, 1990). This could have a marked effect on tumour invasion behaviour. A future experiment could be further developments of this 3-D co-culture brain tumour invasion model by using biopsy tumour spheroids. Characteristics of selectivity and uptake extent of drug delivery systems with passive or active delivery could be evaluated in such a co-culture model.

It is hoped that this co-culture model of biopsy tumour spheroids and the regional organotypic brain slice will be helpful in assessing effectiveness of drug carriers delivering therapeutic agents in reaching the target cells and deleterious effects on the host cells, which can't be easily carried out in animal model or traditional 2-D cell culture model. However, it must be said that this model could only answer behaviour of drug delivery system when they reach the target tissue and the blood brain barrier which limits drug carrier delivery to the brain is still a major problem to overcome in the drug delivery research area.

REFERENCES

Allémann E., Lerous J.C., Gurny R., and Doelker E. (1993). In vitro extended-release properties of drug-loaded poly (D, L-lactic acid) nanoparticles produced by a salting-out procedure. *Pharm Res* **10** 1732-1737

Allen C. Maysinger D., Eisenberg A. (1999) Nano-engineering block copolymer aggregates for drug delivery. *Colloid Surface B* **16** 3-2

Alonso M.J., Losa C., Calvo P., and Vila-Jato J.L. (1991). Approaches to improve the association of amikanci sulphate to poly (cyanoacrylate) nanoparticles. *Int J Pharm* **68** 69-76

Alyautdin R.N., Gothier D., Petrov V., Kharkevich D., and Kreuter J. (1995). Analgesic activity of the hexapeptide dalargin adsorbed on the surface of polysorbate 80-coated poly (butyl cyanoacrylate) nanoparticles. *Eur J Pharm Biopharm* **41** 44-48

Alyautdin R.N., Petrov V.E., Langer K., Berthold A., Kharkevich D.A., and Kreuter J. (1997). Delivery of loperamide across the blood-brain barrier with polysorbate 80-coated polybutylcyanoacrylate nanoparticles. *Pharm Res* **14** 325-328

Alyautdin R.N., Tezikov E.B., Ramge P., Kharkevich D.A., Begley D.J., and Kreuter J. (1998). Significant entry of tubocurarine into the brain of rats by adsorption to polysorbate 80-coated polybutylcyanoacrylate nanoparticles: an in vivo brain perfusion study. *J Microencapsulation* **15** 67-74

Anderson R.G.W., Brown M.S., Beisiegel U., and Goldstein J.L. (1982). Surface distribution and recycling of the low-density lipoprotein receptor as visualized with antireceptor antibodies. *J Cell Biol* **93** 523-521

Anderson R.G, and Orci L. (1988). A view of acidic intracellular compartments. *J Cell Biol* **106** 539-543

Andersson A-M., Moran N., Gaardsvoll H., Linnemann D., Bjerkvig R., Laerum O.D., and Bock E. (1991) Characterization of NCAM expression and function in BT4C and BT4Cn glioma cells. *Int J Cancer* **47** 124-129

Athanasiou K.A., Niederauer G.G, and Agrawal C.M. (1996). Sterilization, toxicity, biocompatibility and clinical applications of polylactic acid/polyglycolic acid copolymers. *Biomaterials* **17** 93-102

Attawia M.A., Uhrich K.E., Botchwey E., Fan M., Langer R., and Laurencin C.T. (1995). Cytotoxicity testing of poly (anhydride-co-imides) for orthopedic applications. *J Biomed Mater Res* **29** 1233-1240

Avers C.J. (1976). Cell biology. D. Van Nostrand Company, London

Bahr B. (1995). Long-term hippocampal slices: a model system for investigating synaptic mechanisms and pathological processes. *J Neurosci Res* **42** 294-305

Banker G.A. (1980). Trhophic interactions between astroglial cells and hippocampal neurons in culture. *Science* **209** 809-810

Barichello J.M., Morishita M., Takayama K., and Nagai T. (1999). Encapsulation of hydrophilic and liphphilic drugs in PLGA nanoparticles by the nanoprecipitation method. *Drug Dev Ind Pharm* **25** 471-476

Béliveau R., Delbecchi L., Beaulieu E., Mousseau N., Kachra Z., Berthelet F., Moumdjian R., and Masetro R. (1999). KaExpression of matrix metalloproteinases and their inhibitors in human brain tumors. *Ann N Y Acad Sci.* **886** 236-239

Bellail A.C., Hunter S.B., Brat C.T., and VanMeir E.G. (2004). Microregional extracellular matrix heterogeneity in brain modulates glioma cell invasion. *Int J Biochem Cell Biol.* **36** 1046-1069

Berthiaume F., Moghe P.V., Toner M., and Yarmush M. L. (1996). Effect of extracellular matrix topology on cell structure, function, and physiological responsiveness: hepatocytes cultured in a sandwich configuration. *FASEB J* **10** 1471-1484

Bjerkvig R., Tonnesen A., Laerum O.D., and Backlund E.O. (1990). Multicellular tumour spheroids from human gliomas maintaind in organ culture. *J Neurosurg* **72** 463-475

Bjorge L., Hakulinen J., Wahlstrom T., Matre R., and Meri S. (1996). Complement regulatory proteins in ovarian malignancies. *Int J Cancer* **68** 1-12

Birnbaum D.T., Kosmala J.D., Henthorn D.B., and Peppas L.B. (2000). Controlled release of β-estradiol from PLAGA microparticles: the effect of organic phase solvent on encapsulation and release. *J Control Rel* **65** 375-387

Blunk T., Hochstrasser D.F., Sanchez J.C., Müller B.W., and Müller R.H. (1993). Colloidal carriers for intravenous drug targeting: plasma protein adsorption patterns on surface-modified latex particles evaluated by two-dimensional polyacrylamide gel electrophoresis. *Electrophoresis* **14** 1382-1387

Bocca C., Caputo O., Cavalli R., Gabriel L., Miglietta A., and Gasco M.R. (1998). Phagocytic uptake of fluorescent stealth and no-stealth solid lipid nanoparticles. *Int J Pharm* **175** 185-193

Bodmeier R., and McGinity J.W. (1987). Polylactic acid microspheres containing quinidine base and quinidine sulfate preared by the solvent evaporation technique: I. methods and morphology. *J Microencapsulation* **4** 279-288

Bodmeier R., Oh K.H., and Chen H. (1989). The effect of the addition of low molecular weight poly (DL-lactide) on drug release from biodegradable poly (DL-lactide) drug delivery systems. *Int J Pharm.* **51** 1-8

Bodey B., Bodey B. Jr., Siegel S.E., and Kaiser H.E. (2000a). Significant differences in the matrix metalloproteinase expression profiles of spontaneous medulloblastomas/primitive neuroectodermal tumors as compared with their xenografted, established tumor cell line derived counterparts. *In Vivo* **14** 675-682

Bodey B., Bodey B.Jr., Siegel S.E., and Kaiser H.E. (2000b). Matrix metalloproteinase expression in childhood medulloblastomas/primitive neuroectodermal tumors. *In Vivo* **14** 667-673

Bolteus A.J., Berens M.E., and Pilkington G.J. (2001). Migration and invasion in brain neoplasms. *Curr Neurol Neurosci Rep* **1** 225-232

Borchard G., Audus K.L., Shi F., and Kreuter J. (1994). Uptake of surfactant-coated poly (methyl- [2-^{14}C]) methacrylate)-nanoparticles by

bovine brain microvessel endothelial cell monolayers, *Int J Pharm* **110** 29-35

Borsi J.D., Csaki C., Ferencz T., and Oster W. (1996). Administration of Ethyol (amifostine) to a child with medulloblastoma to ameliorate hematological toxicity of high dose carboplatin. *Anticancer Drugs* **7** 121-126.

Brash J.L.(1996). Behavior of proteins at interfaces. **1** 682-688

Breitenbach A., Pistel K.F., and Kissel T. (2000). Biodegradable comb polyesters. Part II. Erosion and release properties of poly (vinyl alcohol)-g-poly (lactic-*co*-glcolic acid) *Polymer* **41** 4781-4792

Brem H., Mahaley M.S. Jr., Vick M.A., Black K.L., Schold S. C. Jr., Burger P.C., Friedman A.H., Ciric I.S., Eller T.W., and Cozzens J.W. (1991). Interstitial chemotherapy with drug polymer implants for the treatment of recurrent gliomas. *J Neurosurg* **74** 441-446

Brigger I., Chaminade P., Marsaud V., appel M., Bestnard M., Gurny R., Renoir M., and Couvreur P. (2001). Tamoxifen encapsulation within polyethylene glycol-coated nanospheres. A new antiestrogen formulation. *Int J Pharm* **214** 37-42

Brismar H., Trepte O., and Ulfhake B. (1995). Spectra and fluorescence lifetimes of Lissamine Rhodamine, Tetramethylrhodamine Isothiocyanate, Texas Red, and Cyanine 3.18 fluorophores: influences of some environmental factors recorded with a confocal laser scanning microscope. *J Histochem Cytochem* **43** 699-707

Brown A.G. (1991). Nerve cells and nervous systems: an introduction to neuroscience. Springer-verlag, London

Brown W.V. (1974). Textbook of cytology. Second Edition The C.V. Mosby company, USA.

Buntner B., Nowak M., Bero M., Dobrzynski P. and Kasperczyk J. (1996). Controlled release of 17β-estradiol from D , L -lactide/ ε -caprolactone copolymers. *J Bioact Compat Polym* **11** 110–116.

Busch H., Fujiwara E., and Firszt D.C. (1961). Studies on the metabolism of radioactive albumin in tumor-bearing rats. *Cancer Res.* **21** 371-377

Carino G.P., Jacob J.S., and Mathiowitz E. (2000). Nanoshpere based oral insulin delivery. *J Control Release* **65** 261-269

Cascone M.G., Pot P.M., and Lazzeri L. (2002). Release of dexamethsaone from PLGA nanoparticles entrapped into dextran/poly(vinyl alcohol) hydrogels. *J Mater Sci-Mater M* **13** 265-269

Castello M.A., Clerico A., Deb G., Dominici C., Fidani P., and Donfrancesco A. (1990). High-dose carboplatin in combination with etoposide (JET regimen) for childhood brain tumors. *Am J Pediatr Hematol Oncol* **12** 297-300

Chang C.H., Housepian E.M. and Herbert C.Jr. (1969). An operative staging system and a megavoltage radiotherapeutic technique for cerebellar medulloblastoma. *Radology* **93** 1351-1359

Chasteigner S.de, Fessi H., Devissaguet J.P., and Puisieux F. (1996). Comparative study of the association of itraconazole with colloidal drug carriers. *Drug Dev Res* **38** 125-133

Chatterjee S.S., and Nöldner M. (1994). An aggregate brain cell culture model for studying neuronal degeneration and regeneration. *J Neural Transm (suppl)* **44** 47-60

Chawla J.S., and Amiji M.M. (2003). Cellular uptake and concentrations of Tamoxifen upon administration in poly (ε -caprolactone) nanoparticles. *AAPS Pharm Sci* **5** 28-34

Chen C.S., Mrksich M., Huang S., Whitesides G.M., and Ingber D.E. (1997). Geometric control of cell life and Death. *Science* **276** 1425-1428

Chicurel M.E., Chen C.S., and Ingber D.E. (1998). Cellular control lines in the balance of forces. *Curr Opin Cell Biol* **2** 232-239

Choquet D., Felsenfeld D.P., and Sheetz M.P. (1997). Extracellular matrix rigidity causes strengthening of integrin-cytoskeleton linkages. *Cell* **88** 39-48

Chorny M., Fishbein I., Danenberg H.D., and Golomb G. (2002) Lipophilic drug loaded nanospheres prepared by nanoprecipitation: effect of formulation variables on size, drug recovery and release kinetics. *J Control Release* **83** 389–400

Chung N.S., and Wasan K.M. (2004). Potential role of the low-density

lipoprotein receptor family as mediators of cellular drug uptake. *Adv Drug Deliv Rev* **56** 1315-1334

Conner S.D. and Schmid S.L. (2003). Regulated portals of entry into the cells. *Nature* 422 37-44

Couvreur P., Kante B., Roland M., and Speiser P. (1979a). Adsorption of antineoplastic drugs to poly alkylcyanoacrylate nanoparticles and their release characteristics in a calf serum medium. *J Pharm Sci* **68** 1521-1524

Couvreur P., Kante B., Roland M., Guiot P., Baudhuin P., and Speiser P. (1979b). Polycyanoacrylate nanocapsules as potential lysosomotropic carriers: preparation, morphological and sorptive properties. *J Pharm Pharmacol* **31** 331

Couvreur P., Barratt G., Fattal E., Legrand P., and Vauthier C. (2002). Nanocapsule technology: a review. *Crit Rev Drug Deliv Syst* **19** 99-134

Cukierman E., Pankov R., Stevens D.R., and Yamada K.M. (2001). Taking cell-matrix adhesions to the third dimension. *Science* **294** 1708-1712

Cukierman E., Pankov R., and Yamada K.M. (2002). Cell interactions with three dimensional matrics. *Curr Opin Cell Biol* **14** 633-639

De Bouard S., Christov C., Guillamo J.S., Kassar-Duchossoy L., Palfi S., Leguerinel C., Masset M., Cohen-Hagenauer O., Peschanski M., and Lefrancois T. Invasion of human glioma biopsy specimens in cultures of rodent brain slices: a quantitative analysis. *J Neurosurg* **97** 169-176

Demoy M., Andreux J.-P., Weingarten C., Gouritin B., Guiloux V., and Couvreur P. (1999). In vitro evaluation of nanoparticles spleen capture. *Life Sci* **64** 1329-1337

Demuth T., and Berens M.E. (2004) Molecular mechanisms of glioma cell migration and invasion. *J Neuroonc* **70** 217-228

Domb A.J., Rock m., Schwartz J., PerkinC., Yipchuck G., Broxup B., and Villemure J.G. (1994). Metabolic disposition and elimination studies of a radiolabelled biodegradable polymeric implant in the rat brain. *Materials* **15** 681-688

Douglas S.J., Davis S.S., and Illum L. (1987). Nanoparticles in drug delivery *Crit Rev Ther Drug Carrier Syst* **3** 233-261

Duncan R., and Sat Y-N. (1998). Tumor targeting by enhanced permeability and retention (EPR) effect. *Ann Oncol* **9** 39-50

Edelman B.D., and Keefer E.W. (2005). A cultural renaissance: in vitro cell biology embraces three-dimensional context. *Exp Neurol* **192** 1-6

Enam S.A., Rosenblum M.L., Edvardsen K. (1998). Role of extracellular matrix in tumor invasion: migration of glioma cells along fibronectin-positive mesenchymal cell precesses. *Neurosurg* **42** 599-608

Engebraaten O., Bjerkvig R., Lund-Johansen M., Wester K., Pedersen P.H., Mork S., Backlund E.O., and Laerum O.D. (1990). Interaction between human brain tumour biopsies and fetal rat brain tissue in vitro. *Acta Neuropathol (Berl)* **81** 130-140

Erni C., Suard C., Freitas S., Dreher D., Merkle H.P., and Walter E. (2002). Evaluation of cationic solid lipid microparticles as synthetic carriers for the targeted delivery of macromolecules to phagocytic antigen-presenting cells. *Biomaterials* **23** 4667-4676

Everett D.H. (1988). Basic principle of colloid science Royal society of chemistry, London

Fessi H., Puisieux F., Devissaguet J. Ph., Ammoury N., and Benita S. (1989). Nanocapsule formation by interfacial polymer deposition following solvent displacement. *Int J Pharm* **55** R1-R4

Fidler I.J. (1991). Cancer metastasis. *Br Med Bull* **47** 157-177

Finn P., Bjerkvig R., and Pilkington G. (1997). The role of growth factors in the malignant and invasive progression of intrinsic brain tumours. *Anticancer Research* **17** 4163-4172

Flint O.P. (1983). A micromass culture method for rat embryonic neural cells. *J Cell Sci* **61** 247-262

Folkman J. and Greenspan H.P. (1975). Influence of erometry on control of cell growth. *Biochim Biophys Acta* **417** 211-236

Fonseca C., Simões S., Gaspar R. (2002). Paclitaxel-loaded PLGA nanoparticles: preparation, physicochemical characterization and in vitro anti-tumoral activity. *J Control Release* **83** 273-286.

Foster K.A., Yazdanian M., and Audus K.L. (2001). Microparticulate uptake mechanisms of in-vitro cell culture models of the respiratory epithelium. *J Pharm Pharmacol* **53** 57-66

Fournier E., Passirani C., Montero-Menei C.N., and Benoit J.P. (2003). Biocompatibility of implantable synthetic polymeric drug carriers: focus on brain biocompatibility. *Biomaterials* **24** 3311-3331

Frier M. (1981). Phagocytosis in *Progress in Radiopharmacology* North Holland, Amsterdam

Friese A., Seiller E., Quack G., Lorenz B., and Kreuter J. (2000). Increase of the duration of the anticonvulsive activity of a novel NMDA receptor antagonist using poly (butylcyanoacrylate) nanoparticles as a parenteral controlled release system. *Eur J Pharm Biopharm* **49** 103-109

Gähwiler B.H. (1988). Organotypic cultures of neural tissue. *Trends Neurosci* **11** 484-490

Gähwiler B.H. Capogna M., Debanne D., Mckinney R.A., and Thompson S.M. (1997). Organotypic slice cultures: a technique has come of age. *TINS* **20** 471-477

Galindo-Rodriguez S., Allémann E., Fessi H., and Doelker E. (2004). Physicochemical parameters associated with nanoparticl formation in the salting-out, emulsification-diffusion, and nanopricipitation methods. *Pharm Resear* **21** 1428-1439

Garber B.B., and Moscona A.A. (1972). Reconstruction of brain tissue from cell suspensions. I. Aggregation patterns of cells dissociated from different regions of the developing brain. *Dev Biol* **27** 217-234

Gessner A., Waicz R., Lieske A., Paulke B., Mader K., and Müller R.H. (2000). Nanoparticles with decreasing surface hydrophobicities: influence on plasma protein adsorption. *Int J Pharm* **196** 245-249

Ghose T., Nairn R.C., and Fothergill J.E. (1962). Uptake of proteins by malignant cells. *Nature* **196** 1108-1109

Gibbs E.M., and Lienhard G.E. (1984). Fluid-phase endocytosis by isolated rat adipocytes. *J Cell Physiol* **121** 569-575

Gilbertson R.J. (2004). Medulloblastoma: signaling a change in treatment. *The Lancet* **5** 209-218

Gipps E., Groscurt P., Kreuter J., and Speiser P.P. (1987). The effects of poly (alylcynoacrylate) nanoparticles on human normal and malignant nesenchymal cells in vitro. *Int J Pharm* **40** 23-31

Goldstein J.L., Brown M.S., Anderson R.G.W., Russell D.W., and Schneider W.J. (1985). Receptor-medicated endocytosis-concepts emerging from the LDL receptor system. *Annu Rev Cell Biol* **1** 1-39

Goodenough D.A., Goliger J.A., and Paul D.L. (1996). Connexins, connexons, and intercellular communication. *Annu Rev Biochem* **65** 475-502

Gophferich A. (1996). Mechanisms of polymer degradation and erosion. *Biomaterials* **17** 103-114

Goppert T.M. and Muller R.H. (2003). Plasma protein adsorption of Tween 80- and poloxamer 188-stabilized solid lipid nanoparticles. *J Drug Target* **11** 225-231

Gordon S. (1995). The macrophage. *Bioessays* **17** 977-986

Görner T., Gref R., Michenot D., Sommer R., Tran M.N. and Dellacherie E. (1999). Lidocaine-loaded biodegradable nanopheres. I. Optimization of the drug incorporation into the polymer matrix. *J Control Release* **57**, 259-268.

Govender T, Stolnik S., Garnett M. C., Illum L. and Davis S. S. (1999). PLGA nanoparticles prepared by nanoprecipitation: drug loading and release studies of a water soluble drug, *J Control Release* **57** 171-185

Govender T., Riley T., Ehtezazi T., Garnett M.C., Stolink S., Illum L., and Davis S.S. (2000). Defining the drug incorporation properties of PLA-PEG nanoparticles. *Int J Pharm* **199** 95-110

Gulyaev A.E., Gelperina S.E., Skidan I.N., Antropov A.S., Kivman G.Y., and Kreuter J. (1999). Significant transport of doxorubicin into the brain with polysorbate 80-coated nanoparticles. *Pharm Research* **16** 1564-1569

Hay E.H. (1991). Cell biology of extracellular matrix, second ed., Plenum Press, New York

Harper G.R., Davis S.S., Davies M.C., Norman M.E., Tadros T.F., Taylor D.C., Irving M.P., Waters J.A., and Watts J.F. (1995). Influence of surface coverage with poly (ethylene oxide) on attachment of sterically stabilized microspheres to rat Kupffer cells in vitro. *Biomaterials* **16** 427-439

Heinsman N.W.J.T., Valente A.M., Smienk H.G. F., Padt A., Franssen M. C. R., Groot A., and Riet K.V. (1999). The effect of ethanol on the kinetics of lipase-mediated enantioselective esterification of 4-methyloctanoic acid and the hydrolysis of its ethyl ester. *Biotechnol Bioeng* **76**193-199

Helin E., Salmi A.A., Vanharanta R., Vainionpaa. (1999). Measles virus replication in cells of myelomonocytic lineage is dependent on cellular differentiation stage. *Virology* **253** 35-42

Hintz R. J., and Johnson K.C. (1989). The effect of particle size distribution on dissolution rate and oral absorption, *Int J Pharm* **51** 9-17

Holtzman E. (1989) Lysosomes. Plenum Press, London

Hombreiro-Pérez M., Siepmann J., Zinutti C., Lamprecht A., Ubrich N., Hoffman M., Bodmeier R. and Maincent P. (2003). Non-degradable microparticles containing a hydrophilic and/or a lipophilic drug: preparation, characterization and drug release modeling, *J Control Release* **88** 413-428

Honegger P., Lenoir D., and Favrod P. (1979). Growth and differentiation of aggregating fetal brain cells in serum-free defined medium. *Nature* **82** 305-308

Hopkins C.R. (1983). Cell biology-the importance of the endosome in intracellular traffic. *Nature* **305** 684-685

Hopkins C.R. (1986). Membrane boundaries involved in the uptake and intracellular processing of cell-surface receptors. *Trends Biochem Sci* **11** 473-477

Hrabětová S. and Nicholson C. (2004). Contribution of dead-space microdomains to tortuosity of brain extracelluar space. *Neurochem Int* **45** 467-277

Huang X., and Brazel C.S. (2001). On the importance and mechanism of burst release in matrix-controlled drug delivery systems. *J Controlled Release* **73** 121-136

Ibrahim H., Bindschaedler C., Doelker E., Buri P., ad Gurny R. (1992). Aqueous nanodispersions prepared by a salting-out process. *Int J Pharm* **87** 239-246

Illum L., Davis S.S., Wilson C.G, Thomas N.W., Frier M., and Hardy J.G. (1982). Blood clearance and organ deposition of intravenously administered

colloidal particles. The effect of particles size, nature and shape. *Int J Pharm* **12** 135-146

Illum L., Hunneyball I.M., and Davis S.S. (1986a). The effect of hydrophilic coatings on the uptake of colloidal particles by the liver and by peritonela macrophages. *Int J Pharm* **29** 53-65

Illum L., Khan M.A., Mak E., and Davis S.S. (1986b). Evaluation of carrier capacity and release characteristics for poly (butyl 2-cyanoacrylate) nanoparticles. *Int J Pharm* **30** 17-28

Illum L., Davis S.S., Müller R.H., Mak E., and West P. (1987). The organ distribution and circulation time of intravenously injected colloidal carriers sterically stabilized with a block copolymer poloxamine 908. *Life Sci* **40** 367-370

Ingber D.E., Dike L., Hansen L., Karp S., Liley H., Maniotis A., McNamee H., Mooney D., Plopper G., Sims J *et al*: (1994). Celllar tensegrity: exploring how mechanical changes in the cytoskeleton regulate cell growth, migration, and tissue pattern during morphogenesis. *Int Rev Cyto* **150** 173-224

Ishida T., Harashima H., and Kiwada H. (2001). Interactions of liposomes with cells in vitro and in vivo: opsonins and receptors. *Curr Drug Metab* **2** 397-409

Ishii I., Tomizawa A., Kawachi H., Suzuki T., Kotani A., Koshushi I., Itoh H., Morisaki N., Bujo H., Saito Y., Ohmori S., and Kitada M. (2001). Histological and functional analysis of vascular smooth muscle cells in a novel culture system with honeycomb-like structure. *Atherosclerosis* **158** 377-384

Jacobsen P.F., Jenkyn D.J., and Paradimitriou J.M. (1985). Establishment of a human medulloblastoma cell line and its heterotransplantation into nude mice. *Journal of Neuropathology and applied Neurology* **44** 422-485

Jain R. A., Rhodes C. T., Railkar A. M., Waseem Malick A. and Shah N.H. (2000). Controlled release of drugs from injectable in situ formed biodegradable PLGA microspheres: effect of various formulation variables. *Eur J Pharm Biopharm* **50** 257-262

Jameela S.R., Suma N., Misra A., Raghuvanshi R., Ganga S. and Jayakrishnan A. (1996). Poly (ε-Caprolactone) microspheres as a vaccine carrier. *Curr Sci* **70** 669–671

Janmey P. A. (1998). The cytoskeleton and cell signaling: component localization and mechanical coupling. *Physiol Rev* **78** 763-781

Jeong B. Bae Y.H., and Kim S.W. (2000). Drug release from biodegradable injectable thermosensitive hydrogel of PEG-PLGA-PEG triblock copolymers. *J Control Release* **63** 155-163

Jeong Y.I., Shim Y.H., Choi C.Y., Jang M.K., Shin G.M., and Nah J.W. (2003). Surfactant-free nanoparticles of poly(DL-lactide-*co*-glycolide) prepared with poly(L-lactide)/ poly(ethylene glycol). *J Appl Polym Sci* **89** 1116-1123

Jung S., Kim H.W., Lee J.H., Kang S.S., Rhu H.H., Jeong Y.I., Yang S.Y., Chung H.Y., Bae C.S., Choi C., Shin B.A., Kim K.K., and Ahn K.Y. (2002). Brain tumor invasion model system using organotypic brain-slice culture as an alternative to in vivo model. *J Cancer Res Clin Onco* **28** 469-76.

Kaczarek E., Zapf S., Bouterfa H., Tonn J., Westphal M., and Giese A. (1999). Dissecting glioma invasion: interrelation of adhesion, migration and intercellular contacts determine the invasive phenotype. *Int J Dev Neurosci* **17** 625-641

Kallinteri P., Higgins S., Hutcheon G.A., St Pourcain C.B., and Garnett M.C. (2005). Novel functionalized biodegradable polymers for nanoparticle drug delivery systems. *Biomacromolecules* **6** 1885-1894

Kandel E.R., Schwartz J.H., and Jessel T.M., (1991). Principles of neural science, third ed., Prentice Hall International, London

Kim S.Y., Shin I.G., and Lee Y.M. (1998). Preparation and characterization of biodegradable nanospheres composed of methoxy poly(ethylene glycol) and DL-lactide block copolymer as novel drug carriers. *J Control Release* **56** 1-3

Kim S.H., Jeong J.H., Chun K.W., and Park T.G. (2005). Target-specific cellular uptake of PLGA nanoparticles coated with poly (L-lysine)-poly (ethylene glycol)-folate conjugate. *Langmuir* **21** 8852-8857

Kleihues P., and Cavenee W.K. (2000). World Health Organisation classification of tumours: *Pathology and genetics of tumours of the nervous system* Lyon. IARC Press

Konan N.Y., Gurny R., and Allémann E. (2002). Preparation and

characterization of sterile and freeze-dried sub-200 nm nanoparticles. *Int J Pharm* **233** 239-252

Koochekpour S., Merzak A., and Pilkington G.J. (1995). Extracellular matrix proteins inhibit proliferation, upregulate migration and induce morphological changes in human glioma cell lines. *Eur J Cancer* **31A** 375-380

Kostarelos K., Emfietzoglou D., Papakostas A., Yang W.H., Ballangrud A., and Sgouros G. (2004). Binding and interstitial penetration of liposomes within avascular tumor spheroids. *Int J Cancer* **112** 713-721

Kreuter J. (1994). Nanoparticles, in: J. Kreuter (Ed.), *Colloidal Drug Delivery Systems*, Marcel Dekker, New York, 219-342

Kreuter J., Alyautdin R.N., Kharkevich D.A., and Ivanov A.A. (1995). Passage of peptides through the blood-brain barrier with colloidal polymer particles (nanoparticles). *Brain Res* **674** 171-174

Kreuter J., Petrov V.E., Kharkevich D.A., and Alyautdin R.N. (1997). Influence of the type of surfactant on the analgesic effects induced by the peptide dalargin after its delivery across the blood-brain barrier using surfactant-coated nanoparticles. *J. Control Release* **49** 81-87

Kreuter J. (2001). Nanoparticulate systems for brain delivery of drugs. *Adv drug deliv rev* **47** 65-81

Kreuter J., Shamenkov D., Petrov V., Ramge P., Cychutek K., Koch-Brandt C., and Alyautdin R. (2002). Apolipoprotein-mediated transport of nanoparticl-bound drugs across the blood-brain barrier. *J Drug Target* **10** 317-325

Kubiak c., Couvreur P., Manil L, and Clausse B. (1989). Increased cytotoxicity of nanoparticle-carriered adriamycin in vitro and potentiation by verapamil and amiodarone. *Biomaterials* **10** 553-556

Kubikl T. Bogunia-Kubik K., and Sugisaka M. (2005). Nanotechonology on duty in medical applications. *Curr Pharm Biotechnol* **6** 17-33

La S.B., Okano T. and Kataoka K. (1996). Preparation and Characterization of the Micelle-Forming Polymeric Drug Indomethacin-Incorporated Poly(ethylene oxide)-Poly(β-benzyl L-aspartate) Block Copolymer Micelles. *J Pharm Sci* **85** 85-90

Labhasetwar V., Song C., Humphrey W., Shebuski R. and Levy R.J. (1998). Arterial uptake of biodegradable nanoparticles: effect of surface modifications. *J Pharm Sci* **87** 1229–1234

Lacoulonche F., Gamisans F., Chauvet A., Garcia M.L., Epsina M. and Egea M.A. (1999). Stability and in vitro drug release of Flurbiprofen loaded poly (ε-caprolactone) nanospheres. *Drug Dev Ind Pharm* **25** 983–993

Langer K., Seegmüller E., Zimmer A., and Kreuter J. (1994). Characterization of polybutylcyanoacrylate nanoparticles: quantification of PBCA polymer and dextran. *Int J Pharm* **110** 21-27

Leenslag J.W. Pennings A.J., Bos R.R.M., Rozema F.R., and Boering G. (1987). Resorbable materials of poly (L-lactide): VI. Plates and screws for internal fracture fixation. *Biomaterials* **8** 70-73

Leger J.M., Ries L.A., Smith M.A., Warren J.L., Heineman E.F., Kaplan R.S., and Linet M.S. (1999). Cancer surveillance series [corrected]: brain and other central nervous system cancers: recent trends in incidence and mortality. *J Natl Cancer Inst* **91** 1382-90

Legong K.W., D'Amore P., Marletta M., and Langer R. (1986). Bioerodible polyanhydrides as drug carrier matrices. II. Biocompatibility and chemical reactivity. *J Biomed Mater Res* **20** 51-64

Lefevre F., Garnotel R., Georges N., and Gillery P. (2001). Modulation of collagen metabolism by the nucleolar protein fibrillarin. *Exp Cell Res* **271** 84-93

Leo E., Brina B., Forni F., and Angela M. (2004). In vitro evaluation of PLA nanoparticles containing a lipophilic drug in water-soluble or insoluble form. *Int J Pharm* **278** 133-141

Leong K.W., Brott B.C., and Langer R. (1985). Bioerodible polyanhydrides as drug-carrier matrices. I. Characterization, degradation and release characteristics. *J Biomed Mater Res* **19** 941-955

Levitt P., and Rakic P. (1980). Immunoperoxidase localization of glial fibrillary acidic protein in radial glial-cells and astrocytes of the developing rhesus-money brain. *J Comp Neurol* **193** 815-840

Li S., Girod-Holland S., and Vert, M. (1996). Hydrolytic degradation of poly (DL-lactic acid) in the presence of caffeine base. *J Control Release* **40** 41-53

Liotta L.A. (1986). Tumor invasion and metastases-role of the extracellular matrix: Rhoads Memorial Award lecture. *Cancer Res* **46** 1-7

Ma W., Fitzgerald W., Liu Q.Y., O'shaugnessy T.J., Maric D., Lin H.J., Alkon D.L., and Barker J.L. (2004). CNS stem and progenitor cell differentiation into functional neural circuits in three-dimensional collagen gels. *Exp Neurol* **190** 276-288

MacDonald T.J., Declerck Y.A., and Laug W.E. (1998). Urokinase induces receptor mediated brain tumor cell migration and invasion. *J Neurooncol* **40** 215-226

Maeda H., Wu J., Swawa T., Matsumura Y., and Hori K. (2000). Tumor vascular permeability and EPR effect in macromolecular therapeutics: a review. *J Controlled Rel* **65** 271-284

Magenheim B., Levy M.Y., and Benita S. (1993). A new in vitro technique for the evaluation of drug release profile from colloidal carriers-ultrafiltration technique at low pressure. *Int J Pharm* **94** 115-123

Mani N., Park M.O., and Jun H.W. (2004). Microencapsulation of a hydrophilic drug into a hydrophobic matrix using a salting-out procedure I: development and optimization of the process using factorial design. *J Microencapsul* **21** 125-135

Mareel M.M., Van Roy F.M., and Bracke M.E. (1993). How and when do tumor cells metastasize? *Crit Rev Oncog* **4** 559-594

Margolis E.K., and Mrgolis R.U. (1993). Nervous tissue proteoglycans. *Experientia* **49** 429-446

Markland P., and Yang V. C. (2000) Biodegradable polymers as drug carrier, *Encyclopedia of Pharmaceutical Technology* Marcel Dekker New York 137-155

Matsusue Y., amamuro T., Oka M. Shikinami Y., Hyon S-H., and Ikada Y. (1992). In vitro and in vivo studies on bioabsorbable ultra-high-strength poly (L-lactide) rods. *J Biomed Marter Res* **26** 1553-1567

Mego J.L. and McQueen J.D. (1965). The uptake of labeled proteins by particulate fractions of tumor and normal tissues after injection into mice. *Cancer Res* 25 865-869

Menei P., Crouc A., Daniel V., Pouplard B.A. and Benoit J.P. (1994). Fate

and biocompatibility of three types of microspheres implanted into brain. *J Biomed Mater Res* **28** 1079–1085

McClean S., Prosser E., Meean E., O'Malley D., Clarke N., Ramtoola Z., and Brayden D. (1998). Binding and uptake of biodegradable poly-DL-lactide micro- and nanoparicles in intestinal epithelia. *Eur J Pharm Sci* **6** 153-163

McLean I.W., and Nakane P.K., (1974).
Periodate-lysine-paraformaldehyde fixative a new fixative for immunoelectron microscopy. *J Histochem and Cytochem* **22** 1077-1083

Mellman I. (1996). Endobytosis and molecular sorting. *Ann Rev Cell Dev Biol* **12** 575-625

Milligan C.E., Cunningham R.J., and Levitt P. (1991). Differential immunochemical markers reveal the normal distribution of brain macrophages and microglia in the developing rat brain. *J Comp Neurol* **314** 125-135

Miyajima M., Koshika A., Okada J., Kusai A. and Ikeda M. (1998). Factors influencing the diffusion-controlled release of papaverine from poly (L-lactic acid) matrix. *J Control Release* **56** 85–94

Moghimi S.M. and Davis S.S. (1994). Innovations in avoiding particles clearance from blood by Kupffer cells: cause for reflection. *Crit Rev Ther Drug Carrier Syst* **11** 31-59

Moghimi S.M., Rajabi-Siahboomi A.R. (2000). Recent advances in cellular, sub-cellular and molecular targeting. *Adv Drug Deliv Rev* **41** 129-133

Moghimi S.M., Hunter A.C., and Murray J.C. (2001). Long-circulationg and target-specific nanoparticles: theory to practice. *Pharmacolo Rev* **53** 283-318

Monsky W.L., Fukumura D., Gohongi T., Ancukiewcz M., Weich H.A., Torchilin V.P., Yuan F., and Jain R.K. (1999). Augmentation of transvascular transport of macromolecules and nanoparticles in tumors using vascular endothelial growth factor. *Cancer Res* **59** 4129-4135

Muller W.A., Steinman R.M., and Cohn Z.A. (1983). Membrane-proteins of the vacuolar system.3.further-studies on the composition and recycling of endocytic vacuole membraine in cultured macrophages. *J Cell Biol* **96** 29-36

Müller R.H., Lherm c., Herbort J., and Couvreur P. (1990). Invitro model for the degradation of alkylcyanoacrylate nanoparticles. *Biomaterials* **11** 590-595

Murphy M.P. and Smith R.A. (2000). Drug delivery to mitochondria: the key to mitochondrial medicine. *Adv Drug Deliv Rev* **41** 235–250

Murthy R.S.R. (1997). Biodegradable polymers. In: Jain, N.K. (Eds.), Controlled and Novel Drug Delivery. CBS Publisher, New Delhi, pp. 27–51.

Moscona A.A. (1961). Rotation-mediated histogenic aggregation of dissociated cells quantifiable approach to cell interactions in vitro. *Exp Cell Res* **22** 455-457

Napper D.H. (1989). Polymeric stabilization of colloidal dispersions. Harcourt Brace Jovanovich, London

Nguyen S.J.T., Haugland H.D.R., and Laerum O.D. (2003). Cell interaction studies of PLA-MePEG nanoparticles. *Int J Pharm* **254** 69-72

Nicholson C., and Tao L. (1993). Hindered diffusion of high molecular weight compounds in brain extracellular microenvironment measured with integrative optical imaging. *Biophys J* **65** 2277-2290

Novak U., and Kaye A.H. (2000). Extracellular matrix and the brain: components and function. *J Chin Neurosci* **7** 280-290

Nystrom B., Olson L., and Ungerstedt U. (1972) Noradrenaline nerve terminals in human cerebral cortices: first histochemical evidence. *Science* **172** 924-926

O'Connor S.M., Stenger D.A., Shaffer, K.M., Maric D., Barker J.L., and Ma W. (2000). Primary neural precursor cell expansion, differentiation and cytosolic Ca^{2+} response in three-dimensional collagen gel. *J Neurosci Methods* **102** 187-195

O'Shaughnessy T.J., Lin H.J., and Ma W. (2003). Functional synapse formation among rat cortical neurons grown on three-dimensional collagen gels. *Neurosci Lett* **340** 169-172

Ozen O., Krebs B., Hemmerlein B., Pekrun A., Kretzschmar H., and Herms J. (2004). Expression of matrix metalloproteinases and their inhibitors in

medulloblastomas and their prognostic relevance. *Clin Cancer Res* **10** 4746-4753

Packer R.J. (1999). Childhood medulloblastoma: progress and future challenges. *Brain Dev* **21** 75-81

Pannese E. (1994). Neurocytology: fine structure of neurons, nerve processes, and neuroglial cells, Stuttgart : Georg Thieme Verlag ; New York : Thieme Medical Publishers

Panyam J., Zhou W.Z., Prabha S., Sahoo S.K. and Labhasetwar V. (2002) Rapid endo-lysosomal escape of poly (D,L -lactide-co-glycolide) nanoparticles: Implications for drug and gene delivery, *FASEB J* **16** 1217–1226

Panyam J., Sahoo S.K., Prabha S., Bargar T., and Labhasetwar V. (2003a). Fluorescence and electron microscopy probes for cellular and tissue uptake of poly (D, L-lactide-co-glycolide) nanoparticles. *Int J Pharm* **262** 1-11

Panyam J., and Labhasetwar V. (2003b). Dynamics of endocytosis and exocytosis of poly (D, L-lactide-co-glycolide) nanoparticles in vascular smooth muscle cells. *Pharm Res* **20** 210-218

Penar P.L., Khoshyomn S., Bhushan A., and Tritton T.R. (1998). Inhibition of glioma invasion of fetal brain aggregates. *In Vivo***12** 75-84.

Peracchia M.T., Gref R., Minamitake Y., Domb A., Lotan N., and Langer R. (1997). PEG-coated nanospheres from amphiphilic diblock and multiblock copolymers: Investigation of their drug encapsulation and release characteristics. *J Control Release* **46** 223-231

Perry V.H., and Gordon S. (1988). Macrophages and microglia in the nervous system. *TINS* **11** 273-277

Perry V.H., Hume D.A., and Gordon S. (1985). Immunohistochemical localization of macrophages and microglia in the adult and developing mouse brain. *Neurosci* **15** 313-326

Peters A., Palay S., and Webter H. (1976). The fine structure of the nervous system: the neurons and supporting cells. W.B.Saunders Company, London.
Pillai O., and Panchagnula R. (2001). Polymers in drug delivery. *Curr Opin Chem Biol* **5** 447-451

Peyrl A., Krapfenbrauer K., Slavc I., Yang J-W., Strobel T. and Lubec G.

(2003). Protein profiles of medulloblastoma cell lines DAOY and D283: Identification of tumour-related proteins and principles. *Proteomics* **2** 1781-1800

Pilkington G.J. (1994). Tumour cell migration in the central nervous system. *Brain Pathol* **4** 157-166

Pilkington G.J., Bjerkvig R., de Ridder L., and Kaaijk P. (1997) In vivo and in vitro models for the study of brain tumour invasion. *Anticancer Res* **17** 4107-4110

Pomeroy S.L., Sutton M.E., Goumnerova L.C., and Segal R.A. (1997). Neurotrophins in cerebellar granule cell development and medulloblastoma. *J Neuroonco* **35** 347-352

Pouliot N., Connolly L.M., Moritz R.M., Simpson R.J., and Burgess A.W. (2000). Colon cancer cells adhesion and spreading on autocrine laminin-10 is mediated by multiple integrin receptors and modulated by EGF receptor stimulation. *Exp Cell Res* **261** 360-371

Puttipipatkhachorn S., Nunthanid J., Yamamoto K., and Peck G.E. (2001). Drug physical state and drug-polymer interaction on drug release from chitosan matrix films. *J Control Release* **75** 143-153

Ramge P., Unger R.E., Oltrogge J.B., Zenker D., Begley D., Kreuter J., and Briesen H.V. (2000). Polysorbate-80 coating enhances uptake of polybutylcyanoacrylate (PBCA)- nanoparticles by human and bovine primary brain capillary endothelial cells. *Eur J Neurosci* **12** 1931-1940

Ramge P., Kreuter J., and Lemmer B. (1999). Circadian phase-dependent antinociceptive reaction in mice after i.v. injection of dalargin-loaded nanoparticles determined by the hot-plate test and the tail flick test. *Chronobiol Int* **16** 767-777

Raju T., Bignami A., and Dahl D. (1981) In vivo and in vitro differentiation of neurons and astrocytes in the rat embryo. *BMC Dev Biol* **85** 344-357

Ravi Kumar M.V., Kumar N., Domb A.J., and Arora M. (2002). Pharmaceutical polmeric controlled drug delivery systems. *Advances in Polymer Science* **160** 45-117

Riley T., Govender T., Stolnik S., Xiong C.D., Garnett M.C., Illum L., Davis S.S. (1999). Colloidal stability and drug incorporation aspects of

micellar-like PLA-PEG nanoparticles. *Colloids Surf B Biointerfaces* **16** 147-159

Robinson A.P., White T.M., and Mason D.W. (1986). Macrophage heterogeneity in the rat as determined by two monoclonal antibodies MRC OX-41 and MRC OX-42, the latter recognizing complement receptor type 3. *Immunol* **57** 239-247

Rooprai H.K, and McCormick D. (1997). Proteases and their inhibitors in human brain tumours: a review. *Anticancer Res* **17** 4151-62

Rooprai H.K., Liyanage K., Robinson S.F., Kandanearatchi A., Dean A.F., and Pilkington G.J. (1999). Extracellular matrix-modulated differential invasion of human meningioma cell lines in vitro. *Neurosci Lett* **263** 214-216

Rorke L. (1983). The cerebellar medulloblastoma and its relationship to primitive neuroectodermal tumors. *J Neuropathol Exp Neurol* **42** 1-15

Rosen H.B., Chang J., Wnek G.E., linhardt R.J. and Langer R. (1983). Bioerodible polyanhydrides for controlled drug delivery. *Biomaterials* **4** 131-133

Roser M., Fischer D., and Kissel T. (1998). Surface-modified biodegradable albumin nano-and microspheres. II: effect of surface charges on in vitro phagocytosis and biodistribution in rats. *Eur J Pharm Biopharm* **46** 255-263

Ruch R.J. (1994). The role of gap junctional intercellular communication in neoplasia. *Ann Clin Lab Sci* **24** 216-231

Sacks P.G., Oke V., and Mehta K. (1992) Antiproliferative effects of free and liposome-encapsulated retinoic acid in a squamous carcinoma model: monolayer cells and multicellular tumor spheroids. *J Cancer Res Clin Oncol* **118** 490-496.

Sahai E. and Marshall C.J. (2003). Differing models of tumour cell invasion have distinct requirements for Rho/ROCK signaling and extracellular proteolysis. *Nat cell Biol* **5** 711-719

Saggu H., and Pilkington G.J. (1986). Immunocytochemical characterisation of the A15A5 transplantable brain tumour model *in vivo*. *Neuropath Appl Neurobiol* **12** 291-303

Sant S., Nadeau V., and Hildgen P. (2005). Effect of porosity on the release

kinetics of propafenon-loaded PEG-g-PLA nanoparticles. *J Control Release* **107** 203-214

Santini M.T. and Rainaldi G. (1999). Three-dimensional spheroid model in tumor biology. *Pathology* **67** 148-157

Sasaki H., Takakura Y., Hashida M., Kimura T. and Sezaki H. (1984). Antitumour activity of lipophilic produgs of mitomycin C entrapped in liposome or O/W emulsion. *J Pharm Dyn* **7** 120-130

Schwope A.D., Wise D.L., and Howes J.F. (1976). Development of polylactic/glycolic acid delivery systems for use in treatment of narcotic addiction. *Nat Inst Drug Abuse Res Mongre Ser* **January** 13-18

Scherer D., Robinson J.R., and Kreuter J. (1994). Influence of enzymes on the stability of polybutylcyanoacrylated nanoparticles *Int J Pharm* **101** 165-168

Schroeder U., Sabel B.A., and Schroeder H. (1999). Diffusion enhancement of drugs by loaded nanoparticles in vitro. *Prog Neuro-Psychopharmacol & Biol Psychiat* **23** 941-949

Schuler D., Somlo P., Kooos R., Kalmanchey R., and Paraicz E. (1992). Treatment of malignant scala posterior brain tumors in children: the chemotherapy of relapsed medulloblastoma with a dibromdulcitol containing drug regime and pharmacokinetic studies of dibromdulcitol in children. *Med Pediatr Oncol* **20** 312-314

Searle K.H. (2004). Medulloblastoma invasion in vitro: the role of dimensionally and regional specificity. *PhD Thesis, University of Nottingham*

Selak I., Skaper S.D., and Varon S. (1985) Pyruvate participation in the low molecular weight trophic activity for central nervous system neurons in glia-conditioned media. *J Neurosci* **5** 23-28

Serrano M.C., Pagani R., Pena J., and Portoles M.T. (2005) Transitory oxidative stress in L929 fibroblasts cultured on poly (epsilon-caprolactone) films. *Biomaterials* **26** 5827-5834

Shikani A.H., and Domb A.J. (2000). Polymer chemotherapy for head and neck cancer. *Laryngoscope* **110** 907-917

Shive M.S., and Anderson J.M. (1997). Biodegradation and biocompatibility

of PLA and PLGA microspheres. *Adv Drug Deliv Rev* **28** 5-24

Shively M.L., Coonts B.A., Renner W.D., Southard J.L., and Bennet A.T. (1995). Physicochemical characterization of polymeric injectable implant delivery system. *J Control Release* **33** 237-243

Sinha V.R., Bansal K., Kaushik R., Kumria R., and Trehan A. (2004). Poly-ε -caprolactone microsheres and nanospheres: an overview. *Int J Pharm* **278** 1-23

Singhvi R., Kumar A., Lopez G.P., Stephanopoulos G.N., Wang D.I.C., Whitesides G.M., and Ingber D.E. (1994). Engineering cell shape and function. *Science* **264** 696-698

Smits A., Van Grieken D., Martman M., Lendahl U., Funa K., and Nister M. (1996). Coexpression of platelet-drived growth factor α and β receptors on medulloblastomas and other primitive neuroectodermal tumours is consistent with an immature stel cell and neuronal derivation. *Laboratory Investigation* **74** 188-198

Smith P.G., Garcia R., and Kogerman L. (1997). Strain reorganizes focal adhesions and cytoskeleton in cultured airway smooth muscle cells. *Exp Cell Res* **232** 127-136.

Solaro R., Chiellini F., Signori F., Fiumi C., Bizzarri R., and Chiellini E. (2003). Nanoparticle systems for the targeted release of active principles of proteic nature. *J Mater Sci Mater Med* **14** 705-711

Song C.X., Labhasetwar V., Murphy H., Qu X., Humphrey W. R., ShebuskR. J.I., and Levy R. J. (1997). Formulation and characterization of biodegradable nanopatrticles for intravascular local drug delivery. *J Control Release* **43** 197-212

Souhami R., and Tobias J. (1998). Cancer and its management. Third edition. Blackwell Science, London

Steinman R.M., Brodie S.E., and Cohn Z.A. (1976). Membrane flow during pinocytosis. A stereologic analysis *J Cell Biol* **68** 665-687

Stella B., Arpicco S., Peracchia M.t., Desmaële, D., Hoebeke J., Renoir M., D'Angelo J., Cattel L., and Couvreur P. (2000). Design of folic acid-conjugated nanoparticles for drug targeting. *J Pharm Sci* **89** 1452-1464

Sternlicht M.D., and Werb Z. (2001). How matrix metalloproteinases regulate cell behavior. *Annu Rev Cell Dev Biol* **17** 463-516

Stolnik S., Illum L., and Davis S.S. (1995a). Long circulating microparticlculate drug carriers. *Adv Drug Del Rev* **16** 195-214

Stolnik S., Garnett M.C., Davies M.C., Illum L., Bousta M., Vert M. and Davis S.S. (1995b). The colloidal properties of surfactant-free biodegradable nanopheres from poly (β-malic acid-co-benzyl malate)s and poly (lactic acid-co-glycolide) *Coll Surf A* **97** 235-245

Stoppini L., Buchs P.A., and Muller D. (1991). A simple method for organotypic cultures of nervous tissue. *J Neurosci Methods* **37** 173-182

Sun H., Mei L., Song C., Cui X., and Wang P. (2006). The in vivo degradation, absorption and excretion of PCL-based implant. *Biomaterials* **27** 1735-1740

Sundstrom C., and Nilsson K. (1976). Establishment and characterization of a human histiocytic lymphoma cell line (U-937). *Int J Cancer* **17** 565-577

Sutherland R.M. (1988) Cell and environment interactions in tumour microregions: the multicell spheroid model. *Science* **240** 177-84

Tabata Y., Gutta S., and Langer R. (1993). Controlled delivery systems for proteins using polyanhydride microspheres. *Pharm Res* **10** 487-496

Tadors Th.F., and Vincent B. (1980). Influence of temperature and electrolytes on the adsorption of poly (ethylene oxide)-poly(propylene oxide) block copolymers on polystyrene latex and on the stablility of polymer-coated particles. *J Phys Chem* **64** 1575-1580

Taylor P.R., Martinez-Pomares L., Stacey M., Lin H-H., Brown G. D., and Gordon S. (2005). Macrophage receptors and immune recognition. *Annu Rev Immunol* **23** 901-944

Teng Y., Morrison M.E., Munk P., Webber S.E., and Prochazka, K. (1998). Release Kinetics Studies of Aromatic Molecules into Water from Block Polymer Micelles, *Macromolecules* **31** 3578-3587

Terzis A.J.A., Arnold H., Laerum O.-D., and Bjerkvig R. (1994). Interaction between human medulloblastomas and foetal rat brain aggregates in vitro. *Acta Neurochir (Wien)* **126** 11-16

Torchilin V.P., and Trubetskoy V.S. (1995) Which polymers can make nanoparticulate drug carriers long-circulating? *Adv Drug Del Rev* **16** 141-155

Tseng Y.C., Hyon S.H., and Ikada Y. (1990). Modification of the synthesis and investigation of properties for 2-cyanoacrylates. *Biomaterials* **11** 73-79

Uhrich K.E., Cannizzaro S.M., Langer R.S., and Shakersheff K.M. (1999). Polymeric systems for controlled drug release. *Chem Rev* **99** 3181-3198

Van D. B. (1989). The way of endocytosis. *Int Rev Cyto* **117** 131-177

Van Natta F.J., Hill J.W. and Carruthers W.H. (1934). Polymerization and ring formation, ε-caprolactone and its polymers. *J Am Chem Soc* **56** 455–459

Vansnick L., Couvreur P., Christiaens-Ley D., and Roland M. (1985). Molecular weights of free and drug-loaded nanoparticles. *Pharm Res* **1** 36-41

Vihola H., Laukkanen A., Hirvonen J., and Tenhu H. (1998). Binding and release of drugs into and from thermosensitive poly (*N*-vinyl caprolactam) nanoparticles. *Eur J Pharm Sci* **46** 69-74

Van Deurs B., Petersen O.W., Olsens S., and Sandvig K. (1989). The ways of endocytosis. *Int Rev Cytol* **17** 131-177

Washington C. (1990). Drug release from microdisperse systems: a critical review. *Int J Pharm* **58** 1-12

Wattiaux, R., Laurent, N., Conninck, S. W., and Jadot, M. (2000). Endosomes, lysosomes: their implication in gene transfer. *Adv Drug Deliv Rev* **41** 201-208

Wehrl P., Magenheim B., and Benita S. (1995). The influence of process parameters on the PLA nanoparticles size distribution, evaluated by means of factorial design. *Eur J Pharm Biopharm* **41** 19-26

Wikstrand C.J., Friedman H.S., and Bigner D.D. (1991). Medulloblastoma cell-substrate interaction *in vitro*. *Invasion and Metastasis* **11** 310-324

Yamakawa I., Tsushima Y., Machida R., and Watanabe S. (1992) Preparation of neurotensin analogue-containing poly (DL- lactic acid) microspheres formed by oil-in-water solvent evaporation, *J Pharm Sci* **81** 899-903

Yamada K.M., Pankov R., and Cukierman E. (2003). Dimensions and dynamics in integrin function. *Braz J Med Biol Res* **36** 959-966

Yoo H.S., Oh J.E., Lee K.H., and Park T.G (1999). Biodegradable nanoparticlescontaining doxorubicin-PLGA conjugate for sustained release *Pharm Res* **16** 1114-1118

Yoshida d., Watanabe K., Noha M., Takahashi H., Teramoto A., and Surgisaki Y. (2002) Tracking cell invasion of human glioma cells and suppression by anti-matrix metalloproteinase agent in rodent brain-slice model. *Brain tumor Pathol* **19** 69-76

Zambaux M.F., Bonneaux F., Gref R., Maincent P., Dellacherie E., Alonso M.J., Labrude P., and Vigneron C. (1998). Influence of experimental parameters on the characteristics of poly (lactic acid) nanoparticles prepared by double emulsion method. *J Control Rel* **50** 31-40

Zhang L., Hu Y., Jiang X., Yang C., Lu W., and Wang Y.H. (2004). Camptothecin derivative-loaded poly (caprolactone-co-lactide)-b-PEG-b-poly (caprolactone-co-lactide) nanoparticles and their biodistribution in mice *J Control Release* **96** 135-148

Zeltzer P.M., Boyett J.M., Finlay J.L., Albright A.L., Rorke L.B., Milstein J.M. Allen J.C., Stevens K.R., Stanley P., Li H., Wisoff J.H., Geyer J.R., Mcguire-Cullen P., Stehbens J.A., Shurin S.B., and Packer R.J. (1999). Metastasis stage, adjuvant treatment, and residual tumor are prognostic factors for medulloblastom in children: conclusions from the children's cancer group 921 randomized phase III study. *J Clin Oncol* **17** 832-845

Zorov D.B., Kobrinsky E., Juhaszova M., and Sollott S.J. (2004). Examining intracellular organelle function using fluorescent probes: from animalcules to quantum dots. *Circ Res* **95** 239-252

APPENDIX I

Cell culture medium

DAOY cells:

MEM (x10)	10ml
L-glutamine	1ml
NEAA	1ml
Sodium pyruvate	1ml
Sodium bicarbonate	2.5ml
FBS	15ml
SUPW	70ml
	Total: 100ml

U937 cells:

L-glutamine	1ml
FBS	15ml
DMEM	84ml
	Total: 100ml

Primary rat brain cells and organotypic slices:

MEM (x10)	10ml
L-glutamine	1ml
Sodium bicarbonate	5ml
NCS	10ml
SUPW	74ml
	Total: 100ml

APPENDIX II

Formulae for calculating amount of RBITC and RBITC loaded NPs in metabolism studies of RBITC loaded NPs in DAOY monolayer cell culture:

DAOY cells have been incubated with RBITC labelled NPs to allow NP uptake, and then washed to remove excess NPs. Following incubation in the absence of NPs cell culture medium, RBITC has been released. We wish to determine whether the RBITC released is free RBITC or RBITC still encapsulated in NPs. Ultracentrifugation does not clearly separate RBITC from NPs, so the true amount of free drug and NPs in the supernatant following centrifugation needs to be calculated.

The relationship between total amount of RBITC, RBITC diffusing from cytoplasm, and RBITC loaded in NPs can be described by the following equations:

$$W_0 = D_0 + P_0 \quad (1)$$

$$W_c = D_c + P_c \quad (2)$$

W_0: the total amount of RBITC in growth medium before centrifugation

D_0: the amount of free RBITC in growth medium before centrifugation

P_0: the amount of RBITC in NPs before centrifugation

W_c: the total amount of RBITC in supernatant after centrifugation

Dc: the amount of free RBITC in supernatant after centrifugation

Pc: the amount of RBITC in NPs in supernatant after centrifugation

According to the centrifugation study of control samples (Table. 5.1), it could be deduced that there was 77.9% free RBITC and 43.2% NPs in the

supernatant after ultracentrifugation. Since RBITC can be also released from NPs during the 1hr ultracentrifuge period, the amount of RBITC encapsulated by NPs should be smaller than 43.2%. Therefore, the total amount of RBITC in upper supernatant after centrifugation was contributed by free RBITC diffusing from DAOY cells, RBITC released from NPs, and RBITC encapsulated by NPs. In the release study of RBITC *in vitro*, it was found that approximately 2% RBITC was released from NPs into cell culture medium over 1h (see 4.3.3). Thus equation (2) could be expressed as the following:

$$W_c = 0.78\ D_0 + 0.42\ P_0 \qquad (3)$$

Rearranging equation (1) and substituting for D_0 in equation (3), the following expression is found:

$$\begin{aligned} W_c &= 0.78\ (W_0 - P_0) + 0.42 P_0 \\ &= 0.78\ W_0 - 0.78 P_0 + 0.42 P_0 \\ &= 0.78\ W_0 - 0.36 P_0 \end{aligned} \qquad (4)$$

Rearranging equation (1) and substituting for P_0 in equation (3) gives:

$$\begin{aligned} W_c &= 0.78\ D_0 + 0.42\ (W_0 - D_0) \\ &= 0.78 D_0 + 0.42\ W_0 - 0.42 D_0 \\ &= 0.36 D_0 + 0.42 W_0 \end{aligned} \qquad (5)$$

Thus amount of NPs recycled into the cell culture medium and amount of free RBITC diffusing out of cells can be calculated using following equations: Rearranging equation (4)

$$P_0 = \frac{0.78 W_0 - W_c}{0.36} \qquad (6)$$

Rearranging equation (5)

$$D_0 = \frac{W_c - 0.42 W_0}{0.36} \qquad (7)$$

APPENDIX III

Website address of website images

Website image 1: Principle of flow cytometry

http://www.rudbeck.uu.se/cellanalys/flowpic.html

Website image 2: Principle of confocal laser scanning microscopy

http://www.cnse.caltech.edu/Research02/reports/mumbru1f2.jpg